Metropolitan-scale quantum networks with diamond qubits
Applied quantum networks for business & society

van der Enden, K.L.

DOI
10.4233/uuid:ccccf0fb-89b3-4c1d-be03-0f3cbdcc15a9

Publication date
2025

Document Version
Final published version

Citation (APA)
van der Enden, K. L. (2025). *Metropolitan-scale quantum networks with diamond qubits: Applied quantum networks for business & society*. [Dissertation (TU Delft), Delft University of Technology]. https://doi.org/10.4233/uuid:ccccf0fb-89b3-4c1d-be03-0f3cbdcc15a9

Metropolitan-scale quantum networks with diamond qubits

Applied quantum networks for business & society

Proefschrift

ter verkrijging van de graad van doctor
aan de Technische Universiteit Delft,
op gezag van de Rector Magnificus prof. dr. ir. T.H.J.J. van der Hagen,
voorzitter van het College voor Promoties,
in het openbaar te verdedigen vrijdag 7 maart 2025 om 12:30 uur.

door

Kian Louran van der Enden

Master of Science in Applied Physics,
Technische Universiteit Delft, Nederland.

Dit proefschrift is goedgekeurd door de promotor:
Prof. dr. ir. R. Hanson

Samenstelling promotiecommissie:

Rector Magnificus,	voorzitter
Prof. dr. ir. R. Hanson,	Technische Universiteit Delft, promotor
Prof. dr. S.D.C. Wehner,	Technische Universiteit Delft, promotor
Onafhankelijke leden:	
Dr. M. van den Bossche,	Thales Alenia Space, Frankrijk
Dr. ir. J. Cramer,	Universiteit Leiden
Prof. dr. ir. L.P. Kouwenhoven,	Technische Universiteit Delft
Prof. dr. A.F. Otte,	Technische Universiteit Delft
Prof. Dr. rer. nat. habil. A. Reiserer,	Technische Universität München, Duitsland
Dr. T. van der Sar,	Technische Universiteit Delft, reservelid

Cover art by: Generated by Kian van der Enden using Midjourney 6.1 with manual edits in Inkscape.
Printed by: Gildeprint - The Netherlands.

ISBN 978-94-6384-749-0

An electronic version of this dissertation is available at
https://repository.tudelft.nl.

We don't do this "thing" 'cause it's permitted.
We do it because we have to.
*We do it because we're **compelled**.*

Rorschach, *Watchmen*

Contents

SUMMARY

The internet revolutionized the world by giving computers the ability to communicate with each other. It transformed computing, how we design new technology, the way we run our economy, people's social life and so much more. In the pursuit to go beyond the limits of current *classical* computing, we have set out to build quantum computers, consisting of quantum bits (qubits), that can solve complex computational challenges that their classical counterparts cannot. However, the current internet does not support quantum computer communication. We need a new type of internet: the *quantum internet*. It is *entanglement* generation between the so-called *quantum nodes* of these rudimentary *quantum networks* that enables the exchange of *quantum information* between them, allowing the quantum computers to communicate. Just like the internet did for the computer, the quantum internet will revolutionize quantum computing. Among many applications, it enables secure, distributed quantum computing, driving the future of privacy-enhanced powerful computing. There are different qubit platforms that allow for this *quantum communication*. Impressive progress has been made in the last decades culminating in the realization of small quantum networks in lab environments up to three nodes. Still, a formidable challenge remained: pushing the boundary beyond the lab to a deployed system that can operate in less ideal circumstances, without the locality of signals that ensure the precise control of parameters necessary for entanglement generation. This thesis tackles the challenge of real-world quantum networks in two ways.

In 'Part I - Experimental' we present the successful development of a scalable quantum network hardware platform for long-distance deployment and independent operation of quantum nodes. We built nodes based on nitrogen-vacancy center qubits in diamond, incorporated with frequency conversion from visible (637nm) to telecom wavelengths (1588nm). With these, we successfully generated entanglement between two quantum nodes located in two cities in the Netherlands. We generate this entanglement in a *heralded* way, to deliver a 'live' entangled state that can be used for further quantum processing, exactly how a future quantum internet should operate.

In 'Part II - Business & Society' we develop an understanding of the consequences of future quantum networks for existing industries and society as a whole. First, we discuss an in-depth use case analysis of the quantum internet within the automotive industry, identifying mutually beneficial regions of interest. Then, we evaluate the status of the development of a responsible future quantum internet, revealing that efforts should continue to make quantum ecosystem stakeholders aware of the potential for malicious applications of a quantum internet.

I conclude by urging commercialization of a quantum internet. I suggest specific quantum-related products that are likely to be useful in the coming years. I finalize by highlighting that an opportunity presents itself for a quantum internet operator to deliver a commercial full-stack quantum network hardware infrastructure. This can serve as crucial catalyst towards useful quantum computing.

SAMENVATTING

Het internet heeft de wereld veranderd door computers met elkaar te laten communiceren. Dit heeft technologie, economie en sociale interacties volledig veranderd. Nu streven we naar de ontwikkeling van *kwantumcomputers* die met kwantumbits (qubits) complexe problemen kunnen oplossen die klassieke computers niet aankunnen. Om deze computers te laten communiceren is een nieuw type internet nodig: het *kwantuminternet*. Het genereren van *verstrengeling* tussen de *kwantumnodes* van deze rudimentaire *kwantumnetwerken* maakt de uitwisseling van *kwantuminformatie* tussen elkaar mogelijk, waardoor de kwantumcomputers kunnen communiceren. Dit maakt veilige en gedistribueerde kwantumcomputing mogelijk. Hoewel kleine kwantumnetwerken in laboratoria al zijn gerealiseerd, blijft de uitdaging om deze technologie buiten het lab te laten werken, zonder de lokaliteit van signalen die de precieze controle garanderen voor het genereren van verstrengeling. Dit proefschrift richt zich het ontwikkelen van kwantumnetwerken voor de echte wereld op twee manieren.

In 'Deel I - Experiment' bespreken we de succesvolle ontwikkeling van een schaalbaar kwantuminternet hardware platform dat werkt op lange afstand tussen de kwantumnodes. We bouwden nodes gebaseerd op qubits bestaand uit een stikstof-gat combinatie (NV-center) in diamant, gekoppeld met frequentieconversie van zichtbare (637nm) naar telecomgolflengten (1588nm). Hiermee hebben we verstrengeling gegenereerd tussen twee kwantumnodes in twee steden in Nederland. Deze verstrengeling is gemaakt op zo'n manier dat er een verstrengelde toestand ontstaat die gebruikt kan worden in kwantumberekeningen, precies zoals een toekomstig kwantuminternet zou moeten werken.

In 'Deel II - Business & maatschappij' ontwikkelen we inzicht in de gevolgen van een toekomstig kwantuminternet voor bestaande industrieën en de maatschappij als geheel. Eerst bespreken we een use case analyse van het kwantuminternet binnen de auto-industrie, waarbij we wederzijdse regio's van interesse identificeren. Vervolgens evalueren we de status van de ontwikkeling van een verantwoord toekomstig kwantuminternet. Hier is uitgekomen dat inspanningen moeten worden voortgezet om belanghebbenden van het kwantum-ecosysteem bewust te maken van het potentieel voor kwaadwillige toepassingen van een kwantuminternet.

Ik sluit af door aan te dringen op de vermarkting van een kwantuminternet. Ik stel specifieke kwantumgerelateerde producten voor die de komende jaren hun nut zullen bewijzen. Ik sluit af door te benadrukken dat er een kans is voor een kwantuminternet-provider om een commerciële full-stack kwantuminternet hardware-infrastructuur te leveren. Dit kan dienen als cruciale drijfveer voor nuttige kwantumcomputing.

I

EXPERIMENTAL

I.1

INTRODUCTION

The goal of the Web is to serve humanity. We build it now so that those who come to it later will be able to create things that we cannot ourselves imagine.

Tim Berners-Lee

I.1.1. A SHORT HISTORY OF THE INTERNET

It took roughly 30 years of technological development to go from a commercially available computer, the Z1 built in 1938 by Konrad Zuse [1], to a (government) demonstration project of the first ever network of computers in 1969: ARPANET [2, 3]. Under the guidance of dr. Leonard Kleinrock, several computers the size of a decent studio apartment were housed in research institutes on the west coast of the United States and connected to a dedicated telephone line. With specific technology and rudimentary protocols in place, the computers were ready to share digital information. Famously, the first attempt to do a *remote login* failed spectacularly after typing only 2 letters by grad student Charley Kline at UCLA, severing the connection. After a full hour of tinkering, the remote login was successful and history had been made. It was now possible to interconnect computers over long distances. It only took 13 years for the four initial connections to grow into dozens of locations all across the USA, including several satellite(!) connections to traverse oceans, becoming an intercontinental network.

Jumping ahead to 2024, we can recognize how far interconnected computers have come since the ARPANET days. Most people on earth have some access to a computer that is interconnected with others through a complex network of radio towers, copper wires, satellite connections, line-of-sight laser connections or through a *data-highway* of fiber infrastructure under land and ocean [4–6]. All these physical networks together form, what we now call, the *internet*. These connections are managed by different internet service providers (ISPs), relying on standardized protocols embedded in hardware products to let every data packet find its way from its sender to its targeted receiver, wherever they may be located in the world. This complex chain of signal amplifiers and routers, managed by smartly designed software, allow packets from Amsterdam, the Netherlands to be sent through terrestrial networks to Sydney, Australia in about 260 ms [7], literally a blink of an eye[1]. The data highway also allows for sending large amount of data in a short time. Nowadays an at-home 1 Gbit/s internet connection can be purchased in fiber-dense countries, with experimental records pushing the limits in backbone pipelines towards 402 Tbit/s [9]. Unequivocally we can state that access to internet enabled a revolution for computing and subsequently for people's social life, the way we run our economy and how we design new technology.

I.1.2. THE SECOND QUANTUM REVOLUTION

We are at the cusp of a similar revolution driven by quantum technologies, sometimes referred to as the *second quantum revolution* [10]. Although our current (connected) computers are marvels of technology and capability, they have computational limits based on their classical approach to data processing. However, by the realization that the laws of quantum physics could be used to process data in a fundamentally different way, the revolutionary field of quantum computing was born [11]. In this world we do not encode information in bits, but encode quantum information in qubits (quantum bits) [12]. Throughout the years, many quantum algorithms were introduced that could be run on a general-purpose quantum computer built from these qubits that would provide speed-

[1] $\approx 300\,\mathrm{ms}$ [8]

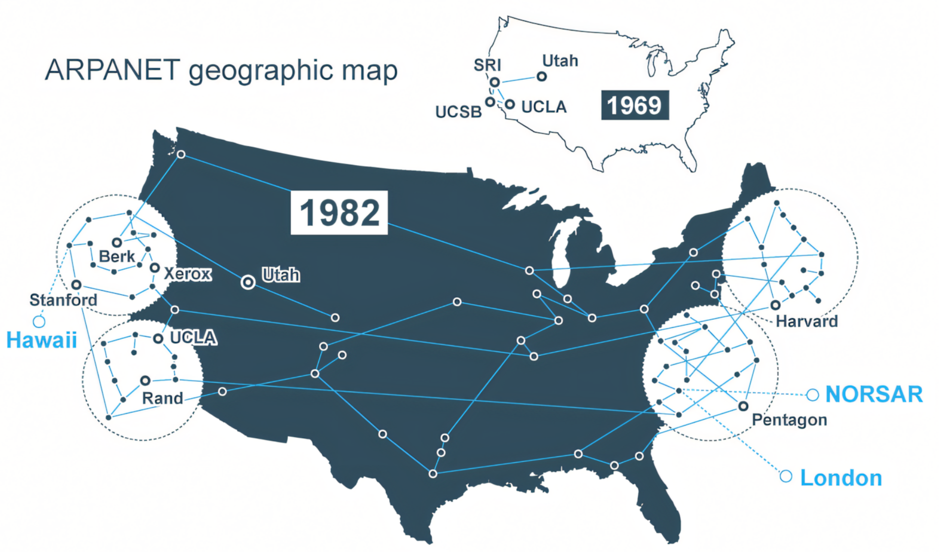

Figure I.1.1: ARPANET evolution from 1969 to 1982. Figure courtesy of PortSwigger [3].

ups over classical equivalents [13, 14]. They provide significant computational speed-ups for chemistry simulations [15, 16], searching through data [17], matrix operations [18] and prime factorization [19], to name a few. Especially the latter has become famously known as Shor's algorithm, which would allow a powerful quantum computer to break public-key cryptography schemes that are used to encrypt most of today's internet traffic[2] [20].

At the same time, quantum *communication* as research field made strides in its own lane. As the name suggests, this field aims to **(1)** secure classical communication between different locations using quantum phenomena or **(2)** to enable quantum devices to *communicate with each other*. Many landmark experiments have been performed making use of the fundamental property of quantum entanglement. Entangled photons enable applications in (1), where the property of entanglement is used to generate (classical) keys between two different locations: quantum key distribution (QKD) [21–24]. This field has matured to the point of commercialization, where many vendors offer turn-key QKD systems of various flavors [25–29]. Although useful from a security point of view, the usability of these systems generally is limited to *key* generation.

To go beyond key generation, we need the photons to be entangled to stationary qubits. Implementations can include trapped atoms [30], trapped ions [31], quantum dots [32] or color-centers [33, 34] entangled to photons. The last decades saw progress in using these qubit-photon entangled pairs to enable entanglement generation *between* stationary qubits [35–41], exactly enabling this chip-to-chip communication of the mentioned (2) above. This ability to generate entanglement between quantum computers allowed for other *quantum network* purposes, such as quantum state teleportation [42–45], prove fun-

[2]The **S** in HTTP**S** means your connection is encrypted with a type of public-key cryptography scheme

damental properties of physics [46] and other forms of distributed quantum computing. This brings us to the most important reason for developing quantum networks:

Quantum networks are the **only** way through which quantum computers can share quantum information.

We develop these quantum networks because just like the internet did for computing:

Quantum networks will revolutionize quantum computing.

Quantum networks are the catalyst to scaling quantum computers with chip-to-chip communication, connecting future high-performance quantum computing centers (HPQCs) and bridging the interface between different kinds of quantum computing platforms [47], to build a full fledged quantum internet [48, 49]. There are applications we know of that are only able to work in quantum networks, some of which are: distributed quantum computing [50], secure delegated quantum computing in the cloud [51, 52], quantum equivalents of message authentication [53], digital signatures [54] and anonymous transmission [55–57]. Leaning on the historical leap the internet has enabled for the computer, we expect many more applications to follow once quantum computers are enabled in connectivity. The argument alone of speeding up the development of useful quantum computers warrants a worldwide push to build scalable quantum networks [58, 59].

In the pursuit of developing these quantum networks, a specific quantum platform has shown incredible versatility both in computing and communication capabilities. The Nitrogen-Vacancy (NV) center in diamond [60] has universal quantum computing control of its electronic qubit [61–65] and can use the surrounding nuclear spins as quantum memory [62, 64, 66, 67]. Simultaneously, it has spin-selective photon emission, allowing for qubit-photon entanglement which makes it compatible with entanglement generation schemes for qubit-qubit entanglement [38]. The entire system that can control the NV center and mediate its entanglement generation is a *quantum node*, which we define in more detail in Chapter I.2.1. The NV center based quantum nodes have been *the* workhorse in solid-state quantum communication showing remote state teleportation between two different quantum chips [44], performing a loophole-free Bell test with 1.2 km distance between the two nodes [46] and, as recent achievement, showed essential quantum networking capabilities within a three-node network [45, 68].

With all these impressive results one formidable challenge was not yet addressed: breaking the wall of the lab. All experiments thus far took place *in the same lab*, or more precisely: they make use of the same hardware devices and make use of the locality of signals to ensure precise control on timing, frequencies, phases and polarization [41, 69, 70], or otherwise are limited in their usability as quantum processing unit and operate as memory [71]. This includes the loophole-free Bell test at 1.2 km distance, which operated effectively as a stretched-out lab [72]. As additional hurdle the photons emitted from the NV center are at a wavelength that limits the distance over which they can be transmitted through fiber (see Section I.2.5). This thesis tackles exactly the challenge of breaking out of the lab: the development of a scalable quantum network hardware platform for long-distance deployment and operation of quantum nodes. Summarizing:

Thesis "Experimental" goal
Design and build an extensible quantum network hardware platform to operate a two-node quantum network at metropolitan scale, running over deployed telecom fiber, and show (heralded) entanglement generation between the nodes.

In achieving this goal we have taken concepts and fundamental know-how of previous NV qubit and network experiments and improved on them to build a quantum network hardware platform capable of performing the above goal. Several improvements include the introduction of the Quantum Frequency Converter (QFC) which converts the lossy NV-wavelength photons to a telecom low-loss wavelength with their quantum properties retained, allowing them to travel tens of kilometers with manageable loss (see Chapter I.2.5). Additionally, we set out to build a system that would be compatible with an entanglement generation scheme where only one photon needs to be measured, instead of two (see Chapter I.2.4). This quadratically increases the rate of entanglement generation, at the trade-off of system complexity by requiring more specialized control over the photons used for entanglement generation. Specifically, we now require the knowledge of the phase of these photons. This practically translates to setting the complete optical phase path, from quantum emitter to detection, to a known setpoint and keeping it there, which we refer to as *phase stabilization* or *synchronization*. We discuss this in detail in Chapter I.2.6 and Chapter I.4.

Lastly, when discussing entanglement, we usually refer to an entanglement *fidelity*, a measure for the quality of the entanglement: it takes a value between 0 and 1 [73]. For the entanglement generation schemes used in this thesis, if the photons would not act as quantum particles, we would obtain a maximum entanglement fidelity of 0.5. This is called the *classical bound*. In order to prove quantum behavior, we set out to show entanglement fidelities that are (within several standard deviations) above that classical bound.

I.1.3. Thesis "Part I" overview

In the following chapters we address the details of the practical challenges, solutions and experiments that together prove that we have succeeded in deploying this quantum network hardware platform.

Chapter I.2 describes the theoretical and practical context of the NV center in diamond and how to use it to generate entanglement between two NV centers. I discuss the challenges of long distance compatibility, introduce the theory and concept of two distinct ways we design a QFC and how and what phase *exactly* we have to stabilize. Lastly, I give an overview of the hardware control stack built specifically for modular and long-term operation of a quantum node.

Chapter I.3 is the first experiment where the first iteration of the quantum network hardware platform was used. Here we prove that we can generate indistinguishable photons from distinguishable sources by performing a Hong-Ou-Mandel interference experiment. Using two distinct NV qubits operating at different frequencies on each of the nodes, we show that separate QFCs with individual feedback mechanisms can generate output photons that are around 90% indistinguishable from another. Importantly, this experiment showed the long-duration experimental capabilities of the hardware platform. While operating in the same lab, the entire system was run as if it was already fully deployed at large distances from another, fully proving the working principle of independent operation of quantum nodes.

Chapter I.4 introduces the technical background of the phase stabilization scheme that is the essential building block to enable single-click entanglement generation between two quantum nodes. We discuss which different paths within a quantum network require phase stabilization, what type of noise is introduced in those paths and the feedback bandwidth we therefore need to properly curb this phase noise. We show the technical layout of the scheme and how an analog feedback system is designed for that allows for limitless feedback range. Lastly, we show the performance of the total phase stabilization system and individually per feedback loop.

Chapter I.5 presents the crowning results of this thesis by achieving the goal that was set out. We show the full overview of the quantum network hardware platform and its capabilities. We characterize the system while the nodes are in the same lab in Delft by verifying entanglement generation in post-selection, and show a fidelity above the classical bound. Then, after moving half of the entire system to The Hague, we have two quantum nodes are in two cities in the Netherlands, linked together by 25 km of deployed fiber. We repeat the experiment in a fully heralded way, which is how one would run a *real* quantum network to enable complex applications. Here, the fidelity is significantly above the classical bound as well. This successfully concludes the experiments performed with the quantum network hardware platform.

Chapter I.6 summarizes the outcomes of Part I of this thesis and presents the outlook of the field of quantum networks as I perceive it to be.

REFERENCES

[1] F. L. Bauer, *Origins and Foundations of Computing: In Cooperation with Heinz Nixdorf MuseumsForum,* (Springer Science & Business Media, 2009) p. 78.

[2] B. M. Leiner, V. G. Cerf, D. D. Clark, R. E. Kahn, L. Kleinrock, D. C. Lynch, J. Postel, L. G. Roberts, and S. Wolff, *A brief history of the internet,* SIGCOMM Comput. Commun. Rev. **39**, 22–31 (2009).

[3] J. Leyden, *ARPANET anniversary: The internet's first transmission was sent 50 years ago today,* test1 (2019).

[4] D. Comer, *Computer Networks and Internets* (Prentice Hall, 2009).

[5] X, a division of Google LLC, *Taara: Fast, affordable connectivity using beams of light,* Accessed through Wayback Machine 19 July 2024 (2024).

[6] ITU, *Infrastructure connectivity map,* (2024).

[7] WonderNetwork, *Ping time between Amsterdam and Sydney,* Accessed through Wayback Machine 4 August 2023 (2023).

[8] I. Fatt and B. A. Weissman, *Physiology of the eye: an introduction to the vegetative functions* (Butterworth-Heinemann, 2013).

[9] B. J. Puttnam, R. S. Luis, I. Phillips, M. Tan, A. Donodin, D. Pratiwi, L. Dallachiesa, Y. Huang, M. Mazur, N. Fontaine, H. Chen, D. Chung, V. Ho, D. Orsuti, B. Boriboon, G. Rademacher, L. Palmieri, R. Man, R. Ryf, D. T. Neilson, W. Forysiak, and H. Furukawa, *402 Tb/s GMI Data-Rate OESCLU-Band Transmission,* in *Optical Fiber Communication Conference (OFC) 2024* (Optica Publishing Group, 2024) p. Th4A.3.

[10] J. P. Dowling and G. J. Milburn, *Quantum technology: the second quantum revolution,* Philosophical Transactions of the Royal Society of London. Series A: Mathematical, Physical and Engineering Sciences **361**, 1655–1674 (2003).

[11] R. P. Feynman, *Simulating physics with computers,* International Journal of Theoretical Physics **21**, 467–488 (1982).

[12] B. Schumacher, *Quantum coding,* Physical Review A **51**, 2738–2747 (1995).

[13] C. H. Bennett, E. Bernstein, G. Brassard, and U. Vazirani, *Strengths and weaknesses of quantum computing,* SIAM Journal on Computing **26**, 1510 (1997).

[14] S. Jordan, *Quantum algorithm zoo,* Accessed through Wayback Machine 24 June 2024 (2011).

[15] A. Aspuru-Guzik, A. D. Dutoi, P. J. Love, and M. Head-Gordon, *Simulated quantum computation of molecular energies,* Science **309**, 1704 (2005).

[16] M. B. Hastings, D. Wecker, B. Bauer, and M. Troyer, *Improving quantum algorithms for quantum chemistry,* Quantum Info. Comput. **15**, 1–21 (2015).

I.1

[17] L. K. Grover, *A fast quantum mechanical algorithm for database search,* in *Proceedings of the twenty-eighth annual ACM symposium on Theory of Computing*, STOC '96 (Association for Computing Machinery, New York, NY, USA, 1996) pp. 212–219.

[18] D. S. Abrams and S. Lloyd, *Quantum algorithm providing exponential speed increase for finding eigenvalues and eigenvectors,* Phys. Rev. Lett. **83**, 5162 (1999).

[19] P. Shor, *Algorithms for quantum computation: discrete logarithms and factoring,* in *Proceedings 35th Annual Symposium on Foundations of Computer Science* (1994) pp. 124–134.

[20] E. Rescorla, *The Transport Layer Security (TLS) Protocol Version 1.3,* RFC 8446 (2018).

[21] A. K. Ekert, *Quantum cryptography based on Bell's theorem,* Physical Review Letters **67**, 661 (1991).

[22] C. H. Bennett and G. Brassard, *Quantum cryptography: Public key distribution and coin tossing,* Theoretical Computer Science Theoretical Aspects of Quantum Cryptography – celebrating 30 years of BB84, **560**, 7 (2014).

[23] R. Van Meter, *Quantum key distribution,* in *Quantum Networking* (John Wiley & Sons, Ltd, 2014) Chap. 5, pp. 91–111.

[24] R. C. Berrevoets, T. Middelburg, R. F. L. Vermeulen, L. D. Chiesa, F. Broggi, S. Piciaccia, R. Pluis, P. Umesh, J. F. Marques, W. Tittel, and J. A. Slater, *Deployed measurement-device independent quantum key distribution and bell-state measurements coexisting with standard internet data and networking equipment,* Communications Physics **5** (2022).

[25] M. Stanley, Y. Gui, D. Unnikrishnan, S. Hall, and I. Fatadin, *Recent progress in quantum key distribution network deployments and standards,* Journal of Physics: Conference Series **2416**, 012001 (2022).

[26] ID Quantique, *Quantum-Safe Security Products,* Accessed through Wayback Machine 10 May 2024 (2024).

[27] Toshiba, *Quantum Key Distribution - What Is QKD? How Does It Work?* , Accessed through Wayback Machine 7 Jan 2024 (2024).

[28] MagiQ Technologies, *MagiQ QPN™| Network Security | Somerville, MA,* Accessed through Wayback Machine 10 May 2024 (2024).

[29] Quintessence Labs, *QOptica™ Quantum Key Distribution Product Sheet,* Accessed through Wayback Machine 17 May 2024 (2024).

[30] J. Volz, M. Weber, D. Schlenk, W. Rosenfeld, J. Vrana, K. Saucke, C. Kurtsiefer, and H. Weinfurter, *Observation of entanglement of a single photon with a trapped atom,* Phys. Rev. Lett. **96**, 030404 (2006).

[31] B. B. Blinov, D. L. Moehring, L.-M. Duan, and C. Monroe, *Observation of entanglement between a single trapped atom and a single photon,* Nature **428**, 153 (2004).

[32] R. Uppu, L. Midolo, X. Zhou, J. Carolan, and P. Lodahl, *Quantum-dot-based deterministic photon–emitter interfaces for scalable photonic quantum technology,* Nature Nanotechnology **16**, 1308 (2021).

[33] E. Togan, Y. Chu, A. S. Trifonov, L. Jiang, J. Maze, L. Childress, M. V. G. Dutt, A. S. Sørensen, P. R. Hemmer, A. S. Zibrov, and M. D. Lukin, *Quantum entanglement between an optical photon and a solid-state spin qubit,* Nature **466**, 730 (2010).

[34] M. Ruf, N. H. Wan, H. Choi, D. Englund, and R. Hanson, *Quantum networks based on color centers in diamond,* Journal of Applied Physics **130**, 070901 (2021).

[35] D. L. Moehring, P. Maunz, S. Olmschenk, K. C. Younge, D. N. Matsukevich, L.-M. Duan, and C. Monroe, *Entanglement of single-atom quantum bits at a distance,* Nature **449**, 68–71 (2007).

[36] S. Ritter, C. Nölleke, C. Hahn, A. Reiserer, A. Neuzner, M. Uphoff, M. Mücke, E. Figueroa, J. Bochmann, and G. Rempe, *An elementary quantum network of single atoms in optical cavities,* Nature **484**, 195 (2012).

[37] J. Hofmann, M. Krug, N. Ortegel, L. Gérard, M. Weber, W. Rosenfeld, and H. Weinfurter, *Heralded Entanglement Between Widely Separated Atoms,* Science **337**, 72 (2012).

[38] H. Bernien, B. Hensen, W. Pfaff, G. Koolstra, M. S. Blok, L. Robledo, T. H. Taminiau, M. Markham, D. J. Twitchen, L. Childress, and R. Hanson, *Heralded entanglement between solid-state qubits separated by three metres,* Nature **497**, 86–90 (2013).

[39] R. Stockill, M. J. Stanley, L. Huthmacher, E. Clarke, M. Hugues, A. J. Miller, C. Matthiesen, C. Le Gall, and M. Atatüre, *Phase-Tuned Entangled State Generation between Distant Spin Qubits,* Physical Review Letters **119**, 010503 (2017).

[40] L. Stephenson, D. Nadlinger, B. Nichol, S. An, P. Drmota, T. Ballance, K. Thirumalai, J. Goodwin, D. Lucas, and C. Ballance, *High-Rate, High-Fidelity Entanglement of Qubits Across an Elementary Quantum Network,* Physical Review Letters **124**, 110501 (2020).

[41] V. Krutyanskiy, M. Galli, V. Krcmarsky, S. Baier, D. Fioretto, Y. Pu, A. Mazloom, P. Sekatski, M. Canteri, M. Teller, J. Schupp, J. Bate, M. Meraner, N. Sangouard, B. Lanyon, and T. Northup, *Entanglement of Trapped-Ion Qubits Separated by 230 Meters,* Physical Review Letters **130**, 050803 (2023).

[42] C. H. Bennett, G. Brassard, C. Crépeau, R. Jozsa, A. Peres, and W. K. Wootters, *Teleporting an unknown quantum state via dual classical and einstein-podolsky-rosen channels,* Physical Review Letters **70**, 1895–1899 (1993).

[43] D. Bouwmeester, J.-W. Pan, K. Mattle, M. Eibl, H. Weinfurter, and A. Zeilinger, *Experimental quantum teleportation,* Nature **390**, 575 (1997).

I.1

[44] W. Pfaff, B. J. Hensen, H. Bernien, S. B. van Dam, M. S. Blok, T. H. Taminiau, M. J. Tiggelman, R. N. Schouten, M. Markham, D. J. Twitchen, and R. Hanson, *Unconditional quantum teleportation between distant solid-state quantum bits,* Science **345**, 532 (2014).

[45] S. L. N. Hermans, M. Pompili, H. K. C. Beukers, S. Baier, J. Borregaard, and R. Hanson, *Qubit teleportation between non-neighbouring nodes in a quantum network,* Nature **605**, 663 (2022).

[46] B. Hensen, H. Bernien, A. E. Dréau, A. Reiserer, N. Kalb, M. S. Blok, J. Ruitenberg, R. F. L. Vermeulen, R. N. Schouten, C. Abellán, W. Amaya, V. Pruneri, M. W. Mitchell, M. Markham, D. J. Twitchen, D. Elkouss, S. Wehner, T. H. Taminiau, and R. Hanson, *Loophole-free Bell inequality violation using electron spins separated by 1.3 kilometres,* Nature **526**, 682 (2015).

[47] M. J. Weaver, P. Duivestein, A. C. Bernasconi, S. Scharmer, M. Lemang, T. C. v. Thiel, F. Hijazi, B. Hensen, S. Gröblacher, and R. Stockill, *An integrated microwave-to-optics interface for scalable quantum computing,* Nature Nanotechnology **19**, 166 (2024).

[48] H. J. Kimble, *The quantum internet,* Nature **453**, 1023 (2008).

[49] S. Wehner, D. Elkouss, and R. Hanson, *Quantum internet: A vision for the road ahead,* Science **362**, eaam9288 (2018).

[50] M. Caleffi, M. Amoretti, D. Ferrari, J. Illiano, A. Manzalini, and A. S. Cacciapuoti, *Distributed quantum computing: A survey,* Computer Networks , 110672 (2024).

[51] A. Broadbent, J. Fitzsimons, and E. Kashefi, *Universal Blind Quantum Computation,* in *2009 50th Annual IEEE Symposium on Foundations of Computer Science* (2009) pp. 517–526.

[52] J. F. Fitzsimons and E. Kashefi, *Unconditionally verifiable blind quantum computation,* Physical Review A **96**, 012303 (2017).

[53] H. Barnum, C. Crépeau, D. Gottesman, A. Smith, and A. Tapp, *Authentication of quantum messages,* in *The 43rd Annual IEEE Symposium on Foundations of Computer Science, 2002. Proceedings.* (IEEE, 2002) pp. 449–458.

[54] D. Gottesman and I. Chuang, *Quantum Digital Signatures,* arXiv:quant-ph/0105032 (2001).

[55] M. Christandl and S. Wehner, *Quantum Anonymous Transmissions,* in *Advances in Cryptology - ASIACRYPT 2005*, edited by B. Roy (Springer, Berlin, Heidelberg, 2005) pp. 217–235.

[56] J. Bouda and J. Sprojcar, *Anonymous Transmission of Quantum Information,* in *2007 First International Conference on Quantum, Nano, and Micro Technologies (ICQNM'07)* (2007) pp. 12–12.

[57] A. Unnikrishnan, I. J. MacFarlane, R. Yi, E. Diamanti, D. Markham, and I. Kerenidis, *Anonymity for practical quantum networks,* Phys. Rev. Lett. **122**, 240501 (2019).

[58] Horizon Europe, *Quantum Internet Alliance - Phase1,* .

[59] IQM Quantum Computers, OpenOcean, Lakestar, and The Quantum Insider (TQI), *State of quantum 2024 report,* (2024).

[60] M. W. Doherty, N. B. Manson, P. Delaney, F. Jelezko, J. Wrachtrup, and L. C. Hollenberg, *The nitrogen-vacancy colour centre in diamond,* Physics Reports **528**, 1 (2013).

[61] F. Jelezko, T. Gaebel, I. Popa, A. Gruber, and J. Wrachtrup, *Observation of coherent oscillations in a single electron spin,* Phys. Rev. Lett. **92**, 076401 (2004).

[62] M. V. G. Dutt, L. Childress, L. Jiang, E. Togan, J. Maze, F. Jelezko, A. S. Zibrov, P. R. Hemmer, and M. D. Lukin, *Quantum Register Based on Individual Electronic and Nuclear Spin Qubits in Diamond,* Science **316**, 1312 (2007).

[63] R. Hanson, V. V. Dobrovitski, A. E. Feiguin, O. Gywat, and D. D. Awschalom, *Coherent Dynamics of a Single Spin Interacting with an Adjustable Spin Bath,* Science **320**, 352 (2008).

[64] L. Robledo, L. Childress, H. Bernien, B. Hensen, P. F. A. Alkemade, and R. Hanson, *High-fidelity projective read-out of a solid-state spin quantum register,* Nature **477**, 574 (2011).

[65] W. Pfaff, *Quantum measurement and entanglement of spin Quantum bits,* PhD Thesis, Delft University of Technology (2013).

[66] T. H. Taminiau, J. J. T. Wagenaar, T. van der Sar, F. Jelezko, V. V. Dobrovitski, and R. Hanson, *Detection and control of individual nuclear spins using a weakly coupled electron spin,* Phys. Rev. Lett. **109**, 137602 (2012).

[67] C. Bradley, J. Randall, M. Abobeih, R. Berrevoets, M. Degen, M. Bakker, M. Markham, D. Twitchen, and T. Taminiau, *A Ten-Qubit Solid-State Spin Register with Quantum Memory up to One Minute,* Physical Review X **9**, 031045 (2019).

[68] M. Pompili, S. L. N. Hermans, S. Baier, H. K. C. Beukers, P. C. Humphreys, R. N. Schouten, R. F. L. Vermeulen, M. J. Tiggelman, L. dos Santos Martins, B. Dirkse, S. Wehner, and R. Hanson, *Realization of a multinode quantum network of remote solid-state qubits,* Science **372**, 259 (2021).

[69] T. van Leent, M. Bock, F. Fertig, R. Garthoff, S. Eppelt, Y. Zhou, P. Malik, M. Seubert, T. Bauer, W. Rosenfeld, W. Zhang, C. Becher, and H. Weinfurter, *Entangling single atoms over 33 km telecom fibre,* Nature **607**, 69 (2022).

[70] C. M. Knaut, A. Suleymanzade, Y.-C. Wei, D. R. Assumpcao, P.-J. Stas, Y. Q. Huan, B. Machielse, E. N. Knall, M. Sutula, G. Baranes, N. Sinclair, C. De-Eknamkul, D. S. Levonian, M. K. Bhaskar, H. Park, M. Lončar, and M. D. Lukin, *Entanglement of nanophotonic quantum memory nodes in a telecom network,* Nature **629**, 573 (2024).

I.1

[71] J.-L. Liu, X.-Y. Luo, Y. Yu, C.-Y. Wang, B. Wang, Y. Hu, J. Li, M.-Y. Zheng, B. Yao, Z. Yan, D. Teng, J.-W. Jiang, X.-B. Liu, X.-P. Xie, J. Zhang, Q.-H. Mao, X. Jiang, Q. Zhang, X.-H. Bao, and J.-W. Pan, *Creation of memory–memory entanglement in a metropolitan quantum network,* Nature **629**, 579 (2024).

[72] B. Hensen, *Quantum Nonlocality with Spins in Diamond*, PhD Thesis, Delft University of Technology (2016).

[73] M. A. Nielsen and I. L. Chuang, *Quantum Computation and Quantum Information: 10th Anniversary Edition* (Cambridge University Press, 2010).

I.2

METHODS

In this chapter we discuss the requirements of a quantum node to be compatible for long-distance quantum networks, the fundamentals of NV-center physics and how we use them to generate entanglement as communication qubit. We finalize by giving an overview of the quantum network hardware platform that was designed and built to support independent and remote operation of quantum nodes.

I.2.1. A long-distance compatible quantum network node

A large-scale *quantum internet* [1] distributes entanglement between *quantum nodes* to enable complex quantum networking applications [2]. A range of experiments over the past decades have shown increasingly complex capabilities of quantum networks based on different qubit platforms [3–12], which includes off-chip interaction between multiple nodes within the same lab or building. Previous work has defined what properties such a node requires to have in order to operate in an interconnected quantum network [13]. In this thesis we redefine these properties for long-distance compatible quantum network nodes:

Quantum node requirements for long-distance quantum networks

1. **Communication qubits that can be entangled with flying qubits.** Qubits on separate nodes are to be entangled through the flying qubits.
2. **Preservation of qubit state** during the time necessary to verify heralded entanglement (6) and availability of memory qubits for subsequent usage of the entangled state in quantum network applications.
3. **Universal quantum control** of the communication and memory qubits.
4. **Independent node operation** to allow scaling in the number of nodes demanded by the large physical distance between the nodes, resulting in a significant communication delay between them.
5. **Minimization of transmission losses** to allow for tens of kilometer separation between nodes
6. **Real-time heralded delivery of entangled states** to the quantum processing unit enabled by feed-forward capabilities to allow executing complex quantum network applications.

The experiments in this thesis satisfy all above requirements except for the usage of specific memory qubits besides the communication qubit. In the following sections we discuss the physical realization and implementation of the requirements using diamond-based quantum chips that allow for the realization of a metropolitan distance quantum network.

I.2.2. The NV center in diamond

The nitrogen vacancy (NV) center in diamond is an atomic defect in the diamond's lattice where two carbon atoms are replaced by one nitrogen atom and leaving a vacancy [14], see Fig. I.2.1A. This creates the neutrally charged NV^0 from the combined wavefunction of the leftover dangling bonds: two from the nitrogen and three from the surrounding carbons to form a spin-1/2 system. Upon capturing of an electron the NV^- state is achieved, forming a negatively charged spin-1 system. The NV^- has useful quantum properties that can be exploited for quantum networking purposes [15], which we will continue to discuss in this chapter and refer to simply as NV.

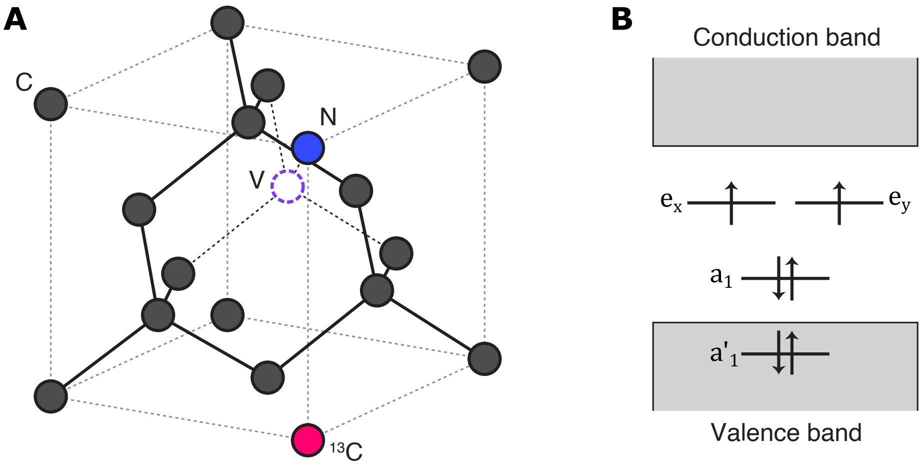

Figure I.2.1: **The nitrogen vacancy center in diamond**. **A** Schematic of the atomic structure of the NV center in the diamond lattice. The nitrogen (blue) is located next to the vacancy (purple striped), surrounded by carbon atoms (black). A nearby ^{13}C isotope is shown (pink). **B** Molecular orbitals of NV$^-$ formed by the atomic orbitals, showing that the ground and first excited state are in the band gap. Image adapted from Pfaff [16] and Bernien [17].

As depicted in Fig. I.2.1B, 4 molecular orbitals are formed from the atomic orbitals. The two degenerate orbitals e_x and e_y each have one electron in a triplet configuration and the two lowest orbitals contain two electrons each. Since the ground state and first excited state lie within the band gap, it is possible to exchange between these states without losing the electron to the conduction band. This allows for coherent state manipulation of the electron while being enclosed in a solid-state system.

The ground state of the spin triplet is optically coupled to the excited states ^{3}E as shown in Fig. I.2.2A, allowing for decay back to the ground state in three ways. Indirect decay occurs via the singlet states upon emission of an infrared photon. Direct decay occurs in two ways, either off-resonantly mediated by phonon emission denoted as phonon sideband (PSB) decay, or resonantly around 637 nm in the zero-phonon line (ZPL). PSB photons are unsuitable for entanglement generation due to their inherent interaction with the environment, although they account for over 97% of the emitted photons. The entanglement-compatible ZPL photons are emitted with a probability of ≈2.55% [18].

At room temperature the excited states ^{3}E interact strongly with the lattice vibrations, making them no longer resonantly addressable [19]. We will use the NV center at low temperatures (< 10 K) where resonant and individual addressing of the excited states is possible. The dominant role for phonon interaction shifts at these temperatures to mediate decay to the singlet states. The individual addressability of the excited states allows generating spin-photon entanglement and state readout, see Section I.2.4. The phonon mixing and spin-flip probability of the excited states via the singlet decay channel

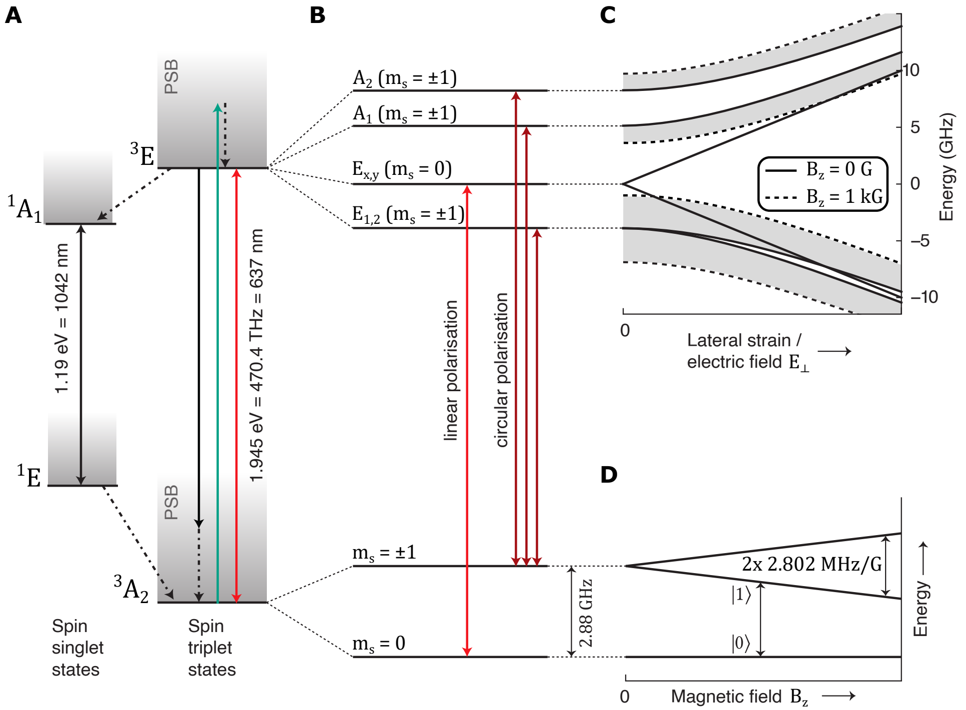

Figure I.2.2: **Level structure of NV$^-$** . **A** Excitation and emission of the spin triplet states can occur resonantly around 637 nm in the zero-phonon line (ZPL), or off-resonantly in the phonon sideband (PSB). The spin singlet states act as additional decay channel through coupling of $^3E \leftrightarrow {}^1A_1$. **B** The ground state is split between the $m_s = 0$ and $m_s = \pm 1$ states and the excited state is split by spin-spin and spin-orbit interactions, creating individually addressable transitions at temperatures < 10 K. Optical transitions are spin selective as shown. **C** Excited energy levels are electric field dependent which is first order equivalent to lateral strain. Solid lines show the energy levels at externally applied magnetic field $B_Z = 0$, dotted lines are the energy levels at $B_Z = 1$ kG [20]. The shaded region is drawn to clarify which solid and dotted lines belong to the same energy level. **D** The $m_s = \pm 1$ states are split with externally applied magnetic field through the Zeeman effect, allowing for a qubit space definition. Image adapted from Pfaff, Bernien and Pompili [13, 16, 17].

allows for spin initialization to $m_s = \pm 0$ using selective resonant driving on the $m_s = \pm 1$ transitions, also referred to as *spin-pumping*.

The excited state energies are electric field dependent which is first order equivalent to lateral strain. The local lattice system around the NV center determines the lateral strain component, and is commonly around 0-5GHz for the low-strain samples used and produced for quantum network experiments. Different energy level mixing occurs at specific strain regimes, which reduces the spin-preserving cyclicity of the resonant driving, e.g. E_y crossing E_2 [20, 21]. For completeness, Fig. I.2.2C includes the shift of the excited state energy levels for externally applied magnetic field up to 1 kG [20], showing that this level landscape is multi-parameter dependent. In experiments where the natural emission frequency of the NV is used to generate the flying qubits meant for entanglement generation, the frequency of the resonant transition will have to overlap with the other

NV(s) to fulfill the criteria of photon indistinguishability. With different magnetic fields, different natural strain and few gigahertz control over externally applied electric fields [9], matching NV-NV frequency overlap can be a challenge. To fulfill requirement (4) of Section I.2.1 and to solve the NV-NV overlap challenge, we shift the frequency tuning ability from on-chip gating to the frequency conversion process, which we will discuss in Section I.2.5.2. This allows for a favorable strain NV to operate without the necessity for externally applied electric field.

Optical addressing and photon collection efficiency are optimal when the emission of an NV center's dipole axis is perpendicular to the surface of the substrate. We use NVs that have an orientation along the (111) axis on a substrate grown along the (100) direction and cleaved on (111) to obtain the desired NV-to-surface perpendicular orientation. This approach is chosen as NV centers in samples grown in this orientation occur with a 97% probability with their axis along the [111] direction [22]. To combat total internal reflection and improve the collection efficiency even further a hemispherical solid immersion lens (SIL) is milled around an NV center [17]. Additionally an anti-reflection coating is deposited to allow improved discrimination between the reflection of the excitation pulse and the emission of photons. Next to the SILs gold strips are deposited to allow delivery of DC and AC fields. The diamond sample is subsequently bonded to a printed circuit board (PCB) which provides accessibility to external connections and allows mounting on a cryogenic holder.

I.2.3. COMMUNICATION QUBIT

We enable the generation of entanglement between remote quantum network nodes by interacting and measuring flying qubits (photons) that are themselves entangled to the communication qubits of the nodes. We can define a communication qubit of the NV center by using the electronic ground state and split the $m_s = \pm 1$ states by applying an external magnetic field. The Hamiltonian of this system, if we neglect external electric field and strain contributions, is given by

$$H_{\mathrm{GS}}/\hbar = DS_z^2 + \gamma_e(S_x B_x + S_y B_y + S_z B_z), \tag{I.2.1}$$

where $\hbar$ is the reduced Planck constant, $D = 2\pi \times 2.88$ GHz the zero-field splitting between the $m_s = 0$ and $m_s = \pm 1$ states, $\gamma_e = 2\pi \times 2.802$ MHz/G is the electron gyromagnetic ratio, S_i are the spin-1 Pauli matrices and B_i the magnetic field along $\hat{i}$. The full ground state Hamiltonian, including the electric field dependence and ^{14}N and ^{13}C splitting, see [14, 23]. For a small applied constant magnetic field of 30 G we can split the $m_s = \pm 1$ states with almost 100 MHz and define a qubit space to $|0\rangle \equiv m_s = 0$ and $|1\rangle \equiv m_s = 1$ with a ≈ 3 GHz level splitting. We can resonantly drive the qubit transitions using microwave pulses of $100 - 300$ns at $\approx 99\%$ fidelity, where the total pulse power defines the rotation θ around the axis $\hat{\phi}$ on the equator plane of the Bloch sphere, which is set by the phase of the pulse [13]. We achieve universal rotational control $R_{\hat{\phi}}(\theta)$, satisfying requirement (3) of Section I.2.1 for the communication qubit.

We drive the excited state transitions with laser light of varying wavelengths, strengths and durations for different purposes. Initialization of $|0\rangle$ is done by resonant driving $E_{1,2}$

or $A_{1,2}$ on the order of 1-10µs with a fidelity up to 99.7% [24]. State readout is performed by resonantly driving only the $m_s = 0$ transition for > 3µs, where E_x is preferred at low strain and low magnetic field, due to its higher cyclicity over E_y. The fidelity of this single-shot readout (SSRO) can be up to 95% [17, 25].

Upon laser light interaction with the NV^- , there is a non-zero probability to lose the electron and flip back to the neutral NV^0 state. We can off-resonantly repump this state to NV^- with 515 nm or use the resonant ZPL of NV^0 around 575 nm. The off-resonant repump is used in conjunction with $m_s = 0$ and $m_s = \pm 1$ driving and photon counting thresholds to determine if the NV is indeed in the negative charge configuration and whether the used laser light is at resonance with the transitions. This subroutine is called a Charge Resonance (CR) check, is used before almost all NV experiments and takes several milliseconds on average to complete. We refer to [13, 26] for more information on the exact operation of the CR check.

I.2.3.1. Coherence

The communication qubit has to be able to retain its quantum information during hundreds of microseconds of delay between remote quantum nodes at tens of kilometers distance. The NV is proven to be a remarkable qubit system to support these conditions. We discuss the coherence times of the energy relaxation of the qubit state (T_1) as well as the dephasing time with decoupling (T_2^{DD}) and without (T_2^*).

In the context of qubit manipulation, we define T_1 as the decay time of the qubit population after initialization into one of the computational basis states. In practice, we first initialize the NV center with high-fidelity in the $|1\rangle$ state, after which we can measure how long it takes for the qubit population to be mixed between $|0\rangle$ and $|1\rangle$. Interaction of external light and microwave fields are the media through which coupling to the qubit and excitation paths occurs, which determines the limit of the coherence time. Upon sufficient suppression of these externals, the T_1 of the NV exceeds 1 hour [27]. The experiments in this thesis where communication qubit storage is used all operate far below this limit at < 1 ms, making the T_1 relaxation time not the limiting factor in qubit state fidelity.

The dephasing time T_2^* is defined by the amount of (unknown) drifting of the phase of a superposition state such as $|x\rangle = \left(|0\rangle + e^{i\phi}|1\rangle\right)/\sqrt{2}$ by the coupling of the qubit state to noise sources in the lattice. The total of all those coupling strenghts and frequencies combined result in a dephasing: random procession of the superposition state around the equator of the Bloch sphere. The T_2^* for the diamond samples used in this thesis is around 5 µs, with noise sources mainly being the 1.1% abundant ^{13}C spin-1/2 atoms. There are several techniques to extend the dephasing time. In this thesis we use the spin-echo effect, where a superposition state receives a single spin-flip pulse after a time t_E, after which the dephasing inverts and refocuses to obtain the original superposition state at time $2t_E$ [28, 29]. This technique can be used to extend T_2^{DD} up to a second when using many spin-flip pulses $2t_E$ apart [27]. Characterization of this echo time for two separate NV centers is performed in Chapter I.5.

The NV center and its environment can be called a *quantum processing unit* due to the extension of its qubit processing capabilities from the NV center to the spin-1/2 ^{13}C nuclear spins in its local environment. These memory qubits are addressable through the

NV center itself and can be used as qubit state register locally [23, 30, 31] or in networked experiments [9, 10, 32]. This makes the quantum network node complete the fulfillment of requirements (2) and (3) on qubit storage and control capabilities.

I.2.4. ENTANGLEMENT GENERATION

Where in classical networking the transmission of classical bits is mediated by encoded bursts of light or electronic macroscopic signals, a quantum network requires entanglement as medium to transfer quantum information. Several techniques for entangling communication qubits are used across different quantum hardware platforms [33]. Any entanglement generation procedure between two communication qubits first requires entangling the communication qubit with a flying qubit. Especially the physical property that this entangled state will be encoded in differs between platforms. Most used are frequency encoding [3], polarization encoding [4, 5, 8, 11, 34], time-bin encoding [35–38] and photon number state encodings [39–41]. The emission of the NV center is compatible with the latter two, where the time-bin encoding is a two photon scheme and the photon number state encoding is a single photon scheme. For an NV center this can be achieved by generating a superposition state

$$|\mathrm{NV}\rangle = \sqrt{\alpha}\,|0\rangle_c + \sqrt{1-\alpha}\,|1\rangle_c\,, \tag{I.2.2}$$

and subsequent selective excitation of the $|0\rangle$ transition ($E_{x/y}$) to obtain the spin-photon entangled state

$$|\mathrm{NV, photon}\rangle = \sqrt{\alpha}e^{i\phi_{\mathrm{opt}}}\,|0\rangle_c\,|1\rangle_p + \sqrt{1-\alpha}\,|1\rangle_c\,|0\rangle_p\,, \tag{I.2.3}$$

where the designations of c and p are for the communication and the photon as flying qubit, respectively and ϕ_{opt} is the optical phase of the flying qubit. This sequence is practically achieved by first using a calibrated microwave pulse that achieves the superposition state defined by $\alpha = [0, 1]$. The selective excitation of the $|0\rangle$ transition is accomplished by sending in the exact amount of energy that saturates the transition named an *optical* π pulse. Such a pulse is carefully shaped to saturate the transition within a few nanoseconds and then be fully extinguished (> 120 dB) to reduce the overlap of excitation light and natural emission decay of the photon as much as possible [42].

From the spin-photon entanglement description we can expand to (stationary) qubit-qubit entanglement with the two and single photon entanglement protocols. First we introduce the concept of photon indistinguishability in combination with beam splitters, two key parameters necessary in the process of entanglement generation.

I.2.4.1. INDISTINGUISHABILITY

The art of generating entanglement mediated by flying qubits comes down to controlling the interaction that the flying qubits have and allowing a form of *shared ignorance*. There are two requirements in achieving erasure of information on the source of the flying qubits. First, a (balanced) beam splitter where incoming photons (a, b) are either transmitted or reflected into separate output ports (c, d). Second, in order for those photons to show quantum behavior, they have to be indistinguishable in all physically relevant parameters. In our case, this is spatial, frequency, polarization and arrival time. If both requirements are guaranteed then the so-called Hong-Ou-Mandel effect occurs where simultaneous arriving photons on the beam splitter will bunch towards the same output port [43]. The beam splitter operators are defined as

I.2

$$a_a^\dagger = \frac{1}{\sqrt{2}}\left(a_c^\dagger + a_d^\dagger\right), \tag{I.2.4}$$

$$a_b^\dagger = \frac{1}{\sqrt{2}}\left(a_c^\dagger - a_d^\dagger\right), \tag{I.2.5}$$

showing that two incoming photons on different input ports both bunch to the same output ports

$$\begin{aligned} a_a^\dagger a_b^\dagger |0\rangle &= \frac{1}{2}\left(|2_c 0_d\rangle + |1_c 1_d\rangle - |1_c 1_d\rangle - |0_c 2_d\rangle\right), \\ &= \frac{1}{\sqrt{2}}\left(|2_c 0_d\rangle - |0_c 2_d\rangle\right) = |\Psi_{\mathrm{HOM}}\rangle, \end{aligned} \tag{I.2.6}$$

with a probability of 1/2 for each pair of input photons to together go one of the two output ports. In other words, if we define a measurement operator that measures the coincidence of two photons arriving at *different* output ports, i.e. $M_{\mathrm{coinc}} = |1_c\rangle\langle 1_c| \otimes |1_d\rangle\langle 1_d|$, the measurement outcome for coincidences of the above state will be $\mathrm{Tr}\left(|\Psi_{\mathrm{HOM}}\rangle\langle\Psi_{\mathrm{HOM}}| M_{\mathrm{coinc}}\right) = 0$.

In reality the arriving photon can have distinguishable properties as described above, which add to the photonic mode $d_i^\dagger = a_i^\dagger |D_i\rangle$ [44], turning the beam splitter operators into

$$d_a^\dagger |0\rangle = \frac{1}{\sqrt{2}}\left(|1_c 0_d\rangle |D_a\rangle + |0_c 1_d\rangle |D_a\rangle\right), \tag{I.2.7}$$

$$d_b^\dagger |0\rangle = \frac{1}{\sqrt{2}}\left(|1_c 0_d\rangle |D_b\rangle - |0_c 1_d\rangle |D_b\rangle\right). \tag{I.2.8}$$

If we apply the above operators again as $d_a^\dagger d_b^\dagger |0\rangle = |\Psi_{\mathrm{D}}\rangle$, if we measure the coincidence probability

$$p_{\mathrm{coinc}} = \mathrm{Tr}\left(|\Psi_{\mathrm{D}}\rangle\langle\Psi_{\mathrm{D}}| M_{\mathrm{coinc}}\right) = \frac{1}{2}\left(1 - |\langle D_a|D_b\rangle|^2\right). \tag{I.2.9}$$

When photons are fully distinguishable $\langle D_a|D_b\rangle = 0$, the coincidence probability is completely classical and dictated by the 50/50 individual probabilities of photons being transmitted or reflected. However, in the quantum case and absolute indistinguishability $\langle D_a|D_b\rangle = 1$, there are no coincidences, retrieving the state of Eq. I.2.6. From this we can extrapolate that any quantum state that has residual distinguishability (usually due to system limitations) will always be capped in fidelity of the entangled state due to the probability of classical interference taking place.

I.2.4.2. Two photon protocol

The two photon protocol is a time-bin entanglement protocol developed by Barret and Kok [35]. The protocol describes two rounds of spin-photon entanglement with a spin flip in between, creating a superposition state of the stationary qubit with an *early* or *late* generated flying qubit. This requires to first create an equal superposition state (i.e. $\alpha = 0.5$ in Eq. I.2.2). The single node development of the communication flying qubit state can be described as

$$\begin{aligned} \frac{1}{\sqrt{2}}(|0\rangle_c + |1\rangle_c) &\xrightarrow{\text{sp-ph}} \frac{1}{\sqrt{2}}\left(|0\rangle_c |E\rangle_p + e^{i\phi_1} |1\rangle_c |0\rangle_p\right) \\ &\xrightarrow{\pi} \frac{1}{\sqrt{2}}\left(|1\rangle_c |E\rangle_p + e^{i\phi_1} |0\rangle_c |0\rangle_p\right) \\ &\xrightarrow{\text{sp-ph}} \frac{1}{\sqrt{2}}\left(|1\rangle_c |E\rangle_p + e^{i\Delta\phi_{\text{opt}}} |0\rangle_c |L\rangle_p\right) = |\psi\rangle, \end{aligned} \tag{I.2.10}$$

where $\Delta\phi_{\text{opt}}$ is the optical phase difference between the two rounds of excitation. Practically, the time between the two excitation rounds is about 100-300ns, in which the phase difference between the first and second round will be small, allowing us to assume $\Delta\phi_{\text{opt}} \approx 0$ in the following calculations. When both the stationary qubits undergo this exact protocol, the flying qubits are overlapped on a beam splitter and assuming indistinguishability, we obtain the state

$$\begin{aligned} |\psi\rangle_A |\psi\rangle_B = 1/2\sqrt{2}\,[(|01\rangle + |10\rangle)_{AB}\,(|E_c L_c\rangle - |E_d L_d\rangle) + \\ (|01\rangle - |10\rangle)_{AB}\,(|E_c L_d\rangle - |E_d L_c\rangle)], \end{aligned} \tag{I.2.11}$$

where A,B are stationary qubits of the nodes and c, d the output port of the beam splitter (and thus the detector). We select on the syndrome of one photon measurement, thus we have dropped the zero photon number states on the output ports. We see that upon detecting a photon in the same (cc, dd) or different port(cd, dc), we obtain the entangled Bell state

$$|\Phi^{\pm}\rangle_{AB} = \frac{1}{\sqrt{2}}(|01\rangle \pm |10\rangle). \tag{I.2.12}$$

Due to having to measure a photon in both rounds, the success probability of this protocol is

$$P_{bk} = \frac{1}{2}\eta_A \eta_B, \tag{I.2.13}$$

with η_i the probability of measuring a photon originating from quantum node i. In most quantum network layouts the photon measurement probability from each node is designed to be approximately the same, making this protocol scale quadratically in measurement probability, which is unfavorable for the entanglement generation rate when η_i is small. However, an upside to this protocol is that the maximum attainable fidelity is close to 1, limited by the phase difference between excitation rounds [19]. We can trade-off this fidelity for entanglement rate by using a single photon protocol, which we will discuss in the next section.

I.2.4.3. Single photon protocol

The spin-photon entangled state presented in Eq. I.2.3 is the starting port of the single photon protocol [39–41], where now $\alpha = (0, 0.5]$. If we prepare both nodes in this state, overlap the flying qubits on a beam splitter and ensure indistinguishability, the combined entangled state becomes

$$\begin{aligned} |\psi\rangle_A |\psi\rangle_B =& \alpha/\sqrt{2}\,|00\rangle_{AB}\left(|2_c0_d\rangle - |0_c2_d\rangle\right) \\ &+ \sqrt{(\alpha-\alpha^2)/2}\left(|01\rangle_{AB} + e^{i\Delta\phi_{\mathrm{opt}}}|10\rangle_{AB}\right)|1_c0_d\rangle \\ &+ \sqrt{(\alpha-\alpha^2)/2}\left(|01\rangle_{AB} - e^{i\Delta\phi_{\mathrm{opt}}}|10\rangle_{AB}\right)|0_c1_d\rangle \\ &+ (1-\alpha)\,|11\rangle_{AB}\,|0_c0_d\rangle\,, \end{aligned} \tag{I.2.14}$$

up to a global phase, and $\Delta\phi_{\mathrm{opt}}$ is the optical phase difference from both nodes at the beam splitter. We are only interested in the conditional event of a photon detection, allowing us to omit the last term. Furthermore, since the current single photon detectors in our experiments are not photon-number resolving, we can rewrite $|2_c0_d\rangle \equiv |1_c0_d\rangle, |0_c2_d\rangle \equiv |0_c1_d\rangle$. For photon-number resolving detectors this error still persists when the arrival probability of a photon is low, i.e. $\eta_i^2 \ll \eta$, and detection efficiency of measuring two photons is small. Together, the density matrix representation of the state upon heralding of a single detection event is thus

$$\rho_{AB} = (1-\alpha)\,|\Phi^{\pm}(\Delta\phi)\rangle\langle\Phi^{\pm}(\Delta\phi)| + \alpha\,|00\rangle\langle 00|_{AB}\,, \tag{I.2.15}$$

where now

$$|\Phi^{\pm}(\Delta\phi)\rangle = \frac{1}{\sqrt{2}}\left(|01\rangle \pm e^{i\Delta\phi_{\mathrm{opt}}}|10\rangle\right), \tag{I.2.16}$$

showing that a phase dependent Bell state is generated with probability $1-\alpha$, and a separable state is introduced with probability α. Since we are unable to distinguish between the two scenarios, the maximum fidelity of the entangled state is therefore

$$F = 1 - \alpha, \tag{I.2.17}$$

making α also known to be the parameter of *protocol error* as it is inherent to the scheme. Although it is possible for $\{\alpha \to 0, \alpha \neq 0\}$, this impacts the success probability of the scheme, which is given by

$$P_{sc} = \alpha\left(\eta_A + \eta_B\right), \tag{I.2.18}$$

making a low alpha infeasible to achieve reasonable entanglement rates, even for η_i approaching 1. With an approximate quadratic speedup, this entanglement scheme is favored over the Barret-Kok for low η_i, with the trade-off of introducing the added complexity to know $\Delta\phi$. To continuously use the generated entangled state for further processing, the $\Delta\phi$ is required to be set to a known value while the entanglement is generated. Practically this translates to the requirement of phase stabilization while performing entanglement generation attempts. We will discuss the techniques used for phase stabilization in Section I.2.6, show its technical implementation in Chapter I.4 and integrated in quantum network experiments in Chapter I.5. Further technical details on the single photon entanglement scheme can be found in [42].

I.2.4.4. ENTANGLEMENT VERIFICATION

We verify entanglement on the generated Bell states by computing the fidelity with regards to the target state as

$$F = \langle\Phi|\,\rho\,|\Phi\rangle\,, \tag{I.2.19}$$

with ρ the density matrix of the entangled state generated in the experiment. To reconstruct the complete density matrix one can measure the correlation of all 16 measurement bases $\langle ab\rangle : a, b \in \{X, Y, Z, I\}$, performing full state tomography. This is a time consuming task, since many correlation events will have to be recorded per basis to reconstruct the density matrix with low error. Instead, we can directly estimate the fidelity by measuring the non-zero elements of the density matrix and calculate the fidelity as

$$F = \frac{1}{4}\left(1 \pm \langle XX\rangle \pm \langle YY\rangle - \langle ZZ\rangle\right) \tag{I.2.20}$$

where the $\pm$ corresponds to the $\Phi^{\pm}$ Bell state. This method allows for measuring the fidelity with a smaller uncertainty in the same amount of time and is used in Chapter I.5 for characterizing the entangled state generated over the metropolitan link.

I.2.5. LONG DISTANCE COMPATIBILITY

As quantum networks aim to scale beyond lab environments, compatibility with commercial telecom fiber infrastructure is necessary to enable growth in number of nodes, mediate larger distances between nodes and allow for freedom in routing choices. The installation of new fiber is expensive, time consuming and uncertain in timelines [45, 46], hence compatibility with existing deployed fiber for quantum purposes allows immediate access to complex backbones of dense fiber structures at different levels. It offers metropoles with fiber-dense areas and long-haul lines with low attenuation, few splices and geographically placed in *straight lines* between large hubs [47].

As it stands now, the transmission of single photons for generating entanglement requires its own *dark fiber*: a fiber that carries no other light besides the customers'. As the entanglement protocols rely on single photon counting in small time windows, any additionally added *noise* photons on such a line can cause a faulty outcome of believing entanglement has been created. This means that a quantum channel will always have to be used alongside a classical channel, now implemented with two fibers instead of one, which is comparable to currently used dedicated classical data lines that operate in full duplex. Reducing the amount of fibers is possible, co-propagation of single photons with classical signals is possible for quantum key distribution purposes [48] and has been achieved for both wavelength division [49] or combined with time-multiplexed techniques [50]. For the experiments in this thesis however, this would have added even more complexity and potentially additional losses or sources of infidelity of the entangled state, and was decided to be left as future engineering challenge.

Commonly used deployed fiber is silica based, which has served the telecommunications industry well in the last decades when commercial development allowed for affordable and low-loss fibers [51]. The attenuation of light traveling through a silica fiber changes as function of wavelength due to several physical phenomena, as shown

I.2

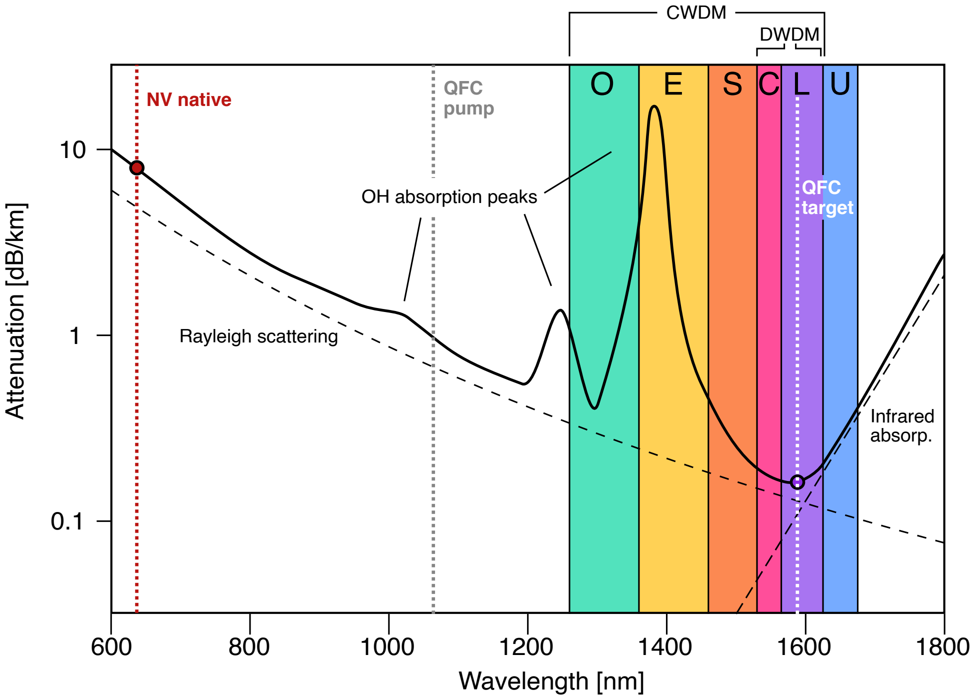

Figure I.2.3: Attenuation of light traveling through silica fiber at different wavelengths. The fundamental limits of attenuation are dictated by Rayleigh scattering, infrared absorption and OH absorption in the silica. The (O, E, S, C, L, U) bands are commonly used in the telecommunications industry due to their lower attentuation range, if the OH absorption peak of the E-band is circumvented. The (O to L) and (C,L)- bands are used for course and dense wavelength division multiplexing (CWDM, DWDM), respectively. The NV native wavelength at 637 nm is at high attenuation with respect to the telecom bands. The target wavelength after quantum frequency conversion (QFC target) is at the lowest attenuation around 1588 nm, after difference frequency generation of the NV native and QFC pump (1064 nm), see Section I.2.5.1.

in Fig. I.2.3. Theoretical limits are due to Rayleigh scattering and infrared absorption, and practical challenges in the form of the presence of hydroxyl (OH) ions, which are absorbent around several wavelengths. To reach the furthest distances, the telecommunications industry settled on defining 6 bands (O, E, S, C, L, U) in the wavelength region with the lowest attenuation, only needing to circumvent one large attenuation peak at the bottom of the E-band. The entire range up to the L-band is used for standard coarse wavelength division multiplexing (CWDM) for classical signal connectivity. The lowest loss bands (C, L) are used for dense wavelength division multiplexing (DWDM) to squeeze in as much bandwidth as possible in the most attenuation-favorable wavelength regime.

Also shown in Fig. I.2.3 is the attenuation of the wavelength of the photons emitted from the NV center. In the ideal case this attenuation is around 8 dB km^{-1} [36], making distances beyond few kilometers infeasible to achieve using silica fibers: the photon rate reduction is simply too large to obtain reasonable entanglement rates. In fact, it would be the most favorable for quantum signals to have the lowest attenuation per kilometer possible. We therefore used a frequency conversion device that would retain the quantum properties of the photon passing through it, while converting the NV single photons from 637 nm to a target frequency in the L-band at 1588 nm [52], which ideally has only approximate 0.25 dB km^{-1} loss. In the following section we go into detail on frequency conversion and the systems used in this thesis.

I.2.5.1. QUANTUM FREQUENCY CONVERSION: THEORY

The concept of frequency conversion follows from understanding the behavior of light in nonlinear media (NLM), which are materials where the polarization density $\boldsymbol{P}$ responds non-linearly to the electric field $\boldsymbol{E}$ of the light. In this thesis we focus on three-wave mixing (TWM) within a nonlinear medium to achieve difference-frequency generation (DFG) such that two input modes (NV photon, pump) result in one output mode (telecom L-band photon). We introduce the necessary theory of nonlinear optics to understand the mechanics of TWM and the boundary conditions necessary to do DFG. For more detailed background on the (vast) field of nonlinear optics we refer to [53–55].

DIFFERENCE FREQUENCY GENERATION

In nonlinear media the optical susceptibility χ is electric field dependent. Under weak electric field dependence, we can power expand χ as

$$\chi = \chi^{(1)} + \chi^{(2)}\boldsymbol{E} + \chi^{(3)}\boldsymbol{E}^2 + \cdots, \tag{I.2.21}$$

where χ^n refers to the n-th order susceptibility. Combined with the relationship between polarization, susceptibility and electric field $\boldsymbol{P} = \epsilon_0\boldsymbol{\chi}\boldsymbol{E}$ makes

$$\boldsymbol{P} = \epsilon_0\chi^{(1)}\boldsymbol{E} + \epsilon_0\chi^{(2)}\boldsymbol{E}^2 + \epsilon_0\chi^{(3)}\boldsymbol{E}^3 + \cdots. \tag{I.2.22}$$

We focus on the first interaction term where field interacts with itself which we refer to as $P_2 = \epsilon_0\chi^{(2)}\boldsymbol{E}^2$. For the case of interest, we want to turn two incoming frequencies into one, thus we define the electric field as superposition of two distinct frequency components

$$\tilde{\boldsymbol{E}}(t) = E_1 e^{-i\omega_1 t} + E_2 e^{-i\omega_2 t} + \text{c.c.}, \tag{I.2.23}$$

where ‘c.c.’ refers to the complex conjugates of the previous terms. This makes the nonlinear polarization

$$\begin{aligned}\boldsymbol{P}^{(2)}(t) = \epsilon_0\chi^{(2)}\Big[&E_1^2 e^{-2i\omega_1 t} + E_2^2 e^{-2i\omega_2 t} + 2E_1E_2 e^{-i(\omega_1+\omega_2)t}\\ &+2E_1E_2 e^{i(\omega_1-\omega_2)t} + \text{c.c.}\Big] + 2\epsilon_0\chi^{(2)}\left[E_1E_1 + E_2E_2\right].\end{aligned}$$

We can rewrite this to the shorthand

$$\boldsymbol{P}^{(2)}(t) = \sum_n P(\omega_n)e^{-i\omega_n t}, \tag{I.2.24}$$

where we can divide the complex amplitudes of the different frequency components into

$$
\begin{aligned}
P(2\omega_1) &= \epsilon_0\chi^{(2)}E_1^2 && \text{(SHG)},\\
P(2\omega_2) &= \epsilon_0\chi^{(2)}E_2^2 && \text{(SHG)},\\
P(\omega_1+\omega_2) &= 2\epsilon_0\chi^{(2)}E_1E_2 && \text{(SFG)},\\
P(\omega_1-\omega_2) &= 2\epsilon_0\chi^{(2)}E_1E_2^* && \text{(DFG)},\\
P(0) &= 2\epsilon_0\chi^{(2)}(E_1E_1^*+E_2E_2^*) && \text{(OR)}.
\end{aligned}
$$

We label every component based on the process that they describe: the second-harmonic generation (SHG) of each frequency with itself, sum-frequency generation (SFG) of both frequencies added, optical rectification (OR) and difference-frequency generation (DFG) where the output frequency is the substraction of the inputs. We rewrite $\omega_3 = \omega_1 - \omega_2$ to $\omega_t = \omega_{\mathrm{NV}} - \omega_{\mathrm{pump}}$, to represent the frequencies of the system used in this thesis of (target) telecom, NV center and QFC pump laser wavelengths, respectively.

We can solve the wave equation for the polarization that now includes the nonlinear component $P\left(\omega_{\mathrm{NV}} - \omega_{\mathrm{pump}}\right)$ and obtain a relationship between the amplitude of the two input fields and the generated output field that is driven by energy exchange between the electric fields and the polarization. Over the length of the interaction in the nonlinear medium, a constant phase change between the field and polarization occurs. The length over which the transfer of energy from the polarization into the field takes place is the coherence length. When the output field phase maintains a fixed relationship with the nonlinear polarization, it is the most efficient at extracting energy from the incident fields. This occurs at perfect phase matching, which is defined at $\Delta\boldsymbol{k} = 0$ where

$$\Delta\boldsymbol{k} = \boldsymbol{k}_{\mathrm{NV}} - \boldsymbol{k}_{\mathrm{pump}} - \boldsymbol{k}_{\mathrm{t}}, \tag{I.2.25}$$

and we can turn the vector $\boldsymbol{k_i} = k_i$ in the case for collinear interaction of the photons, which describes the use case of our conversion systems. The coherence length is defined as

$$L_{\mathrm{coh}} = 2/\Delta k, \tag{I.2.26}$$

where we see that for $\Delta k = 0$ the coherence length is infinite, which means that there is constructive transfer of energy from input fields to the output field over the total interaction length within the nonlinear medium. This perfect phase matching can be achieved with several methods, one of which is birefringent phase matching (BPM). By tuning the propagation angle of the light through a birefringent medium, the difference in refractive indices for the two input fields is compensated, however this requires strong interaction fields to achieve an efficient conversion process [56]. We will discuss the implementation of a frequency conversion process using birefringent phase matching in Section I.2.5.4.

In the case of $\Delta k \neq 0$ the intensity of the output field oscillates, where energy is exchanged back and forth between the input and output modes. We can engineer the nonlinear material in such a way that the destructive interference part is replaced by a constructive interference part by flipping the crystal axis, which flips the induced

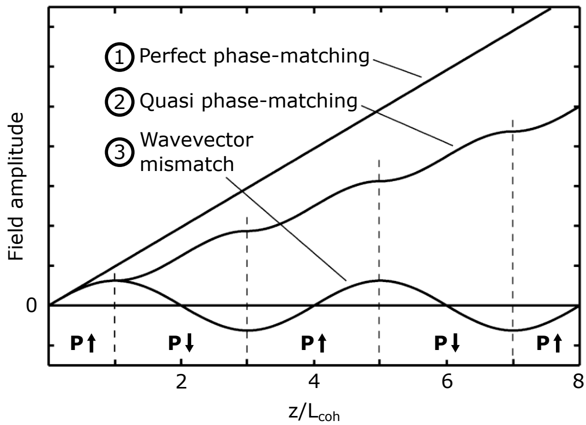

Figure I.2.4: Field amplitude of the converted light field as function of the interaction distance in the birefringent material for different phase-matching situations. For perfect phase-matching and bulk material at ① we see a constant increase in field amplitude. Using periodic poling of the polarization of the material we can achieve quasi phase-matching at ②. For no phase matching at ③ we periodically destructively interfere to generate no target field on average. Image adapted from [54].

polarization direction. Upon repeating of this process, we constantly constructively interfere through the entirety of this *poled* material, which is called quasi-phase matching (QPM). This changes Eq. I.2.25 to

$$\Delta \boldsymbol{k} = \boldsymbol{k}_{\mathrm{NV}} - \boldsymbol{k}_{\mathrm{pump}} - \boldsymbol{k}_{\mathrm{t}} - \frac{2\pi}{\Lambda}, \tag{I.2.27}$$

where Λ is the poling period, which is optimal for $\Lambda = 2L_{\mathrm{coh}}$ to achieve as much constructive interference as possible. We present the physical implementation of this type of conversion in Section I.2.5.3.

For orthogonal polarization inputs (NV and pump) the phase matching conditions are denoted Type-I and Type-II for the same or orthogonal polarization of the input (NV) and output (telecom) photons. Type-0 is reserved for same polarization inputs and outputs.

It has been shown that DFG with QPM can convert $\lambda_{\mathrm{NV}} = 637\,\mathrm{nm}$ with $\lambda_{\mathrm{pump}} = 1064\,\mathrm{nm}$ to $\lambda_{\mathrm{t}} = 1588\,\mathrm{nm}$, also denoted in the spectrum in Fig. I.2.3. It even can convert the photons and retain their quantum properties [52], giving it the name *quantum frequency conversion*. However, any error in the periodicity of the crystal used for QPM also causes spontaneous parametric downconversion photons (SPDC) which adds constant background noise photons that reduce the signal-to-noise (SNR) ratio of the entanglement generation procedure. We will continue discussing the implications of an engineered implementation of these techniques in the following sections.

I.2.5.2. QUANTUM FREQUENCY CONVERSION: IMPLEMENTATION

In this thesis we have used both QPM and BPM to achieve frequency conversion of NV photons. In Chapter I.3 we show the indistinguishability of converted photons from distinguishable NV centers by using a QFC built using a waveguide integrated periodically poled Lithium Niobate crystal (ppLN). In Chapter I.5 we use a cavity enhanced

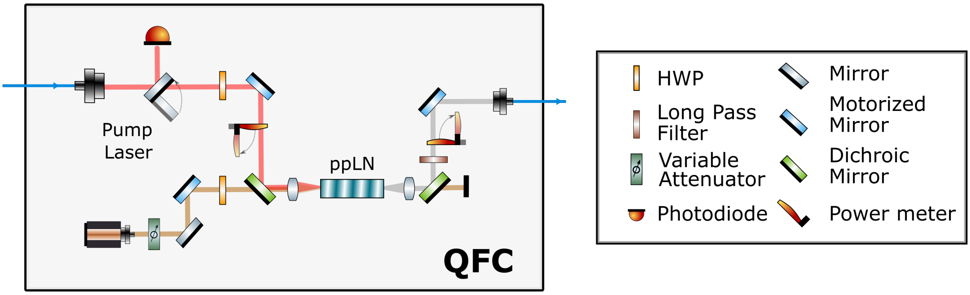

Figure I.2.5: **Schematic drawing of the ppLN QFC**. Light from the ZPL path ($\lambda_{\mathrm{NV}} = 637\,\mathrm{nm}$) couples from fiber to free-space (top left), where flippable mirrors direct the light to a local APD or toward the ppLN, to be co-propagating with pump laser light ($\lambda_{\mathrm{pump}} = 1064\,\mathrm{nm}$). Flippable power meters are used for characterization and debugging purposes. Image adapted from Ubbens [20].

monocrystalline bulk crystal based QFC system (NORA QFC), which is co-developed with Fraunhofer Institute for Laser Technology (ILT), to use in one quantum node to perform conversion of photons for entanglement generation. In the following section we first discuss the experimental implementation of the ppLN based QFC, followed by the description of the noise-reduced implementation of the NORA QFC. For a complete comparison and analysis, we refer to [56].

I.2.5.3. PPLN QFC

A detailed graphical representation of the ppLN QFC system is shown in Fig. I.2.5. Light from the free-space optics that can be either NV light or laser light is coupled into the QFC from a polarization maintaining (PM) fiber. A flip in mirror allows for probing the ZPL path at $\lambda_{\mathrm{NV}} = 637\,\mathrm{nm}$, usually used to confirm *local* performance of the quantum node where ZPL photons need to be collected, unrelated to the conversion process. We have steerable mirrors for incoupling to optimize coupling into the ppLN waveguide, as well as for coupling to the output fiber. Flippable power meters are used to have a quantitative measure for the conversion efficiency when using a ~100 nW probing laser light at λ_{NV}. The pump laser $\lambda_{\mathrm{pump}} = 1064\,\mathrm{nm}$ operates at ~200 mW, where control over the power can be achieved using a variable attenuator. All input light bundles are coupled into the waveguide with the ppLN integrated where Type-0 phase matching is achieved. The output bundle is filtered to remove λ_{pump} and transmit mostly $\lambda_{\mathrm{t}} = 1588\,\mathrm{nm}$. All mentioned control elements are necessary to operate the QFC remotely and adjust the exact alignment to achieve the highest efficiency possible. Typical efficiency of this system (front-to-end) is around 50% with an spectral density of noise photons (NSD) to be $250\,\mathrm{s}^{-1}\,\mathrm{pm}^{-1}$ ($2100\,\mathrm{s}^{-1}\,\mathrm{GHz}^{-1}$) [52]. In noise sensitive experiments this NSD warrants additional specific spectral filtering that is done before single photon measurement. For a strictest possible bandwidth of 50 MHz (limited by the bandwidth of the down-converted photons from the NV center at ≈12.7 MHz), the ppLN waveguide QFC therefore adds error counts with a rate of approximately $100\,\mathrm{s}^{-1}$.

I.2.5.4. NORA QFC†

NOISE REDUCED APPROACH (NORA) CONCEPT

We propose a TWM scheme without the use of a periodically poled material and waveguiding structures, i.e., TWM in a monocrystalline bulk material. This approach requires birefringent phase matching for efficient conversion, which requires orthogonal polarization of the interacting waves. For most NLM, the effective nonlinearity is smaller if the phasematching condition is met for Type-I or Type-II configuration compared to the effective nonlinearity in Type-0 configuration in the case of quasi phasematching in pp-NLM. To overcome this challenge, larger pump laser intensities are required, which can be achieved by resonantly enhancing the pump laser power in an optical cavity. Relying on active stabilization of the cavity, which can be accomplished with low-cost electronic components, enables maintaining efficient conversion while the pump wavelength is tuned, resulting in a tunable output wavelength. Since the central wavelength of photons emitted by NV-center qubits can drift by up to 10 MHz, a tunable QFC output wavelength is required to maintain indistinguishable telecom photons. Whereas similar setups have been proposed for QFC [57–59] and photon-pair generation [60], they incorporate periodically-poled crystals and passively stabilized cavities to achieve the required efficiency.

Here monocrystalline KTA is chosen as the NLM, exhibiting a broad transparency range between 0.5 to 3.5 µm [61] and high threshold to laser-induced damage. The phase matching condition is met in type-II configuration, i.e., the high-intensity pump field and the converted telecom photons have perpendicular polarization. Numerical simulations are performed to approximate the required laser power and crystal length for efficient conversion. With this scheme, an internal conversion efficiency as high as 80 % can be reached. With pump laser power up to 400 W available for the experiments, an internal efficiency of approximately 60 % is expected. Since due to the free-space interaction no single-mode waveguide coupling (which can result in losses up to 40 % [62, 63]) is required, the overall device efficiency is expected to reach similar values as in waveguide-based setups with larger internal conversion efficiency.

NORA DESIGN

The NORA QFC is schematically shown in Fig. I.2.6. The 30 mm-long NLM KTA is placed in a bow-tie cavity (length 46 cm) consisting of three HR-coated mirrors (R_{HR} =99.95 %) and one coupling mirror (R_{in} =99 %), in which the incident (coupled) pump power is enhanced by a factor of 40 (60). Two cavity mirrors have a ROC of 100 mm, resulting in a focus diameter of roughly 100 µm inside the NLM.

An amplified fiber laser (NKT ADJUSTIK Y10 and BOOSTIK Y10) provides up to 9 W pump power with a tuning range of 160 GHz. To maintain resonant enhancement at any time, one cavity mirror is mounted to a piezoelectric actuator. A feedback loop implementing the Hänsch-Couillaud locking scheme [64] provides an error signal. Further components are half-wavelength (quarter-wavelength) retardation plates (HWP, QWP)

† This section appears in the publication: J. F. Geus et al., *Low-noise short-wavelength pumped frequency down-conversion for quantum frequency converters*, Optica Quantum 2, 189 (2024).

I.2

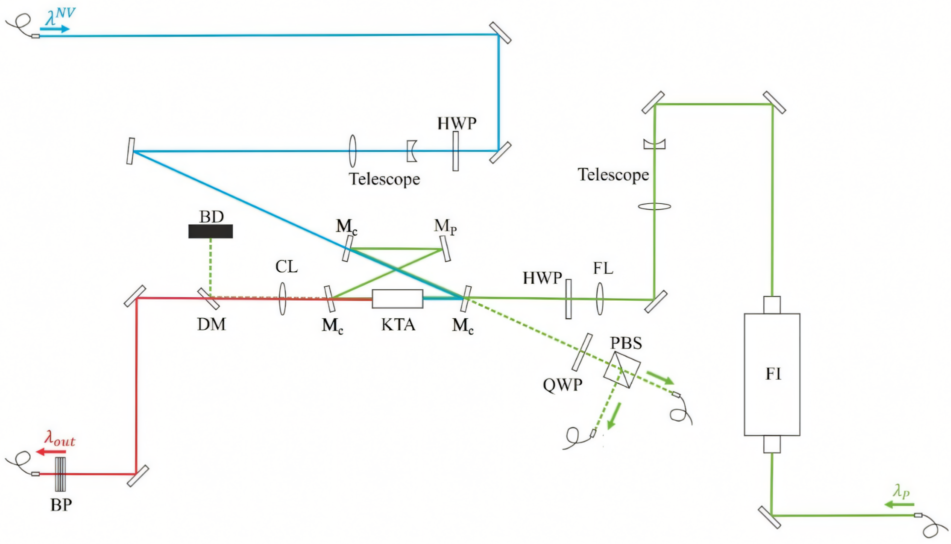

Figure I.2.6: **Schematic drawing of the NORA QFC.** The enhancement cavity consists of three mirrors (MC) and one which is mounted to a piezoelectric actor to control the cavity length (MP). The nonlinear crystal (KTA) is placed such that the cavity mode's focus is centered inside of it. At the device's signal input/output and pump input, the interacting waves are coupled from free space to fiber or vice versa, indicated by the respective arrow. The solid blue (green, red) lines indicate the beam path of 637 nm (1064 nm, 1589 nm) light, whereas dashed lines denote reflected light and leakages from the cavity, which are either used to implement the cavity control via the Hänsch-Couillaud method or to be filtered from the output field by a dichroic mirror (DM) and further long-pass and band-pass filters (BP). The converted light is coupled to a single-mode fiber behind the BP. Additional components are a Faraday-isolator (FI), half-waveplates (HWP), a quarter-waveplate (QWP), focusing and collimation lens (FL, CL), a polarizing beam splitter (PBS) and a beam dump (BD).

rotating the polarization state of the two input fields and various elements (Telescopes, collimation lens (CL), focusing lens (FL)) for efficient coupling of the fields into the cavity and single-mode optical fiber, respectively. To reduce the coupling of any stray-light or residual pump light into the optical fiber, the converted light is filtered spectrally by several band-pass and edge-pass filters (BP, optical density of 20 at 1064 nm). The type-II phasematching condition is met at a crystal orientation of $\Theta \approx 90°, \Phi \approx 30°$ and a crystal temperature 130 °C, where Θ equals the angle between the propagating light and the crystal's z-axis and Φ being the angle between the propagating light and the crystal's x-axis measured in the x-y plane. A precise measurement of the angles was not possible due to the limited space between mirrors and crystal.

In this configuration a maximum internal conversion efficiency of 60(5) % is measured at a circulating pump power of 360(40) W. Behind the filter stack (transmission T_{BP} =90 %, bandwidth (FWHM) $\Delta\lambda$ =3.14(7) nm, center-wavelength $\lambda_{BP} = \lambda_{out}$) and after coupling to a single-mode optical fiber (SMF28, coupling efficiency η_{FC} =80(6) %), the external conversion efficiency is measured to equal 43(5) %. The NSD of this configuration is in the order of single counts per picometer, which is two orders of magnitude smaller than in the formerly discussed ppLN QFC at comparable conversion efficiencies.

I.2.6. PHASE STABILITY

In employing the single photon protocol we require the optical phase of the interfering photonic modes $\Delta\theta$ to be known and kept constant, as the fidelity of the entangled state is directly related to the uncertainty of $\Delta\theta$. This requires that any phase stabilization scheme needs to be of sufficient bandwidth to keep the phase uncertainty as low as possible, traded-off to its implementation complexity and system compatibility with the requirements of entanglement generation. For the phase stabilization schemes used in this thesis we detect the phase from interfering optical signals by heterodyne detection. Two input optical fields with amplitude I_1, I_2 and frequencies ω_1, ω_2 incident on a balanced beam splitter generate the output fields

$$I_{3,4} = I_1 + I_2 \pm 2\sqrt{I_1 I_2}\,(\cos((\omega_1 - \omega_2)\,t) + \Delta\theta)\,. \tag{I.2.28}$$

These optical fields have a symmetric output to the detection arms of the beam splitter ($I_{3,4}$), where the intensity fluctuates with $\Delta\omega = \omega_1 - \omega_2$ and has phase $\Delta\theta$. The advantage of this detection scheme is that the intensity of the inputs does not need to be known in order to extract $\Delta\theta$, given that we know what $\Delta\omega$ is. We can even make use of the fact that one input field is allowed to be small, provided that the other is large, allowing us to extract phase differences from interfering optical fields of wide intensity ranges. Additionally, both arms of the beam splitter carry individually all the information about the phase difference. In most heterodyne systems, the frequency difference between the fields is of order $1 - 500$MHz, the operating range of generic analog signal processing equipment. Feedback of $\Delta\theta$ to the known *phase setpoint* is performed by (fast) frequency shifting of the optical light fields using Acousto Optical Modulators (AOMs), which are doubly used as amplitude modulators. The AOMs that are used introduce an optical frequency shift of 200 MHz, disciplined by input RF waves and mediated by acoustic waves, which is tunable with ~MHz around its setpoint. By frequency shifting these input RF waves as function of time on the AOM, we effectively shift the optical phase with endless feedback (i.e. feedback is not limited by phase slips), a technique we use extensively in the following Chapters where entanglement generation is performed. For more background information on phase detection and stabilization techniques, we refer to the excellent write-up in [44].

I.2.7. QUANTUM NETWORK HARDWARE PLATFORM

In this section we discuss the higher level approach of the newly developed *quantum network hardware platform*. The entirety of the hardware control stack that is used in this thesis operates at the *physical layer* of the quantum network stack [65]. On its own, the physical layer already consists of several layers itself, as shown in Fig. I.2.7.

I.2.7.1. HARDWARE CONTROL STACK

Instructions are disciplined by the **sequencer** layer, which consists of self-contained experimental code written in Python 3.x using the open-source framework of Quantum

I.2

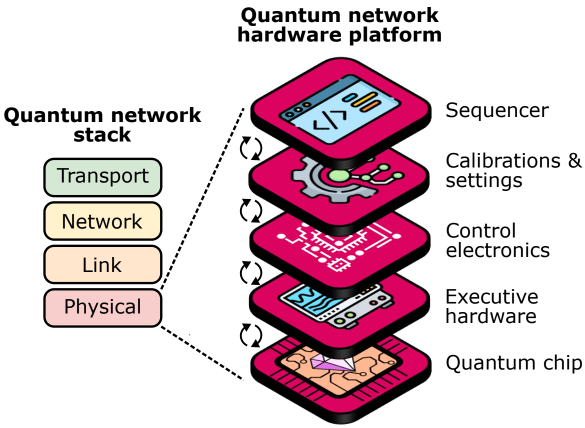

Figure I.2.7: The quantum network stack's [65] hardware layer consists of its own stack, which we refer to as the **quantum network hardware platform**. There, all layers interact with its nearest neighbor to control quantum behavior at the chip-level, that through *executive hardware* and *control electronics* is set up through *calibrations & settings* and overall controlled by *sequencer* code. The top four icons on the right hand side have been designed by Freepik from Flaticon.com and Freepik.com.

Measurement Interface (QMI) [66] in addition to libraries of device drivers that communicate to the **control electronics** layer. As initial approach to an eventually targeted state machine approach, the **calibrations & settings** layer contains almost all settings for the control electronics and tracks the performance of the system (most related to the qubit on the quantum chip). This layer also has certain autonomy to perform calibrations and record the outcomes. Details on calibrations can be found in Fig. I.3.10 and I.3.11.

The control electronics processes its given instructions and executes its specific functions, including but not limited to: **executive hardware** initialization, DC and/or AC signals on/off and processing of signal recording. These functions all result in executive hardware performing its specific task, which usually is the actual production of the DC and/or AC signals or movement of physical mounts, to name a few. We make this specific distinction between the control and executive electronics because often they *are* different hardware units, e.g. most light field modulators (executive hardware) are radio-frequency driven, which is a signal generated from a different device (control electronics). On the microsecond scale, computational control on a node is performed by dedicated microcontroller (Jağer ADwin-Pro II T12). For (sub-)nanosecond timing control, guaranteed alignment of optical signals for those sent to the quantum chip or received through the network (i.e. heralding signal), an Arbitrary Waveform Generator (AWG) (Zurich Instruments HDAWG) is used. Lastly, the **quantum chip** is the recipient of optical or electronic signals, where executive hardware provides the means to address the quantum chip (optical field or RF) or acts as receiver of signals sent from the chip (photon detection). All layers have mutual interaction due to the duality all being able to receive instructions or signals and send them out to a neighboring layer.

I.2.7.2. MULTIPLE NODES

The sequencer code accommodates for multiple nodes, where multiple calibrations and settings can be taken and applied to the respective nodes. The QMI framework allows for fully network-defined devices, exposed through TCP/UDP connections. USB-like devices are locally initialized through (remote) managed services that take distributed settings and expose their functionality again as TCP/UDP connection. This makes for a system that is can be initialized fully remotely, yet has a single point of control that hooks in or out to the underlying control mechanisms whenever appropriate. In addition we have Graphical User Interfaces (GUIs) that have the ability to interact, observe and intervene with crucial components that can benefit from quick human assessments, e.g. laser frequencies and mode behavior.

I.2.7.3. LONG-TERM NETWORK OPERATION

In the early phases of the experiments pertaining to this thesis it became clear that well-defined hardware layers together with standardized calibrations and system (state) settings and cleverly designed sequencer code would be the key to successful experiments. Especially for comparatively long operation times of several days and systems that are physically distributed, there is no option of a *quick manual fix*. Remote addressability and automated upkeep is the only way for prototype systems like these to be pushed into operation as *deployed* system.

With a properly constructed sequencer layer and calibration suite, (human) operator time can be significantly reduced by making use of a *watchdog* system that handles calibrations, starts experiments and signals on errors it cannot solve itself, see Fig. I.2.8. As example of its operation, the two-photon quantum experiment of Fig. I.3.4 in Chapter I.3 took a total of 412 wall clock hours, operated 78% of the time fully independently, of

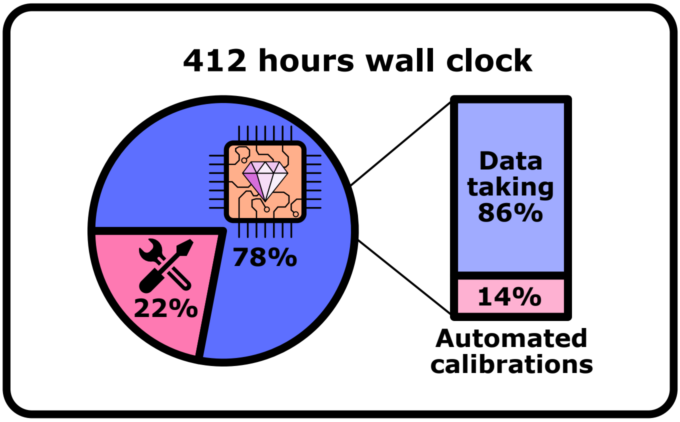

Figure I.2.8: Breakdown of measurement time to obtain the data of Fig. I.3.4 in Chapter I.3. At 412 hours of wall clock time, only 22% required human supervision. The 78% of measurement time was run by a *watchdog* system, where 86% of that time was data taking and 14% automated calibrations. The watchdog could prompt for manual intervention, leading to the aforementioned human supervision time.

which 86% was data taking and the other 14% was automated calibrations. The 22% of operation time where supervision was required consisted of unplanned downtime or system alert triggers where manual intervention was requested for optimal continuation of the experiment. This functionality was extensively used to continue into Chapter I.5, where the entirety of the experiment ran almost completely autonomously with only a handful of manual (brief) interventions.

I.2.7.4. Node temperature stability

To ensure long-term operation beyond active calibrations, passive stability must also be guaranteed. The ZPL collection and QFC operation depend on free-space optics with travel distances of several meters. Temperature changes change the exact photon path ever so slightly due to the movement of the microscope housing, mirrors, filters, lenses and the collection fiber(s). We actively control optimization of coupling to the NV center, the ZPL collection and the local phase interference signal, but alignment corrections help to find local maxima and usually cannot correct for coherent error build up. To ensure weeks of consistent operation and passive stability, it is imperative that the temperature of the optical setup remains as constant as possible. While for most cases this *should* ensured by the lab environment itself, usually (large) room heating, ventilation, and air conditioning (HVAC) control is not sufficient due to several reasons: feedback delays to HVAC systems, directed air streams, cooling capacity limitations, insufficient temperature resolution control, on/off HVAC systems instead of continuous variable cooling/heating control, doors opening/closing at random times and varying number of people at work in the environment.

To solve the above challenge, a fully temperature stabilized box around the crucial parts of the setup was built. With approximate air-sealing of the optical table, the free-space optics, fiber optics and crucial electronics, the heat load from inside this box is

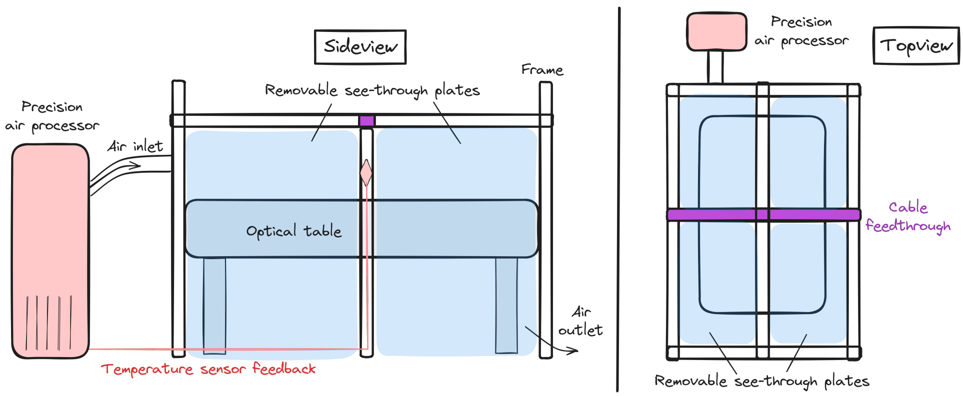

Figure I.2.9: Schematic side- (left) and topview (right) of the temperature controlled box around the crucial parts of the experimental setup. The see-through plates are 4mm transparent polycarbonate. The temperature sensor is placed centered in free-space, which is used as feedback for changing the incoming air temperature by the precision air processor.

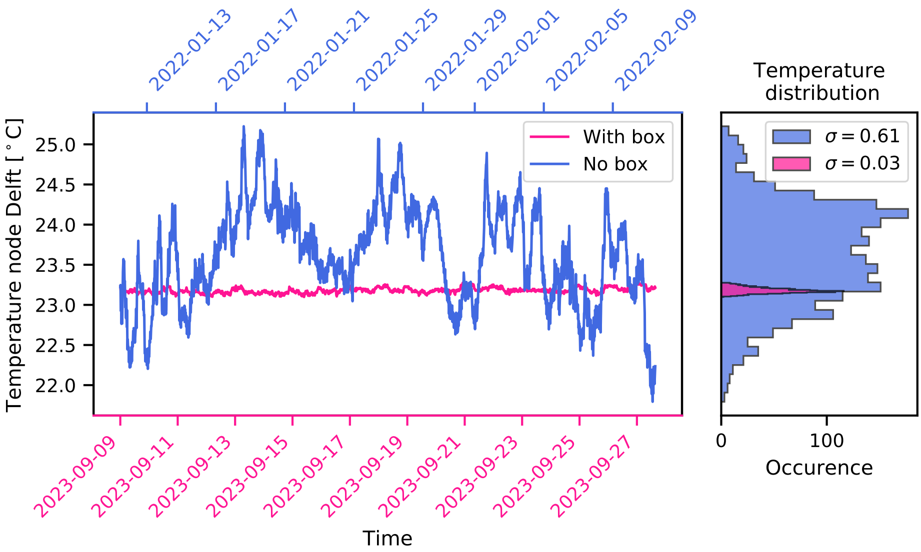

Figure I.2.10: Temperature stability of the ambient temperature of node Delft, uncovered and operating in lab space (blue) or fully boxed and temperature stabilized (pink) as shown in Fig. I.2.9. The time windows were selected as representative and without interruption of *normal* operation, e.g. opening the box for extended amount of time. The right shows the distribution of temperatures with the respective standard deviations, indicating an order of magnitude increase in stability *with* the box. In both cases the temperature sensor was located at the same location as the sensor in Fig. I.2.9.

constant and the temperature gradient from the outside is small. The air inside the box is temperature controlled by a precision air processor (Orion PAP02A-CE), which has 0.01 K resolution control and PID-control with a temperature sensor inside to achieve a target temperature setpoint. With controlled air blowing in on one end, we overpressurize the box and let air slip out on opposite side of the input. A representative comparison between the system fully open to the air or enclosed in the box is shown in Fig. I.2.10. With an order of magnitude improvement in stability, this enhanced system allowed for several weeks to months of optics stability, which greatly contributed to the success of the metropolitan entanglement experiment of Chapter I.5.

I.2

REFERENCES

[1] H. J. Kimble, *The quantum internet,* Nature **453**, 1023 (2008).

[2] S. Wehner, D. Elkouss, and R. Hanson, *Quantum internet: A vision for the road ahead,* Science **362**, eaam9288 (2018).

[3] D. L. Moehring, P. Maunz, S. Olmschenk, K. C. Younge, D. N. Matsukevich, L.-M. Duan, and C. Monroe, *Entanglement of single-atom quantum bits at a distance,* Nature **449**, 68–71 (2007).

[4] S. Ritter, C. Nölleke, C. Hahn, A. Reiserer, A. Neuzner, M. Uphoff, M. Mücke, E. Figueroa, J. Bochmann, and G. Rempe, *An elementary quantum network of single atoms in optical cavities,* Nature **484**, 195 (2012).

[5] J. Hofmann, M. Krug, N. Ortegel, L. Gérard, M. Weber, W. Rosenfeld, and H. Weinfurter, *Heralded Entanglement Between Widely Separated Atoms,* Science **337**, 72 (2012).

[6] H. Bernien, B. Hensen, W. Pfaff, G. Koolstra, M. S. Blok, L. Robledo, T. H. Taminiau, M. Markham, D. J. Twitchen, L. Childress, and R. Hanson, *Heralded entanglement between solid-state qubits separated by three metres,* Nature **497**, 86–90 (2013).

[7] R. Stockill, M. J. Stanley, L. Huthmacher, E. Clarke, M. Hugues, A. J. Miller, C. Matthiesen, C. Le Gall, and M. Atatüre, *Phase-Tuned Entangled State Generation between Distant Spin Qubits,* Physical Review Letters **119**, 010503 (2017).

[8] L. Stephenson, D. Nadlinger, B. Nichol, S. An, P. Drmota, T. Ballance, K. Thirumalai, J. Goodwin, D. Lucas, and C. Ballance, *High-Rate, High-Fidelity Entanglement of Qubits Across an Elementary Quantum Network,* Physical Review Letters **124**, 110501 (2020).

[9] M. Pompili, S. L. N. Hermans, S. Baier, H. K. C. Beukers, P. C. Humphreys, R. N. Schouten, R. F. L. Vermeulen, M. J. Tiggelman, L. dos Santos Martins, B. Dirkse, S. Wehner, and R. Hanson, *Realization of a multinode quantum network of remote solid-state qubits,* Science **372**, 259 (2021).

[10] S. L. N. Hermans, M. Pompili, H. K. C. Beukers, S. Baier, J. Borregaard, and R. Hanson, *Qubit teleportation between non-neighbouring nodes in a quantum network,* Nature **605**, 663 (2022).

[11] V. Krutyanskiy, M. Galli, V. Krcmarsky, S. Baier, D. Fioretto, Y. Pu, A. Mazloom, P. Sekatski, M. Canteri, M. Teller, J. Schupp, J. Bate, M. Meraner, N. Sangouard, B. Lanyon, and T. Northup, *Entanglement of Trapped-Ion Qubits Separated by 230 Meters,* Physical Review Letters **130**, 050803 (2023).

[12] P. Drmota, D. P. Nadlinger, D. Main, B. C. Nichol, E. M. Ainley, D. Leichtle, A. Mantri, E. Kashefi, R. Srinivas, G. Araneda, C. J. Ballance, and D. M. Lucas, *Verifiable blind quantum computing with trapped ions and single photons,* arXiv:2305.02936 (2024).

[13] M. Pompili, *Multi-Node Quantum Networks with Diamond Qubits*, Ph.D. thesis, Delft University of Technology (2021).

[14] M. W. Doherty, N. B. Manson, P. Delaney, F. Jelezko, J. Wrachtrup, and L. C. Hollenberg, *The nitrogen-vacancy colour centre in diamond,* Physics Reports **528**, 1 (2013).

[15] M. Ruf, N. H. Wan, H. Choi, D. Englund, and R. Hanson, *Quantum networks based on color centers in diamond,* Journal of Applied Physics **130**, 070901 (2021).

[16] W. Pfaff, *Quantum measurement and entanglement of spin Quantum bits*, PhD Thesis, Delft University of Technology (2013).

[17] H. Bernien, *Control, measurement and Entanglement of Remote Quantum Spin Registers in Diamond*, PhD Thesis, Delft University of Technology (2014).

[18] D. Riedel, I. Söllner, B. J. Shields, S. Starosielec, P. Appel, E. Neu, P. Maletinsky, and R. J. Warburton, *Deterministic enhancement of coherent photon generation from a nitrogen-vacancy center in ultrapure diamond,* Phys. Rev. X **7**, 031040 (2017).

[19] B. Hensen, *Quantum Nonlocality with Spins in Diamond*, PhD Thesis, Delft University of Technology (2016).

[20] O. Ubbens, *A Unified Model to Predict Excited State Cyclicity of Nitrogen Vacancy Centres in Diamond*, Master's thesis, QuTech, Delft University of Technology (2022).

[21] L. Robledo, L. Childress, H. Bernien, B. Hensen, P. F. A. Alkemade, and R. Hanson, *High-fidelity projective read-out of a solid-state spin quantum register,* Nature **477**, 574 (2011).

[22] M. Lesik, J.-P. Tetienne, A. Tallaire, J. Achard, V. Mille, A. Gicquel, J.-F. Roch, and V. Jacques, *Perfect preferential orientation of nitrogen-vacancy defects in a synthetic diamond sample,* Applied Physics Letters **104**, 113107 (2014).

[23] C. Bradley, J. Randall, M. Abobeih, R. Berrevoets, M. Degen, M. Bakker, M. Markham, D. Twitchen, and T. Taminiau, *A Ten-Qubit Solid-State Spin Register with Quantum Memory up to One Minute,* Physical Review X **9**, 031045 (2019).

[24] T. van der Sar, *Quantum control of single spins and single photons in diamond*, Ph.D. thesis, Delft University of Technology (2012).

[25] N. Kalb, *Diamond-based quantum networks with multi-qubit nodes,* PhD Thesis, Delft University of Technology (2018).

[26] S. Hermans, *Quantum Networks using Spins in Diamond*, Ph.D. thesis, Delft University of Technology (2022).

[27] M. H. Abobeih, J. Cramer, M. A. Bakker, N. Kalb, M. Markham, D. J. Twitchen, and T. H. Taminiau, *One-second coherence for a single electron spin coupled to a multi-qubit nuclear-spin environment,* Nature Communications **9**, 2552 (2018).

I.2

[28] G. d. Lange, Z. H. Wang, D. Ristè, V. V. Dobrovitski, and R. Hanson, *Universal Dynamical Decoupling of a Single Solid-State Spin from a Spin Bath,* Science **330**, 60 (2010).

[29] C. A. Ryan, J. S. Hodges, and D. G. Cory, *Robust Decoupling Techniques to Extend Quantum Coherence in Diamond,* Physical Review Letters **105**, 200402 (2010).

[30] T. H. Taminiau, J. Cramer, T. van der Sar, V. V. Dobrovitski, and R. Hanson, *Universal control and error correction in multi-qubit spin registers in diamond,* Nature Nanotechnology **9**, 171 (2014).

[31] J. Cramer, *Quantum error correction with spins in diamond,* PhD Thesis, Delft University of Technology (2016).

[32] N. Kalb, A. A. Reiserer, P. C. Humphreys, J. J. W. Bakermans, S. J. Kamerling, N. H. Nickerson, S. C. Benjamin, D. J. Twitchen, M. Markham, and R. Hanson, *Entanglement distillation between solid-state quantum network nodes,* Science **356**, 928–932 (2017).

[33] H. K. Beukers, M. Pasini, H. Choi, D. Englund, R. Hanson, and J. Borregaard, *Remote-entanglement protocols for stationary qubits with photonic interfaces,* PRX Quantum **5**, 010202 (2024).

[34] S. Daiss, S. Langenfeld, S. Welte, E. Distante, P. Thomas, L. Hartung, O. Morin, and G. Rempe, *A quantum-logic gate between distant quantum-network modules,* Science **371**, 614 (2021), https://www.science.org/doi/pdf/10.1126/science.abe3150 .

[35] S. D. Barrett and P. Kok, *Efficient high-fidelity quantum computation using matter qubits and linear optics,* Physical Review A **71**, 060310 (2005).

[36] B. Hensen, H. Bernien, A. E. Dréau, A. Reiserer, N. Kalb, M. S. Blok, J. Ruitenberg, R. F. L. Vermeulen, R. N. Schouten, C. Abellán, W. Amaya, V. Pruneri, M. W. Mitchell, M. Markham, D. J. Twitchen, D. Elkouss, S. Wehner, T. H. Taminiau, and R. Hanson, *Loophole-free Bell inequality violation using electron spins separated by 1.3 kilometres,* Nature **526**, 682 (2015).

[37] A. Narla, S. Shankar, M. Hatridge, Z. Leghtas, K. M. Sliwa, E. Zalys-Geller, S. O. Mundhada, W. Pfaff, L. Frunzio, R. J. Schoelkopf, and M. H. Devoret, *Robust concurrent remote entanglement between two superconducting qubits,* Phys. Rev. X **6**, 031036 (2016).

[38] C. M. Knaut, A. Suleymanzade, Y.-C. Wei, D. R. Assumpcao, P.-J. Stas, Y. Q. Huan, B. Machielse, E. N. Knall, M. Sutula, G. Baranes, N. Sinclair, C. De-Eknamkul, D. S. Levonian, M. K. Bhaskar, H. Park, M. Lončar, and M. D. Lukin, *Entanglement of nanophotonic quantum memory nodes in a telecom network,* Nature **629**, 573 (2024).

[39] C. Cabrillo, J. I. Cirac, P. García-Fernández, and P. Zoller, *Creation of entangled states of distant atoms by interference,* Physical Review A **59**, 1025–1033 (1999).

[40] S. Bose, P. L. Knight, M. B. Plenio, and V. Vedral, *Proposal for Teleportation of an Atomic State via Cavity Decay,* Physical Review Letters **83**, 5158 (1999).

[41] P. C. Humphreys, N. Kalb, J. P. J. Morits, R. N. Schouten, R. F. L. Vermeulen, D. J. Twitchen, M. Markham, and R. Hanson, *Deterministic delivery of remote entanglement on a quantum network,* Nature **558**, 268 (2018).

[42] S. L. N. Hermans, M. Pompili, L. D. S. Martins, A. R.-P. Montblanch, H. K. C. Beukers, S. Baier, J. Borregaard, and R. Hanson, *Entangling remote qubits using the single-photon protocol: an in-depth theoretical and experimental study,* New Journal of Physics **25**, 013011 (2023).

[43] C. K. Hong, Z. Y. Ou, and L. Mandel, *Measurement of subpicosecond time intervals between two photons by interference,* Phys. Rev. Lett. **59**, 2044 (1987).

[44] A. J. Stolk, *Going the distance: Metropolitan scale entanglement of NV-centers over deployed telecom fiber,* Ph.D. thesis, QuTech, Delft University of Technology (2024).

[45] Fiber Broadband Association, *Fiber Deployment Annual Report,* (2023).

[46] J. Kim, *Fiber Optic Network Construction: Process and Build Costs,* Accessed through Wayback Machine 8 August 2024 (2024).

[47] ITU, *Infrastructure connectivity map,* (2024).

[48] P. D. Townsend, *Simultaneous quantum cryptographic key distribution and conventional data transmission over installed fibre using wavelength-division multiplexing,* Electronics Letters **33**, 188 (1997).

[49] P. Eraerds, N. Walenta, M. Legré, N. Gisin, and H. Zbinden, *Quantum key distribution and 1 gbps data encryption over a single fibre,* New Journal of Physics **12**, 063027 (2010).

[50] J. Wang, B. J. Rollick, Z. Jia, H. Zhang, and B. A. Huberman, *Time-interleaving enabled co-propagation of qkd with a 10-dbm 100-gb/s qpsk channel over 100-km fiber,* in *49th European Conference on Optical Communications (ECOC 2023)*, Vol. 2023 (2023) pp. 652–655.

[51] W. Gambling, *The rise and rise of optical fibers,* IEEE Journal of Selected Topics in Quantum Electronics **6**, 1084 (2000).

[52] A. Dréau, A. Tchebotareva, A. E. Mahdaoui, C. Bonato, and R. Hanson, *Quantum frequency conversion of single photons from a nitrogen-vacancy center in diamond to telecommunication wavelengths,* Phys. Rev. Appl. **9**, 064031 (2018).

[53] T. Suhara and M. Fujimura, *Waveguide Nonlinear-Optic Devices* (Springer Berlin Heidelberg, 2003).

[54] R. W. Boyd, *Nonlinear Optics*, 3rd ed. (Academic Press, Inc., USA, 2008).

I.2

[55] P. E. Powers and J. W. Haus, *Fundamentals of Nonlinear Optics*, 2nd ed. (CRC Press, Boca Raton, 2017) p. 500.

[56] J. F. Geus, F. Elsen, S. Nyga, A. J. Stolk, K. L. van der Enden, E. J. van Zwet, C. Haefner, R. Hanson, and B. Jungbluth, *Low-noise short-wavelength pumped frequency down-conversion for quantum frequency converters,* Optica Quantum **2**, 189 (2024).

[57] F. Mann, H. M. Chrzanowski, F. Gewers, M. Placke, and S. Ramelow, *Low-noise quantum frequency conversion in a monolithic cavity with bulk periodically poled potassium titanyl phosphate,* Phys. Rev. Appl. **20**, 054010 (2023).

[58] R. Ikuta, T. Kobayashi, T. Yamazaki, N. Imoto, and T. Yamamoto, *Cavity-enhanced broadband photonic rabi oscillation,* Phys. Rev. A **103**, 033709 (2021).

[59] C. E. Vollmer, C. Baune, A. Samblowski, T. Eberle, V. Händchen, J. Fiurášek, and R. Schnabel, *Quantum up-conversion of squeezed vacuum states from 1550 to 532 nm,* Phys. Rev. Lett. **112**, 073602 (2014).

[60] E. Arenskötter, T. Bauer, S. Kucera, M. Bock, J. Eschner, and C. Becher, *Telecom quantum photonic interface for a 40ca+ single-ion quantum memory,* npj Quantum Information **9** (2023), 10.1038/s41534-023-00701-z.

[61] G. Hansson, H. Karlsson, S. Wang, and F. Laurell, *Transmission measurements in ktp and isomorphic compounds,* Appl. Opt. **39**, 5058 (2000).

[62] B. Albrecht, P. Farrera, X. Fernandez-Gonzalvo, M. Cristiani, and H. de Riedmatten, *A waveguide frequency converter connecting rubidium-based quantum memories to the telecom c-band,* Nature Communications **5** (2014), 10.1038/ncomms4376.

[63] N. Maring, D. Lago-Rivera, A. Lenhard, G. Heinze, and H. de Riedmatten, *Quantum frequency conversion of memory-compatible single photons from 606 nm to the telecom c-band,* Optica **5**, 507 (2018).

[64] T. Hansch and B. Couillaud, *Laser frequency stabilization by polarization spectroscopy of a reflecting reference cavity,* Optics Communications **35**, 441 (1980).

[65] A. Dahlberg, M. Skrzypczyk, T. Coopmans, L. Wubben, F. Rozpundefineddek, M. Pompili, A. Stolk, P. Pawełczak, R. Knegjens, J. de Oliveira Filho, R. Hanson, and S. Wehner, *A link layer protocol for quantum networks,* in *Proceedings of the ACM Special Interest Group on Data Communication*, SIGCOMM '19 (Association for Computing Machinery, New York, NY, USA, 2019) p. 159–173.

[66] I. T. Raa, H. K. Ervasti, P. J. Botma, L. C. Visser, R. Budhrani, J. F. van Rantwijk, S. P. Cadot, J. Vermeltfoort, M. Pompili, A. J. Stolk, M. J. Weaver, K. L. van der Enden, D. de Leeuw Duarte, M. Teng, J. van Zwieten, and F. Grooteman, *QMI - Quantum Measurement Infrastructure, a Python 3 framework for controlling laboratory equipment,* (2023).

I.3

TELECOM-BAND QUANTUM INTERFERENCE OF FREQUENCY-CONVERTED PHOTONS FROM REMOTE DETUNED NV CENTERS

A. J. Stolk†, K. L. van der Enden†, M-C. Roehsner, A. Teepe, S.O.F. Faes, S. Cadot, J. van Rantwijk, I. te Raa, R.A.J. Hagen, A.L. Verlaan, B. Biemond, A. Khorev, R. Vollmer, M. Markham, A. M. Edmonds, J.P.J. Morits, E.J. van Zwet, and R. Hanson

Entanglement distribution over quantum networks has the promise of realizing fundamentally new technologies. Entanglement between separated quantum processing nodes has been achieved on several experimental platforms in the past decade. To move towards metropolitan-scale quantum network test beds, the creation and transmission of indistinguishable single photons over existing telecom infrastructure is key. Here we report the interference of photons emitted by remote, spectrally detuned NV center-based network nodes, using quantum frequency conversion to the telecom L-band. We find a visibility of 0.79 ± 0.03 *and an indistinguishability between converted NV photons around* 0.9 *over the full range of the emission duration, confirming the removal of the spectral information present. Our approach implements fully separated and independent control over the nodes, time-multiplexing of control and quantum signals, and active feedback to stabilize the output frequency. Our results demonstrate a working principle that can be readily employed on other platforms and shows a clear path towards generating metropolitan scale, solid-state entanglement over deployed telecom fibers.*

The results of this chapter have been published in PRX Quantum **3**, 020359 (2022).

† These authors contributed equally to this work.

A future quantum internet [1, 2], built using quantum processor nodes connected via optical channels, promises applications such as secure communication, distributed quantum computation, and enhanced sensing [3–5]. In recent years, the generation of entanglement between remote processor nodes has been realized with ions and atoms [6–9], Nitrogen-Vacancy (NV) centers in diamond [10, 11], and quantum dots [12, 13]. Moreover, other platforms such as rare-earth doped crystals [14–16], atom-cloud based memories [17, 18], and mechanical resonators [19] have been used to explore distributed entangled states.

Central to commonly used remote entanglement generation protocols [6, 8–13] is the propagation and interference of single photons that are entangled with stationary qubits in the nodes. Scaling these schemes to many nodes and to long distances poses two main challenges. First, any source of distinguishability between the emitted photons needs to be removed to generate high-fidelity entangled states. Especially for solid-state emitters, this requirement is difficult to meet for a large number of nodes due to variations in the local environment of the emitters. Second, for long-distance connections photon loss in fibers is a dominant factor determining the rate at which the entanglement generation succeeds. Leading platforms for realizing processor nodes [9, 20–24] in a future quantum network have natural emission frequencies in the visible spectrum; fiber losses at these frequencies hinder scaling beyond a few kilometers.

In this work, we show that both challenges can be addressed simultaneously by converting the coherent single-photon emission from NV centers (637 nm) to a single target wavelength in the Telecom L-band (1565-1625 nm) (Fig. I.3.1a). Using the pump lasers to compensate for local detuning and using active stabilization of the frequency of the converted field, we are able to decouple the natural emission wavelength of the emitters from the wavelength used for propagation and interference and build fully independent, modular quantum nodes. We demonstrate that this method enables the removal of spectral offsets over a broad frequency range (>3 GHz). Moreover, the chosen interference wavelength has low propagation losses over commercially available optical fibers, making it suitable for long-range single-photon transmission.

We validate our approach by measuring quantum interference [25] between telecom photons that are frequency converted from the emission of two remote NV-centers that are detuned by more than 100 linewidths. By comparing the data to a detailed model we extract both the major noise sources and the underlying indistinguishability of the converted NV photons.

I.3.1. Independent quantum network nodes

We employ two independently operated quantum network nodes separated by a few meters on different optical tables. The nodes are connected to a midpoint located in two separate 19-inch racks. The relevant elements are depicted in Fig. I.3.1c. Each node operates a single diamond NV center as stationary qubit, hosted in a closed-cycle cryostat at $T \approx 4K$. The relevant energy levels and optical transitions of the NV qubit are depicted in Fig. I.3.1b. The spin reset transition is used for spin initialization into $m_s = 0$ (fidelity > 0.99). We use the transition to the $E_{x/y}$ excited state to generate single photons: a coherent optical π-pulse (≈2 ns) brings the NV center to the excited state, followed by spontaneous emission (lifetime ≈12 ns [26, 27]). Both setups employ their own lasers and

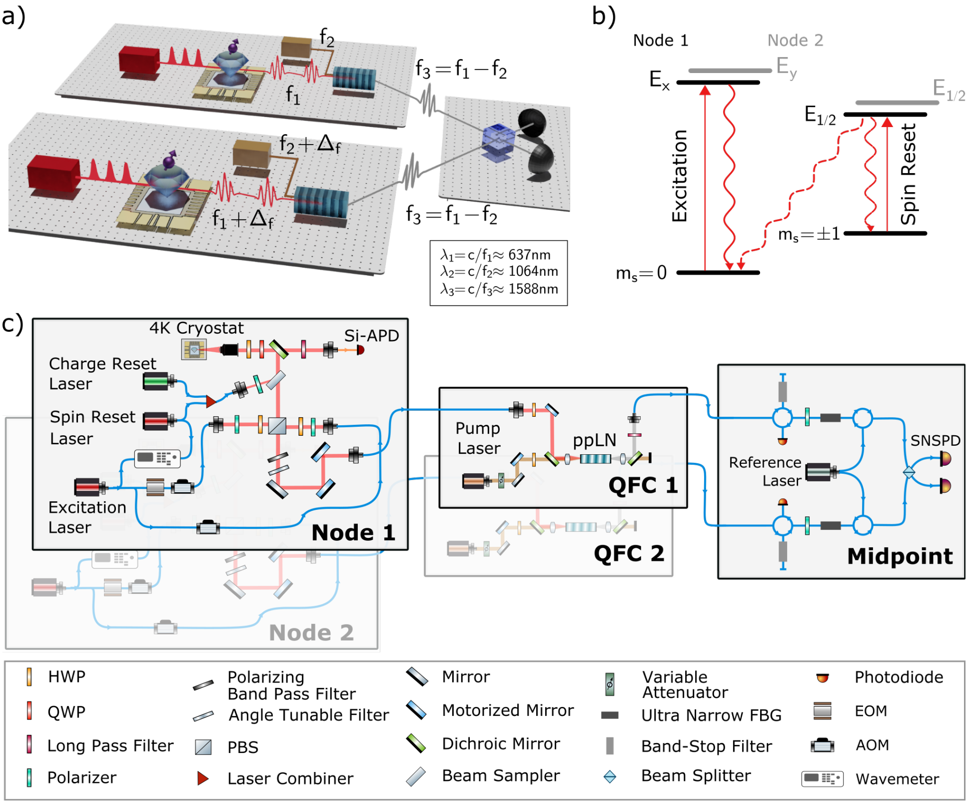

Figure I.3.1: **Lay-out of the two independent network nodes and the midpoint.** a) Schematic of the main components of the set-up. Pulses excite the NV center, which emits single photons through spontaneous decay. The photons are converted to telecom wavelength and guided towards a midpoint placed in the neighboring lab, where they interfere on a beamsplitter I.3.6.1. b) NV center level structure showing the spin levels in the ground state and the relevant optical transitions. The optical transitions of the two nodes have different energies due to local variations in strain (see text). c) Detailed schematic showing the optics used for full operation of the system. The nodes are identical, and no hardware is shared between the systems. Each node has a set of charge reset, spin reset and excitation laser, which are modulated, combined and focused via a high NA objective onto the NV center. The Phonon side-band (PSB) (Zero-phonon line (ZPL)) emission from the NV center is filtered using frequency (polarization) filtering and coupled into a multi (single-) mode fiber. The PSB emission is measured locally on an APD, while the ZPL emission is sent to the QFC module. Stabilization light is split off from the excitation path, and brought into the single-photon path via a polarizing beamsplitter. The QFC module contains remotely controllable optics to align the input, pump and converted fields to the waveguide on the ppLN crystal that converts both the single-photons and stabilization light. Polarization maintaining (PM) fibers transport the photons to a midpoint where the single photons are filtered and separated from the stabilization light using a combination of in-fibre filters. The single photons interfere on a beamsplitter and are measured by SNSPDs, while the stabilization light interferes with the reference laser and is measured on a photodiode.

optical components that deliver and collect light to the NV center.

The nodes are equipped with a (nominally identical) Quantum Frequency Conversion (QFC) module. Here the light at 637 nm is converted to 1588 nm via a single-step Difference Frequency Generation (DFG) process. This process has previously been shown to preserve entanglement between the photon and an NV center qubit [28]. The QFC modules are based on waveguides in a periodically poled Lithium Niobate crystal (ppLN), where the large non-linear coefficient facilitates conversion of single photons using a strong 1064 nm pump field. Various remotely controllable components allow for the remote and automated optimization of the QFC modules. While this single-step conversion has the upside of using a prevalent commercially available pump laser, it has the challenge of introducing spontaneous parametric down-conversion noise at the target wavelength by the pump laser due to imperfections in the crystal domains [29].

After free-space filtering to remove the bright pump light, the frequency-converted light is guided to a central midpoint. In the midpoint, a series of filters separate photons at the target wavelength from stabilization light and filter out noise photons. To achieve a high suppression of any broad-band background light, we use a two-step filtering process. First, we use a reflection off a narrow Band-Stop filter of 0.35 nm, followed by transmission through an ultra-narrow (FWHM of ~50 MHz) Fiber Bragg Grating (abbreviated with UNF). The filters are connected via circulators, and an in-fiber polarizer is used to ensure optimal performance of the UNF (Fig. I.3.1B). After filtering, we interfere the two paths using a 50 : 50 beam splitter, and detect the photons using single-photon superconducting nanowire detectors (SNSPDs).

I.3.2. Realizing spectral stability via feedback

For solid-state emitters, the local environment can influence the emission properties directly via electric, magnetic or strain fields. For instance, for NV centers in nominally low-strain samples the local strain environment can shift the emission frequency by more than 1000 times the linewidth [30]. While direct tuning of emission wavelength is in principle possible on several platforms, e.g. by strain [31] or via static electric fields [10, 13], the range of tunability is in general limited. Also, direct tuning brings additional complexities in the device fabrication and can add significant experimental overhead.

We show that we can use the QFC process to remove the spectral offset between the NV emission without the need for direct tuning of the optical transition. An analogous scheme has recently been used on spectrally distinct quantum dots [32, 33]; a key difference is that the NV center host diamond also contains a long-lived matter qubit and can function as a processing node in a quantum network [23]. Using resonant excitation spectroscopy we find the optical transition frequency used for single-photon generation at each node (Fig. I.3.2a). We observe that these transition frequencies are separated by approximately 3 GHz (about 100 natural linewidths), as shown in Fig. I.3.2B.

To bring the NV photons to the same target frequency, we realize a scheme that locks the pump laser at each node to the frequency difference between the excitation laser at that node (and hence the NV emission frequency) and a joint Telecom reference laser at the midpoint. To achieve this lock, we use a split-off of the excitation laser, offset in frequency by a fixed 400 MHz, as stabilization light (see Fig. I.3.2D). We propagate

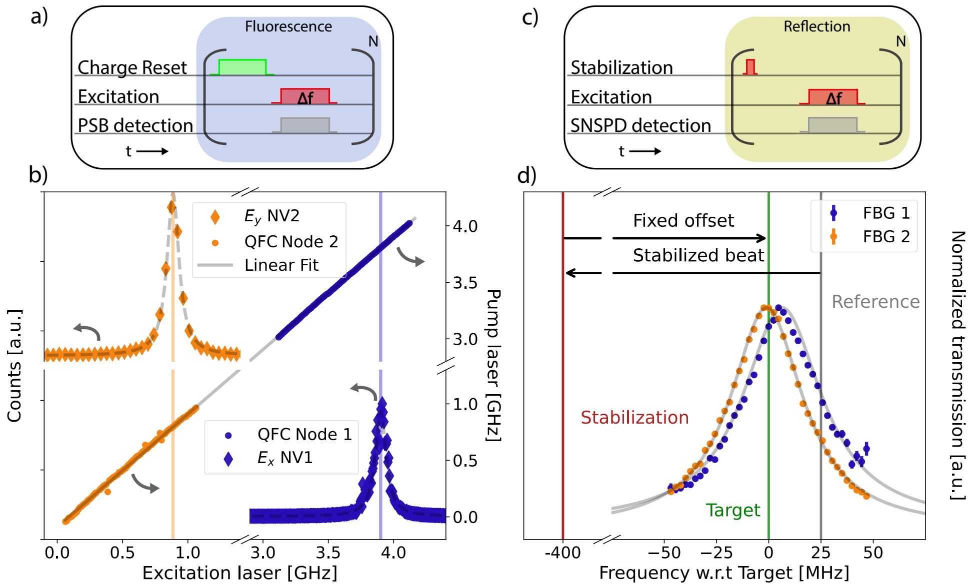

Figure I.3.2: **Removing spectral offset using conversion.** a) Fluorescence measurement sequence used in b). A charge reset pulse is followed by repeated resonant excitation, during which fluorescence in the PSB is monitored. b) Resonant excitation spectra at Node 1 (Node 2) shown in blue (orange) diamonds, revealing the frequencies of the optical transitions (vertical lines) used for photon generation. The horizontal axis shows the optical excitation frequency with respect to a 470 477 GHz offset. Grey dotted lines are Lorentzian fits. The right vertical axis shows the frequency of the QFC pump with respect to a 281 635 GHz offset. Blue and orange dots show the QFC pump laser frequency when the stabilization is active. Solid grey line is linear fit. c) Pulse schematic for measuring the transmission through the ultra-narrow filter (UNF) shown in d). Reflections from the excitation light off the sample surface, which follow the same path as the resonant NV emission, are converted to the target telecom frequency and measured on the SNSPDs. The excitation frequency is swept by modulating the AOM frequency (see Fig. I.3.1c). Transmission data is corrected for the frequency dependence of the losses in the AOMs. d) Layout of relevant laser frequencies and transmission data of the ultra-narrow filters (UNF). The UNF transmissions (blue and orange dots) are actively stabilized via their temperature to half transmission of the reference laser (grey vertical line). The stabilization light (red vertical line) is detuned from the target (green vertical line) and therefore reflected off the UNF (see main text).

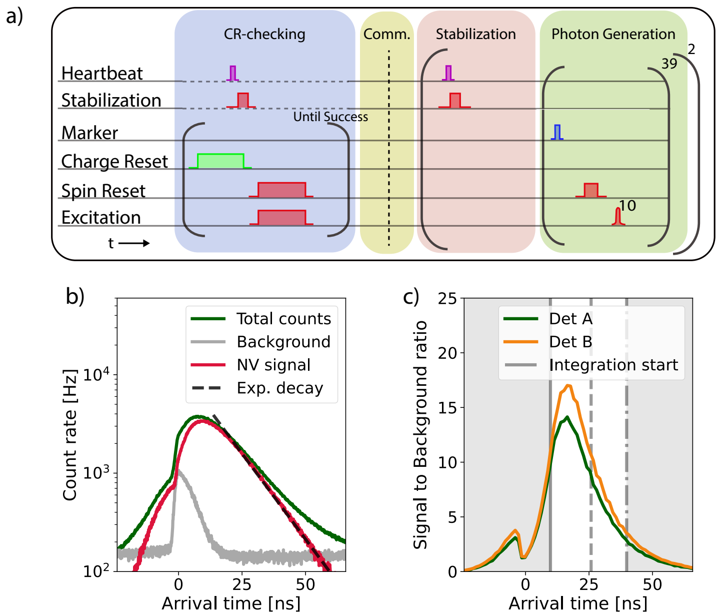

Figure I.3.3: **Generating single-photons using a fixed heartbeat.** (a) Measurement sequence for synchronized generation of single-photons using a distributed heartbeat. For detailed timing see Supplementary Info I.3.5. (b) Histogram of SNSPD counts in a single excitation round, averaged over $\approx 2.8 \times 10^{11}$ repetitions and analyzed in 80 ps bins. The measured count rate (green) is a combination of background (grey) and NV fluorescence (red), which is calculated by subtracting the background from the total counts. The dotted line depicts exponential decay with 12.5 ns lifetime and serves as a guide to the eye. The NV signal before time 0, the peak of the excitation pulse, is due to the non-perfect extinction ratio of the devices generating the optical excitation pulse. The background data was taken continuously over 24 hours to include any drifts that occur over the same timescale as the signal data. (c) Signal-to-background ratio for both detectors as calculated from data in (b) (solid lines). The solid vertical grey line shows the start of our chosen detection window, whereas the dashed (dash-dotted) line shows the end for the data shown in Fig. I.3.4a (Fig. I.3.4b). The difference between the two curves is due to non-equal detector performances.

this stabilization light through the same frequency-conversion path as the NV photons. Due to the frequency offset, the stabilization light is reflected at the UNF, travelling backwards towards the first circulator where it exits (see Fig. I.3.1c). Light from the joint reference laser is inserted at the second circulator, from where it propagates in opposite direction through the transmission flank of the UNF, also exiting on the first circulator. Here, the interference with the stabilization light is measured on a photo diode yielding the error signal for the lock (see Supplementary Info I.3.9). We close the loop by applying feedback to the pump laser, imprinting the same frequency shift on both the single photons and stabilization light. By transmitting the reference laser 25 MHz detuned from the transmission peak of the second ultra narrow filter, the DC amplitude on the same photo diode serves as an error signal for active temperature stabilization of the UNF. Typical transmission profiles of the temperature-stabilized UNFs and the respective light-field frequencies are shown in Fig. I.3.2d. The small deviation from ideal peak transmission at the target frequency is due to unaccounted background voltage of the photo diode and the slight difference in FWHM of the two UNFs. The remaining thermal drifts of about 1 MHz have only a minor (~1%) effect on the transmission (see Supplementary Information I.3.6.11 and I.3.12). Note that the part of the reference light that is reflected off the ultra-narrow filter exits the circulator towards the SNSPDs and thus needs to be taken into account when designing the experimental sequence (see next section).

We verify our frequency locking by sweeping the excitation laser and monitoring the resulting pump laser frequency in Fig. I.3.2b. We observe the expected linear relationship: a change in excitation laser frequency is precisely compensated by the pump laser frequency to always yield the same target frequency across the full tuning range. A linear fit yields the target frequency of (1587.5298 ± 0.0001) nm. This data demonstrates the ability of our frequency-locked down-conversion system to robustly compensate for a wide range of detunings.

I.3.3. PHOTON GENERATION AT THE TARGET TELECOM WAVELENGTH

We now turn to the generation of single telecom photons by the nodes as used for the measurement of two-photon quantum interference at the midpoint. The measurement sequence involves four stages (see Fig. I.3.3), which are synchronized across the nodes by a fixed electronic "heartbeat" every 200 µs. This heartbeat is derived from a GPS-disciplined atomic clock positioned in the midpoint, which is distributed over telecom fibers via the White Rabbit Precision Time Protocol [34]. The first 2.5 µs following each heartbeat are used for the error signal generation for the frequency lock. This scheme allows the frequency lock to operate without knowledge of the state of the nodes, which reduces the complexity and rounds of communication needed. Moreover, it enables the autonomous operation of each of the nodes, using their own independent hardware to control the NV center and generate single photons.

In the first stage of the measurement sequence, a Charge-Resonance (CR) check is performed at each node to ensure that the NV centers are in the correct charge state and their transitions are on resonance with their respective spin reset and excitation lasers [10, 35]. In case a CR check fails, a charge reset laser pulse is applied and a new CR check is started; this protocol is repeated until success. Importantly, the CR check can be run in parallel with the frequency locking as the stabilization light for the lock does not reach the NV center nor the local PSB detectors; hence the CR checks can run independently of the heartbeat. The second phase starts once the CR check is passed on a node, where a digital trigger from the micro-controller signals the readiness to the other node. After the readiness of both nodes has been communicated, the heartbeat at which they move to the third stage is agreed upon (Fig. I.3.3a and Supplementary Info I.3.5 for timings and more information).

The third stage of the measurement sequence is used for the time-multiplexed frequency stabilization, as described above. In the fourth stage, we repeatedly apply a block consisting of a spin reset pulse (1.5 µs) followed by 10 optical π-pulses, ideally generating a train of 10 NV photons. A time-tagged digital signal marks the times at which the photon generation takes place. This block is repeated 39 times per heartbeat period. After two

I.3

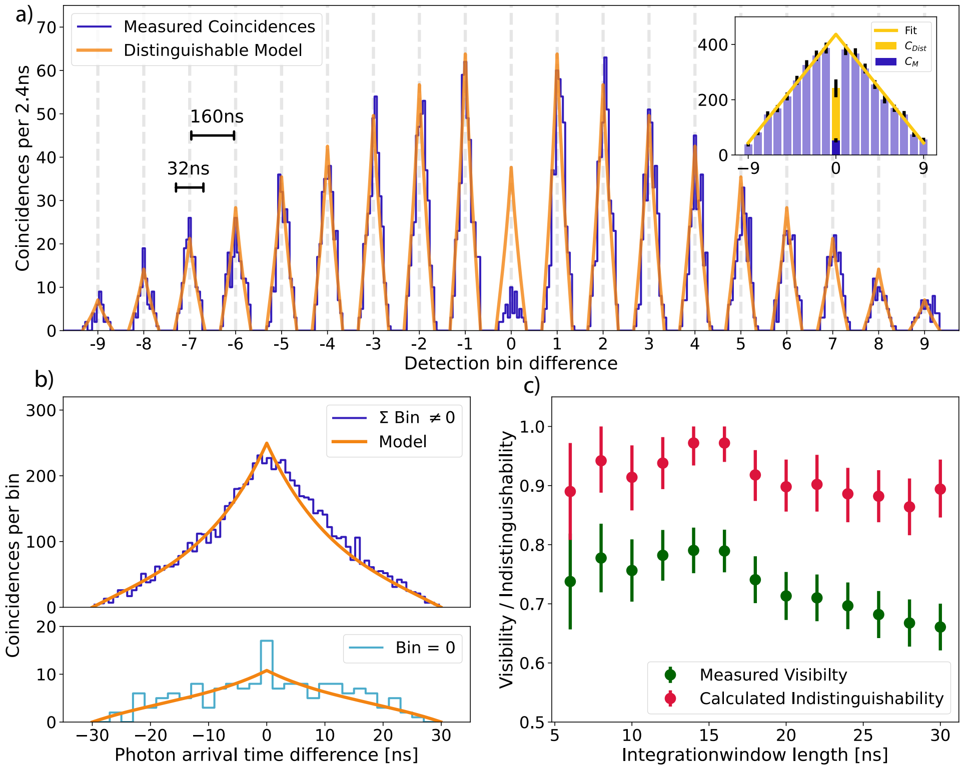

Figure I.3.4: **Two-photon quantum interference at telecom wavelength.** a) Histogram of measured coincidences (blue) for the analyzed time-bins, overlaid with a model assuming distinguishable photons (orange), based on independently determined parameters. Histogram binsize is 2.4 ns. Vertical lines depict the time-origin of each detection bin difference. Horizontal scale bars show the relevant timescales in and between the detection bin difference. Inset: extraction of the interference visibility, corrected for the imbalance of measured photons per excitation of the two nodes, using a linear fit to the total counts per bin difference (see text). b) Histogram showing temporal shape of the non-zero (zero) bin difference coincidences shown at the top (bottom) panel. We overlay the data with the same model (see Supplementary Info), taking into account brightness and background rates and indistinguishability of converted NV photons of 0.9 (see c)). Binsize for top (bottom) panel is 0.8 ns (2 ns) c) Measured visibility and extracted indistinguishability of converted NV photons for varying window length. Errorbars for visibility/indistinguishability are $1\sigma/68\%$ confidence interval. Green (blue) circled points indicate data corresponding to the window length shown in Fig. I.3.4a (Fig. I.3.4b).

heartbeat periods, the system returns to the first stage (CR checks). Note that during the third and fourth stage, time-multiplexing the operations on the NV center and the error signal generation for the frequency lock is critical as the stabilization light and the reference light both leak into the single-photon detection path.

We analyze the resulting telecom photon detection rate in Fig. I.3.3b (green line). We show the events observed in a single detector, aggregated over all single excitation rounds and both nodes. We denote $t = 0$ as the relative time of excitation. A sharp increase in count rate is observed when the ≈2 ns-wide optical π-pulse starts, followed by a slower decay dominated by spontaneous emission of the NV centers.

A data set displaying only the noise counts and the counts due to leakage of the excitation π-pulse (grey line) is independently generated by detuning the excitation laser by 1 GHz. The observed uniform background consists of intrinsic detector darkcounts (5 Hz per detector), counts induced by detector blinding from leaked reference and stabilization light (35 Hz per detector), and SPDC photons from the QFCs (≈150 Hz per detector). The leakage of the excitation π-pulse reflected off the sample is clearly visible. By subtracting this background from the data, we isolate the frequency-converted NV signal (red) displaying the characteristic exponential decay.

In remote entanglement experiments, the effect of noise counts can be mitigated by defining a heralding detection time window: only photon counts in this window are taken as valid entanglement heralding events [10]. In general, setting the heralding window involves a trade-off between high signal-to-background and thus high fidelity (favouring shorter windows) and success rate (favouring longer windows). In Fig. I.3.3c we plot the signal-to-background ratio (SBR) for the two detectors as a function of photon detection time. The SBR is bounded on one side by the leaked excitation pulse and on the other side by the NV signal approaching the uniform background. For the analysis of the two-photon interference visibility (Fig. I.3.4a), we apply a detection window in which the average SBR exceeds 10 (Fig. I.3.3c, up to dashed line). For a more detailed comparison of our model to the data (Fig. I.3.4b) we use an extended window (up to dash-dot line). In order to maintain the same SBR throughout the experiment, we employ a system of automatic optimization based on the live monitoring and processing of the single photon detection events (see Supplementary Info I.3.6.5, I.3.10 and I.3.11).

I.3

I.3.4. TWO-PHOTON QUANTUM INTERFERENCE

Next we investigate the distinguishability of the photons emitted by the two nodes by analyzing their quantum interference. For two fully indistinguishable photons impinging on the input ports of a balanced beam splitter, quantum interference leads to vanishing probability to detect one photon in each output port [25], while for fully distinguishable photons this probability is 0.5 [36, 37]. From the (properly normalized) coincidence counts in the two detectors we can thus extract the distinguishability of the photons.

Figure I.3.4a) shows the measured coincident detections between the two output arms without any background subtraction. Each excitation round is treated as a “detection bin” in which a photon can arrive. We analyze the coincidences per block of 10 excitation pulses, defined as a click in both detectors in the same or two different detection bins. This leads to a maximum detection absolute bin difference of 9 and a coincidence probability increasing linearly towards 0 bin difference. We overlay the data with a model based on independently determined parameters, treating the photons as completely distinguishable (see Supplementary Information). For the non-zero bin differences, in which the NV photons are fully distinguishable by their arrival time difference of at least 10x the lifetime, the model shows excellent agreement with the measured coincidences. In stark contrast, we observe a strong reduction in measured coincidences compared to the model for the zero bin difference. This drop in coincidences when the photons arrive in the same bin is the hallmark of two-photon quantum interference and forms the main result of this work.

The observed visibility is defined as $V = 1 - \frac{C_M}{C_{Dist}}$, with C_M the measured number of coincidences, and C_{Dist} the coincidences we would have measured at zero bin difference in case the photons were completely distinguishable. In the inset of Fig. I.3.4a we show the method of extracting the visibility. First we use a linear fit to the total distinguishable coincidences per detection bin difference to get C_E, the extrapolated coincidences for 0 bin difference. From this value we extract C_{Dist}, by correcting for the imbalanced emission rates (see Supplementary Inf I.3.6.6). The resulting visibility is $V = 0.79 \pm 0.03$, which is well above the classical bound of 0.5 [36, 37], proving the successful demonstration of quantum interference of single photons in the telecom L-band.

A more detailed picture of the temporal shape of the coincidences allows us to test our model with more precision (Fig. I.3.4b). The accumulated coincidences for non-zero bin difference (top panel) show a characteristic shape dominated by the exponential decay of the NV emission. The data is well described by our model that takes into account the temporal shape of the NV-NV, background-NV and background-background coincidence contributions (derivation in Supplementary Info I.3.6.8). The temporal histogram of coincidences within the same bin (bottom panel) shows a good match with the temporal shape predicted by our model. In particular, we observe no reduction of coincidences at 0 time delay, consistent with the visibility being limited by background counts rather than frequency differences between emitted photons [38, 39].

With our knowledge of the background and signal rates we can extract the degree of indistinguishability of the emission coming from our NV centers. We perform a Monte-Carlo simulation of our dataset using the independently determined parameters and apply Bayesian inference to find the most likely value of the indistinguishability, given our measured result (see Supplementary Info I.3.6.9 and I.3.7).

In Fig. I.3.4c we plot the visibility and the extracted photon indistinguishability for increasing detection time window lengths. While the visibility drops for longer windows consistent with the decreasing signal-to-background ratio, the indistinguishability of the NV photons remains high around 0.9. We note that this latter value is similar to values found for NV-NV two-photon quantum interference without frequency conversion [11], confirming that our conversion scheme including the frequency stabilization to a single target wavelength preserves the original photon indistinguishability, and enables solid-state entanglement generation via entanglement swapping.

I.3.5. Conclusion and Outlook

We have shown quantum interference of single photons emitted by spectrally distinct NV centers, by converting them to the same telecom wavelength. We have demonstrated an actively stabilized Quantum Frequency Conversion scheme using Difference Frequency Generation on fully independent nodes. The design and implementation allow for the scheme to be used at large distances. Furthermore, the techniques can be readily transferred to other quantum emitters in the visible regime with minimal adaptations to the conversion optics and control schemes used.

Future improvements to our system can increase the performance in multiple ways. First, adapting our optical design to prevent detector blinding by the stabilization light can lower the detector contribution to the background counts to the design level of 5 Hz. Second, a different approach to the QFC technique based on a bulk crystal may remove the (currently dominating) SPDC background noise due to poling irregularities. Third, the signal level of collected coherent photons from the NV centers could be improved significantly by use of an open microcavity [40, 41]. In particular, achieving a fraction of coherent emission of 46% as reported in Ref. [40] would raise the signal-to-background ratio above 200. Finally, by extending the hardware we can stabilize the optical phase of the single photons emitted by the NV centers, enabling entanglement generation upon heralding of a single photon [23].

By combining the protocols demonstrated here with established spin-photon entangling operations and photon heralding at the midpoint [10, 11], remote NV centers can be projected in an entangled state via telecom photons. Owing to the low propagation loss of these photons and extendable control scheme, our results pave the way for entanglement between solid-state qubits over deployed fiber at metropolitan scale.

I.3.6. SUPPLEMENTARY MATERIALS

I.3.6.1. OPTICAL SET-UP

Our experiments are performed using two nominally identical quantum network nodes. Each node houses a Nitrogen-Vacancy (NV) center in a high-purity type-IIa chemical-vapor-deposition diamond cut along the ⟨111⟩ crystal orientation (Element Six). Both samples have a natural abundance of carbon isotopes. Fabrication of solid immersion lenses and an anti-reflection coating on the diamond samples enhances the photon-collection efficiencies from the NV centers. The ground-state spin levels are split using a small permanent magnetic field aligned with the NV axis of $\approx 30\,\mathrm{G}$.

Experimental equipment used for each node is summarized in Tab. I.3.1. Node 1 and 2 are in the same laboratory, around 7 m apart. The optical fibers that connect Node 1 and 2 with the first midpoint 19" rack containing the filters are PM fibers of 3 m and 10 m long, respectively. After the filters, both are connected to the beamsplitter and subsequently the SNSPDs in a separate 19" rack in the room next door with 10 m long PM fibers.

Details of the optical lay-out of the free-space and in-fibre optics used are shown in figure 1B. For initialization in the correct charge and spin state, we use a combination of off-resonant (515 nm) and resonant (637 nm) excitation respectively. Both lasers are combined using in-fibre optics, and coupled into the free-space part using a beam sampler optimized for transmission. For single-photon generation, we use a second resonant laser tuned to a spin-preserving transition. Both resonant lasers are stabilized using a wave meter. The main part of the excitation light passes electro- and acoustic- optical modulation (EOM and AOM) for fast switching, and is coupled into the free-space path using a central polarizing beam splitter (Thorlabs). Combined, this light is guided to the high NA microscope objective (Olympus 100x 0.9NA) using a dichroic mirror (DM) (Semrock), after which the polarization is set at an optimum for cross-polarization. The second part of the excitation laser is sent to a separate set of AOMs that provide an offset in frequency to form the stabilization light and coupled in on the opposite side of the central PBS. The main purpose of this light is to provide a fixed frequency reference of the single photons generated by the excitation light, and its purpose can be extended to stabilize the phase of the relevant phases for entanglement generation [23, 42].

Emission from the NV-centre propagates backwards through the set-up, where the phonon side-band (PSB) is separated from the main path using the DM, filtered by additional long-pass filters (Semrock) and coupled into a multi-node fibre to be detected locally by an APD (LaserComponents). During the measurement, detection in this path is used for live monitoring and diagnostic purposes. The resonantly emitted photons in the zero-phonon line (ZPL) are guided to the central PBS, separated from the excitation light based on polarization (Thorlabs), and filtered using a band pass filter (Semrock). We use a deformable mirror and a set of motorized mirrors to couple in both the single photons and frequency control light simultaneously into the same PM SMF. Using these components, we can periodically optimize the coupling remotely, greatly improving the long-term performance and remote operation capabilities. By coupling into a fibre, we can decouple the alignment of the free-space optics from the QFC optics, simplifying the set-up and allowing for easy exchange of different QFC modules (full details of equipment list in Tab. I.3.1 and I.3.2.

I.3.6.2. Overview of timing electronics

Interfering photons emitted by two NV centres with high fidelity places strict requirements on the arrival time and thus the generation time of the single photons. Future long distances between our nodes prevent us from using a single waveform generator to meet these requirements, and a more scalable approach is needed, which we have employed for the current experiment. The lay-out is shown in figure I.3.14 (full equipment in I.3.3), showing how a single GPS disciplined clock is shared across the nodes via White-Rabbit enabled switches. The resulting synchronization pulses are then coherently split and distributed to the devices requiring timing synchronization. The microcontrollers EVENT cycles are externally triggered by a 1 MHz pulse. The AWG sequencers are referenced externally by the 10 MHz. Furthermore, the waveform generation inside the AWG is triggered using the 5 kHz heartbeat, after which the AWG sequencer can realize a sub nanosecond delay. Together, this allows for the long range synchronization of the experimental sequence with a jitter of 100 ps.

For future experiments, the heartbeat can be adjusted by changing the settings of the heartbeat generator. This would allow to run the frequency stabilization at a higher rate needed for the higher feedback bandwidth for phase-locking of two remote excitation lasers.

I.3.6.3. Overview experimental sequence.

The experimental sequence is given in more detail in Fig. I.3.5. The CR-check procedure contains a bright off-resonant charge reset pulse to probabilistically re-ionize the NV centre into the negative charge state. We then verify that the lasers are resonant with the right transitions by monitoring the fluorescence during excitation with both the spin reset and excitation laser. The counts during this interval are compared to a threshold determined before the experiment. If past this threshold, we assume to be on resonance and in the right charge state. This procedure is repeated until success, and has a typical passing rate of 5 – 10%, taking on average 1.5 ms[35]. The amount of experimental sequences per CR-checking round is a balance between ionization to the NV^0 state during the sequence and data rate. At the start of each CR-check we find the NV centres to be ionized in about 10% of the cases per node.

The communication between the nodes signalling the ready state is done by exchanging a digital trigger between the micro-controllers in charge of the CR-check process. By using the predetermined travel time of the communication, each micro-controller can calculate the next available starting time upon receiving the digital trigger of the opposite node. Using this information it triggers the AWG in advance of that heartbeat, reliably triggering the AWGs that switch to playing the waveforms that generate the optical pulses needed for photon generation. During the live analysis of the data, the experiment markers are used to signal the generation of single photons. These markers are in sync with the heartbeat present on the midpoint, and allow for the faithful recovery of the single photon events. Future improvements can be made by actively heralding the arrival of photons in the midpoint, conditioned on receiving the experiment signal.

I.3.6.4. DATA COLLECTION AND PROCESSING

The data taken shown in Fig. I.3.3 and Fig. I.3.4 was taken over the course of 17 days. To allow for long-duration remote experiments, we operate the set-ups with minimal manual in-situ intervention, and employ a multitude of automatic calibrations. We determined the amount of data to collect by using previous measurements of coincidence rates and targeting an approximate statistical errorbar of 3% on the measured visibility.

The data was collected in batches of ≈ 24 hours, during which the set-up was operating fully autonomously. Remote monitoring was made possible by live viewing in a Grafana dashboard showing performance and environmental data pushed to a database. Live warnings of parameters that went outside pre-defined ranges provided 24/7 warnings, and the possibility to manually intervene remotely. After each block of 24 hours, manual routine inspections were done to check the sample and set-up status. As an example of the benefits of this system, the interference data was collected over a period of 17 days, of which 78% of the wallclock time under autonomous operation of the complete system, during which no human operator actively controlled the experiment.

DATA PROCESSING

We employ various data processing steps during the experiment. First, all the raw data generated by the Adwin counting modules describing the result of the CR-checking process on the nodes is written to disk every ≈ 2 of minutes, and a next block of measurements is started. Simultaneously the stream of time tags of all synchronizations (heartbeat and experiment marker), and all SNSPD events outside of the blinding window, are tagged using 80 ps bins, and saved to disk on dedicated node PCs every couple of seconds, totalling to ≈ 1.2Tb of uncompressed data.

Because performing the analysis on large amounts of raw data is challenging, we employ live processing that generates significantly smaller files. This processing stores only the photon events that might be of interest for further analysis, by looking at the time bins where converted single photons from the nodes are expected to arrive in the midpoint (see Fig. I.3.5). The data stored when an event occurs is given in Tab. I.3.4, which can be extracted from the combined stream of timetagged events from all 3 timetaggers. One experiment marker can have more than one event (e.g. coincidences). The size of this dataset is less than 0.5% of the raw data generated, making it much more manageable.

While analyzing the coincidence data we noticed that some blocks contain many events that happen at time intervals much shorter than the dead time of our detectors (20 ns). We suspect that these events are due to (yet unexplained) resonances in the biasing electronics of the SNSPDs. To filter out these events we ignore blocks of measurements in which more than 2 detection events have happened in a single 160 ns window for both the SNSPDs. We can give an upper bound on how many events we would expect of this kind based on our signal rate by taking the maximum singles detection rate in Fig. I.3.3b (3000 Hz) for the full duration of the 160 ns. Then, the probability of having more than 2 counts in both nanowires simultaneously is given by $P(C>2)^2$ with

$$P(C>2) = 1 - P(C=0) - P(C=1) - P(C=2) \tag{I.3.1}$$

the chance of having more than 2 counts in one nanowire. For the amount of repetitions of our experiment ($282226000000 \approx 2.8 * 10^{11}$), we thus conservatively expect 0.015 of these occurrences. When applying this filter we remove ≈ 36 blocks which equates to 0.05% of the total data.

I.3.6.5. AUTOMATED CALIBRATIONS

Keeping multiple nodes at their pre-calibrated performance level in parallel requires an automated calibration framework, in which several setup-specific calibrations can be performed both in parallel and successively, where the order of calibrations is conditional on setup specific inter-dependencies. After a constant amount of optical excitations, each node's performance is evaluated against several parameters that are indicative for the NV photon emission, conversion and collection rate per node, listed below in Sec. I.3.6.5. Every parameter has a specific threshold chosen to reflect the manually calibrated performance level at the time of initialization of each dataset taken per day. A visual representation of the automated calibration framework is shown in Fig. I.3.10. Violation of the pre-calibrated parameter thresholds triggers adding specific calibrations to the 'calibration queue', where the calibrations are ordered by setup specific inter-dependencies and subsequently executed, parallelizing calibrations on nodes as much as possible.

Every individual calibration that will block the optical path output of the QFC temporarily freezes the frequency lock's feedback loop for the duration of the calibration, schematically shown in Fig. I.3.11. We require this when calibrating the QFC efficiency with path-blocking flip-in power meters, as well as using a diagnostic flip-in mirror to measure NV excitation resonant laser light and photons coupling in to the QFC. The lock feedback loop is resumed after every such a calibration to ensure the locking feedback scheme can keep up with longer term drifts of the locking beat frequency.

EVALUATED PERFORMANCE PARAMETERS

- **Count-per-shot of PSB photons ($\mathbf{CPS_{PSB}}$)**: The amount of photon detections in the PSB per excitation attempt contains information on how well we address the relevant transition with the optical excitation pulse. A reduction in CPS_{PSB} can thus trigger all available node-related calibrations, including re-calibration of the power of the excitation pulse, but only of the specific node on which this is detected.

- **Average CR-check passing rate**: Indicative of the stability of optical addressability of the NV center's transitions.

- **Fixed amount of optical excitations**: Recalibration of each node is performed regardless of performance thresholds after a fixed amount of attempts, both for logging purposes of small drifts as well as certainty about bringing the setup to a well calibrated known state, mitigating any drifts we could not observe while the experiment is live.

- **Count-per-shot of telecom photons from NV excitation ($\mathbf{CPS_{tel}}$)**: The amount of single telecom photons incident on the SNSPD detectors per excitation attempt show a performance of the entire node: the entire optical path the single photons traverse until detection at the SNSPD detectors. This also includes the intrinsic performance of the QFC, which is calibrated separately.

These measurements also enable us to collect the data crucial for the further analysis of the two-photon quantum interference: the probability of detecting a photon from Node 1 or 2 in detector A and B and the rate of background counts detected in detector A and B. An overview of the average value and standard deviation per measurement dataset is shown in Fig. I.3.6. How these values are used for further calculations is explained in the next section.

I.3.6.6. MODEL OF COINCIDENCE PROBABILITIES

In this section we will give details on the model used to calculate the expected coincidence probabilities assuming both completely distinguishable photons and (partially) indistinguishable photons with an indistinguishability η. We collect coincidences in 19 distinct difference bins (-9 ... 9) which are generated as follows: Once both nodes have indicated their ready-state we perform 10 pulsed excitations. This results in 10 consecutive time windows in which we can detect single photons emitted from the NV centers. For each detected photon we are looking for photon coincidences (i.e. events for which also the other detector clicked). We consider coincidence events where both photons were detected in the same time window (these coincidences are shown in the zero-difference bin) as well as photon detections in different time windows. Depending on the difference in time window number we assign these coincidences to one of the 19 possible bin number differences, numbered from -9 to 9, as shown in Fig. I.3.4a of the main text. Due to the finite number of time windows, the probability of detecting a coincidence decreases for higher bin number differences. The probability of detecting a coincidence for any given bin number difference is thus given by $P_{det} = sP_{coinc}$ with the scaling factor $s = 10 - |bin|$ where bin is the bin number difference. The probability of detecting a coincidence is:

$$P_{coinc} = P_{NVNV} + P_{NVDC} + P_{DCDC} \tag{I.3.2}$$

where P_{NVNV} is the probability of a coincidence between two photons emitted by an NV center, P_{NVDC} is the probability of a coincidence between an NV emitted photon and a dark count (or other noise or background count) and P_{DCDC} is the probability of a coincidence between two dark counts.

I.3

For the non-zero bin number differences these probabilities are given by

$$P_{NVNV} = p_{1A}p_{2B} + p_{1B}p_{2A} + p_{1A}p_{1B} + p_{2A}p_{2B} \tag{I.3.3}$$
$$P_{NVDC} = p_{DC_A}(p_{1B} + p_{2B}) + p_{DC_B}(p_{1A} + p_{2A}) \tag{I.3.4}$$
$$P_{DCDC} = p_{DC_A}p_{DC_B} \tag{I.3.5}$$

where $p_{1(2)A(B)}$ is the probability of a photon emitted by node 1 (2) to be detected in detector A (B) and $p_{DC_A(B)}$ is the probability of a dark count in detector A (B). All these parameters are measured during the experiment by having excitation rounds from only a single node interleaved with the normal excitation rounds.

As the single emitter nature of our NV center does not permit two photons from the same NV within one time window (up to a small probability of double excitation which we neglect in this model), in the zero bin number difference P_{NVNV} reduces to the following expression:

$$P_{NVNV,0bin} = (p_{1A}p_{2B} + p_{1B}p_{2A})(1-\eta) \tag{I.3.6}$$

while P_{NVDC} and P_{DCDC} remain the same. Here η is the indistinguishability, which represents the reduction of the probability of getting an coincidence from NV contributions. This single parameter in our model takes into account the possible sources of distinguishibility such as spectral/temporal offset and polarization differences.

I.3.6.7. Calculating the visibility with unbalanced emitters

We define Visibility using the ratio between coincidence counts in the case that photons are fully distinguishable C_{dist} and coincidence counts we measured, C_M.

$$V = 1 - \frac{C_M}{C_{dist}} \tag{I.3.7}$$

We can directly extract C_M from our experiment, as it corresponds to the measured coincidences in the zero-difference bin. In our model, it is given by filling in Eq. I.3.6 and I.3.3 into Eq. I.3.2:

$$P_M = (p_{1A}p_{2B} + p_{1B}p_{2A})(1-\eta) + p_{DC_A}(p_{1B} + p_{2B}) + p_{DC_B}(p_{1A} + p_{2A}) + p_{DC_A}p_{DC_B} \tag{I.3.8}$$

However, we do not have such direct access to C_{dist}. To extract C_{dist} from measured parameters we fit the number of coincidences in the non-zero bins using a linear fit (as shown in Figure 4 of the main text), and use this to extrapolate the value in the zero-bin, which we will call C_E. This extrapolation will overestimate the coincidences we would get in the zero bin number difference for perfectly distinguishable photons as the non zero bin number differences also include coincidences of photons emitted from the same NV, a case that does not occur in the zero bin number difference. To determine the necessary correction we compare the probability of a coincidence in the zero bin number difference for $\eta = 0$

$$P_{dist} = (p_{1A}p_{2B} + p_{1B}p_{2A}) + p_{DC_A}(p_{1B} + p_{2B}) + p_{DC_B}(p_{1A} + p_{2A}) + p_{DC_A}p_{DC_B} \tag{I.3.9}$$

with P_E, the probability for an extrapolated zero-bin using the fit of the non-zero bins

$$P_E = (p_{1A}p_{2B} + p_{1B}p_{2A}) + (p_{1A}p_{1B} + p_{2A}p_{2B}) + p_{DC_A}(p_{1B} + p_{2B}) + p_{DC_B}(p_{1A} + p_{2A}) + p_{DC_A}p_{DC_B} \tag{I.3.10}$$

Resulting in the following correction for the C_E, where we use $C_E = P_E N_{attempt}$

$$C_{dist} = C_E - (p_{1A}p_{1B} + p_{2A}p_{2B})N_{attempt} \tag{I.3.11}$$

Here we have used the number of experimental attempts $N_{attempt}$ (i.e. the number of excitation pulses sent to the NV center over the course of the entire experiment). We note that in case the used beamsplitter is strongly imbalanced this would also affect the number of coincidences in the zero bin number difference. In particular, our determined indistinguishability would be scaled by an additional correction factor to $\eta(1 - \frac{(R-T)^2}{(R^2+T^2)})$ with the beam splitter reflectivity R and transmitivity T. Using the specified values of our beam splitter $R = 0.496$ and $T = 0.504$, we find that this effect is on the order of $\eta(1-10^{-4})$ and we therefore neglect it in our model.

I.3.6.8. MODEL OF TEMPORAL SHAPE OF DISTINGUISHABLE COINCIDENCES

The analysis of the measured coincidences with respect to their arrival time difference holds a vast amount of information of the (relative) emitter properties. In our case, it is difficult to extract detailed information about the NV centres from the measured coincidences in the zero-difference bin as the vast majority of these coincidences involves background counts. We can, however, model the different temporal shape of the three contributions as mentioned in I.3.2 in the non-zero difference bins. Analogous to Kambs [39] we start by writing down the photon wave-packets of the individual events. The single photon wave function an NV-centre from spontaneous emission (ignoring any spectral and phase information) is given by

$$\phi_{NV}(t) = \frac{1}{\sqrt{\tau(e^{\frac{-T_{start}}{\tau}} - e^{\frac{-T_{end}}{\tau}})}} e^{-\frac{t}{2\tau}} H(t - T_{start})(1 - H(t - T_{end})) \tag{I.3.12}$$

where τ =12.5 ns the lifetime of the excited state. We can define $W(t) \equiv H(t - T_{start})(1 - H(t - T_{end})$ to be the selected window with start(end) time $T_{start}(T_{end})$ both larger than 0. $H(t)$ is the Heaviside step function. Here we have chosen $t = 0$ to be the moment the infinitely short optical excitation would have arrived in the detector as the start of the exponentially decaying wave-packet. We now assume that both NV centres have the same excited state lifetime, and the beamsplitter ratio to be perfect. The joint detection probability is given by:

$$P_{joint}(t, \Delta t) = \frac{1}{4}|\phi_i(t+\Delta t)\phi_j(t) - \phi_j(t+\Delta t)\phi_i(t)|^2 \tag{I.3.13}$$

A background photon at the beamsplitter is modeled as a process that has a uniform probability density in time:

$$P_{DC}(t) = \frac{1}{(T_{end} - T_{start})} W(t) \tag{I.3.14}$$

Here we assume that the contribution of background noise is constant in time, which is a good approximation for the darkcounts of the detector and SPDC noise coming from the QFC process. For the excitation pulse leakage this approximation does not hold, but we assume this error to be small if we limit the amount of pulse light in our analysis window. For completely distinguishable events the interference term in the joint detection probability drops out, and it simplifies to:

$$P_{joint}^{dist}(t,\Delta t) = \frac{1}{4}(P_i(t+\Delta t)P_j(t) + P_j(t+\Delta t)P_i(t)) \tag{I.3.15}$$

with $P_i(t) = |\phi_i(t)|^2$. To obtain the second order cross-correlation function we integrate over the detection times of the single photons. The NV-NV contribution is therefore given by:

$$\mathcal{G}^{(2)}_{NVNV}(\Delta t) = \int_{-\infty}^{\infty} \frac{1}{4}\, 2P_{NV}(t')P_{NV}(t'+\Delta t)dt' = \tag{I.3.16}$$

$$\frac{1}{2\tau^2(e^{\frac{-T_{start}}{\tau}} - e^{\frac{-T_{end}}{\tau}})^2} \int_{-\infty}^{\infty} e^{-\frac{t'}{\tau}} e^{-\frac{t'+\Delta t}{\tau}} W(t')W(t'+\Delta t)dt' \tag{I.3.17}$$

We can solve this integral by breaking it up for positive and negative Δt, and absorbing the Heavisides accordingly in the integration limits. For $\Delta t > 0$ we get:

$$\begin{aligned}\frac{1}{2\tau^2(e^{\frac{-T_{start}}{\tau}} - e^{\frac{-T_{end}}{\tau}})^2} &\int_{T_{start}}^{T_{end}-\Delta t} (e^{-\frac{t'}{\tau}} e^{-\frac{t'+\Delta t}{\tau}})\, dt' \\ &= \frac{1}{4\tau(e^{\frac{-T_{start}}{\tau}} - e^{\frac{-T_{end}}{\tau}})^2}(-e^{\frac{-2T_{end}-\Delta t}{\tau}} + e^{\frac{-2T_{start}+\Delta t}{\tau}})\end{aligned} \tag{I.3.18}$$

For $\Delta t < 0$ we get:

$$\begin{aligned}\frac{1}{2\tau^2(e^{\frac{-T_{start}}{\tau}} - e^{\frac{-T_{end}}{\tau}})^2} &\int_{T_{start}-\Delta t}^{T_{end}} (e^{-\frac{t'}{2\tau}} e^{-\frac{t'+\Delta t}{2\tau}})\, dt' \\ &= \frac{1}{4\tau(e^{\frac{-T_{start}}{\tau}} - e^{\frac{-T_{end}}{\tau}})^2}(-e^{\frac{-2T_{end}+\Delta t}{\tau}} + e^{\frac{-2T_{start}-\Delta t}{\tau}})\end{aligned} \tag{I.3.19}$$

which, after combining both, arrive at the expression for $\Delta t \in [-(T_{end} - T_{start}), T_{end} - T_{start}]$:

$$\mathcal{G}_{NVNV}(\Delta t) = \frac{1}{4\tau(e^{\frac{-T_{start}}{\tau}} - e^{\frac{-T_{end}}{\tau}})^2}(e^{\frac{2T_{start}+|\Delta t|}{\tau}} - e^{\frac{2T_{end}-|\Delta t|}{\tau}}) \tag{I.3.20}$$

As a sanity check, we can integrate $\mathcal{G}_{NVNV}(\Delta t)$ over the interval $[-(T_{end} - T_{start}), T_{end} - T_{start}]$, to get the overall probability to get a coincidence in our window:

$$\int_{-(T_{end}-T_{start})}^{T_{end}-T_{start}} \mathcal{G}_{NVNV}(\Delta t)d\Delta t \tag{I.3.21}$$

which, by separately integrating the for negative and positive Δt results in

$$\frac{1}{4\tau(e^{\frac{-T_{start}}{\tau}} - e^{\frac{-T_{end}}{\tau}})^2}\tau\left((e^{\frac{-T_{start}}{\tau}} - e^{\frac{-T_{end}}{\tau}})^2 + (e^{\frac{-T_{start}}{\tau}} - e^{\frac{-T_{end}}{\tau}})^2\right) = \frac{1}{2} \tag{I.3.22}$$

This is what we would expect for two completely distinguishable photons. Following the same approach, we can calculate the integral for the NV-DC as

$$\mathscr{G}^{(2)}_{NVDC}(\Delta t) = \int_{T_{start}}^{T_{end}} \frac{1}{4}(P_{NV}(t'+\Delta t)P_{DC}(t') + P_{DC}(t'+\Delta t)P_{NV}(t'))\,dt' = \tag{I.3.23}$$

$$\frac{e^{\frac{-T_{start}}{\tau}} - e^{-\frac{T_{end}-|\Delta t|}{\tau}} + e^{-\frac{T_{start}+|\Delta t|}{\tau}} - e^{\frac{-T_{end}}{\tau}}}{4\tau(T_{end}-T_{start})(e^{\frac{-T_{start}}{\tau}} - e^{\frac{-T_{end}}{\tau}})} \tag{I.3.24}$$

For the DC-DC contribution we get

$$\mathscr{G}^{(2)}_{DCDC}(\Delta t) = \int_{T_{start}}^{T_{end}} \frac{1}{4}(P_{DC}(t'+\Delta t)P_{DC}(t') + P_{DC}(t'+\Delta t)P_{DC}(t'))\,dt'$$

$$= \frac{(T_{end}-T_{start}) - |\Delta t|}{2(T_{end}-T_{start})^2} \tag{I.3.25}$$

that both integrate to $\frac{1}{2}$ over the coincidence window.

Figure I.3.13 shows the shapes of these cross-correlation functions for the different contributions of coincidences in the experiment. The difference between NV-DC and DC-DC contributions is minimal, but the NV-NV shape is clearly distinguishable from the noise sources. The plot in Fig. I.3.4b in the main text is a weighted sum of the three shapes. The weights of for the different contributions are calculated using Eq. I.3.3- I.3.5 and the data shown in Fig. I.3.6. For the numerical values of input parameters used see Tab. I.3.6 For the indistinguishable case, we use the same temporal shape as the distinguishable, and scale the amplitude with $1-\eta$. This is a valid approximation where polarization difference are the dominant contribution with respect to any temporal or spectral effects.

I.3.6.9. MONTE-CARLO BASED DERIVATION OF INDISTINGUISHABILITY USING BAYESIAN INFERENCE

As a next step we use our model to derive an expression for the indistinguishablity η. Due to the stochastic nature of the coincidences observed in our measurement, the calculation of the indistinguishability using standard error propagation like the variance formula can lead to non-physical results for the indistinguishability being in its confidence interval. We prevent this by using Bayesian Inference to find a more accurate confidence interval. In words, we want to know the most likely indistinguishability η_{opt}, given the set of measured coincidences C_M and C_E. Equations I.3.8 and I.3.10 and the number of attempts $N_{attempts}$ give us a direct way of calculating C_M and C_E, based on $p_{1(2)A(B)}$, $p_{DC_{A(B)}}$ (denoted $\bar{\theta}$ in short) and η as described in I.3.6.6. The strategy is then to simulate many realizations of our experiment with η_i the only free parameter, via a Monte-Carlo simulation. We then use the outcomes of these simulations to calculate the likelihood of a certain η, given our measured C_M and C_E via Bayes rule:

$$P(\eta,\bar{\theta}|\bar{M}) = \frac{P(\bar{M}|\eta,\bar{\theta})P(\eta,\bar{\theta})}{P(\bar{M})} = \frac{P(\bar{M}|\bar{\theta},\eta)P(\eta,\bar{\theta})}{\sum_i P(\bar{M}|\bar{\theta},\eta_i)P(\eta_i,\bar{\theta})} \tag{I.3.26}$$

where $P(a|b)$ is the probability of a given b, $\bar{M}$ is the observed measurement outcomes C_M and C_E, and $\bar{\theta}$ the vector containing the parameters that fully describe our experiment.

$P(\eta, \bar{\theta})$ is the probability of the set of parameters *before* our measurement, the so called prior. The only unknown parameter is η, for which we take a uniform distribution on the interval $[0, 1]$, to reflect the assumption of no prior knowledge. All the other parameters θ_j in $\bar{\theta}$ are assumed to be normally distributed, with the mean and variance determined by the independent samples during the measurement, see previous section I.3.6.4 and I.3.6.

Algorithm 1 Monte-Carlo simulation routine to find likelyhood of η_i, based on the inputs $\bar{\theta}$ and $\bar{M}$

for η_i in $[0 \ldots 1]$ **do**
    for θ_j in $\bar{\theta}$ **do**
        Draw N times input parameters $\theta_{\mathbf{n}}$ from $\mathcal{N}(\mu_j, \sigma_j^2)$
        Calculate N values for P_E^n and P_M^n according to eq. S8 and S10
    end for
    for n in $[0, 1, \ldots, N]$ **do**
        Draw K realizations of the measurement outcomes
        $C_E^{Sim} = \text{Poisson}(P_E^n * N_{\text{attempts}})$ and $C_N^{Sim} = \text{Poisson}(P_M^n * N_{\text{attempts}})$
        Store C_E^{Sim} and C_M^{Sim} in array
    end for
    Calculate fraction $\frac{\sum[(C_E^{Sim} = C_E) \wedge (C_M^{Sim} = C_M)]}{N * K}$, which is equal to $P(\bar{M}|\eta, \bar{\theta})$
    Calculate likelyhood of η_i using eq. S23 and store the value.
end for

The algorithm to calculate the posterior distribution of η for a given set of $\bar{\theta}$ and $\bar{M}$ is given in algorithm 1. It captures both the uncertainty in the input parameters $\bar{\theta}$, as well as the statistical fluctuations introduced by the stochastic nature of measuring a rate of coincidences. In our case, the uniform chosen prior means that the normalized likelyhood function produced by the algorithm is directly the probability density function (pdf) for the left hand side of Eq. I.3.26. The pdf's for the calculated indistinguishability of the data shown in Fig. I.3.4a and b are shown in Fig. I.3.7. Here we can clearly see the asymmetry of the calculated distributions, and their cut-off at the maximum of 1. To report this likelyhood as a single value with 'errorbars', we chose the maximum of the likelyhood to be our datapoint, and calculate a symmetric 68% confidence interval around the most likely η. For the datapoints where the most likely indistinguishability is closest to 1, a symmetric confidence interval, with 34% of the probability on either side can not be taken, and asymmetric intervals are used.

I.3.6.10. SNSPD BLINDING INDUCED BACKGROUND

The current lay-out of the in-fibre optics guides the reflected part of the reference light through the same port of the circulator as the single-photons. Therefore the power is aimed directly at the nanowires of the SNSPDs, blinding the dectectors. Additionally, because of the beamsplitter in front of the detectors, the reference light reflected from both UNFs interferes, making the output power oscillate in time. To prevent latching, the manufacturer placed anti-latching shunt resistors in the circuits to prevent the loss of photon counting over timescales of >milliseconds.

However, during the early investigation of the time multiplexing of frequency stabilization with single photon generation, we noticed a blinding-power dependent elevated darkcount rate, persisting long (>10 µs after the end of the blinding pulse. By scanning the incident power on one of the nanowires in a controlled manner (Fig. I.3.8, we can see a clear power dependence of this effect. We reduce the additional background counts to a constant manageable level of 30 Hz by moving our single photon generation by ≈45 µs, and optimizing the reference light power in-situ. Further improvement to the in-fibre optics that reduce the backpropagated power through the FBG and active attenuation shielding the detectors can be employed in the future to remove this background contribution.

I.3.6.11. UNF STABILITY

The UNFs are enclosed in an well-isolated box, with a heating pad and thermometer, temperature controlled by a Team Wavelength TC5. This controller provides ~0.1 mK control of the temperature setpoint. Due to non-homogeneous distribution of temperature inside the box and fluctuating temperature gradients coming from outside the box, with a fixed temperature setpoint we observe significant drift of the UNF frequency if not actively stabilized to a target frequency.

The UNFs are frequency stabilized by measuring the power incident on the detector (Thorlabs PDB482C-AC) that measures the frequency lock beat, extracted as a voltage from a monitoring port of the detector. We stabilize the temperature controller setpoint of the UNF to the relative half-of-maximum transmission point. We calibrate the maximally measured power through each individual UNF by temperature-sweeping them, effectively changing the position of the filters in frequency space. In this calibration, there is no correction for the noise incident on or coming from the detector, . After calibration, we feedback the measured transmission power back to the temperature setpoint of the temperature controller of the UNF with a software implemented PI-control loop.

TRANSMISSION STABILITY

Due to inherent inaccuracies in the active stabilization described above, a spread of transmission powers of the UNFs with respect to their setpoint at the relative half-of-maximum transmission point is observed. This occurs due to the limitation in accuracy of the actual temperature control at the filter and other drifts of fixed in-fiber components in the path that passes through the UNF. Such a drift in frequency of the UNF maximum transmission point results in a reduction of NV photon transmission probability, however the NV conversion target frequency is unaffected. To determine the exact UNF frequency shift with respect to the setpoint, we start with the Cauchy-distribution fit in Fig. I.3.2d of the transmission power T of the reference laser through the filter with respect to frequency f:

$$T(f) = \frac{I}{1+\left(\frac{(f-f_0)}{\gamma}\right)^2} + B, \tag{I.3.27}$$

where f_0 is the location of the filter, 2γ the filter FWHM and I and B a relative scaling factor and offset to background, respectively. We can relate the offset from the half-of-maximum transmission point to a frequency shift on this characteristic shape of the filter by rewriting the above function to be a function of transmission

$$f = f_0 - \gamma\sqrt{-1 + \frac{I}{(T(I+B) - B)}}, \tag{I.3.28}$$

obtaining f by using the filter-specific fit parameters obtained from Eq. I.3.27. The root-minus solution is chosen according to the boundary condition that appropriately reflects the direction of change in frequency for a change in transmission power. With Eq. I.3.28 we can convert a representative stabilized 70 h set of second-interval transmission power data to a relative shift in frequency of the filter with respect to the the half-of-maximum transmission point, in the assumption that all transmission power drift is due to the shift in UNF frequency. The transmission power is not corrected for any other drifts of in-fiber components between the power-stabilized reference laser emission and detection at the beat detector. The residual frequency instability for both filters is shown in Fig. I.3.12.

NV PHOTON TRANSMISSION

From this frequency instability we can calculate the change in average transmission probability of converted photons emitted from the NV center through the UNFs. The emitted NV photons with natural linewidth of $2\gamma_{\mathrm{NV}} \approx 12.7\,\mathrm{MHz}$ [26] have a frequency distribution as the Cauchy distribution

$$P(f) = \frac{1}{\pi\gamma_{\mathrm{NV}}\left(1 + \left(\frac{(f - f_{NV})}{\gamma_{\mathrm{NV}}}\right)^2\right)}, \tag{I.3.29}$$

where f_{NV} is the frequency of our target wavelength (see Fig. I.3.2). We can treat the UNFs as frequency dependent transmission devices, i.e. the Cauchy fit parameters used for Fig. I.3.2D can be used to construct the *probability* of transmission $T_{\mathrm{p}}(f)$ of an incident photon by setting $I = 1, B = 0$ in Eq. I.3.27, resulting in $T(f = f_0) = 1$. The probability of the NV photon transmitting through the UNF filter is then

$$P_{\mathrm{t}} = \int_{-\infty}^{\infty} P(f)\, T_{\mathrm{p}}(f)\, df. \tag{I.3.30}$$

Using the above equation we can calculate the relative change in transmission probability from each UNF's fitted parameters and all frequencies $f_0 \pm 1\,\mathrm{MHz}$, the interval where almost all of the occurrences of the measured filter shift are located. Using numerical methods to approximate the above integral we find that the total transmission of the NV photon is reduced to $\approx 75\%$(UNF1) and $\approx 77\%$ (UNF2) with the filters at the half-of-maximum transmission setpoint, excluding any losses incurred in the physical implementation. For the UNF stability data shown in Fig. I.3.12 we obtain a transmission change of at most $\approx 1.5\%$(UNF1) and $\approx 0.4\%$ (UNF2) for $f_0 \pm 1\,\mathrm{MHz}$ that would solely be ascribable to the frequency shift of the UNFs.

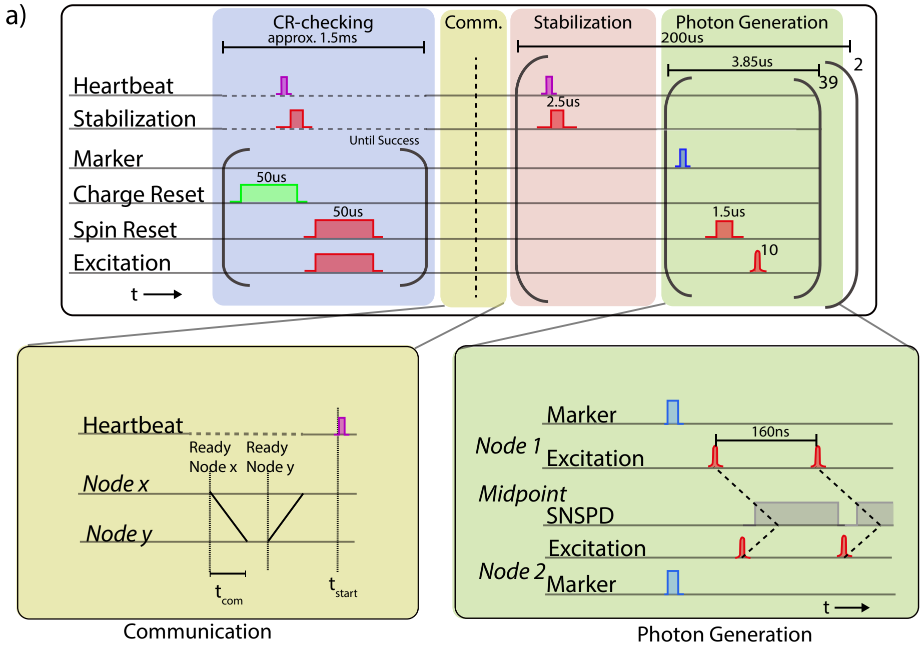

Figure I.3.5: . Schematic showing pulses played during the experiment. The timescale is indicated above the pulses and sequence stages. The communication step (bottom left) is symmetric whether node1 or node2 succeeds first in passing the CR check. The heartbeat where the next stage is started is shown. Using the Marker signals, the corresponding coincidence windows in the SNSPDs in the midpoint can be calculated.

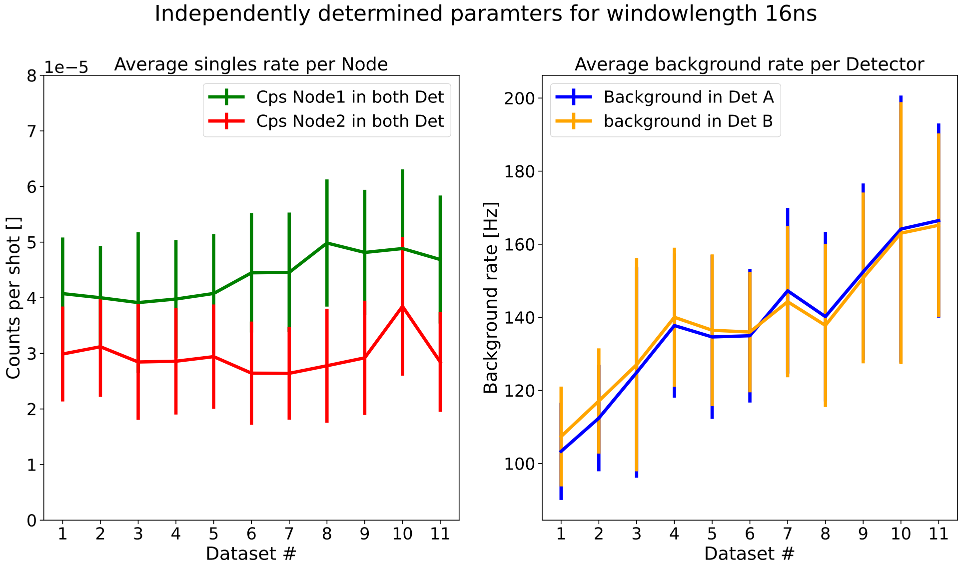

Figure I.3.6: Average of the independently measured parameters for one of the analyzed integration windows. Individual data sets are about 24 hours of measurement. The error-bar on the values is the standard error of the mean. For each datapoint,the parameter is measured during at approximately 2 minute intervals. The signal rate is calculated in the fluorescence window after the excitation as shown in figure I.3.3. The average background rate is calculated using data in between the pulses, far away from the optical excitation and fluorescence. These parameters can be calculated for the different windowlengths using the same dataset. The rise of the background counts during the experiment is currently not understood.

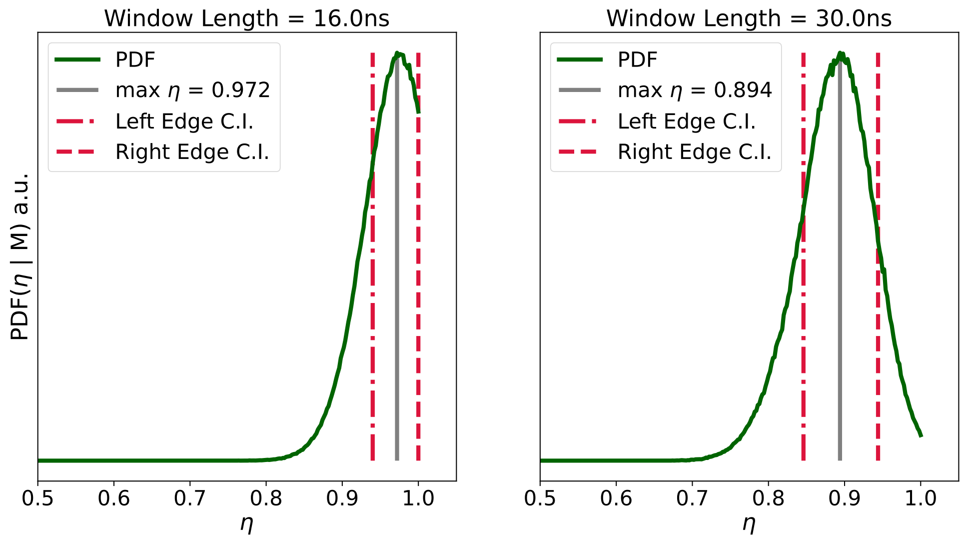

Figure I.3.7: Probability density functions generated by the Monte-Carlo simulations, used for the calculation of the indistinguishability shown in the main text and figureI.3.4. A clear optimum is seen for both the distributions. The asymmetric confidence intervals are the result of the distribution being close to 1, as shown by the distribution for the left figure.

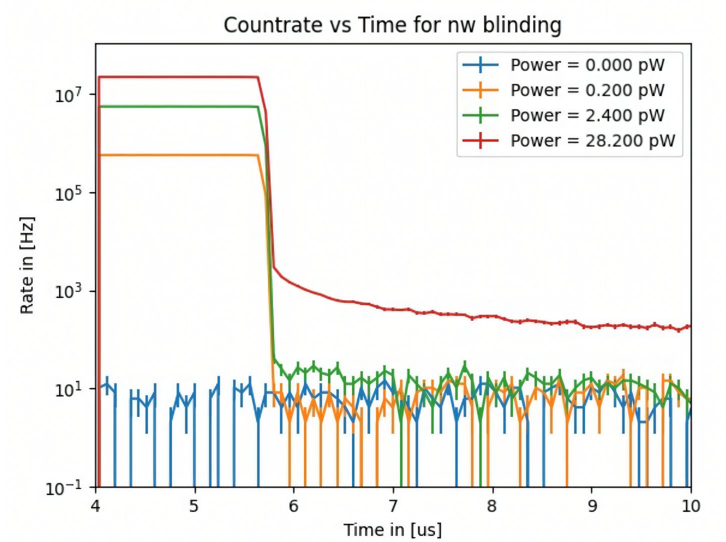

Figure I.3.8: Rate of measured events after a bright blinding pulse in the superconducting nanowire single photon detectors. After the bright pulse we measure an elevated background level as compared to no blinding pulse applied. This effect persists for tens of microseconds, forcing us to delay the single photon generation by more than 45 µs with respect to the frequency stabilization measurement. The optimal powers used during the experiment is not shown, and was optimized in-situ.

I.3

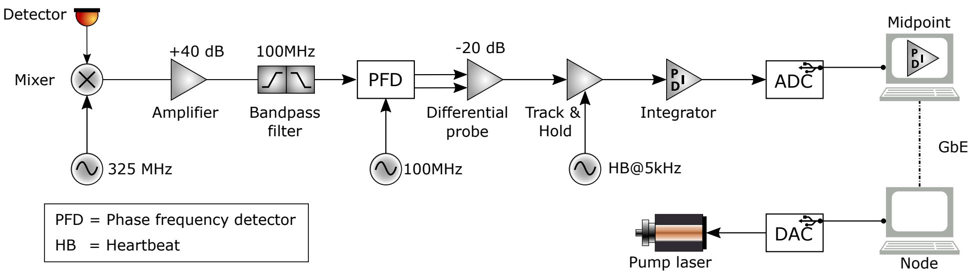

Figure I.3.9: Schematic of frequency lock hardware for one arm of the two-node setup. The optical beat is down-mixed with 325 MHz and then further processed using standard electronics components. The feedback loop is closed using a pair of ADC/DAC over a Gigabit Ethernet connection, resulting in a feedback rate of $\sim 500\,\mathrm{Hz}$.

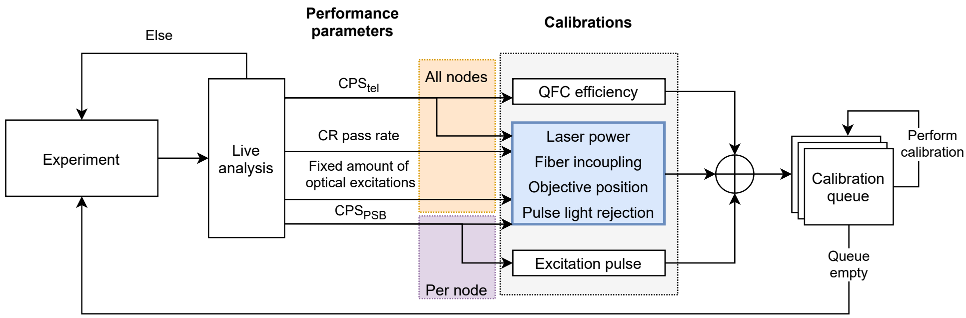

Figure I.3.10: Schematic visualization of the automated calibration framework. At fixed intervals of NV excitation attempts, we perform live an analysis of several variables that triggers specific calibrations per node or on all nodes. The order in which the possible calibrations are performed in the queue is the same as the order in which they are shown in the schematic, reading from top to bottom.

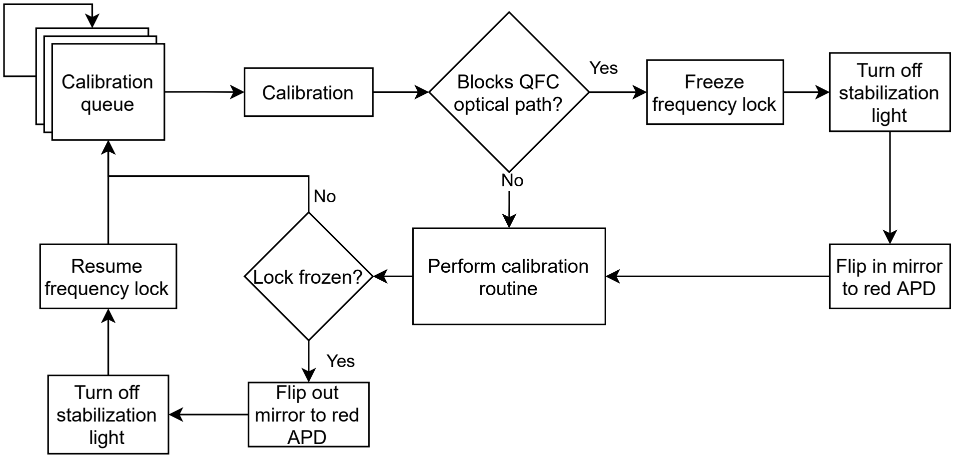

Figure I.3.11: Schematic showing the decision logic deciding if the frequency lock should be frozen before performing a calibration routine. To ensure proper handoff of setup-equipment control, the stabilization light is always turned off before any calibration is started whilst freezing the feedback, if this calibration will block the optical path going through the QFC. Resuming of the lock is an exact reversal of this process, where the stabilization light has to be turned on before the lock's feedback loop is resumed, otherwise no locking beat will be generated.

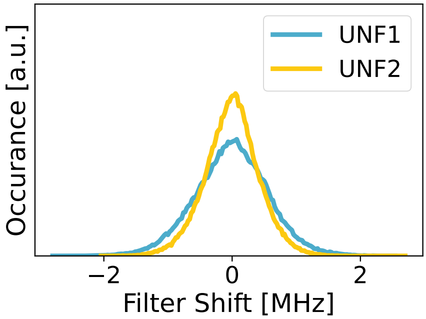

Figure I.3.12: Histogram of the calculated filter shift of both UNFs with respect to their half-of-maximum transmission setpoint over a representative frequency-stabilized 70 h set of second-interval transmission power measurements, in the assumption that all transmission power drift is due to the shift in UNF frequency. From the NV photon and filter overlap we calculate to have at most a change of ≈ 1.5% in transmission power for a change in filter frequency of ±1 MHz, covering approximately 92% and 97% of the spread in filter shift, for UNF1 and UNF2, respectively.

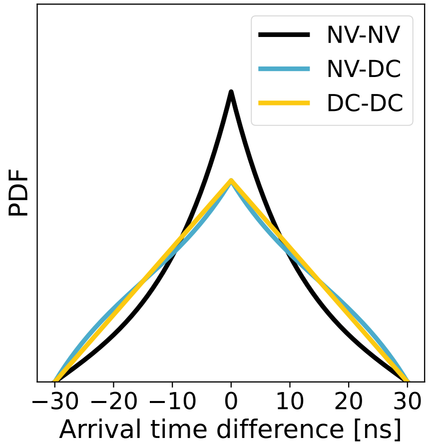

Figure I.3.13: Temporal shape of the three contributions of our model explained in section I.3.6.6 and I.3.6.8.

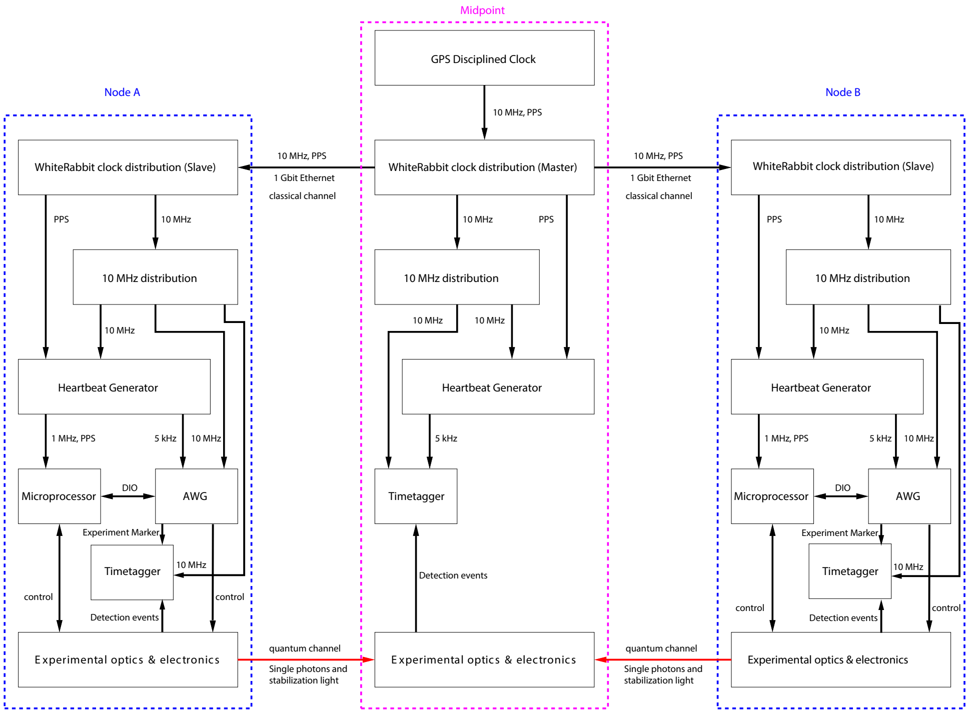

Figure I.3.14: Schematic overview of hardware to synchronize events across the experiment. All connections that distribute the critical timing signals are propagated over telecom fibres on a dedicated fibre. The data that is generated by the timetaggers is sent over the network to a single PC that processes the data. Both the raw and processed data are stored to disk.

Table I.3.1: Experimental equipment used in the two nodes.

Equipment name	Part name/number
Cryostat	Montana Instruments Cryostation S50
Positioners	Microscope objective on 3x PI E-873
Micro-controller	Jäger ADwin-Pro II T12
Arbitrary Waveform Generator AWG	Zürich Instruments HDAWG-8
Excitation laser	Toptica DL pro 637 nm
Spin reset laser	Toptica DL pro 637 nm
Charge reset laser	Cobolt 06-01 515 nm
Reference laser	NKT Photonics 1550 nm Koheras ADJUSTIK E15 PM FM
EOM	Jenaoptik AM635b
AOM	Gooch and Housego Fibre Q 637nm
AOM Driver	Time Base DIM-3000
APD	Laser Component COUNT-10C Photon Countng Module
SNSPDs	Quantum Opus 00-NPD-1588-HDE

Table I.3.2: QFC equipment used in the two nodes.

Equipment name	Part name/number
Pump laser	NKT Photonics 1064 nm Koheras ADJUSTIK Y10 PM FM
Pump laser amplifier	NKT Photonics Koheras BOOSTIK HP
Non-linear Crystal	Custom ppLN crystal NTT
Remote Piezo mirrors	Newport AG-M100n

Table I.3.3: Timing Hardware

Equipment name	Part name/number
GPS-disciplined clock	Stanford Research Systems FS752
Frequency Distribution, between nodes (10MHz, PPS)	OPNT WRS-3/18 White Rabbit Switch
Frequency Distribution, local (10MHz)	Pulse Research Lab PRL-4110
Heartbeat Generator	Tektronix AFG 31022
Micro-controller	Jäger ADwin-Pro II T12
Arbitrary Waveform Generator (AWG)	Zürich Instruments HDAWG-8
Time Tagger	PicoQuant MultiHarp 150 4N

Table I.3.4: Entry in filtered dataset

Field name	Field description	Field data-type
trigger index	Experiment Marker index preceding event in midpoint	uint64
node1 trigger timestamp	Absolute timestamp of corresponding Experiment marker on node1	uint64
node2 trigger timestamp	Absolute timestamp of corresponding Experiment marker on node2	uint64
detection bin index	Index of detection bin this event is detected in	uint32
detA counts	Number of counts measured by nanowire A for this event	uint16
detB counts	Number of counts measured by nanowire B for this event	uint16
detA relative timestamp	Timestamp w.r.t. the start of detection bin of first count measured in nanowire A	int32
detB relative timestamp	Timestamp w.r.t. the start of detection bin of first count measured in nanowire B	int32

Table I.3.5: Frequency lock hardware

Equipment name	Part name/number
Balanced photodetector	Thorlabs PDB482C-AC
Mixer	MiniCircuits ZX05-1l+
Amplifier	Femto DHPVA-201
Bandpass filter	MiniCircuits SBP-100+
Downmix signal generator 325 MHz	AnaPico APSin6010
Beat reference generator 100 MHz	AnaPico APSin6010
Phase-Frequency-Detector	AnalogDevices HMC3716LP4E
Differential probe	Pintek DP-60HS
Track & Hold	Texas Instruments OPA1S2384
Integrator	NewFocus LB1005
ADC, DAC	Analog Discovery 2

Table I.3.6: Numerical values of inputs to calculation and simulations

Window length [ns]	$p_1\,[10^{-5}]$	$p_2\,[10^{-5}]$	$p_{DC_A}\,[10^{-6}]$	$p_{DC_B}\,[10^{-6}]$	C_M	C_{dist}
6	2.1 ± 0.4	1.4 ± 0.4	0.84 ± 0.1	0.84 ± 0.1	13 ± 4	92.37 ± 0.32
8	2.7 ± 0.4	1.8 ± 0.4	1.12 ± 0.15	1.12 ± 0.13	19 ± 4	154.7 ± 0.4
10	3.2 ± 0.4	2.1 ± 0.4	1.40 ± 0.19	1.40 ± 0.17	30 ± 5	221.7 ± 0.5
12	3.7 ± 0.4	2.4 ± 0.4	1.67 ± 0.22	1.68 ± 0.20	37 ± 6	297.9 ± 0.6
14	4.1 ± 0.4	2.7 ± 0.4	1.95 ± 0.26	1.96 ± 0.23	44 ± 7	367.6 ± 0.6
16	4.4 ± 0.4	2.9 ± 0.4	2.23 ± 0.30	2.24 ± 0.27	53 ± 7	436.9 ± 0.7
18	4.7 ± 0.4	3.1 ± 0.4	2.51 ± 0.34	2.52 ± 0.30	74 ± 9	496.5 ± 0.7
20	5.0 ± 0.4	3.2 ± 0.4	2.8 ± 0.4	2.79 ± 0.33	93 ± 10	558.9 ± 0.8
22	5.2 ± 0.4	3.4 ± 0.4	3.1 ± 0.4	3.1 ± 0.4	103 ± 10	611.1 ± 0.8
24	5.4 ± 0.4	3.5 ± 0.4	3.3 ± 0.4	3.4 ± 0.4	118 ± 11	662.9 ± 0.9
26	5.5 ± 0.4	3.6 ± 0.4	3.6 ± 0.5	3.6 ± 0.4	133 ± 12	708.5 ± 0.9
28	5.7 ± 0.4	3.7 ± 0.4	3.9 ± 0.5	3.9 ± 0.5	148 ± 12	749.5 ± 0.9
30	5.8 ± 0.4	3.7 ± 0.4	4.2 ± 0.6	4.2 ± 0.5	159 ± 13	785.7 ± 0.9

REFERENCES

[1] H. J. Kimble, *The quantum internet,* Nature **453**, 1023 (2008).

[2] S. Wehner, D. Elkouss, and R. Hanson, *Quantum internet: A vision for the road ahead,* Science **362** (2018), 10.1126/science.aam9288.

[3] A. Ekert and R. Renner, *The ultimate physical limits of privacy,* Nature **507**, 443 (2014).

[4] L. Jiang, J. M. Taylor, A. S. Sørensen, and M. D. Lukin, *Distributed quantum computation based on small quantum registers,* Physical Review A **76**, 062323 (2007).

[5] D. Gottesman, T. Jennewein, and S. Croke, *Longer-Baseline Telescopes Using Quantum Repeaters,* Physical Review Letters **109**, 070503 (2012).

[6] D. L. Moehring, P. Maunz, S. Olmschenk, K. C. Younge, D. N. Matsukevich, L.-M. Duan, and C. Monroe, *Entanglement of single-atom quantum bits at a distance,* Nature **449**, 68 (2007).

[7] S. Ritter, C. Nölleke, C. Hahn, A. Reiserer, A. Neuzner, M. Uphoff, M. Mücke, E. Figueroa, J. Bochmann, and G. Rempe, *An elementary quantum network of single atoms in optical cavities,* Nature **484**, 195 (2012).

[8] J. Hofmann, M. Krug, N. Ortegel, L. Gérard, M. Weber, W. Rosenfeld, and H. Weinfurter, *Heralded Entanglement Between Widely Separated Atoms,* Science **337**, 72 (2012).

[9] L. Stephenson, D. Nadlinger, B. Nichol, S. An, P. Drmota, T. Ballance, K. Thirumalai, J. Goodwin, D. Lucas, and C. Ballance, *High-Rate, High-Fidelity Entanglement of Qubits Across an Elementary Quantum Network,* Physical Review Letters **124**, 110501 (2020).

[10] H. Bernien, B. Hensen, W. Pfaff, G. Koolstra, M. S. Blok, L. Robledo, T. H. Taminiau, M. Markham, D. J. Twitchen, L. Childress, and R. Hanson, *Heralded entanglement between solid-state qubits separated by three metres,* Nature **497**, 86 (2013).

[11] P. C. Humphreys, N. Kalb, J. P. J. Morits, R. N. Schouten, R. F. L. Vermeulen, D. J. Twitchen, M. Markham, and R. Hanson, *Deterministic delivery of remote entanglement on a quantum network,* Nature **558**, 268 (2018).

[12] A. Delteil, Z. Sun, W.-b. Gao, E. Togan, S. Faelt, and A. Imamoğlu, *Generation of heralded entanglement between distant hole spins,* Nature Physics **12**, 218 (2016).

[13] R. Stockill, M. Stanley, L. Huthmacher, E. Clarke, M. Hugues, A. Miller, C. Matthiesen, C. Le Gall, and M. Atatüre, *Phase-Tuned Entangled State Generation between Distant Spin Qubits,* Physical Review Letters **119**, 010503 (2017).

[14] I. Usmani, C. Clausen, F. Bussières, N. Sangouard, M. Afzelius, and N. Gisin, *Heralded quantum entanglement between two crystals,* Nature Photonics **6**, 234 (2012).

I.3

[15] M. l. G. Puigibert, M. F. Askarani, J. H. Davidson, V. B. Verma, M. D. Shaw, S. W. Nam, T. Lutz, G. C. Amaral, D. Oblak, and W. Tittel, *Entanglement and nonlocality between disparate solid-state quantum memories mediated by photons,* Phys. Rev. Research **2**, 013039 (2020).

[16] D. Lago-Rivera, S. Grandi, J. V. Rakonjac, A. Seri, and H. de Riedmatten, *Telecom-heralded entanglement between multimode solid-state quantum memories,* Nature **594**, 37 (2021).

[17] C. W. Chou, H. de Riedmatten, D. Felinto, S. V. Polyakov, S. J. van Enk, and H. J. Kimble, *Measurement-induced entanglement for excitation stored in remote atomic ensembles,* Nature **438**, 828 (2005).

[18] Y. Yu, F. Ma, X.-Y. Luo, B. Jing, P.-F. Sun, R.-Z. Fang, C.-W. Yang, H. Liu, M.-Y. Zheng, X.-P. Xie, W.-J. Zhang, L.-X. You, Z. Wang, T.-Y. Chen, Q. Zhang, X.-H. Bao, and J.-W. Pan, *Entanglement of two quantum memories via fibres over dozens of kilometres,* Nature **578**, 240 (2020).

[19] R. Riedinger, S. Hong, R. A. Norte, J. A. Slater, J. Shang, A. G. Krause, V. Anant, M. Aspelmeyer, and S. Gröblacher, *Non-classical correlations between single photons and phonons from a mechanical oscillator,* Nature **530**, 313 (2016).

[20] D. Hucul, I. V. Inlek, G. Vittorini, C. Crocker, S. Debnath, S. M. Clark, and C. Monroe, *Modular entanglement of atomic qubits using photons and phonons,* Nature Physics **11**, 37 (2015).

[21] V. Krutyanskiy, M. Meraner, J. Schupp, V. Krcmarsky, H. Hainzer, and B. P. Lanyon, *Light-matter entanglement over 50 km of optical fibre,* npj Quantum Information **5**, 72 (2019).

[22] S. Daiss, S. Langenfeld, S. Welte, E. Distante, P. Thomas, L. Hartung, O. Morin, and G. Rempe, *A quantum-logic gate between distant quantum-network modules,* Science **371**, 614 (2021).

[23] M. Pompili, S. L. N. Hermans, S. Baier, H. K. C. Beukers, P. C. Humphreys, R. N. Schouten, R. F. L. Vermeulen, M. J. Tiggelman, L. dos Santos Martins, B. Dirkse, S. Wehner, and R. Hanson, *Realization of a multinode quantum network of remote solid-state qubits,* Science **372**, 259 (2021).

[24] T. van Leent, M. Bock, F. Fertig, R. Garthoff, S. Eppelt, Y. Zhou, P. Malik, M. Seubert, T. Bauer, W. Rosenfeld, W. Zhang, C. Becher, and H. Weinfurter, *Entangling single atoms over 33 km telecom fibre,* Nature **607**, 69 (2022).

[25] C. K. Hong, Z. Y. Ou, and L. Mandel, *Measurement of subpicosecond time intervals between two photons by interference,* Phys. Rev. Lett. **59**, 2044 (1987).

[26] M. L. Goldman, M. W. Doherty, A. Sipahigil, N. Y. Yao, S. D. Bennett, N. B. Manson, A. Kubanek, and M. D. Lukin, *State-selective intersystem crossing in nitrogen-vacancy centers,* Phys. Rev. B **91**, 165201 (2015).

[27] N. Kalb, P. C. Humphreys, J. J. Slim, and R. Hanson, *Dephasing mechanisms of diamond-based nuclear-spin memories for quantum networks,* Phys. Rev. A **97**, 062330 (2018).

[28] A. Tchebotareva, S. L. N. Hermans, P. C. Humphreys, D. Voigt, P. J. Harmsma, L. K. Cheng, A. L. Verlaan, N. Dijkhuizen, W. de Jong, A. Dréau, and R. Hanson, *Entanglement between a diamond spin qubit and a photonic time-bin qubit at telecom wavelength,* Phys. Rev. Lett. **123**, 063601 (2019).

[29] J. Pelc, C. Langrock, Q. Zhang, and M. Fejer, *Influence of domain disorder on parametric noise in quasi-phase-matched quantum frequency converters,* Optics letters **35**, 2804 (2010).

[30] M. Ruf, M. IJspeert, S. van Dam, N. de Jong, H. van den Berg, G. Evers, and R. Hanson, *Optically coherent nitrogen-vacancy centers in micrometer-thin etched diamond membranes,* Nano Letters **19**, 3987 (2019).

[31] S. Meesala, Y.-I. Sohn, B. Pingault, L. Shao, H. A. Atikian, J. Holzgrafe, M. Gündoğan, C. Stavrakas, A. Sipahigil, C. Chia, R. Evans, M. J. Burek, M. Zhang, L. Wu, J. L. Pacheco, J. Abraham, E. Bielejec, M. D. Lukin, M. Atatüre, and M. Lončar, *Strain engineering of the silicon-vacancy center in diamond,* Phys. Rev. B **97**, 205444 (2018).

[32] J. H. Weber, B. Kambs, J. Kettler, S. Kern, J. Maisch, H. Vural, M. Jetter, S. L. Portalupi, C. Becher, and P. Michler, *Two-photon interference in the telecom c-band after frequency conversion of photons from remote quantum emitters,* Nature Nanotechnology **14**, 23 (2019).

[33] X. You, M.-Y. Zheng, S. Chen, R.-Z. Liu, J. Qin, M. C. Xu, Z. X. Ge, T. H. Chung, Y. K. Qiao, Y. F. Jiang, H. S. Zhong, M. C. Chen, H. Wang, Y. M. He, X. P. Xie, H. Li, L. X. You, C. Schneider, J. Yin, T. Y. Chen, M. Benyoucef, Y.-H. Huo, S. Hoefling, Q. Zhang, C.-Y. Lu, and J.-W. Pan, *Quantum interference between independent solid-state single-photon sources separated by 300 km fiber,* arXiv:2106.15545 (2021).

[34] E. F. Dierikx, A. E. Wallin, T. Fordell, J. Myyry, P. Koponen, M. Merimaa, T. J. Pinkert, J. C. J. Koelemeij, H. Z. Peek, and R. Smets, *White rabbit precision time protocol on long-distance fiber links,* IEEE Transactions on Ultrasonics, Ferroelectrics, and Frequency Control **63**, 945 (2016).

[35] L. Robledo, L. Childress, H. Bernien, B. Hensen, P. F. A. Alkemade, and R. Hanson, *High-fidelity projective read-out of a solid-state spin quantum register,* Nature **477**, 574 (2011).

[36] H. Paul, *Interference between independent photons,* Rev. Mod. Phys. **58**, 209 (1986).

[37] F. Bouchard, A. Sit, Y. Zhang, R. Fickler, F. M. Miatto, Y. Yao, F. Sciarrino, and E. Karimi, *Two-photon interference: the hong–ou–mandel effect,* Reports on Progress in Physics **84**, 012402 (2021).

[38] T. Legero, T. Wilk, A. Kuhn, and G. Rempe, *Time-resolved two-photon quantum interference,* Applied Physics B **77**, 797 (2003).

[39] B. Kambs and C. Becher, *Limitations on the indistinguishability of photons from remote solid state sources,* New Journal of Physics **20**, 115003 (2018).

[40] D. Riedel, I. Söllner, B. J. Shields, S. Starosielec, P. Appel, E. Neu, P. Maletinsky, and R. J. Warburton, *Deterministic enhancement of coherent photon generation from a nitrogen-vacancy center in ultrapure diamond,* Phys. Rev. X **7**, 031040 (2017).

[41] M. Ruf, M. Weaver, S. van Dam, and R. Hanson, *Resonant excitation and purcell enhancement of coherent nitrogen-vacancy centers coupled to a fabry-perot microcavity,* Phys. Rev. Applied **15**, 024049 (2021).

[42] R. Hanson, N. Kalb, P. Humphreys, and E. van Zwet, *Photon exchange based quantum network and method of operating such a network,* (2020).

I.4

EXTENDABLE OPTICAL PHASE SYNCHRONIZATION OF REMOTE AND INDEPENDENT QUANTUM NETWORK NODES OVER DEPLOYED FIBERS

A. J. Stolk, J. J. B. Biemond, K. L. van der Enden, L. van Dooren, E.J. van Zwet, and R. Hanson

Entanglement generation between remote qubit systems is the central tasks for quantum communication. Future quantum networks will have to be compatible with low-loss telecom bands and operate with large separation between qubit nodes. Single-click heralding schemes can be used to increase entanglement rates at the cost of needing an optically phase-synchronized architecture. In this paper we present such a phase synchronization scheme for a metropolitan quantum network, operating in the low-loss telecom L-band. To overcome various challenges such as communication delays and optical power limitations, the scheme consists of multiple tasks that are individually stabilized. We characterize each task, identify the main noise sources, motivate the design choices and describe the synchronization schemes. The performance of each of the tasks is quantified by a transfer-function measurement that investigates the frequency response and feedback bandwidth. Finally we investigate the resulting optical phase stability of the fully deployed system over a continuous period of 10 hours, reporting a short-term stability standard deviation of $\sigma \approx 30\,\mathrm{deg}$ *and a long-term stability of the average optical phase to within a few degrees. The scheme presented served as a key enabling technology for an NV-center based metropolitan quantum link. This scheme is of interest for other quantum network platforms that benefit from an extendable and telecom compatible phase synchronization solution.*

The results of this chapter have been published in Physical Review Applied **23** (1), 014077 (2025).

I.4.1. INTRODUCTION OPTICAL PHASE IN QUANTUM NETWORKS

Quantum networks [1] hold the promise to revolutionize the way people exchange information. A central task of a quantum network is the generation of entanglement between (end-)nodes, in which the entanglement can be stored, manipulated and processed [2]. In general, protocols to generate entanglement between stationary qubits involve the emission, transmission and joint measurement of flying qubits, encoded in a photon state, see Fig. I.4.1a. A common configuration envisioned for a future large scale quantum internet is the combination of nodes, which house the stationary qubits, and midpoints, where the flying qubit from different nodes are sent to. These nodes are connected via deployed telecom fiber to midpoints, that provide synchronization, interference and detection tasks, see Fig. I.4.1b.

Photon loss in the connecting fibers decreases the rate at which entanglement between the nodes is generated, with the exact scaling depending on the photonic qubit encoding used. For example, for frequency encoding [3], polarization encoding [4–8], and time-bin encoding [9–12], the entangling rate scales linearly with the photon transmission η between the nodes. In contrast, for photonic encoding using number states (0 or 1 photon) [13, 14] the rate scales favourably with $\sqrt{\eta}$, yielding significantly higher rates in the typical scenario of substantial photon loss (i.e. for $\eta \ll 1$). However, with this encoding the resulting entangled state phase ϕ is proportional to the optical phase difference between the two paths to the midpoint (θ_1 and θ_2, see Fig. I.4.1a)), leading to the additional experimental requirement that this optical phase difference at the time of interference in the midpoint needs to be known [1].

If the phase deviates from the chosen setpoint by $\delta\phi$, the maximum fidelity achievable is given by $F(\delta\phi) = \frac{1}{2}(1+\cos(\delta\phi))$. In a larger network, the single photons are originating from multiple sources at distant locations, where the phase is affected at many length- and time-scales. Any attempt to stabilize this phase needs to take into account unwanted light from either conversion or the synchronization methods used, that degrade the fidelity of the entangled state. This puts stringent requirements on any classical stabilization light co-propagating with the quantum channel.

Entanglement generation using photonic number state encoding, hereafter called single-click protocol, has been demonstrated in atoms [16], (hole-)spins in semi-conductors [17, 18], ensemble-based quantum memories [19, 20], and between single rare-earth ions in cavities [21]. Specifically, the implementation of this protocol on the Nitrogen Vacancy (NV-) center in diamond [22] resulted in orders of magnitude faster entanglement generation than the preceding experiments on the same platform that used time-bin encoding [10, 15, 23]. This allowed for the extension to a multi-node network on which distributed quantum protocols can be realized [24, 25]. So far these experiments have not dealt with the additional requirements of large separation between nodes or telecom compatibility, allowing them to simplify their design. Our approach forms an essential part of a metropolitan quantum link realized in the Netherlands, where solid-state entan-

[1] For time-bin encoding the entangled state phase is dependent on the optical phase difference picked up between the two time bins. Thus, optical phase stability is required only on this timescale which is typically below 500ns [10, 12, 15]

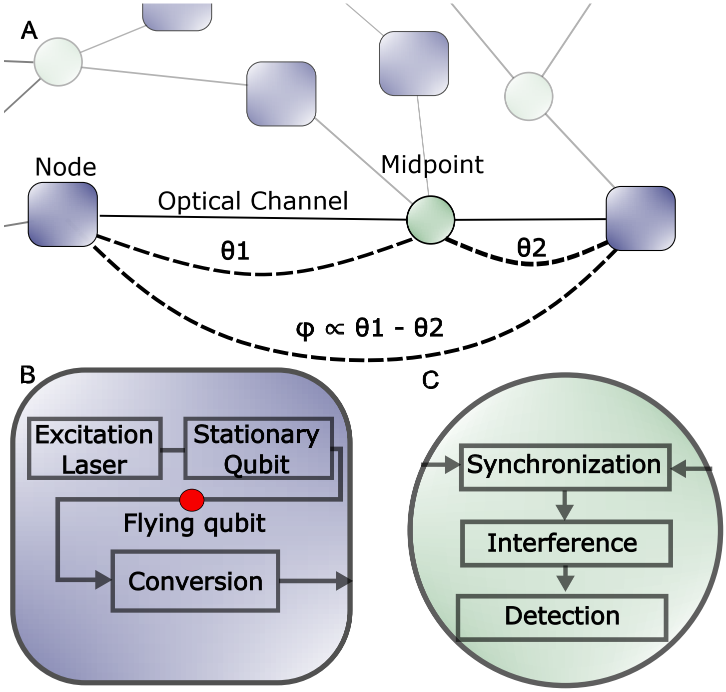

Figure I.4.1: **Schematic overview of elements in a Quantum Network. A)** Many nodes can be connected by sending flying qubits over optical channels towards a central midpoint. The optical path from excitation in the node, to detection in the midpoint, gives rise to an optical phase, θ. When using the Fock-state encoding of the flying qubit for entanglement generation, the resulting entangled state phase ϕ is proportional to the difference between the optical phases. B) Elements needed to generate entanglement between stationary qubits, via the exchange of flying qubits. If the flying qubits are photons not compatible with deployed infrastructure, frequency conversion can be used to significantly lower the propagation losses. C) Upon arrival in the midpoint, the phase of the incoming photonic qubits needs to be stabilized, after which they can be interfered and subsequently detected. The outcome of this detection heralds entanglement between the stationary qubits in the nodes.

glement is generated between two NV-based quantum nodes using 25 km of deployed telecom fiber[26].

A key challenge for the implementation of the single-click protocol for entanglement generation over large distances is the strict requirement on the optical phase stability. Large physical separation between the end nodes adds even more complexity to the system, as fast fluctuation of the optical phase can only be synchronized by using high-bandwidth feedback, where the propagation-delay of information exchange between locations becomes potentially problematic. Furthermore, directly sharing of optical phase references between the nodes beforehand becomes challenging when the distance between the nodes becomes larger and the excitation lasers are in the visible wavelengths. The duration of this stability is demanded for the full duration of the time it takes to analyze (or in the future, end-user protocol runtime) the entangled state that is being generated. A robust, extendable and highly synchronized solution is therefore a key enabler for future quantum networks at scale. Currently, experiments over deployed fiber that use optically coherent between the nodes have been realized with Twin-Field Quantum Key Distribution (TF-QKD), where ultra-stable reference cavities and narrow-linewidth telecom lasers (< 1Hz) were used to reduce the phase-noise in the link. These systems are not compatible when interfacing with solid-state quantum nodes.

In this work we propose, implement and verify an optical phase synchronization scheme between remote and independent quantum nodes operating in the telecom band. The structure of the paper is as follows. In the following section we provide the broader scope in which our phase synchronization scheme is developed and the challenges it is aiming to solve. In the section after that, we provide a full system overview and provide information on the various noise sources that occur in the system. We describe the division of the full system into smaller synchronization tasks, which are subsequently individually described, where the control-layout, noise spectrum and feedback performance are discussed. We then verify the synchronization of the full system at work using measurements of the optical phase between the nodes deployed in the network. Finally we conclude by highlighting the benefits of our scheme, as well as give an outlook on broader applications and further improvements.

I.4.2. Phase-stabilization for entanglement generation using NV-center based processors and telecom fibers

The NV center is an optically active defect in a diamond lattice, of which the electronic spin state forms the basis of many previous demonstrations of solid-state entanglement generation in a network [10, 15, 24]. The entanglement generation can be briefly described in three steps: (1) the generation of single photons by resonant excitation and spontaneous emission, (2) the collection, possible frequency conversion, and propagation towards a central beamsplitter, and (3) a measurement of a single photon. The schematic in the top of Fig. I.4.2 shows the important optical components needed to perform the entanglement generation.

Single-photons are generated by carving short (1.5 ns FWHM) optical pulses from a tap-off from a continuous laser. This excitation light is routed to the NV-center housed in a 4 K cryostat via in-fiber and free-space optics. Spin-selective, resonant excitation followed by spontaneous emission, generates single photons emitted by the NV-center (Fig. I.4.2a, left). Around 3% of the photon-emission is not accompanied by a phonon emission, the so called Zero-Phonon line (ZPL). These photons are coherent with the laser field used for excitation, and are entangled with the spin-state of the NV-center. The ZPL photons are collected into a single-mode fiber, and guided to a Quantum Frequency Converter (QFC), similar to previous work [27, 28], that maintains the entanglement between the photon and the NV spin [29].

In the QFC process, the single-photons are mixed with a high-power pump (1064 nm) inside a non-linear medium, which is phase-matched for a Difference Frequency Generation process (Fig.I.4.2a). This converts the single photons from the original 637 nm to 1588 nm in the telecom L-band. This process is crucial to reduce propagation losses, and also serves as a method to remove any frequency difference between the different NV-centers used for entanglement generation. For more details see previous experiments [30].

After the frequency conversion, the single-photons propagate over the deployed fibers towards a central location called the midpoint, shown in Fig. I.4.2a on the right. There the incoming photons are spectrally filtered via transmission through an Ultra-narrow Filter (UNF, FWHM 50 MHz), and guided to an in-fiber beamsplitter, where the modes of the two nodes interfere. At this point, the relative optical phase is crucial for the entanglement generation when using the single click protocol. The resulting modes behind the beamsplitter are measured using Superconducting Nanowire Single Photon Detectors (SNSPDs), that perform a photonic Bell-state measurement on the combined photon mode. The outcome of this measurement heralds the spin-state of the NV-centers in an entangled state.

For this configuration of a qubit platform we highlight a few specific challenges of synchronizing the optical phase.

Firstly, the free-space and in-fiber optics is sensitive to resonances when placed on an optical table together with a closed-cycle cryostat inducing vibrations, showing up as phase noise on the single photon field. Depending on the mechanical frequencies and stability, a moderate feedback bandwidth is needed to get rid of these fluctuations. Furthermore, careful design of the optics should be done to limit these mechanical vibrations, to reduce the phase-noise that is present due to this effect.

Second, the optical path that requires phase-synchronization is inherently optically connected with a two-level quantum system on one end, and sensitive single-photon detectors on the other end. This constrains the optical powers that can be used for the phase synchronization, and makes the design of the whole system more complex. For instance, unwanted reflections at fiber to fiber connectors or free-space to matter interfaces can lead to crosstalk between the synchronization tasks and entanglement generation. The careful balancing of optical powers and illumination times of light that is incident on the NV-center, as well as the extra shielding of the SNSPDs with Variable Optical Attenuators (VOAs) are additions to allow for a more stable optical phase without reducing the coherence of the NV-center or blinding of the SNSPDs.

Third, when using optical fibers over large distance, the thermal expansion can introduce variations that expand the fiber in the same direction for days. Because we only stabilize the relative phase, large drift in fiber length introduces many phase-slips of 2π, which results in a non-negligible difference between the stabilized phase and optical phase of interest, see I.4.9.2. This is due to the fact that the stabilization light propagates over the long fiber with slightly different frequency than the photons with which we generate entanglement. In our case, when using an offset of 400 MHz, residual phase error $\Delta\theta$ is $\Delta\theta = M\,360\,(\frac{f_{NV}-f_{stab}}{f_{stab}}) = M\,7.6\times10^{-4}$ degrees, where M is the number of phaseslips. For deployed fibers of kilometers long, many centimeters of expansion/contraction occurs on the timescale of days, corresponding to millions of phaseslips. This makes it significant for continuous operation of entanglement generating networks over large fiber networks.

Fourth, propagating high power optical pulses over long fibers can create a significant background at the single photon level both due to double Rayleigh scattering [31], and via interfaces such as connectors and splices. This puts limits on the shot-noise limited feedback bandwidth one can achieve using this classical light, without inducing more background photons in the SNSPDs.

In the following section we discuss our approaches to tackle all these challenges, given the boundary conditions as discussed in the previous sections. We identify three subtasks that can be synchronized independently, resulting in the synchronization of the relative phase of the single-photon fields between two NV-center nodes.

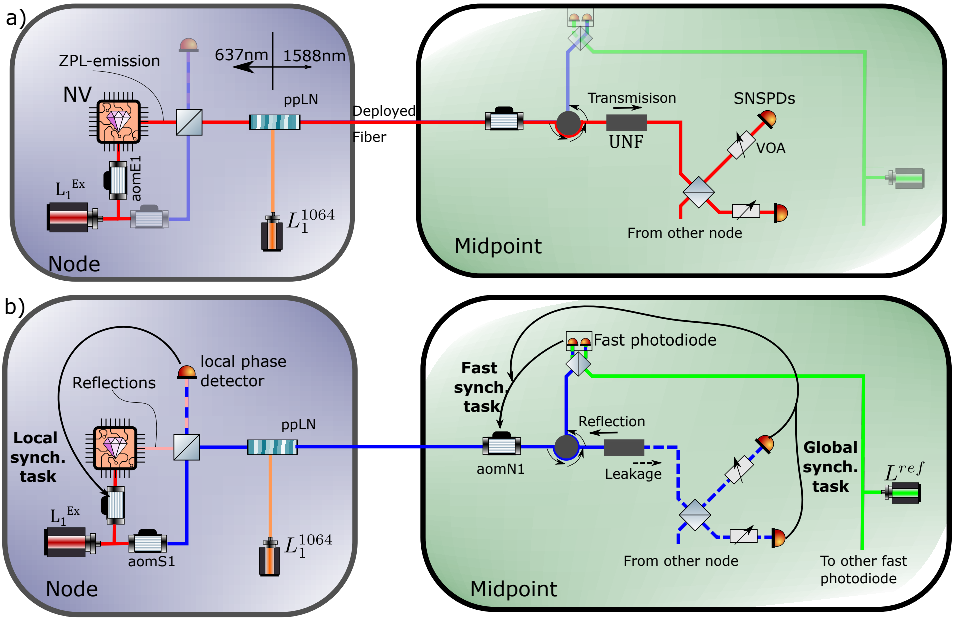

Figure I.4.2: **Schematic of optical lay-out with sources, detectors and optical phase actuators. a)** Optical paths for entanglement generation. At the node light from the excitation laser (red) excites the NV center, yielding single photons at the ZPL wavelength (in red) through spontaneous emission which are converted and routed to the midpoint. There the single photons are passed through an AOM and an ultra-narrow FBG (UNF) for spectral filtering. Overlapping the incoming photon with the photon from the other node on a central beamsplitter, they are measured using SNSPDs. As described in the main text, the relative phase at this beamsplitter is crucial in the entanglement generation. **b)** The lay-out of the phase synchronization schemes to achieve the synchronized phase at the beamsplitter in the midpoint. The laser used for excitation of the NV-center is split and offset in frequency to generate stabiliation light (in blue). In addition reflections of the excitation light (shown pink) coming from the diamond surface, are generated which guided to the 'local phase detector', interfering with part of the stabilization light. This error signal is used to feedback the local synchronization task. The stabilization light is also converted and sent to the midpoint, following the same optical path as the single-photons. There the stabilization light co-propagates with the single photons until it hits the UNF in the rejection band, where most of the stabilization is reflected and routed towards the fast photo-diode, ultimately interfering at the 'fast detector' with light from a reference laser (green). This error signal is used to synchronize the fast task. Leakage stabilization light passes through the FBG (blue dotted line) and reaches the central beamsplitter at the midpoint and the SNSPDs. Similarly, light from Node 2 arrives at the midpoint to arrive at the same beamsplitter, interfering with the light from Node 1. This beat can be measured by the SNSPDs, and the error signal is used to stabilize the global synchronization task.

I.4.3. SYSTEM OVERVIEW AND NOISE SOURCES

An overview of the optical layout that enables synchronization is shown in Fig. I.4.2b. The strategy to divide the phase synchronization for NV-based networks in multiple subtasks was first divised and implemented in Ref. [24], which we extend in this work to suit the additional challenges of telecom operation and large node separation. In this section we identify those sub tasks, showing which optical paths are used where error-signals are generated and subsequently what actuator is used to achieve the synchronization. In Fig. I.4.3 we describe the synchronization subtasks in more detail, giving an overview of the individual components used.

To achieve the ultimate goal of synchronizing the ZPL photons coming from different nodes, an additional light field is added on both nodes, enabling optical phase synchronization at higher optical powers. This stabilization light is generated at both nodes from the same laser that also excites the NV, and is offset in frequency using a similar set of AOMs. This stabilization light is optically overlapped with light coming from the cryostat using a beamsplitter on the node, where the majority is transmitted and overlaps with the reflections coming from the diamond chip. This reflection is used to synchronize the ZPL light to the stabilization light via a local interferometer in the node, see Fig. I.4.2b, left. This interferometer stabilization, called the local synchronization task, is discussed in Section I.4.4, and effectively makes the stabilization light a good phase reference coherent with the ZPL light. The part of the stabilization light that does not go to the local photodiode, propagates via the same fiber as the ZPL photons, via the QFC to the midpoint. Fast phase disturbances in the fiber and phase noise from the excitation and pump lasers are now present on both the stabilization light and ZPL light. The stabilization light is separated from the ZPL using a spectral filter due to the frequency offset of 400 MHz. The stabilization light is synchronised to light from a telecom reference laser by means of frequency modulation by of an AOM driver. We do this by generating an error signal on a balanced photodetector, as shown in Fig. I.4.2b. This is called the fast synchronization lock and is described in more detail in Section I.4.5.

Finally, the SNSPDs are used to assess the optical powers of the stabilization light to each detector, generating a single-photon detector based detection scheme for interference measurement. The error signal is generated using stabilization light that is leaking through the spectral filter at both arms, and meets on the central beamsplitter connecting the two arms, see Fig. I.4.2b. This measurement is inherently of low bandwidth, limited by the low powers used, and the SNSPDs' maximum count rate of $1\,\mathrm{MC\,s^{-1}}$. Higher bandwidths would demand lower integration times, and introduce too high shotnoise. Based on this phase measurement, the setpoint of the fast synchronization task 1 is altered. This allows the synchronization of the stabilization light combining from the two nodes, closing the synchronization scheme. As length variations (caused e.g. by temperature variations) over the long deployed fiber will generate non-negligible phase variations between light at the ZPL and stabilization frequency, this length variation is measured and the frequency-induced phase variation is compensated. Using this compensation, synchronization between ZPL light from both nodes is achieved, cf. Section I.4.6.

Hence, 3 distinct synchronization tasks have been identified. Each of these synchronization tasks are performed using heterodyne phase measurements, and are described in more detail in the following three sections. An overview of the three tasks and their

I.4

Table I.4.1: Summary of synchronization tasks.

Synchronization task	**Light sources generating error signal and used actuator**	**Distortions and dominant frequency range**	**Heterodyne frequency**	**Achieved feedback bandwidth**
Local synchronization at the node	Reflected excitation light from Quantum Device and stabilization light measured on photodiode. Feedback implemented on AOM of excitation light.	• mechanical vibrations of objective lens w.r.t sample, 10 Hz-5 kHz • thermal drift of free space/fiber optics <1 Hz	400 MHz ±750 Hz	3 kHz
Fast synchronization at the midpoint	Stabilization light of selected node and reference light, measured on fast detector. Feedback via AOM acting on both the stabilization light and single photons. Actuator desaturation is done via the pumplaser of QFC.	• thermal effects on deployed fiber <10 Hz • mechanical vibrations of deployed fiber 1 Hz-5 kHz • phase noise in excitation laser, pumplaser and reference laser 1 kHz-50 kHz	215 MHz +0/-1500 Hz	224 kHz
Global synchronization at the midpoint	Stabilization light of node 1 and 2 measured on SNSPDs. Compensation through the setpoint of the fast synchronization loop from node 1.	• thermal drift at midpoint <10 Hz	1500 Hz	~50 Hz

description, including noise sources, heterodyne frequency and feedback bandwidth is shown in Table I.4.1. A full theoretical description of the synchronization tasks, underlying assumptions and the conditions that must be met for them to function is given in the supplementary information I.4.9.2.

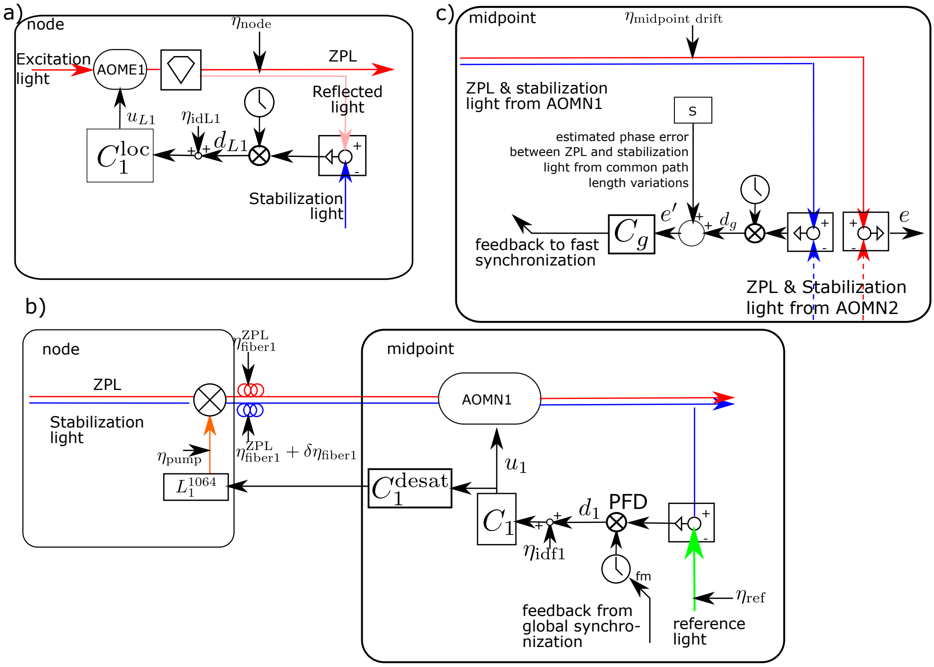

Figure I.4.3: **Control scheme including main distortions. a) Local synchronization.** At the nodes, light exciting the NV is modulated using AOME1, where the controller C_1^{loc} applies a frequency modulation of the sine generator driving the AOM. This modulation depends on the heterodyne measurement of the beat between reflected and stabilization light at a balanced detector. Main noise sources are the phase noise of the excitation laser and mechanical vibrations and drift that are not shared by the stabilization light and the ZPL light (η_{node}). **b) Fast synchronization.** Subsequently, ZPL and stabilization light are frequency-converted by mixing with a 1064nm-pumplaser, and this light travels from both nodes to the midpoint. The stabilization light is separated from the ZPL light and interferes on a balanced detector with the reference laser, where the demodulation is performed with a Phase Frequency Detector (PFD). The PFD output is fed to a synchronization controller C_1 which modulates the ZPL and stabilization light with aomN1. This fast controller suppresses mechanical distortions $\eta_{\text{fiber}}^{\text{ZPL}}$ shared between ZPL and stabilization light and phase noise from the excitation- and pumplaser, i.e. $\eta_{\text{excitation}}$ and η_{pump}. A varying setpoint to the fast synchronization task on node 1 is supplied by the global synchronization task. **c) Global synchronization**. The phase error between stabilization light at the SNSPDs is measured to suppress phase drifts $\eta_{\text{midpoint drift}}$ in the optical paths at the midpoint between reference laser and fast detectors, as well as between the fast detectors and the SNSPDs. This heterodyne measurement uses the SNSPD count rates as error signal. The global controller C updates the setpoint of the fast synchronization task of node 1. Since larger length variations will occur over the deployed fiber, a phase error will be introduced between ZPL and stabilization light, which is estimated using fiber-length measurements and compensated through S. Homodyne interference between ZPL light also is measured using the SNSPDs. The interference between ZPL light (red) is used in the entanglement generation process, and the error e directly reduces the maximum fidelity thereof.

I.4.4. LOCAL SYNCHRONIZATION AT THE NODE

The local synchronization tasks consists of ensuring that the reflected excitation light from the Quantum Device is phase-synchronized to the stabilization light. In this manner, we also ensure phase synchronization between the ZPL photons and the stabilization light. Namely, the ZPL light emitted at the NV center is phase-synchronous with the excitation light as they run over the same optical path[2]. The reflected excitation light is separated from the ZPL light based on polarisation using a free space beamsplitter. The stabilization light enters the system at the other input, after which we use a set of birefringent α-Bariumborate (αBBO) crystals to maximize the complex overlap between the orthogonally polarized reflected beam and the stabilization light. These crystals can correct for static differences in tip-tilt and translation errors between the stabilization and reflected light. After this optimization, we project both beams in a common polarization mode using a polarizer, and measure a sufficient interference signal using a photodiode. After demodulation, an analogue proportional controller with roll-off filter is used to generate a frequency-modulating signal for the AOM driver of AOME1, see Fig. I.4.2.

To assess the performance of this control loop, a *linear* system identification experiment is performed for each of the synchronization tasks, as show in Fig. I.4.3a. Within each synchronization task we can identify a 'plant'. The plant is defined as the combination of the processing and actuation of the error signals (e.g. d_{L1} to u_{L1}). It consists of the actions of the frequency-modulation of a digital clock, amplification to drive the AOM, interference detection and demodulation of the electrical signal. While the frequency shifting behaviour of the AOM and subsequent demodulation via an analogue diode-based double balanced mixer are in practice nonlinear, we assume a linear input-output behaviour of the plant, which matches our observations.

To identify this subsystem[3] in series with the controller we use a commonly used technique of injecting an additional but known broadband noise signal on the actuator (η_{idL1} and η_{idL1} in Fig. I.4.3a. By measuring the resulting output with the feedback on and off and comparing them we can calculate important performance parameters such as the open-loop transfer function of the plant. We can also record the spectral densities of the residual phase noise. For more information see the supplementary information.

We show the result of this analysis for the local synchronization task in Fig. I.4.4. It shows that a bandwidth of ~3 kHz is obtained [4], where the gain reaches a value of ~ 0.5 in Fig. I.4.4a. The free-running Power Spectral Density (PSD) shown in Fig. I.4.4b (orange) has the features of slow drifts below 10 Hz, as well as mechanical resonances between 100 Hz to 1000 Hz. By integrating the PSD when the controller is enabled (Fig. I.4.4b, blue), we reach a cumulative phase error of 12° RMS, as shown in Fig. I.4.4c.

[2] There is a small optical path difference between the emitter location and light reflected off the diamond surface, which can be kept constant via spatial optimization of the microcsope objective.

[3] In contrast to the final operation, the stabilization light is constantly available, i.e. the 2.5 µs 'dark' periods every 10 µs period are avoided for the identification experiments.

[4] To define the synchronization bandwidth, we use the 0dB point of the open loop dynamics, given by the controller and plant of the system.

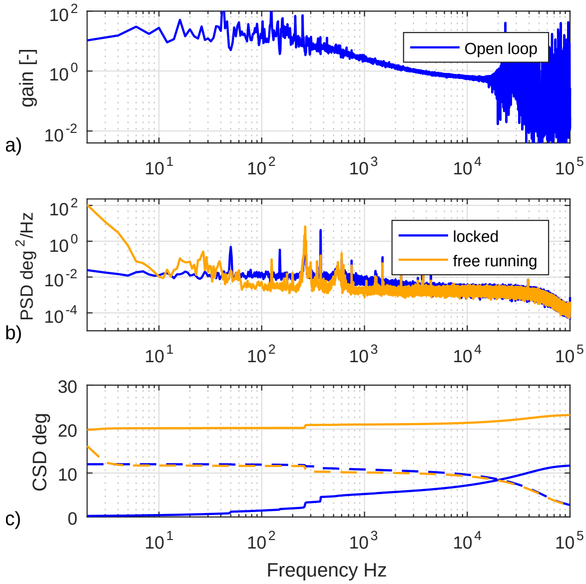

Figure I.4.4: **Performance of local synchronization task**. a) Identified linear dynamical relation between control output u_{L1} and demodulation output d_{L1} (demodulated around DC as used as control input), called plant. b) Power Spectral Density and c) Cumulative (solid) and Inverse (dotted) Cumulative Spectral Density of residual phase error with (blue) and without (orange) feedback, measured without additional noise injection.

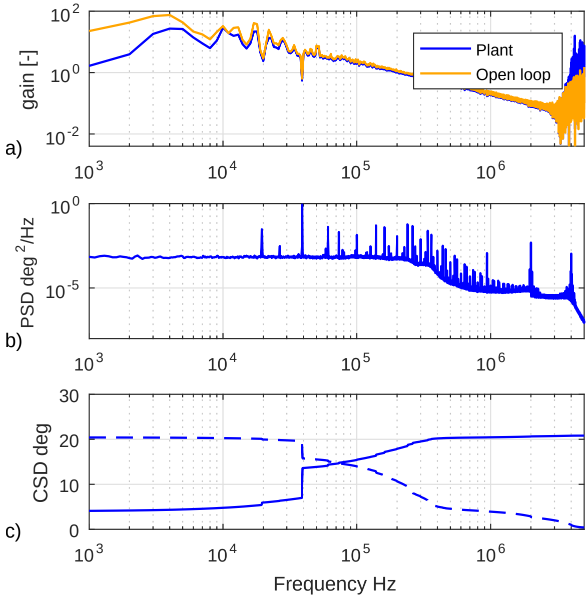

Figure I.4.5: **Performance of fast synchronization task.** a) Identified linear dynamical relation between control output u_1 and demodulation output d_1 (demodulated around DC as used as control input), called plant, and between control input and demodulation output, i.e. the open-loop behaviour. b) Power Spectral Density and c) Cumulative and Inverse Cumulative Spectral Density of residual phase error.

I.4.5. Fast synchronization at the midpoint

Both fast synchronization loops at the midpoint have the goal to synchronize the stabilization light of the nodes to light of the same reference laser which is located in the midpoint, see Section I.4.3b and Fig. I.4.3b, and have the same design for both arms coming from Node 1 and Node 2, and we discuss the workings in the context of Node 1. After conversion and subsequent arrival in the midpoint, stabilization light of the node and reference light interfere and is measured with a balanced photodetector, demodulated using a phase frequency detector (PFD) and then passed to an analog controller $C1$ of proportional-integral type. The output of this controller is then used for frequency modulation of the AOM AOMN1. To limit the frequency-modulation range of this AOM to avoid reduced optical transmission, de-saturation is required, which is performed via additional feedback to the pump laser frequency back at the node. This control signal is sent over an User Datagram Protocol (UDP) connection (update frequency 500 Hz) from the midpoint to the node.

To identify the synchronization performance, we used the same techniques as outlined for the local synchronization task. The resulting open-loop transfer function is identified and shown in Fig. I.4.5a. It shows that a 220 kHz control bandwidth is achieved. By integrating the 'locked' PSD of the residual phase noise (Fig. I.4.5b), we find the cumulative phase error of 21° RMS, as shown in Fig. I.4.5c. The achieved bandwidth is realized by the short distance between error-signal generation and actuation, and fast servo control for error signal processing. Spectral data of the recorded signals is shown as a supplementary figure at the top of Fig. I.4.8a.

I.4.6. Global synchronization

The global synchronizing feedback is required to suppress low-frequent phase drifts in the optical paths at the midpoint between reference laser and fast detectors, as well as between the fast detectors and the SNSPDs, schematically depicted in Fig. I.4.3c. A heterodyne phase error measurement is obtained from the SNSPD measurement by converting the single-photon count rate to well-defined pulses using an analog pulse stretcher, subtracting both pulse signals and lowpass-filtering the result. Employing a small frequency offset between the stabilization light between the nodes, we can detect a heterodyne beat at 1500 Hz, still below the relatively low bandwidth of the error signal generated with the SNSPDs, while making the measurement insensitive to power fluctuations (see Table I.4.1 for details). The error signal is processed and fed back by changing the setpoint of one of the fast synchronization scheme by an amount determined by controller C', which affects the phase shift introduce by AOMN1, cf. [32]. A proportional controller is used in this setup.

We compensate the expected phase differences between stabilization and ZPL light over the deployed fibers (i.e., $\delta\eta_{\mathrm{fiber1}}$ and $\delta\eta_{\mathrm{fiber2}}$, which will occur due to the optical frequency mismatch, combined with length variations over these fibers (see also I.4.9.2). Exploiting the measurement of these length variations using roundtrip-time measurements, estimates $\tilde{\delta}\eta_{\mathrm{fiber1}}$ and $\tilde{\delta}\eta_{\mathrm{fiber2}}$ are obtained in subsystem S in Fig. I.4.3, cf. [33].

The performance of the global synchronization is illustrated in Fig. I.4.6, where the spectrum with and without this feedback is shown. The dominant noise-sources are below 10 Hz, as seen in the unlocked PSD of the phase noise in Fig. I.4.6. This is because all high-frequency noise is removed by the fast synchronization task, and only slow drifts remain. This controller yields a cumulative phase error of 8° RMS, as shown in Fig. I.4.6c.

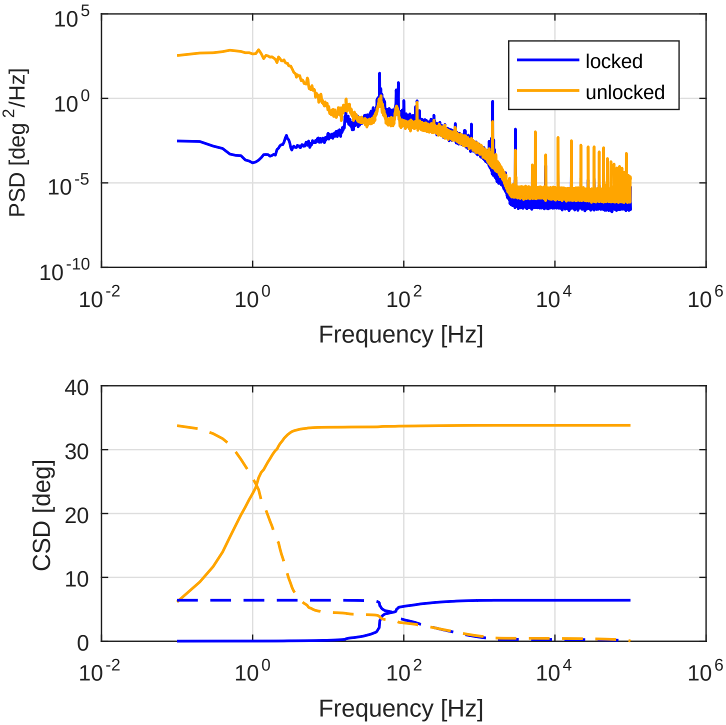

Figure I.4.6: **Performance of global phase synchronization**. Power Spectral Density (top) and Cumulative and Inverse Cumulative Spectral Density (bottom) of residual phase error.

I.4.7. SYNCHRONIZATION RESULT ON RELATIVE PHASE BETWEEN REMOTE NODES.

We now measure the performance of the complete system when all the synchronization tasks are active. We evaluate the system by measuring the phase error e between the excitation lasers of the both nodes, see Fig. I.4.3c. The system is deployed at three locations in the Netherlands, where the nodes are separated by ≈10 km, connected to the midpoint by 10 km and 15 km of fiber between the cities The Hague and Delft respectively.

We assess the optical performance by using classical light fields reflected off the diamond surface, which should result in homodyne interference, and allows us to access the relative optical phase between the nodes. This light originates in the nodes and travels the same optical path as the ZPL photons (which are coherent with this light), up to a small propagation through the diamond sample. The intensity of this reflected light can be adjusted on the nodes (>1 kC$\,s^{-1}$), allowing for quick integration times and high signal-to-noise ratio in the SNSPDs. We conduct this measurement under identical conditions as an entanglement generation experiment. This means that the powers of the optical fields, both reflected and direct, and their on/off modulation are done in the way one does during entanglement generation. The reflected laser pulses are located at the same location in the sequence as where the optical excitation would be, making the phase measured in this experiment a good metric for the expected performance.

The interference and subsequent measurement by the SNSPDs of this reflected light is show in Fig. I.4.7a, with clear interference shown in the region where the light fields overlap in time. The contrast of this interference can be corrected for imbalance of the incident power, and by sweeping the phase setpoint a full fringe can be taken (Fig. I.4.7b). Fitting these fringes with a single cosine $I = \frac{1 \pm C\cos(\phi+\phi_0)}{2}$, we can retrieve the contrast C and setpoint ϕ_0 of the synchronised system. By assuming that the loss of contrast C is solely due to a normally distributed residual phase error, we calculate its standard deviation from the contrast which is $\sigma_{measured}$ =35.5°. This matches well with the expected residual phase noise, which would be the quadratic sum of all five independent synchronization tasks: $\sigma_{total} = \sqrt{2\sigma^2_{local} + 2\sigma^2_{fast} + \sigma^2_{global}}$ =34.9°. By repeating this measurement and recording both contrast and setpoint, we can characterize the long-term behaviour of the phase synchronization system (Fig. I.4.7c). We find that the phase synchronization is stable over a time-span of more than ten hours, showing a high contrast. The long term drift (Fig. I.4.7d) of the phase setpoint is almost completely explained by the aforementioned offset in phase due to the combination of the frequency offset and long fiber length variation, which was calculated but not compensated in this test. The resulting phase setpoint distribution is shown in the bottom right of Fig I.4.7d, showing a sharp distribution around a setpoint of 0°.

I.4.8. Discussion and Outlook

We have designed, built and evaluated an extendable phase synchronization scheme to enable entanglement generation between solid-state emitters, compatible with the telecom L band and large node separation. The phase synchronization is achieved between two independent excitation lasers, which are integrated in an NV-center quantum network node, connected over deployed fibers. The introduction of stabilization light allows to generate reliable phase measurements with low shotnoise and enable the ability to guide the stabilization light to an alternative detector. Therefore we can use two distinct feedback loops at the midpoint, to compensate both the high-frequent distortions via a balanced photodetector but also compensate the low-frequent distortions using the SNSPDs, achieving synchronization at the central beamsplitter where the single-photon paths of two distant nodes interfere. The separation of the overall synchronization task and tailoring the control schemes to the specific noise present allow us to realize high-performing synchronization using independent excitation lasers and at a metropolitan scale node separation. By making the synchronization tasks robust against drifts of optical power and compensating for large fiberlength variations, phase stability sufficient for entanglement generation is achieved for more than 10 hours .

Our implementation has a few advantages. First, our method only requires the distribution of a phase reference in the RF domain, e.g. 10 MHz, over the network. This can be done over deployed fiber using the White Rabbit [34] protocol, and is easily distributed locally via amplified buffers. Second, due to the choice of AOMs as feedback actuators and additional offloading on the pump laser of the QFC, the system has both a fast step response, and the feedback range is only limited by the QFC conversion bandwidth. Additionally, the achieved feedback bandwidth lowers the requirements on the linewidth of our lasers used on the nodes, simplifying their design and avoiding complex optical reference distribution. Furthermore, the design allows the reduction of the optical intensity of signals that could interfere with the entanglement generation, by using heterodyne schemes. This boosts the signal-to-noise ratio of the generated error signal, and at the same time limits the crosstalk with the quantum system and single-photon emission.

This scheme also allows for scaling the number of nodes in the network. The most straightforward way of scaling would be in a star pattern, as all the incoming nodes could be continuously synchronized with the same optical reference. To establish a connection between two nodes, one has to switch the incoming photons to the same beamsplitter. With the appropriate feedback speed one can make the newly switched paths phase-stable before the photons arrive from the remote nodes. A similar approach can be taken on a line-configuration with multiple midpoints if the frequency difference between the optical references used at each midpoint can be kept reasonably small, below the feedback bandwidth of the fast synchronization.

Further improvements can be made for the local and fast subtasks, which we will discuss starting with the local synchronization task. Currently the fully analog and integral nature via feedback on an AOM causes a high gain at low frequencies. This means that it is sensitive to small analog input offsets to this AOM when the errorsignal generation is paused. This results in the reduction of the free-evolution time, the time that the phase stays synchronised without feedback. Using a proportional feedback or a fast digital controller could circumvent this. The residual phase noise present in the fast synchronization could be reduced in a number of ways. Excitation lasers with less phase-noise would lead to a direct improvement of the performance. Additionally, more in-depth tuning of the control to the noise-spectrum measured could deal more effectively with the noise. Further investigations into the exact noise spectrum and more complex control techniques could further enhance the performance of the fast synchronization.

As a conclusive demonstration of the system we recently used it to generate heralded entanglement between two NV-centers over deployed metropolitan fiber [26]. Here, the phase synchronization was time-multiplexed with the emission of single-photons by the NV-centers. Being compatible with many different qubit platforms, the architecture presented in this work can form the basis for future developments and implementations generating large-scale entanglement over deployed fiber networks.

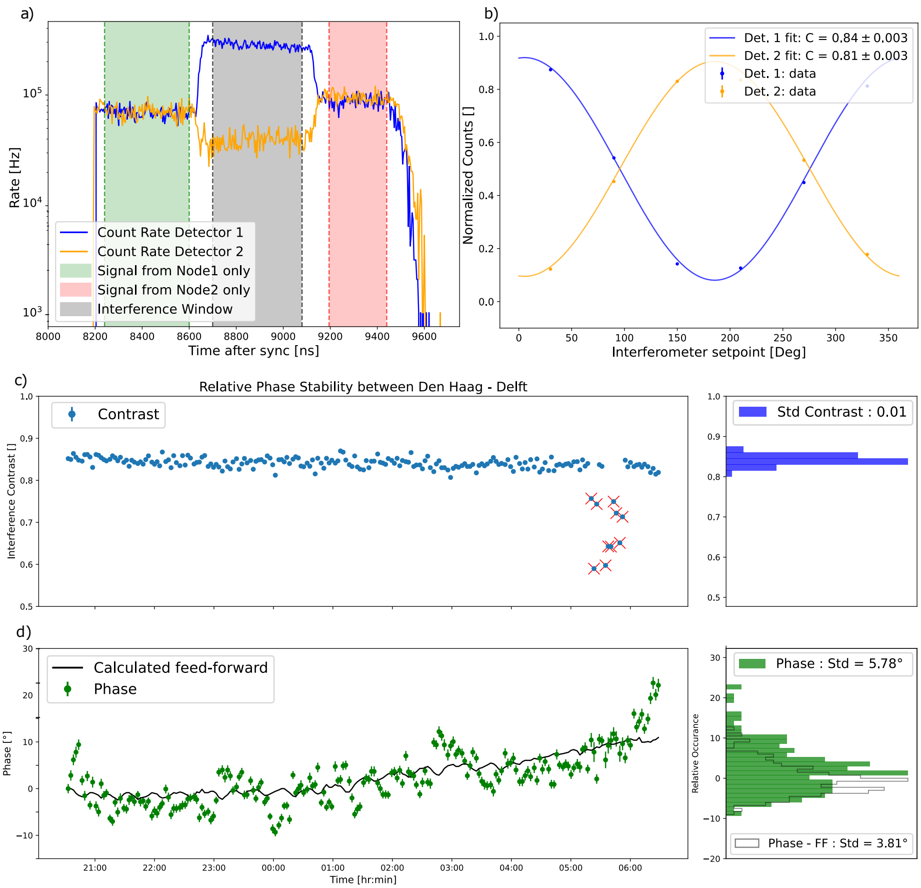

Figure I.4.7: **Performance of the total system performing phase synchronization. a)** Interference of reflections of the excitation lasers from the diamond chip from, as measured by the SNSPDs in the midpoint. The blue (orange) line indicate the rate of photons incident on the first (second) detector. The shaded indicate regions in time where only light from Node 1 (green) or Node 2 (red) is present show no interference. In the overlapping region (grey), the light interferes and is directed to predominantly one detector, indicating interference of the weak laser fields. **b)** By sweeping the local oscillator of the global synchronization task in Fig I.4.3c, we change the setpoint of the interference, directing light into one or the other detector, as show by change of preferred direction to detector 1 (blue) or 2 (orange). By correcting the count rates for imbalance, we can fit these oscillations with a single cosine, recovering the relative phase of the excitation lasers of the two nodes. The imperfect contrast of this oscillation represent the residual phase noise in the system at timescales below the measurement time (≈seconds). **c)** Measurement of the relative optical phase between the paths coming from Delft and The Hague over a timespan of ten hours. We measure a constant average contrast over the full duration of more than 200 measurement, with the exception of a group of 10 measurements. These were the result of one of the excitation lasers lasing multi-mode, as picked up by a separate monitoring scope. **d** The measured relative phase shows a small drift over this time-frame, without the compensation for phase slips due to large fiber drifts (green, see I.4.9.2). Plotting the calculated feed-forward based on the round-trip time between the two nodes and the midpoint shows the correlation. When taking this feed-forward into accounts, the resulting spread standard deviation of the phase setpoint is below 4° over the course 10 hours (white histogram).

I.4.9. SUPPLEMENTARY MATERIALS

I.4.9.1. SYSTEM IDENTIFICATION DETAILS

We injected additional noise at the location shown in Fig. I.4.3 while the control loop is active and measured the signals u_{L1} and the demodulated output d_{L1} of the local synchronization loop. Throughout the paper, these measured interference powers $x(t_i), i = 1,\ldots,N$, are analysed by subsequently taking the Hilbert transform to compute the phase of the resulting analytical signal [35]. Additionally we can plot the spectral content measured during the identification experiments. This is done with Welch's averaged periodogram method [36], and is shown in Fig. I.4.8. We repeat this analysis for the fast synchronization loop, injecting noise, monitoring the signals and demodulated output, and perform the analysis. The spectral content of the measurements are show in Fig. I.4.8, with the analysis in the main text.

For the global synchronization task injecting noise posed a challenge, and we therefore only measured the residual phase error under open/closed loop conditions.

I.4

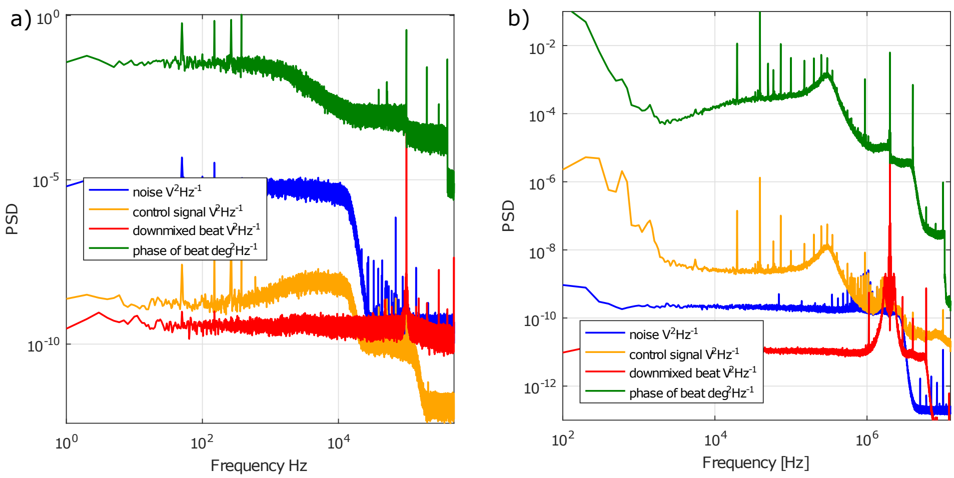

Figure I.4.8: **System identification of synchronization tasks**.a) Power Spectral Density of noise injected before the controller η_{idL1}, control output signal u_{L1}, measured beat signal m_{L1} (analoguely downmixed to 100 kHz), and phase error on this signal, respectively, for the local synchronization task. b) Power Spectral Density of noise injected before the controller η_{idf1}, control output signal $u1$, measured beat signal $m1$ (analoguely downmixed to 2 MHz), and phase error on this signal, respectively, for the fast synchronization task.

I.4.9.2. THEORETICAL DESCRIPTION OF SYNCHRONIZATION RESULT

Here we give a theoretical description of the phase synchronization scheme, and determine the conditions that must hold for the phase synchronization to succeed. We start off by describing some definitions and assumptions underlying the analysis and provide a schematic that includes all relevant fields and optical paths. This allows us to define the central stabilization task we want to achieve, and how we achieve it by breaking up the task into smaller synchronization tasks.

Definitions and assumptions

We make the following definitions and assumptions in the derivation of the phase conditions:

- In propagating the fields we treat them all as monochromatic plane waves that propagate along the optical axis, the $\hat{z}$ direction. We can therefore write the complex wavefunction of a field with frequency f_i in a medium with refractive index n_l depending on time t and space z as

$$U(z,t) = Ae^{j\phi_i} = Ae^{j(\omega_i t - k_i z)} \tag{I.4.1}$$

  with A being a constant, $\omega_i = 2\pi f_i$ and $k_i = \frac{n\,\omega_i}{c}$ with c the speed of light in vacuum and n the refactive index. We ignore all effects of a varying spatial intensity distribution or curvature of the wavefront in free space.

- We treat reflection and transmission through the Ultra-narrow filter as having no impact on the phase, an assumption that is true if the central frequency is kept stable, and the reflection is far away from the resonance of the filter.

- We assume that the change in refractive index for small frequency differences (<1 GHz) or temperature variations are negligible.

- All clocks (RF sources as references in the synchronization) used in the scheme are coherent with each other. This is realized by providing a 10 MHz External Reference to each of the signal generators, and finding clock settings that minimize any non-idealities in the signal generation of the devices used.

We make extensive use of heterodyne interference, which is the interference of two fields of different frequencies. When measuring the intensity of this field with a photodiode, the combined field intensity is described as

$$I = |U_1 + U_2|^2 = |U_1|^2 + |U_2|^2 + U_1^* U_2 + U_1 U_2^* \tag{I.4.2}$$

Filling in two plane waves of equal amplitude $\sqrt{I_0}$ at the start of the lasers, but different frequencies and initial phase, we get

$$I(t) = 2I_0 + 2I_0 \cos\big((\omega_2 - \omega_1)t + \frac{n}{c}(\omega_1 D_1 - \omega_2 D_2) + (\theta_2 - \theta_1)\big), \tag{I.4.3}$$

where THz-frequencies are dropped. The intensity is varying in time with the difference of the two frequencies of the original waves (called a beat), with change of the distances D_1 and D_2, and with a phase given by the initial phases of the two fields. This allows us to use the photodiode to generate an error signal that contains both the difference frequency $\omega_1 - \omega_2 = \Delta\omega$ and the relative phase of the two optical waves. By choosing the frequency difference of the two optical fields in the RF regime (<1 GHz), we can use RF-generators, mixers, amplifiers and filters to stabilize this errorsignal. This synchronizes the two fields, and adjusts for frequency variations, drifts of the distances to the point of interference, and phase jumps due to the linewidth of the laser. This is the underlying principle to stabilize the relative optical phase of two optical fields, at a certain location in space.

It is useful to give a proper definition of what we mean when we say two phases are synchronized. When two optical fields in a task are *synchronized*, it means that at a specific point in space z_s, the two fields $U_1(z_s,t)$ and $U_2(z_s,t)$ have a phase relation that can be written as

$$\left(Arg(U_1(z_s,t)) - Arg(U_2(z_s,t))\right) - \omega_{clock} t \equiv \eta(t) \tag{I.4.4}$$

with ω_{clock} the clock frequency of the RF-source used in the signal processing and $\eta(t) - \mu \ll \pi$ the residual phase error and μ a constant. For sampling frequencies much smaller than the feedback bandwidth (and therefore slower than phase residuals), these samples are independent of their evaluation time $t_i, \imath = 0,1,2,...$, and thus follow a probability distribution with constant parameters in time, i.e.

$$\eta(t_i) \in \mathcal{N}(\mu,\sigma),\ i = 0,1,2,..., \tag{I.4.5}$$

where, for small angles, $\mathcal{N}$ is a normal distributed variable with mean μ and standard deviation σ. Experimentally we can choose $\mu \in [0,2\pi]$ by changing the clock setpoint used for the stabilization, and $\sigma \ll \pi$ gives the performance of the synchronization: smaller σ indicates better synchronization performance. For the special case where $\omega_{clock} = 0$, or when one has access to a source coherent with the clock, one can sample the distribution $\mathcal{N}$. For entanglement generation experiments this conditions holds, where the sampling occurs at the measurement of a single-photon every couple of seconds.

ERRORS DUE TO LARGE LENGTH VARIATIONS

Suppose we have two coherent, co-propagating fields U_1 and U_2 with different frequencies ω_1,ω_2, on a long fiber with length L. The first field is (perfectly) synchronized at the end of the fiber $z = L$ with a phase actuator that works **on both** U_1 and U_2, with the phase setpoint $\theta_{Ref} := \frac{nL\omega_1}{c}$. The phase that the field U_2 has at $z = L$ is than given as

$$\varphi_2\big|_{z=L} = \frac{nL\omega_2}{c} = \theta_{Ref} + \frac{n\,L(\omega_2-\omega_1)}{c} = \theta_{Ref} + \frac{n\,L(\omega_2-\omega_1)}{c}, \tag{I.4.6}$$

which is at a constant offset of θ_{ref}. This means the synchronization task of U_1 is also synchronizing U_2, it is no longer varying in time, albeit at a constant offset. If now the fiber expands to length $L+\Delta L$, the synchronization tasks aims for phase $\varphi_1\big|_{z=L+\Delta L} \to \theta_{Ref}$. Hence,

$$\begin{aligned}\varphi_2\big|_{z=L+\Delta L=\frac{n\,(L+\Delta L)\omega_2}{c}} \\ &= \frac{n\,(L+\Delta L)\omega_1}{c} + \frac{n\,(L+\Delta L)(\omega_2-\omega_1)}{c} \\ &= \theta_{Ref} + \frac{n\,L(\omega_2-\omega_1)}{c} + \frac{n\,\Delta L(\omega_2-\omega_1)}{c} \\ &= \frac{n\,L\omega_2}{c} + \theta_{err}(\Delta L),\end{aligned} \tag{I.4.7}$$

with $\theta_{err}(\Delta L) = \frac{n\,\Delta L(\omega_2-\omega_1)}{c}$ an additional term, indicating the phase of U_2 has moved with respect to its original position at L, and is no longer synchronized. therefore we have to be careful in exchanging phase terms of fields that are co-propagating and synchronized over long fibers, but at slightly different frequencies. Using the numbers in our system, $\Delta\omega = 2\pi \times 400$ MHz, and a ΔL of 2 cm expansion of the fiber would result in a $\theta_{err}(0.02)$ of $10°$ of phase error. Given the low thermal expansion coefficient of silica of $\frac{dL}{dT} = 5.5 \times 10^{-}7\,\mathrm{m\,K^{-1}}$, this effect only happens when large fiber lengths and temperature drifts are involved. In the main text, Fig. I.4.7 shows a measurement of this effect, where the value calculated using our accurate timing hardware matches the value measured by the phase interference well.

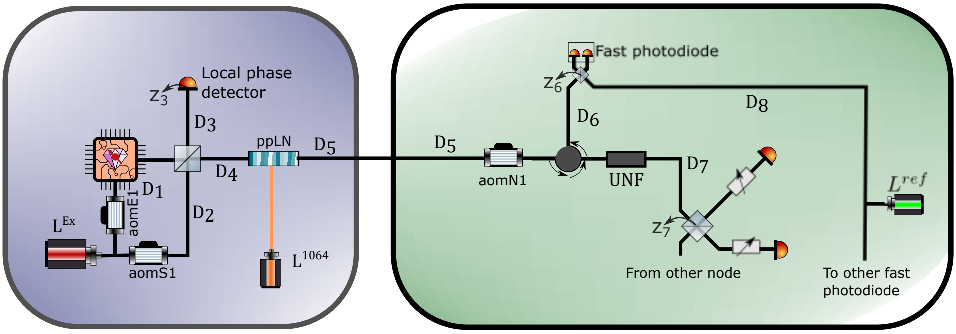

Figure I.4.9: **Schematic showing the division of optical paths in the system, used for deriving the synchronization tasks.** The main synchronization task, and the subdivision of local, fast and global synchronization tasks is given in the main text Fig. I.4.2

For a full overview of all the optical fields used, we refer to Table I.4.2 that gives the typical central frequency, linewidth and powers. In Fig. I.4.9 we show the division of the connection of one node to the midpoint into separate optical paths, used in the derivation of the phase synchronization requirements. These sections ($D1$, $D4$, $D5$ and $D7$) form a continuous path between the excitation laser L^{Ex} and the central beamsplitter in the midpoint where the relevant interference takes place, plus additional sections that are needed to describe the individual synchronization tasks ($D2$, $D3$, $D6$ and $D8$). A short description, typical distances and extra information is given in Table I.4.3.

Table I.4.2: Overview of optical fields.

Optical field	NV emission	Excitation	Reflections	Stabilization	Leakage	QFC Pump	Reference
Typ. wavelength [GHz]	470450	470450	470450	470450.4	470450.4	281759	188691
Typ. linewidth [kHz]	12.3e3	~10	~10	~10	~10	<20	<0.1
Power in local PD	Single photons	~5uW	~1nW	~5uW	-	-	-
Power in Midpoint	Single photons	-	<1pW	~30nW	Single photons (100kHz)	-	~5mW

Table I.4.3: Overview and description of optical paths.

Section	Description	Length [m]	Dominant noise source
D_1	Excitation path, from laser, via AOM, objective and diamond chip to local central beam splitter	10	Objective stage/vibrations and laser phase noise
D_2	Local stabilization light path, from laser, via AOM, free-space optics, to local central beam splitter	10	Fibre optics/vibrations
D_3	Local central beam splitter to local phase projection (Polarizing BS)	2	Long term optics drift/birefringent optics
D_4	Local central beam splitter, via free-space optics, to QFC crystal	2	-
D_5	QFC crystal, via deployed fibers, through EPC, AOM to Ultra-narrow filter	>10e3	Thermal expansion/environmental vibrations
D_6	Backwards reflection off UNF, to BS at fast detector	2	Vibrations/loose fibers
D_7	Transmission through UNF, towards central beam splitter in midpoint	2	Vibrations/loose fibers
D_8	Reference laser, via fibers, to BS at fast detector	2	Vibrations/loose fibers

Central synchronization task

We define the central synchronization task as achieving a stable phase between the photon emission on each node, measured at the location of the central beamsplitter in the midpoint, denoted z_7 in Fig. I.4.9. This is the central requirement for entanglement generation via the single-click protocol, as discussed in the main text. To simplify things, we will first derive the stability of the relative phase between the two excitation lasers on each node, as measured in the central beamsplitter in the midpoint, and then argue that the single photon emission is coherent with this field (see Sec. I.4.9.2).

The time-dependent relative phase at the central beamsplitter can be written as

$$\eta(t) = \phi(t, z_7)^1 - \phi(t, z_7)^2 \tag{I.4.8}$$

where $\phi(t, z_7)^i$ is the phase of the field coming from node i at the location of the central beamsplitter z_7. When all the synchronization tasks are active, the error $\eta(t)$ will be small ($\ll \pi$), and under probabilistic entanglement generation samples this time-dependent phase is sampled, and the errors form a distribution $\mathcal{N}_{Tot}$.

We can write $\phi(t, z_7)$ by following the fields through the setup as shown in the main text Fig. I.4.2. It is given by

$$\phi(t, z_7) = \theta_{Ex} + \frac{n\omega_{Ex}}{c}(D_1 + D_4) - \theta_{1064} + \frac{n'\omega'_{Ex}}{c}(D_5 + D_7) + \omega'_{Ex} t, \tag{I.4.9}$$

where ω_{Ex} the frequency of the excitation laser, $\theta_{Ex/1064}$ are the phases of the excitation and QFC pump laser respectively. The $'$ denotes the fact that the field has been converted, meaning $\omega'_{Ex} = \omega_{Ex} - \omega_{1064}$. For the other node to the midpoint we can write an identical equation, containing the same but uncorrelated terms. In order to synchronize these two fields, we need to get rid of the terms that are varying rapidly in time (see Tab. I.4.3). The next step is to fill in the synchronization conditions guaranteed by the synchronization tasks realized in the setup.

Local synchronization task

The local synchronization task synchronizes the relative phase of the light coming from two paths consisting of $D_1 + D_3$, and $D_2 + D_3$, both starting at the excitation laser and ending at detector z_3. In the path $D_2 + D_3$, the AOM shifts the light in frequency with 400 MHz±750 Hz. Due to the two paths being different polarization states of the light, the actual interference happens after projection into the same state by a polarizer, and subsequent detection by the detector after traveling D_3, which we denote as z_3, see Fig. I.4.2b and Fig. I.4.9. The synchronization error is given by the equation

$$\eta(t)_{loc} = (\phi^A(t, z_3) - \phi^B(t, z_3)) - \omega_{loc} t,$$

and can be written out as

$$\begin{aligned} \omega_{Loc} t + \eta_{loc}(t) = \\ & \left(\theta_{Ex} + \frac{n\omega_{Ex}}{c}(D_1 + D_3) + \omega_{Ex} t\right) \\ & - \left(\theta_S + \frac{n\omega_S}{c}(D_2 + D_3) + \omega_S t\right) \end{aligned} \tag{I.4.10}$$

with θ_{Ex} the phase due to the finite linewidth of the Excitation laser, and ω_S the frequency of the stabilization light and $\omega_{loc} = \omega_{Ex} - \omega_S$ the frequency and θ_{loc} the phase of the clock used as reference. By ensuring that $D_1 - D_2$ is well within the coherence length of the excitation laser, we can write $\theta_{Ex} = \theta_S$. The remaining terms are slowly varying in time with respect to the feedback bandwidth, as shown in the main text I.4.4. The performance parameter σ_{loc} is also given there. We can also write I.4.10 in a different form that makes it easier to use in future derivation as

$$\theta_{Ex} + \frac{n\omega_{Ex}}{c} D_1 = \theta_S + \frac{n\omega_S}{c} D_2 + \frac{n(\omega_S - \omega_{Ex})}{c} D_3 + \eta_{loc}(t), \tag{I.4.11}$$

FAST SYNCHRONIZATION TASK

The next synchronization task we describe is the fast synchronization task. This consist of again two arms, A and B, that meet at the point z_6. Path A is from the excitation laser, via the stabilization split-off (D_2), through the QFC (D_4), over the long deployed fiber (D_5), through the AOM at the midpoint, reflected by the UNF (D_6) to reach z_6. Path B is from the Reference laser directly to z_6 (via D_8), see Fig. I.4.2b and Fig. I.4.9. We can again define the synchronization error for this task as

$$\eta(t)_{fast} = (\phi^A(t, z_6) - \phi^B(t, z_6)) - \omega_{fast}(t),$$

I.4

and filling in the terms we find

$$\omega_{fast}t + \eta_{fast}(t) = \\ \left(\theta_S + \frac{n\omega_S}{c}(D_2 + D_4) - \theta_{1064} + \frac{n'\omega'_S}{c}(D_5 + D_6) + \omega'_S t\right) \\ - \left(\theta_{Ref} + \frac{n\, D_8\, \omega_{Ref}}{c} + \omega_{Ref}\, t\right) \quad \text{(I.4.12)}$$

Where $\omega_{fast} = \omega'_S - \omega_{Ref}$ is the frequency and θ_{loc} the phase of the reference clock used in the fast lock (see Fig. I.4.3b). Again, in order for this synchronization to work, we need to have fast enough feedback with respect to the noise present. Because this equation contains the three phase term due to the linewidth of the lasers ($\theta_{Ex/1064/Ref}$), of which θ_{Ex} is by far the dominant (see Table I.4.2). For long fibers, the term containing the long fibers (D_5) can also induce fast phase fluctuations. We show that we can ensure these conditions in the main text, Fig. I.4.5, and give the performance parameter σ_{fast}. We can rewrite I.4.12 to a more useful form as

$$\theta_S + \frac{n\omega_S}{c}(D_2 + D_4) - \theta_{1064} + \frac{n'\omega'_S}{c}D_5 + \omega'_S t \\ = -\frac{n'\omega'_S}{c}D_6 + \omega_{fast}t + \eta_{fast}(t) + \theta_{Ref} + \frac{n\, D_8\, \omega_{Ref}}{c} \quad \text{(I.4.13)}$$

Global synchronization task

The final synchronization task is the global synchronization, which is the final task that closes the feedback system between the two distant nodes. It takes as input two arms, A and B, that interfere at the point z_7, the central beamsplitter. The fields that are interfering is stabilization light that is leaking *through* the UNF in each arm. This is light that came from the same location as in the fast synchronization task I.4.12, but is now traveling towards the SNSPDs. We can write the optical phase coming from node A/B as

$$\phi^{A/B}(t, z_7) = \theta_{Ex} + \frac{n\omega_S^{A/B}}{c}(D_2^{A/B} + D_4^{A/B}) \\ - \theta_{1064} + \frac{n'\, \omega_S'^{A/B}}{c}(D_5^{A/B} + D_7^{A/B}) + \omega_S'^{A/B}\, t \quad \text{(I.4.14)}$$

We described in the main text that the global synchronization task only needs a small bandwidth (1000 Hz) to be realized. However, equation I.4.14 contains many fast terms, such as the laser linewidth of the Excitation laser. Therefore the global synchronization can only be realized once the fast synchronization condition is met. This becomes apparent when we filling in I.4.13 in I.4.14, giving:

$$\phi^{A/B}(t,z_7) = \eta_{fast}(t) + \theta_{Ref} + \frac{n\, D_8^{A/B}\, \omega_{Ref}}{c} + \frac{n'\, \omega_S^{\prime A/B}}{c}(D_7^{A/B} - D_6^{A/B}) + \omega_S^{\prime A/B} t \quad \text{(I.4.15)}$$

and using that to write down synchronization task error for the global lock:

$$\eta(t)_{glob} = \left(\phi^A(t,z_7) - \phi^B(t,z_7)\right) - \omega_{glob}(t) - \theta_{glob}(t) \quad \text{(I.4.16)}$$

which, when grouping similar terms pairwise, becomes

$$\begin{aligned}\eta(t)_{glob} = \eta^A_{fast}(t) - \eta^B_{fast}(t) + \\ \theta^A_{Ref} - \theta^B_{Ref} + \frac{n\,(D_8^A - D_8^B)\,\omega_{Ref}}{c} + \\ \frac{n'\,\omega_S^{\prime A}}{c}(D_7^A - D_6^A) - \frac{n'\,\omega_S^{\prime B}}{c}(D_7^B - D_6^B) + \\ (\omega_S^{\prime A} - \omega_S^{\prime B})\, t - \theta_{glob}(t)\end{aligned} \quad \text{(I.4.17)}$$

where the super-script$^{A/B}$ denotes the field coming from node 1/2 and $\omega_{glob} = (\omega_S^{\prime A} - \omega_S^{\prime B})$ the frequency and θ_{glob} the phase of the clock used as reference in the global synchronization (see Fig. I.4.3c). We will go over this equation term by term. The first line of the equation are the residual terms from the fast synchronization tasks $\eta^{A/B}_{fast}(t)$, which are the residuals of the fast lock, and therefore too fast for the global synchronization to provide any feedback on. That is why they also appear on the other side of the equation, as they remain an error source in the system. The second line is the phase contribution due to the linewidth of the reference laser and optical path of the delivery of the laser to the fast photo-diodes. By using the same length fibers ($D_8^A \sim D_8^B$) we can minimize both the effect of fiber drifts, as well as the effect of the Reference laser linewidth. The third line of equation I.4.17 shows two terms that are dependent on the distance from the UNF to the two points (fast photo-diode z_6 and central beamsplitter z_7) of interference. These are more difficult to keep equal, and is best practice to keep these fibers in the same optical rack such that they share vibrations/temperature fluctuations. We can also identify the synchronization error of the global synchronization *by itself* by excluding the fast errors and writing as

$$\eta_{glob}(t) = \theta^A_{Ref} - \theta^B_{Ref} + \frac{n\,(D_8^A - D_8^B)\,\omega_{Ref}}{c} + \frac{n'\,\omega_S^{\prime A}}{c}(D_7^A - D_6^A) - \frac{n'\,\omega_S^{\prime B}}{c}(D_7^B - D_6^B) - \omega_{glob}\, t \quad \text{(I.4.18)}$$

Now that we have discussed all three different synchronization tasks and described their synchronization task error, we can go back go to I.4.8 and fill in the synchronization conditions.

Substitution Local synchronization

We start with equation I.4.9 and fill in the local synchronization condition in the form of Eq. I.4.11 to get

$$\phi(t,z_7) = \theta_S + \frac{n\omega_S}{c}D_2 + \eta_{loc}(t) + \frac{n(\omega_S-\omega_{Ex})}{c}D_3 + \frac{n\omega_{Ex}}{c}D_4 - \theta_{1064} + \frac{n'\omega'_{Ex}}{c}(D_5+D_7) + \omega'_{Ex}t \quad \text{(I.4.19)}$$

where the term $\frac{n(\omega_S-\omega_{Ex})}{c}D_3 = \theta_{err}(\Delta D_3)$ is due to the fact that the interference for the local synchronization happens at a distance D_3 away from where the stabilization light ω_S is split off (local beamsplitter). The phase is therefore sensitive to expansion/contraction of D_3, albeit with only the frequency difference of $\omega_S - \omega_{Ex}$. Therefore drifts of D_3 are minimized by making the distance short and housed in a temperature stabilized environment and can be considered constant.

Substitution fast synchronization

In order to fill in the fast synchronization task into eq. I.4.19, we need to substitute all the terms containing ω_{Ex} with ω_S. These fields are co-propagating from the local beamsplitter towards the QFC (D_4) and onward. Because the local synchronization ensure their mutual coherence at the local beamsplitter, and ω_S is stabilized in the midpoint at the fast photodiode, we can follow the substitution method as outlined in Section I.4.9.2, taking into account the expected fiber drifts. The terms containing ω_{Ex} contain the distances D_4, D_5 and D_7. We remark that the drifts in $\theta(\Delta D_4)$ and $\theta(\Delta D_7)$ are negligible when the (fiber) lengths are short($\approx$10 m) and will be considered constant and left out, however $\theta(\Delta D_5)$ can be significant due to the length of D_5 (see Table I.4.3). Completing the substitution gives us:

$$\phi(t,z_7) = \theta_S + \frac{n\omega_S}{c}(D_2+D_4) + \theta_{err}(\Delta D_3,\omega_{loc}) + \eta_{loc}(t) - \theta_{1064} + \frac{n'\omega'_S}{c}(D_5+D_7) + \theta_{err}(\Delta D_5,\omega_{loc}) + (\omega'_S+\omega_{loc})t \quad \text{(I.4.20)}$$

where we have added the error term $\theta_{err}(\Delta D_5,\omega_{loc})$ accordingly. We can now recognize the terms of the fast synchronization task, and filling in the form of eq. I.4.13 we arrive at the expression

$$\phi(t,z_7) = \eta_{loc}(t) + \eta_{fast}(t) + \theta_{err}(\Delta D_5,\omega_{loc}) + \theta_{Ref} + \frac{n\,\omega_{Ref}}{c}D_8 + \frac{n'\omega'_S}{c}(D_7-D_6) + (\omega_{fast}+\omega_{loc})t \quad \text{(I.4.21)}$$

SUBSTITUTION GLOBAL SYNCHRONIZATION

We can now fill in eq. I.4.21 into I.4.8, and use the global synchronization condition (the last four terms of this expression are precisely one half of the global synchronization condition I.4.18), to simplify it into its final form:

$$\begin{aligned}\eta(t) = \eta^A_{loc}(t) + \eta^A_{fast}(t) - \eta^B_{loc}(t)) + \eta^B_{fast}(t) + \\ \theta^A_{err}(\Delta D_5, \omega_{loc}) - \theta^B_{err}(\Delta D_5, \omega_{loc}) + \\ \Omega_{tot}\, t + \eta_{glob}(t)\end{aligned} \quad \text{(I.4.22)}$$

The first line is the performance of the local and fast synchronization task $\eta^{A/B}_{loc/fast}(t)$ of the two nodes, the second line the error due to the expansion/contraction of the long fibers $\theta^{A/B}_{err}(D_5)$. The last line is the global synchronization task performance $\eta_{glob}(t)$, and a time dependent term $\Omega_{tot}\ t$, where $\Omega_{tot} = (\omega^A_{fast} + \omega^A_{loc}) - (\omega^B_{fast} + \omega^B_{loc})$. All the other terms in this equation are either not dependent on time, or we have discussed ways to minimize their effects over longer time duration. The only thing left is then to choose the right frequencies of all the synchronization tasks such that the time dependence of the phase is removed, e.g. $\Omega_{tot} = 0$, with only small variations of $\eta(t)$ remaining in the system.

I.4

SELECTION OF CLOCK FREQUENCIES

As described in the main text, the condition $\Omega_{tot} = 0$ is not the only requirement for the frequencies at which the synchronization tasks operate. Due to shot-noise limitations of the SNSPDs, $\omega'^A_S - \omega'^B_S = \omega_{glob}$ can realistically not exceed 10 kHz, and in order for the feedback bandwidth of the fast synchronization to be fast enough, a high ω_{fast} is needed. The additional requirement of $\omega'^A_{Ex} = \omega'^B_{Ex}$ to generate indistinguishable photons, while the natural frequency $\omega^A_{Ex} - \omega^B_{Ex}$ >1 GHz can be far detuned, adds to the complexity. The flexibility in choosing ω_{1064} on each of the nodes separately deals with this requirement, and shifts both the excitation and stabilization light equally. Considering other experimental details outside the scope of this work regarding the temperature stabilization of the FBGs, we arrive on the choice of frequencies as presented in Table I.4.1. Setting $\omega^{A/B}_{loc} = 400e6 \mp 750$Hz and $\omega^A_{fast} = 215001500$Hz and $\omega^B_{fast} = 215000000$Hz. With these values, the remaining frequency difference between the excitation lasers is:

$$\Omega_{tot} = (215001500 + 399999250) - (215000000 + 400000750) = 0 \quad \text{(I.4.23)}$$

Additionally, this gives us $\omega_{glob} = 1500$Hz, which lies well within the bandwidth of the SNSPDs.

CONCLUSION

We can now return to the central synchronization condition I.4.8 and make the following claim. Given that the conditions

1. Both nodes have the local phase synchronization active (I.4.10),
2. The midpoint synchronizes the Stabilization light to the Reference laser (I.4.12),

3. The Stabilization light of the nodes is synchronized to each other(I.4.17),
4. The known error $\theta_{err}^{A/B}(\Delta D_5)$ is calculated and compensated by adjusting the phase of the clock used for reference in the global synchronizaiton.
5. The phase is sampled at a frequency below the frequency of the noise (I.4.5),
6. The measured residual phase noise in each of the synchronization tasks can be considered independent,

hold we can consider the excitation lasers to be synchronized. Condition six is valid due to the fact that the local synchronization task feedback is done on the excitation laser AOM, and therefore not affected by the synchronization in the midpoint. Additionally the residual phase noise of the fast synchronization is practically zero below the bandwidth of the global synchronization task, see Fig. I.4.5 and I.4.6, making them independent. Given these conditions, then the sampling of the error $\eta(t)$ from Eq. I.4.22 of the phase between the excitation lasers of each node arriving at the central beamsplitter in the midpoint can be written as:

I.4

$$\mathcal{N}_{tot}(\mu_{tot},\sigma_{tot}) + \theta_{offset} \tag{I.4.24}$$

$$\mu_{tot} = \mu_{loc}^{A} + \mu_{loc}^{B} + \mu_{fast}^{A} + \mu_{fast}^{B} + \mu_{glob} \tag{I.4.25}$$

$$\sigma_{tot} = \sqrt{(\sigma_{loc}^{A})^2 + (\sigma_{loc}^{B})^2 + (\sigma_{fast}^{A})^2 + (\sigma_{fast}^{B})^2 + (\sigma_{glob})^2} \tag{I.4.26}$$

where $\mathcal{N}_{tot}(\mu_{tot},\sigma_{tot})$ is the distribution of the total phase error, and $\mathcal{N}_{i}^{A/B}(\mu_i,\sigma_i)$ the mean and standard deviation of resulting distributions of the sampling of the individual synchronization task errors. The value θ_{offset} is a term that contains all the constant phase terms in this derivation. This is the central result of the derivation, and provides the full description of the total synchronization. This result is also experimentally verified in Fig. I.4.7, by measuring the interference of the excitation lasers at the central beamsplitter. The measurement involves the changing of the phase of the RF-clock used for the global synchronization, therefore changing μ_{global}. The measured phase of the oscillation of Fig. I.4.7b is the true 'phase setpoint' of the optical interference of the excitation lasers. The relation between μ_{global} and this phase setpoint is difficult to calculate due to the constant terms neglected in this derivation, currently denoted as θ_{offset}. It can however be measured relatively quickly and consistently, as Fig. I.4.7c shows over the duration of 10 h, showing that its long-term drift is dominated by the terms mentioned in Section I.4.9.24.

I.4.9.3. Relation between optical phase and entangled state phase

The main result of this work shows the stabilization of the optical phase between two remote nodes over telecom fiber. The light with which we show this stability is reflected of the diamond chip, and follows the same optical path towards the midpoint and central beamsplitter. However, during the entanglement generation, the Excitation light is actually:

1. propagating ≈10 µm into the diamond,

2. excitation the Nitrogen Vacancy-center resonantly and subsequent emission of a single photon through spontaneous emission,

3. that propagates ≈10 µm back out of the diamond.

All steps add an additional phase to the optical field that is now a single photon. These factors introduce fixed offsets between the phase investigated in this work, and need to be calibrated using a separate experiment. therefore, a stable optical phase is necessary but not sufficient to generate entanglement between two distant NV-center electron spins. Any drifts in these parameters would change the entangled state phase, and therefore the correlations between the spin states. These processes can be considered constant in time given the following conditions:

1. The path taken towards the NV center is constant in time

2. The path taken from the NV center towards the collection is constant in time and a single spatial mode with well-defined phase.

3. The spontaneous emission process is coherent with the exciting field

Both (1) and (2) are realized by making sure the relative position of the microscope objective used to address the NV center and the diamond sample is stationary during the entanglement generation. Furthermore, if the objective is moved during the operation, a check of the entangled state phase has to be done again. The relative microscope and sample location is one of the limiting factors in keeping a constant entangled state phase. The spontaneous emission is found to be coherent with the excitation field [37], and, because of the short ≈1 ns excitation pulse used, even in the presence of small detunings with the emitter.

I.4

REFERENCES

[1] H. J. Kimble, *The quantum internet,* Nature **453**, 1023 (2008).

[2] S. Wehner, D. Elkouss, and R. Hanson, *Quantum internet: A vision for the road ahead,* Science **362**, 30337383 (2018).

[3] D. L. Moehring, P. Maunz, S. Olmschenk, K. C. Younge, D. N. Matsukevich, L.-M. Duan, and C. Monroe, *Entanglement of single-atom quantum bits at a distance,* Nature **449**, 68 (2007).

[4] S. Ritter, C. Nölleke, C. Hahn, A. Reiserer, A. Neuzner, M. Uphoff, M. Mücke, E. Figueroa, J. Bochmann, and G. Rempe, *An elementary quantum network of single atoms in optical cavities,* Nature **484**, 195 (2012).

[5] J. Hofmann, M. Krug, N. Ortegel, L. Gérard, M. Weber, W. Rosenfeld, and H. Weinfurter, *Heralded Entanglement Between Widely Separated Atoms,* Science **337**, 72 (2012).

[6] L. J. Stephenson, D. P. Nadlinger, B. C. Nichol, S. An, P. Drmota, T. G. Ballance, K. Thirumalai, J. F. Goodwin, D. M. Lucas, and C. J. Ballance, *High-Rate, High-Fidelity Entanglement of Qubits Across an Elementary Quantum Network,* Physical Review Letters **124**, 110501 (2020).

[7] S. Daiss, S. Langenfeld, S. Welte, E. Distante, P. Thomas, L. Hartung, O. Morin, and G. Rempe, *A quantum-logic gate between distant quantum-network modules,* Science **371**, 614–617 (2021).

[8] V. Krutyanskiy, M. Galli, V. Krcmarsky, S. Baier, D. A. Fioretto, Y. Pu, A. Mazloom, P. Sekatski, M. Canteri, M. Teller, J. Schupp, J. Bate, M. Meraner, N. Sangouard, B. P. Lanyon, and T. E. Northup, *Entanglement of trapped-ion qubits separated by 230 meters,* Phys. Rev. Lett. **130**, 050803 (2023).

[9] S. D. Barrett and P. Kok, *Efficient high-fidelity quantum computation using matter qubits and linear optics,* Physical Review A **71**, 060310 (2005).

[10] B. Hensen, H. Bernien, A. E. Dréau, A. Reiserer, N. Kalb, M. S. Blok, J. Ruitenberg, R. F. L. Vermeulen, R. N. Schouten, C. Abellán, W. Amaya, V. Pruneri, M. W. Mitchell, M. Markham, D. J. Twitchen, D. Elkouss, S. Wehner, T. H. Taminiau, and R. Hanson, *Loophole-free bell inequality violation using electron spins separated by 1.3 kilometres,* Nature **526**, 682 (2015).

[11] A. Narla, S. Shankar, M. Hatridge, Z. Leghtas, K. M. Sliwa, E. Zalys-Geller, S. O. Mundhada, W. Pfaff, L. Frunzio, R. J. Schoelkopf, and M. H. Devoret, *Robust concurrent remote entanglement between two superconducting qubits,* Physical Review X **6**, 031036 (2016).

[12] C. M. Knaut, A. Suleymanzade, Y.-C. Wei, D. R. Assumpcao, P.-J. Stas, Y. Q. Huan, B. Machielse, E. N. Knall, M. Sutula, G. Baranes, N. Sinclair, C. De-Eknamkul, D. S. Levonian, M. K. Bhaskar, H. Park, M. Lončar, and M. D. Lukin, *Entanglement of nanophotonic quantum memory nodes in a telecom network,* Nature **629**, 573 (2024).

[13] C. Cabrillo, J. I. Cirac, P. García-Fernández, and P. Zoller, *Creation of entangled states of distant atoms by interference,* Physical Review A **59**, 1025–1033 (1999).

[14] S. Bose, P. L. Knight, M. B. Plenio, and V. Vedral, *Proposal for teleportation of an atomic state via cavity decay,* Physical Review Letters **83**, 5158–5161 (1999).

[15] H. Bernien, B. Hensen, W. Pfaff, G. Koolstra, M. S. Blok, L. Robledo, T. H. Taminiau, M. Markham, D. J. Twitchen, L. Childress, and R. Hanson, *Heralded entanglement between solid-state qubits separated by three metres,* Nature **497**, 86 (2013).

[16] L. Slodička, G. Hétet, N. Röck, P. Schindler, M. Hennrich, and R. Blatt, *Atom-atom entanglement by single-photon detection,* Physical Review Letters **110**, 083603 (2013).

[17] A. Delteil, Z. Sun, W.-b. Gao, E. Togan, S. Faelt, and A. Imamoğlu, *Generation of heralded entanglement between distant hole spins,* Nature Physics **12**, 218–223 (2016).

[18] R. Stockill, M. J. Stanley, L. Huthmacher, E. Clarke, M. Hugues, A. J. Miller, C. Matthiesen, C. Le Gall, and M. Atatüre, *Phase-Tuned Entangled State Generation between Distant Spin Qubits,* Physical Review Letters **119**, 010503 (2017).

[19] D. Lago-Rivera, S. Grandi, J. V. Rakonjac, A. Seri, and H. de Riedmatten, *Telecom-heralded entanglement between multimode solid-state quantum memories,* Nature **594**, 37 (2021).

[20] J.-L. Liu, X.-Y. Luo, Y. Yu, C.-Y. Wang, B. Wang, Y. Hu, J. Li, M.-Y. Zheng, B. Yao, Z. Yan, D. Teng, J.-W. Jiang, X.-B. Liu, X.-P. Xie, J. Zhang, Q.-H. Mao, X. Jiang, Q. Zhang, X.-H. Bao, and J.-W. Pan, *Creation of memory–memory entanglement in a metropolitan quantum network,* Nature **629**, 579–585 (2024).

[21] A. Ruskuc, C.-J. Wu, E. Green, S. L. N. Hermans, J. Choi, and A. Faraon, *Scalable multipartite entanglement of remote rare-earth ion qubits,* (2024).

[22] P. C. Humphreys, N. Kalb, J. P. J. Morits, R. N. Schouten, R. F. L. Vermeulen, D. J. Twitchen, M. Markham, and R. Hanson, *Deterministic delivery of remote entanglement on a quantum network,* Nature **558**, 268 (2018).

[23] W. Pfaff, B. J. Hensen, H. Bernien, S. B. van Dam, M. S. Blok, T. H. Taminiau, M. J. Tiggelman, R. N. Schouten, M. Markham, D. J. Twitchen, and R. Hanson, *Unconditional quantum teleportation between distant solid-state quantum bits,* Science **345**, 532–535 (2014).

[24] M. Pompili, S. L. N. Hermans, S. Baier, H. K. C. Beukers, P. C. Humphreys, R. N. Schouten, R. F. L. Vermeulen, M. J. Tiggelman, L. dos Santos Martins, B. Dirkse, S. Wehner, and R. Hanson, *Realization of a multinode quantum network of remote solid-state qubits,* Science **372**, 259 (2021).

[25] S. L. N. Hermans, M. Pompili, H. K. C. Beukers, S. Baier, J. Borregaard, and R. Hanson, *Qubit teleportation between non-neighbouring nodes in a quantum network,* Nature **605**, 663–668 (2022).

[26] A. J. Stolk, K. L. van der Enden, M.-C. Slater, I. te Raa-Derckx, P. Botma, J. van Rantwijk, J. J. B. Biemond, R. A. J. Hagen, R. W. Herfst, W. D. Koek, A. J. H. Meskers, R. Vollmer, E. J. van Zwet, M. Markham, A. M. Edmonds, J. F. Geus, F. Elsen, B. Jungbluth, C. Haefner, C. Tresp, J. Stuhler, S. Ritter, and R. Hanson, *Metropolitan-scale heralded entanglement of solid-state qubits,* Science Advances **10** (2024), 10.1126/sciadv.adp6442.

[27] A. Dréau, A. Tchebotareva, A. E. Mahdaoui, C. Bonato, and R. Hanson, *Quantum frequency conversion of single photons from a nitrogen-vacancy center in diamond to telecommunication wavelengths,* Physical Review Applied **9**, 064031 (2018).

[28] J. Geus, F. Elsen, S. Nyga, A. J. Stolk, K. L. van der Enden, E. J. van Zwet, C. Haefner, R. Hanson, and B. Jungbluth, *Low-noise short-wavelength pumped frequency downconversion for quantum frequency converters,* Optica Open (2023), 10.1364/opticaopen.23684502.v1.

[29] A. Tchebotareva, S. L. N. Hermans, P. C. Humphreys, D. Voigt, P. J. Harmsma, L. K. Cheng, A. L. Verlaan, N. Dijkhuizen, W. de Jong, A. Dréau, and R. Hanson, *Entanglement between a diamond spin qubit and a photonic time-bin qubit at telecom wavelength,* Phys. Rev. Lett. **123**, 063601 (2019).

[30] A. J. Stolk, K. L. van der Enden, M.-C. Roehsner, A. Teepe, S. O. J. Faes, C. E. Bradley, S. Cadot, J. Van Rantwijk, I. Te Raa, R. A. J. Hagen, A. L. Verlaan, J. J. B. Biemond, A. Khorev, R. Vollmer, M. Markham, A. M. Edmonds, J. P. J. Morits, T. H. Taminiau, E. J. Van Zwet, and R. Hanson, *Telecom-band quantum interference of frequency-converted photons from remote detuned nv centers,* PRX Quantum **3**, 020359 (2022).

[31] J.-P. Chen, C. Zhang, Y. Liu, C. Jiang, W. Zhang, X.-L. Hu, J.-Y. Guan, Z.-W. Yu, H. Xu, J. Lin, M.-J. Li, H. Chen, H. Li, L. You, Z. Wang, X.-B. Wang, Q. Zhang, and J.-W. Pan, *Sending-or-not-sending with independent lasers: Secure twin-field quantum key distribution over 509 km,* Phys. Rev. Lett. **124**, 070501 (2020).

[32] J. J. B. Biemond, A. J. Stolk, K. L. van der Enden, E. J. van Zwet, and A. J. H. Meskers, *Controlled synchronisation at bandwidths beyond the limit of direct synchronisation error measurement,* Patent pending (2023).

[33] J. J. B. Biemond, A. J. H. Meskers, W. D. Koek, A. J. Stolk, K. L. van der Enden, and E. J. van Zwet, *Estimation method of phase difference between two optical channels induced by optical latency variations,* Patent pending (2023).

[34] E. F. Dierikx, A. E. Wallin, T. Fordell, J. Myyry, P. Koponen, M. Merimaa, T. J. Pinkert, J. C. J. Koelemeij, H. Z. Peek, and R. Smets, *White rabbit precision time protocol on long-distance fiber links,* IEEE Transactions on Ultrasonics, Ferroelectrics, and Frequency Control **63**, 945 (2016).

[35] A. Matsuki, H. Kori, and R. Kopayashi, *An extended Hilbert transform method for reconstructing the phase from an oscillatory signal,* Scientific Reports **13** (2023).

[36] P. Welch, *The use of fast fourier transform for the estimation of power spectra: A method based on time averaging over short, modified periodograms,* IEEE Transactions on Audio and Electroacoustics **15**, 70–73 (1967).

[37] C. R. Stroud, *Quantum-electrodynamic treatment of spontaneous emission in the presence of an applied field,* Physical Review A **3**, 1044–1052 (1971).

I.5

METROPOLITAN-SCALE HERALDED ENTANGLEMENT OF SOLID-STATE QUBITS

This person comes up and says "Who's your hero?" I said, "I thought about it. You know who it is?" I said, "It's me in 10 years."

Matthew McConaughey,
Oscar Acceptance for Best Actor in a Leading Role, 2014

A.J. Stolk†, K.L. van der Enden†, M.-C. Slater, I. te Raa-Derckx, P. Botma, J. van Rantwijk, J.J.B. Biemond, R.A.J. Hagen, R.W. Herfst, W.D. Koek, A.J.H. Meskers, R. Vollmer, E.J. van Zwet, M. Markham, A.M. Edmonds, J.F. Geus, F. Elsen, B. Jungbluth, C. Haefner, C. Tresp, J. Stuhler, S. Ritter, and R. Hanson

A key challenge towards future quantum internet technology is connecting quantum processors at metropolitan scale. Here, we report on heralded entanglement between two independently operated quantum network nodes separated by 10km. The two nodes hosting diamond spin qubits are linked with a midpoint station via 25km of deployed optical fiber. We minimize the effects of fiber photon loss by quantum frequency conversion of the qubit-native photons to the telecom L-band and by embedding the link in an extensible phase-stabilized architecture enabling the use of the loss-resilient single-click entangling protocol. By capitalizing on the full heralding capabilities of the network link in combination with real-time feedback logic on the long-lived qubits, we demonstrate the delivery of a predefined entangled state on the nodes irrespective of the heralding detection pattern. Addressing key scaling challenges and being compatible with different qubit systems, our architecture establishes a generic platform for exploring metropolitan-scale quantum networks.

The results of this chapter have been published in Science Advances **10** eadp6442 (2024).

† These authors contributed equally to this work.

I.5.1. Introduction

Future quantum networks distributing entanglement between distant quantum processors [1, 2] hold the promise of enabling novel applications in communication, computing, sensing, and fundamental science [3–6]. Over the past decades a range of experiments on different qubit platforms have demonstrated the rudimentary capabilities of quantum networks at short distances including photon-mediated entanglement generation [7–13]. These short-range qubit networks are useful for testing of improved hardware [14], developing a quantum network control stack [15] and for exploring quantum network protocols in a lab setting [16–18].

The next major challenge is to develop quantum network systems capable of generating, storing and processing quantum information on metropolitan scales. Such systems face several new requirements. First, the large physical distance, the consequential substantial communication times and need for scalability demand that the network nodes operate fully independently. Second, as the optical fibers connecting nodes will extend for tens of kilometers, photon loss becomes a critical parameter that must be mitigated. Third, as advanced network applications require the heralded delivery of shared entangled states ready for further use, the qubit systems must be able to store quantum information for extended times and the network system must be capable of applying real-time feedback to the qubits upon successful entanglement generation.

Recent qubit experiments have shown promising progress towards the latter two criteria, including the integration with efficient quantum frequency converters [19–24], demonstration of long coherence times on qubit systems that can be extended into multi-qubit registers [25, 26] and entanglement generation between nearby qubits via tens of kilometers of optical fiber [27, 28]. In parallel, experiments on ensemble-based quantum memories have pioneered notable advances on the first two criteria [29–32].

Here, we report on the realization of a deployed quantum link between two solid-state qubit nodes separated by 10 km matching all three criteria. The two network nodes are combined with a midpoint heralding station via 25 km of deployed fiber, with all relevant classic and quantum signals propagating over the same fiber bundle in telecom bands (see Fig. I.5.1). We implement an extensible architecture that enables the nodes to operate fully independently at large distance, mitigates the effects of photon loss on the entangling rate and allows for full heralding of entanglement generation. Furthermore, the network architecture features precise polarization and timing control as well as active stabilization of the relative optical phase between photons emitted from the nodes, enabling the use of the loss-resilient single-click protocol for efficient entanglement generation [33, 34]. We benchmark the performance of the architecture by parameter monitoring and by generating entanglement in post-selection. Finally, we use the full network capabilities of heralding and real-time feedback to deliver entangled states shared between the nodes ready for further use. This demonstration establishes a critical capability for future applications and scaling and presents a key milestone towards large-scale quantum networking.

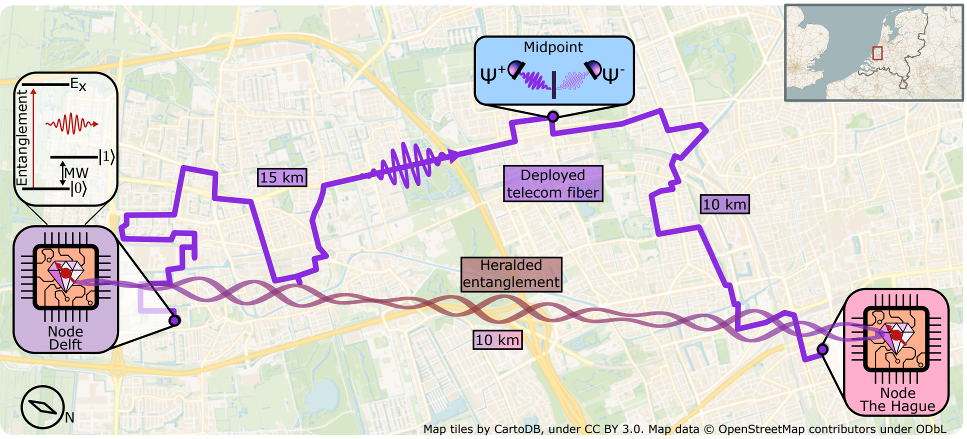

Figure I.5.1: **The metropolitan-scale quantum link.** Cartographic layout of the distant quantum link and the route of the deployed fiber bundle, with similar quantum processor nodes in Delft and The Hague. Fiber length between node Delft and midpoint is 15 km, and between node The Hague and midpoint is 10 km, with losses on the quantum channels at 5.6 dB and 5.2 dB, respectively. Inset to the quantum processor are the used qubit energy levels where the qubit is encoded in the electronic ground state addressable with microwave pulses (MW), and the spin-selective optical transition (λ = 637 nm) is used for entanglement generation and state readout.

I.5.2. RESULTS

I.5.2.1. DEPLOYED QUANTUM NETWORK LINK ARCHITECTURE

In order to meet the challenges of metropolitan-scale entanglement generation, we designed and implemented the control architecture depicted in Fig. I.5.2A. Each node contains a CVD grown diamond chip hosting a Nitrogen-Vacancy (NV) center electronic spin qubit that can be faithfully initialized and read out by resonant laser light and controlled using microwave pulses. The NV center optical transition at 637 nm is used for generating qubit-photon entanglement. Each node is equipped with a stand-alone quantum frequency converter (QFC) unit that converts the 637 nm NV photons down to the telecom L-band at 1588 nm such that photon loss in the deployed fiber is minimized. The QFCs further serve as a tuning mechanism for compensating strain-induced offsets between the native emission frequencies typical for solid-state qubits. Through independent feedback on the frequency of the individual QFC pump lasers, we achieve conversion to a common target wavelength despite the few gigahertz difference in qubit emission frequencies [35]. The QFC in Delft is based on a novel noise-reduced approach (NORA) [36] that produces two orders of magnitude lower background counts than the periodically-poled Lithium Niobate (ppLN) with integrated waveguide based QFC in The Hague [37].

To further mitigate photon loss, we employ the single-click entangling protocol [33, 34, 38] which employs the number basis encoding for the photons. For this protocol the entangling rate favourably scales with the square root of the photon transmission probability across the entire link, as opposed to schemes using photonic polarization or time-bin encoding which exhibit a linear scaling of rate with transmission [7–10, 12–14, 27, 28]. In the single-click protocol, each qubit is first prepared in an unbalanced superposition state $|\psi\rangle = \sqrt{\alpha}\,|0\rangle + \sqrt{1-\alpha}\,|1\rangle$. Application of an optical π-pulse resonant for qubit state $|0\rangle$ and subsequent spontaneous emission then results in qubit-photon entanglement, where the photonic qubit is encoded in the photon number state (0 or 1). Overlap of the photonic states at the beam splitter at the midpoint removes the which-path information, followed by single-photon detection by superconducting nanowire single-photon detectors. Upon measurement of one photon after interference, entanglement of the qubit states is heralded to $|\Psi^{\pm}\rangle = \left(|01\rangle \pm e^{i\theta}|10\rangle\right)/\sqrt{2}$ with maximum fidelity $1-\alpha$, where the $\pm$ sign is set by which output arm the photon was detected in. The entangled state phase θ is dependent on the optical phase difference between the photonic modes arriving at the interference beam splitter from Delft and The Hague. Note that choosing the value of α involves a trade-off between higher signal-to-noise (larger α) and higher fidelity (smaller α). We use $\alpha = 0.25$ in the current work.

This entanglement generation critically relies on photon indistinguishability at the heralding station and therefore all degrees of freedom of the photons (frequency, arrival time, phase, polarization) must be actively controlled at the metropolitan scale. A defining feature of our architecture is that stabilization laser light used for phase locking and polarization stabilization is time-multiplexed with the single-photon signals used for entanglement generation and sent over the same fiber from the nodes to the midpoint. To this end, we operate the link at a pre-defined heartbeat at 100 kHz, defining a common time division. During each heartbeat period of 10 µs, stabilization light is sent to the midpoint continuously, except for a 2 µs period where the entangling photonic states are sent out. This allows for near-continuous stabilization with high feedback bandwidth while performing entanglement generation. Below we discuss the major sources of drift at metropolitan scale affecting the entangled state generation and our strategy for mitigating them.

First, length drift of the deployed fibers can result in reduced overlap of the photonic modes on the beam splitter. The timing of the optical π-pulse is locally controlled and disciplined by an optically linked distributed clock that doubles as Ethernet connection (White-Rabbit protocol [39]) over a dedicated fiber. Fig. I.5.2B shows a histogram of measured offsets in time-of-arrival for the two deployed-fiber segments over 24 hours, with the inset displaying the drift speeds ($\sigma = 5\,\mathrm{ps\,min^{-1}}$). By using this data to compensate for the drift via timing adjustments of the control electronics every ~15 minutes, the offset is kept below 50 ps, much smaller than the photon $1/e$ decay time of 12 ns. The resulting entangled state infidelity due to length drifts is below 0.1%.

Second, as the phase difference of the photonic modes interfering at the beam splitter is imprinted on the entangled state, this phase must be known in order for the generated entangled states to be useful. To achieve a known and constant optical phase setpoint, five individual phase locking loops are implemented across the total link, see Fig. I.5.2A. At each node, a local phase lock is closed between reflection of the resonant excitation light off the qubit device surface and the stabilization laser light via the controllers θ_1 and θ_2, stabilizing the in-fiber and free-space excitation and collection optics. Phase noise from the long fiber and excitation laser is mitigated by the controllers θ_3 and θ_4 via interference of light from the midpoint reference telecom laser and frequency down-converted stabilization light at nanowatt levels. Importantly, analog phase feedback is performed locally at the midpoint directly on the incoming light yielding a high stabilization bandwidth exceeding 200 kHz. Lastly, interference of telecom stabilization light from both nodes at the central beam splitter is measured by the single-photon detectors and input to controller θ_5, closing the global phase lock between the nodes (see Suppl. Mat. for additional details). We note that the modularity of this architecture directly allows for the connection of multiple nodes to the same midpoint in a star topology, as the synchronization of all incoming signals to a central reference and relative phase stabilization between links can be performed using the control system at the midpoint. Fig. I.5.2C displays a histogram of the resulting phase errors during 24 hours of operation. Stable operation is achieved with a few-percent impact on the entangled state fidelity per connection. As this architecture yields full control over the phase difference at the beam splitter, the phase θ of the entangled state can be tuned on demand by adjusting the setpoint of the phase lock (see Suppl. Mat.). In order to maintain the phase lock under frequency drifts at the nodes, two individual feedback loops (ν) between the nodes and the midpoint adjust the frequency of the individual QFC pump lasers at an update rate of 500 Hz. Importantly, this desaturation allows for a large dynamic range of the phase feedback, as required to handle the observed frequency drift range of >50 MHz, see Fig. I.5.2C inset.

Third, polarization drifts, though considerably slower than phase drift, must also be mitigated. To this end, the stabilization light is additionally used for electronic polarization compensation (EPC) at the midpoint. The amplitude of the error signal input at θ_3 and θ_4 is dependent on polarization overlap with an in-fiber polarizer. We use this as input for a gradient ascent algorithm to feedback on the polarization of the incoming light at the midpoint. Data on the deployed link (inset Fig. I.5.2D) shows that polarization drift occurs on second-timescales; our feedback at a few Hz bandwidth keeps the polarization aligned to within a few percent (Fig. I.5.2D). Any remaining polarization mismatch is removed by the polarizers at the cost of a slightly reduced entanglement generation rate.

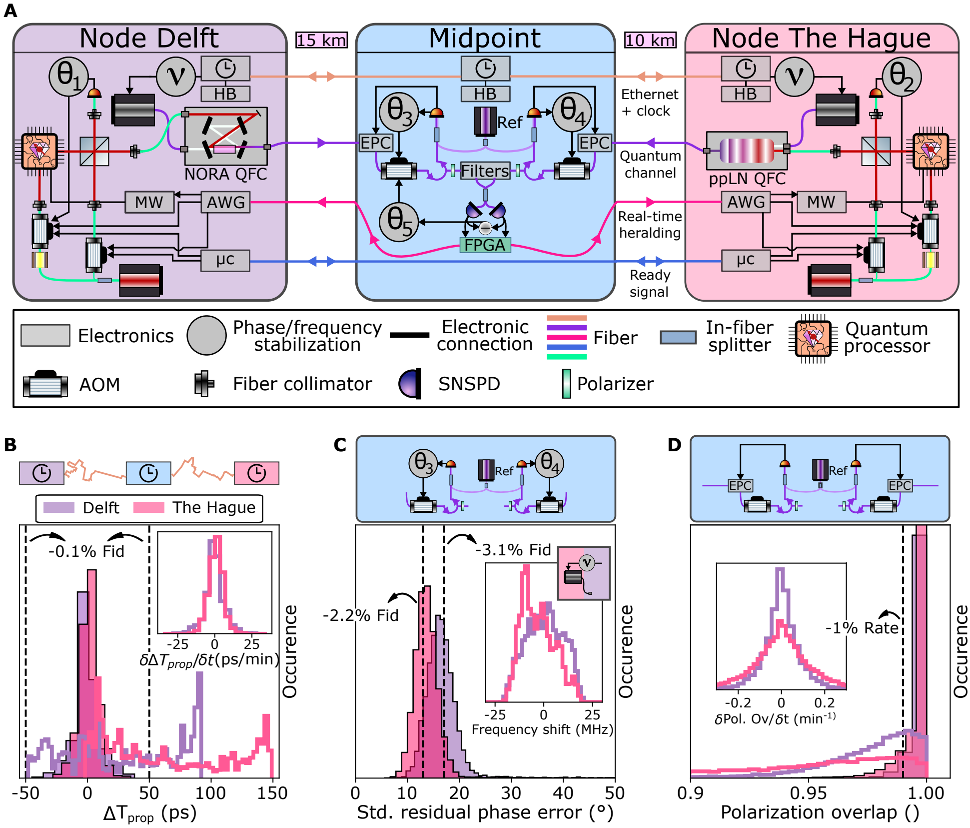

Figure I.5.2: **Quantum node components and metropolitan-scale stabilization performance** **(A)** Detailed components of the quantum nodes and fiber link connections. A micro-controller (μc) orchestrates the experiment, which together with an arbitrary waveform generator (AWG) shapes laser- and microwave (MW) pulses. Solid-state qubit entangled photon emission and stabilization light from each node is converted to the telecom L-band by the NORA (ppLN) based QFC in node Delft (node The Hague) and sent to a central midpoint. There, long distance qubit-qubit entanglement is heralded via single photon measurement (superconducting nanowire single photon detector (SNSPD), efficiency$\approx$ 60%, darkcount rate $\approx 5s^{-1}$) with detection outcomes fed back in real-time. The stabilization light is used for phase locking at the nodes (θ_1,θ_2), at the midpoint (θ_3,θ_4,θ_5) and for phase lock desaturation to the QFC pump lasers at the nodes (ν). The performance of stabilization over the deployed link over 24hrs is shown for **(B)** Time of arrival, **(C)** Phase and frequency and **(D)** Polarization. Hardware providing active feedback (header) keeps these parameter that are drifting over time (line histogram) stable (shaded histograms) by enabling continuous feedback faster than the experienced drifts (insets). Vertical lines show the modeled impact on fidelity and rate.

I.5.2.2. POST-SELECTED ENTANGLEMENT GENERATION OVER A DEPLOYED LINK

We now turn to the performance of the deployed link in generating entanglement between the solid-state qubits at the remote nodes. The proper functioning of all components of our system is first validated in a set of experiments with all devices of the link in a single lab in Delft, showing successful entanglement generation at state fidelities exceeding 0.6 (see Fig. I.5.7). After connecting and calibrating the equipment at the remote locations, we first focus on generating entanglement in post-selection. In this protocol the qubits are measured directly after generating spin-photon entanglement, and successful photon detection at the midpoint is used in post-processing to analyze entanglement generation. This scenario is compatible with quantum key distribution, but does not allow for more advanced protocols as the entangled state is not available for further use [2].

Our implementation of the post-selected entanglement generation is depicted in the space-time diagram of Fig. I.5.3A, where each horizontal grey line depicts one 10 µs heartbeat period. Both nodes signal their start-of-experiment after passing their own charge-resonance check (CR Check) that ensures that the lasers are on resonance with the relevant optical transitions [16]. After communicating their readiness they resolve the earliest heartbeat to start attempting entanglement generation. In the first 20 heartbeat periods both nodes stabilize their local phase, followed by 540 rounds of entanglement generation, with one attempt per heartbeat period. Every seventh entanglement round also contains optical pulses for maintaining stability of the local phase. The operations performed at the nodes for each round are detailed in the pop-out of Fig. I.5.3A. The sequence returns to the CR Check after completing the preset number of rounds.

We characterize the generated non-local states by measuring qubit-qubit correlations in different readout bases. In Fig. I.5.3B we plot the outcomes for the three basis settings split out per detector, showing the expected (anti-)correlations. Combining the outcome probabilities we calculate the correlators $\langle ZZ\rangle$, $\langle XX\rangle$ and $\langle YY\rangle$. Note that as the two detectors herald different Bell states (Ψ^+ vs Ψ^-), the corresponding $\langle XX\rangle$ and $\langle YY\rangle$ correlations have opposite sign. We also plot the values predicted by our detailed model without any free parameters (grey lines, see Suppl. Mat.), and observe good agreement with the data. The asymmetry in the amount of events is caused by a difference in quantum efficiency between the two single-photon detectors. We find that the measured fidelities $F(|\Psi^{\pm}\rangle) = \frac{1}{4} * (1 - \langle ZZ\rangle \pm \langle XX\rangle \pm \langle YY\rangle)$ with respect to the ideal Bell states are significantly above 0.5, proving the generation of post-selected two-qubit entanglement (Fig. I.5.3B). In the above analysis, we included photon emission up to 10 ns after the optical π-pulse. By varying the analysis window of the photon detection, we can explore the trade-off between rate and fidelity (Fig. I.5.3C). We find that the entangled state fidelity slowly decreases with increasing window length, due to the decreasing the signal-to-noise ratio of the photon detection at the midpoint (see inset to Fig. I.5.3C) in addition to the window-size dependent influence of spectral diffusion [35, 38]. Other examples of sources of infidelity are the residual optical phase noise and the probability of double optical excitation, all taken into account by our model (black line, see Suppl. Mat.). At the same time, as more photon detection events are accepted with increasing window length, the success rate increases. The achieved entanglement generation rate reaches 0.48 Hz (success probability per attempt of $7.2 \cdot 10^{-6}$) for a 20 ns window.

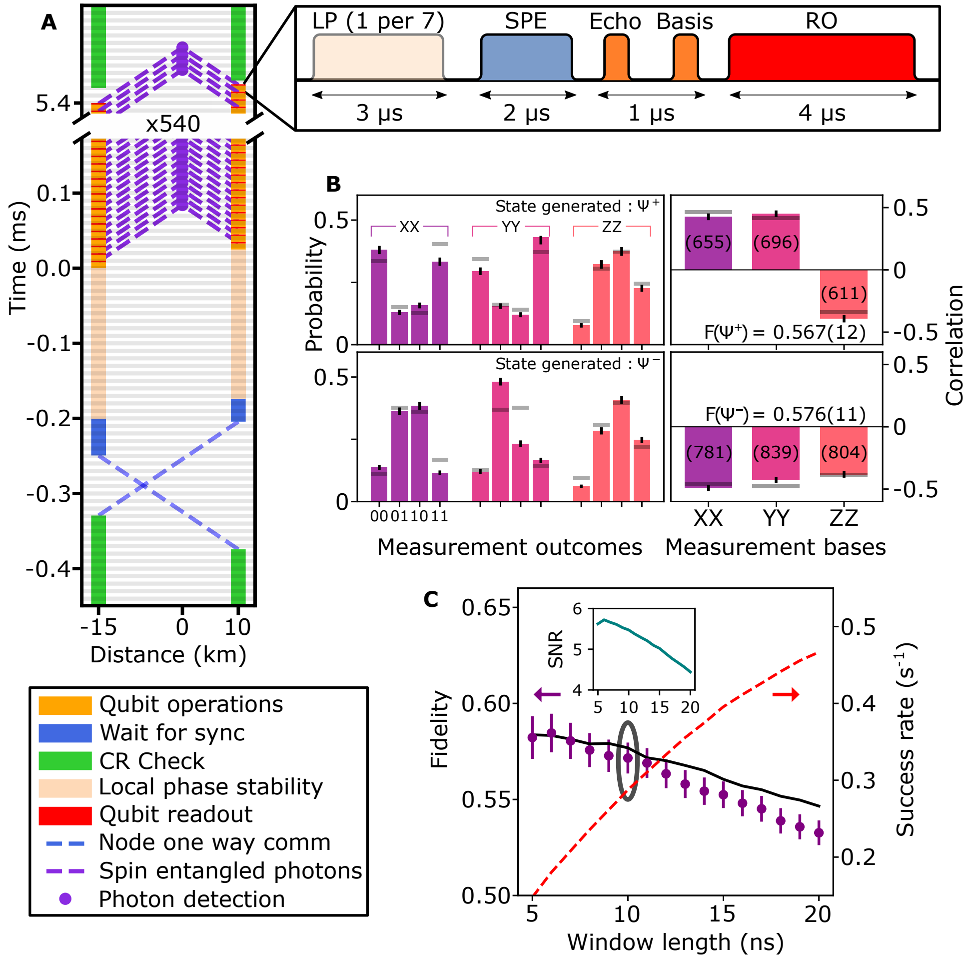

Figure I.5.3: **Post-selected entanglement over the deployed link (A)** Space-time diagram depicting the generation of entanglement in post-selection. Horizontal grey lines indicate the periodic heartbeat of 100 kHz. Local qubit control used to generate entanglement and perform state readout (pop-out) all fit within one heartbeat period of 10 μs. A local phase (LP) pulse is followed by spin-photon entanglement (SPE) generation, an echo and basis selection microwave pulse. Finally, the state is read out (RO).**(B)** Outcome of correlation measurements, with different detector signature for the top and bottom panels. We show the qubit-qubit readout outcomes per correlators(left), as well as the resulting values per correlator (right). The calculated state fidelity is given inside each figure. The number in parenthesis indicates the amount of events recorded for that correlator. Horizontal grey bars indicate the theoretical model. **(C)** Average state fidelity (left vertical axis) and entanglement generation rate (right vertical axis) for varying photon acceptance window length. Circling indicates the window used in (B), black solid line is a model(see Suppl. Mat.). Inset shows signal-to-noise ratio for the various window lengths. All measurement outcomes are corrected for tomography readout errors, errorbars are 1 standard deviation.

I.5.2.3. FULLY HERALDED ENTANGLEMENT GENERATION OVER A DEPLOYED QUANTUM LINK

In a final demonstration that highlights the capabilities of the deployed platform, we generate fully heralded qubit-qubit entanglement. In contrast to the post-selected entanglement generation described above, "live" entangled states are now delivered to the nodes that can be further used for quantum information tasks. Such live entanglement delivery is a fundamental requirement for many future applications of long-range entangled states [2]. We emphasize that this protocol requires that all relevant heralding signals (including which detector clicked) are processed at the node before the entanglement delivery is completed. To this end, we employ the experimental sequence depicted in Fig. I.5.4A. To preserve the qubit states with high fidelity while waiting for the heralding signals to return and be processed, the refocusing echo pulse is applied to the qubits halfway the sequence to dynamically decouple them from spin bath noise in their solid-state environment. Fig. I.5.4B shows the resulting qubit preservation as a function of time depicting periodic revivals of coherence due to interactions with nearby nuclear spins [40]. We note that with established advanced pulse sequences these revivals can be set with high timing resolution and the NV qubit coherence time can be extended towards a second [41]. While the qubits are protected at the nodes, the photons travel to the midpoint in about 52 μs and 73 μs from The Hague and Delft, respectively. An FPGA at the midpoint processes the output of the single-photon detectors, establishing whether a photon was detected in a predetermined time window and in which detector. The electronic output of the FPGA is optically communicated to the nodes, taking another 52 μs (73 μs). There, the signal is detected and processed live to choose the next action. The time at which this final processing is completed per node is indicated by the solid pink lines in Fig. I.5.4B.

We choose to use the first echo revival (orange dotted vertical line in Fig. I.5.4B) after the expected arrival time of the heralding signal to complete the delivery of the entangled state. For these setpoints, a detailed measurement of the echo contrast shows that the wait times introduce a 1.3 (3.2) percent reduction in coherence for node Delft (The Hague). The entanglement generation runs are automatically repeated by the nodes until a successful heralding signal is received from the midpoint. Once such a signal is received, the system jumps to a different control sequence in which a basis selection gate is applied to each qubit followed by single-shot qubit readout. This control sequence incorporates the which-detector information communicated from the midpoint in real time. We exploit this full heralding capability to apply a phase flip conditioned on which detector clicked, thereby delivering the same Bell state $\Psi^- = 1/\sqrt{2}\,(|01\rangle - |10\rangle)$ for each of the two possible heralding signals.

The measured correlations per readout basis are shown in Fig. I.5.4C, showing the expected anti-correlated outcomes for all three bases. The top bars show the outcomes divided per detector, displaying now the same Ψ^- thus showing the successful operation of the real-time feedback. We find that the delivered entangled states have a fidelity of 0.534(15). This result establishes the first demonstration of heralded qubit-qubit entanglement at metropolitan scale, with all the heralding signals processed in real-time and the entangled states delivered ready for further use. Fig. I.5.4D displays the rate-fidelity trade-off in analogy to Fig. I.5.3C, showing a similar trend. The reduction in rate

I.5

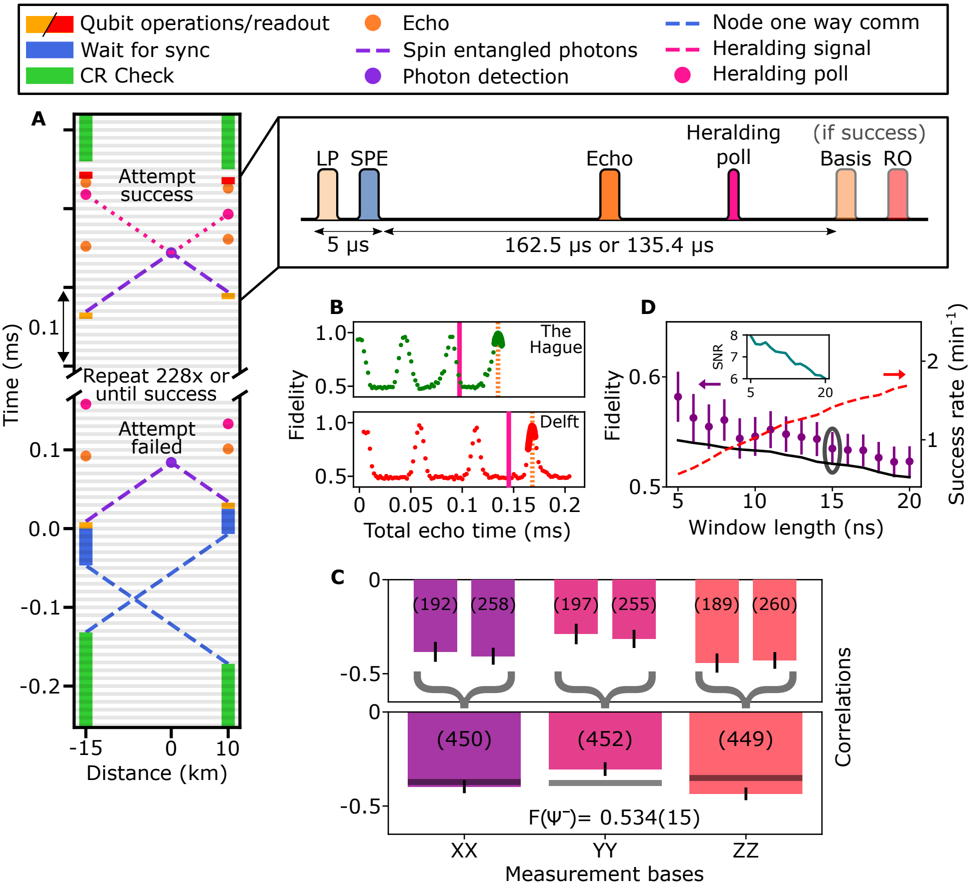

Figure I.5.4: **Fully heralded entanglement over the deployed link (A)** Space-time diagram of fully heralded entanglement generation. An attempt is successful upon registering a heralding signal at the polling time, after which a feed-forward is applied on the qubit and readout is performed. Absence of a heralding signal communicates a failed attempt, where we retry for a maximum of 228 attempts or until success. Pop-out depicts the local qubit control, basis selection and readout pulses. The time between spin-photon entanglement (SPE), heralding poll and basis selection is node-dependent. **(B)** Hahn-echo experiment on the communication qubit, showing the revivals of the coherence [40]. Solid vertical line indicates the heralding poll, the dotted line the time of the basis selection. All times are with respect to echo sequence start. **(C)** Correlation measurement for full heralding, showing both detector outcomes delivering the same Ψ^- state. Upper (lower) plot shows events per detector (combined). Bars indicate data, the number in parenthesis indicate the amount of events. Horizontal lines indicate the theoretical model. **(D)** Average state fidelity (left axis) and entanglement generation rate (right axis) for varying photon acceptance window length. Circling indicates the window used in (C), black line is a model (see Suppl. Mat.). Inset shows signal-to-noise ratio for respective window lengths. Measurement outcomes are corrected for tomography readout errors, errorbars are 1 st.dev.

($0.022\,\mathrm{s}^{-1} = 1.3\,\mathrm{min}^{-1}$ at the pre-defined 15 ns window length) compared to the post-selected case is mainly due to the added communication delay needed for the heralding signal to travel to the nodes, making each attempt a factor of ≈ 20 slower. The observed fidelity vs. window size is well captured by our models, with the reduction in fidelity compared to the post-selected case mainly coming from the additional decoherence and a reduced phase stability (black line, see Suppl. Mat.). The improved SNR (Fig. I.5.4D inset) compared to Fig. I.5.3C is due to an improved trade-off between detection efficiency and dark counts following an optimization of the single-photon detector bias currents.

I.5.3. DISCUSSION

We have realized a deployed quantum link and demonstrated heralded entanglement delivery between solid-state qubits separated at metropolitan scale. The architecture and methods presented here are directly applicable to other qubit platforms [13, 27, 42–45] that can employ photon-interference to generate remote entanglement and frequency conversion to minimize photon losses. Additionally, the ability to phase-lock remote signals without the need for ultra-stable reference cavities can be of use for ensemble-based quantum memories [29–31, 46]. This work can benefit from future developments in the following ways. Real-time correction of false heralds [17] can be realized by using detection events of phonon side-band photons on the nodes, upon which the fidelity of the delivered entangled state improves (see Suppl. Mat.). Near-term developments can substantially improve the signal-to-noise ratio, which is currently limiting the entangled state fidelity (about 30% contribution) through false heralding events and forcing a high value of α (protocol error). For instance, the signal can be substantially boosted by embedding the NV-centre in an open micro-cavity [47, 48] or by using different color centers that exhibit a more efficient spin-photon interface [24, 28, 49, 50]. As a quantitative example, replacing the NV center with a diamond SnV center (which has a 16 times higher probability of coherent photon emission), employing NORA QFCs at all nodes [36] (here used only in the Delft node), and fixing a known imperfection in the local phase stabilization would reduce the residual phase-noise, already increasing the heralded state fidelity to above 80%. Furthermore, improving coherence protection using XY8 sequences and systematic reduction of the remaining small error sources could lift the fidelity beyond 90% (see Table I.5.4). The extensible nature of our architecture opens the door to connecting more than two qubit nodes to a midpoint without additional overhead by locking to the same reference, which, in combination with using local memory qubits [14, 25, 51, 52], would enable the exploration of more advanced protocols on a metropolitan-scale network [17, 18, 53], as well testing quantum control stacks [15] on a distributed multi-node quantum network.

I.5.4. MATERIALS AND METHODS

The experimental set-ups used in this work are built on top of the hardware described in Ref. [35]. A detailed schematic of the quantum nodes, midpoint and their connections is shown in Fig. I.5.2. Hardware control is enabled through use of software based on the Quantum Measurement Infrastructure, a Python 3 framework for controlling laboratory equipment [54]. We will give a brief overview of the relevant parts of the set-up below.

I.5.4.1. QUANTUM NODE

Each node houses a diamond-based quantum processor consisting of a Nitrogen-Vacancy (NV) center electronic spin qubit in the negative charge state. The ground-state spin levels are split using a small permanent magnetic field aligned with the NV axis of ≈ 3 mT, allowing for arbitrary qubit rotations with a microwave pulse frequency of ≈ 2.8 GHz. Initialization, read out and qubit-photon entanglement generation is achieved through resonant excitation at 637 nm.

I.5.4.2. Quantum Frequency Converters

We employ both an in-house built ppLN QFC module and the NORA QFC described in [36]. The NORA QFC mitigates the amount of noise photons generated by the frequency conversion due to imperfections in the waveguide and poling period of periodically poled Lithium Niobate (ppLN) crystals. We compare the NORA QFC to the ppLN QFC in Table I.5.1, and refer to [36] for more information.

I.5.4.3. Phase stability

To allow for phase stability between physically separated setups, we use a prototype TOPTICA DLC DL pro 637 nm employing optical feedback from an additional cavity to reduce the phase noise to < 40 mrad integrated from 100 kHz to 100 MHz. We use a combination of five interferometers with heterodyne detection and feedback that together lock the phase to a controlled setpoint. On both nodes we define local interferometers that lock the excitation laser path to the stabilization path of the respective set-ups. On the midpoint we stabilize the incoming light from each node to the same telecom wavelength reference. The relative optical phase between the nodes is stabilized using interference at the central beam splitter in the midpoint and measured with SNSPDs. The optical fields and respective frequencies used are shown in Fig. I.5.5, and the combination of the stabilization fields with the NV control fields is shown in Fig. I.5.8 and I.5.9. More detail on the phase stability implementation can be found in the Suppl. Mat., Sections I.5.5.1 and I.5.5.2. In addition to phase stability, the midpoint provides polarization control, spectral filtering and single-photon detection (Suppl. Mat. Section I.5.5.4).

I.5.4.4. Midpoint

The midpoint provides phase feedback, polarization control, spectral filtering and single-photon detection. The phase feedback uses frequency modulation of AOMs for phase-locking of the node excitation lasers to the midpoint telecom reference at ≈ 1588 nm. Two Electronic Polarization Controller allow for full control over the polarization state to compensate for fiber drifts. Two low-loss Variable Optical Attenuators (VOAs) shield the SNSPDs from bright stabilization light coming from the nodes. Per node, all the error signals for the phase- and polarization stabilization, and temperature of the ultra-narrow fiber Bragg-grating (FBG) filters are generated on the same balanced photodiode, and subsequently extracted by a combination of power-splitters, bandpass filters and amplifiers. An FPGA development board processes electrical signals to allow for real-time heralding to the nodes of photon detections at the midpoint.

I.5.5. SUPPLEMENTARY MATERIALS

I.5.5.1. EXPERIMENTAL SETUP

The experimental set-ups used in this work are built on top of the hardware described in Ref. [35] and they use software based on the Quantum Measurement Infrastructure, a Python 3 framework for controlling laboratory equipment [54]. In this section we will discuss the hardware changes made that enabled compatibility with metropolitan-scale entanglement generation.

QUANTUM NODE

We exchanged the diamond quantum device of Node The Hague for a newly fabricated one. All parameters of the substrate (Element Six) and device, such as purity, crystal orientation and carbon isotopes are the same as previously reported. To allow for phase stability between physically separated setups, the TOPTICA DLC DL pro 637 nm was exchanged for an upgraded prototype employing optical feedback from an additional cavity to reduce the phase noise to < 40 mrad integrated from 100 kHz to 100 MHz.

QUANTUM FREQUENCY CONVERTERS

As mentioned in the main text, we have replaced one of the in-house built QFC modules with the NORA QFC described in [36]. This design mitigates the amount of noise photons generated by the frequency conversion due to imperfections in the waveguide and poling period of periodically poled Lithium Niobate (ppLN) crystals. Briefly, the novel approach consists of identifying the right bulk material that can be critically phase-matched to perform efficient conversion, and embedding the crystal in a single-resonant cavity to enhance the effective pump power in the conversion process. We compare the NORA QFC to the ppLN QFC in Table I.5.1, and refer to [36] for more information.

PHASE STABILITY ON THE NODES

On both nodes we added the components to define the local interferometers that lock the excitation laser path to the stabilization path of the respective set-ups. We use a combination of up- and down-shift Acousto-Optical Modulators (AOM, Gooch and Housego Fiber-Q), already used for amplitude modulation, to define a 400 MHz frequency offset. The excitation light reflected off the diamond surface is separated from the zero-phonon-line (ZPL) path by a polarizing beam splitter (PBS), where it spatially overlaps with the stabilization light. We guide the light to a set of birefringent crystals that maximize the complex overlap between the orthogonally polarized reflected beam and the stabilization light. A polarizer then selects a common polarization such that both beams can interfere in intensity, after which we focus the light into a multi-mode fiber (core diameter $\approx 100 um$) and measure the interference beat signal using a fast avalanche photodiode (Menlo Systems APD210). After amplification and filtering, we extract the phase of the interference by mixing it with an electronic reference signal generated by a stable RF source (Anapico APSIN6010). The feedback signal generated is passed through a Track-And-Hold amplifier (Texas Instruments OPA1S2384) and input to the Frequency Modulation input of the Excitation light AOM RF-driver (TimeBase DIM3000), which closes the feedback loop. Because the frequency modulation has integral feedback on the phase that can not be switched on/off fast, any bias/offset in the error-signal reduces the free evolution time during which the local phase remains stable. In a future implementation, this actuator will be replaced by a linear phase shifter, and an improvement of the local phase-stability can be realized.

Midpoint

The previous design of the midpoint used for two-photon quantum interference [35] suffered from an increased noise floor due to the presence of bright laser pulses incident on the nanowires every 200 µs. To reach an adequate feedback bandwidth for phase-locking of our excitation lasers to the telecom reference, we have to reduce the period of bright pulses to 10 µs, making this even more challenging. We have made the following improvements to allow for polarization and fast phase feedback, to reduce crosstalk between optical channels and lower the background counts in the SNSPDs:

- Split the high-power reference light into three paths, two used to generate an optical beat to lock the stabilization light coming from each node to the reference laser, and one used to generate an error signal to stabilize the ultra-narrow Fiber-Bragg grating filters.

- Added two low-loss Variable Optical Attenuators (VOAs, Boston Applied Technologies Nanona VOA) that shield the detectors from bright pulses coming from the nodes.

- Added two Electronic Polarization Controller (OZOptics EPC-400-11-1300/1550-9/125-S-3A3A-1-1) to allow for full control over the polarization state to compensate for fiber drifts.

- Added two AOMs to have fast and integral control of the phase of the incoming light, used for phase stabilization.

- Removed one circulator from the design and splicing multiple connectors where the single-photons pass through to reduce single-photon loss

All the error signals for the phase- and polarization stabilization, and the ultra-narrow fiber Bragg-grating (FBG) for one node are generated on the same balanced photodiode (Thorlabs PDB480C-AC), and subsequently extracted by a combination of power-splitter, bandpass filters and amplifiers.

Heralding

To allow for low-latency feedback of photon detections at the midpoint, the midpoint was upgraded with an FPGA development board (Digilent Arty-A7) with custom-built PCBs converting the external pin I/O to SMA connectors with the possibility of 50 Ohm matching. Single photon signals were input on a custom pulse-stretcher, cleaning up the electrical pulse from the SNSPD to a block-like pulse shape of around 1 µs and input on the I/O of the FPGA. The complete I/O of the FPGA is shown in Fig. I.5.13. The acceptance window of sending out a heralding signal is predetermined at the time within a heartbeat period where we expect spin-photon entangled photons to arrive. The exact timing of the acceptance window is derived from the centralized clock and heartbeat signal available at the midpoint. To be able to signal which detector clicked on a photon count, we use two digital pulses to herald, one for the success, and one for which detector clicked. Since the delay in time-of-flight between the nodes is different, the digital pulses need to be aligned individually to arrive at the nodes at the same time within one heartbeat. To clarify, this does not mean they arrived at the same global time at the nodes, but that the digital pulses arrive at the same time modulo the heartbeat (10 μs) at the nodes. Lastly, a local FPGA code loading server was employed that could upload compiled-VHDL that was either manually or automatically generated remotely. A change in timing of sending out pulses could be updated on the underlying VHDL code automatically based on a custom template code. This allowed fast multi-core compilation locally and remote upload to considerably reduce debugging time when determining the required exact timing of the heralding pulses.

I.5.5.2. Phase stabilization in the midpoint

We stabilize the incoming light from each node to the same telecom reference (fast stabilization). The relative optical phase between the nodes is stabilized using interference at the central beam splitter in the midpoint, and measured with the SNSPDs (global stabilization). The optical fields and respective frequencies are shown in Fig. I.5.5, and the distribution of the fields in time shown in Fig. I.5.8 and I.5.9.

Fast stabilization

Part of the stabilization light used in the local phase lock also propagates via the QFC, through the same deployed fiber, to the midpoint. There it is split off in frequency from the single-photons via the FBG, subsequently interfered with a telecom reference laser (NKT Adjustik fiber laser), where a heterodyne interference beat is measured by the balanced photodiode. A phase-frequency detector (Analog Devices HMC3716LP4E) processes this signal by comparing it to a reference signal (Wieserlabs FlexDDS-NG DUAL). Its output serves as the error-signal for a high-speed servo controller (Newport LB1005-S) performing PID control. This controller provides feedback on the AOM to stabilize the incoming light, synchronizing it with the reference at a bandwidth of over 200 kHz. To stay within the low-loss performance of the AOM close to the central frequency, we offload the accumulation of phase error (frequency drifts) to the QFCs at the nodes. This can be done much slower (500 Hz) and makes the feedback only limited by the frequency range of the QFCs ($\gg$1 GHz). The fast feedback removes all high-frequency noise from the incoming light, which contains the excitation laser line-width, as well as phase noise introduced by expansion/contraction and vibrations of the deployed fiber.

Global stabilization

To further compensate phase drift that occurs in the midpoint and to set the relative phase between the incoming optical modes, we employ a control loop based on the stabilization light from both nodes that interferes at the central beam splitter. This light leaks through the FBG, and is of sufficient low power to not blind the SNSPDs. The voltage pulses from the SNSPDs are amplified, and a difference amplifier (Krohn-Hite Model 7000) generates a heterodyne beat by subtracting the count-rates from each detector. This beat is compared to a reference signal (AimTTi) by mixing it and low-pass filtering (150 Hz), generating an error-signal. This is again input to a servo controller (Newport LB1005-S), of which the output is used to modulate the phase of the reference of one of the fast stabilization controllers.

Verifying phase stability

We can verify the performance of the full optical phase stabilization by interfering the two excitation lasers from the nodes at the central beam splitter in the midpoint, using the time-resolved counts in the SNSPDs to generate the error signal. By changing the phase of the reference signal, we can measure a full visibility fringe of the interference. By correcting the measured interference for the imbalance in photon flux from each node, we can calculate the interference contrast, see Fig. I.5.6B. A more in-depth description and technical analysis of the total phase stabilization will be given in a separate manuscript [55].

I.5.5.3. Overview communication times and decisions

In this section we discuss the different optical and electrical pulses or feedback signals that are needed to control this distributed experiment. We will first discuss the local nodes, then which signals are necessary to be timed at the midpoint for single photon processing and phase stability. Lastly, we will discuss how we align the arrival time of the photonic states at the midpoint telecom detectors.

Pulses and timing at node

Since the central clock in the midpoint is distributed to the nodes by the White Rabbit enabled switches, it provides a common reference frame to align the time-of-arrival for each of the entanglement generation attempts, see Section I.5.5.3.

A full timing overview of a single heartbeat length when we perform a full entanglement attempt without heralding is shown in Fig. I.5.8A and with heralding in Fig. I.5.8B. The entanglement generation attempt with heralding contains exactly the same pulses as in Fig. I.5.8A, except for that the time between the spin superposition state generation and basis-selection pulse is at a revival of the spin coherence, as previously shown in the pop-out of Fig. I.5.4A of the main text.

Pulses and timing at midpoint

The laser, electrical and feedback pulses used at the midpoint by design operate agnostically of the experiment that is being run. For about ~8 μs we can perform phase, frequency and FBG stability actions using the interference from the reference light and the incoming stabilization light from the node (see Fig. I.5.9old amplifier is set to ‘hold’ and the VOAs opened fully to allow for single photons to pass through to the SNSPDs.

Time-of-arrival alignment

One of the requirements for indistinguishability of the photons is the time aligned photonic mode overlap at the beam splitter in the midpoint. The timing of the emission of the photonic state determines, together with the time of flight (ToF), the time at which the photonic state arrives from the node at the midpoint. This is especially crucial in the metropolitan distance case, where fiber distance varies with tens of picoseconds per hour (see Table I.5.2). Since we have unbalanced fiber connection lengths between the nodes-midpoint, Node Delft will be allowed to send its photon as soon as possible. Node The Hague has to hold its pulse sequence start for 3 heartbeats. Both nodes require sub-heartbeat timing alignment to align the arrival time of the solid-state entangled photons in the last ~2 µs of the midpoint scheme (Fig. 5). This last alignment step is achieved with the arbitrary waveform generator (AWG, Zurich Instruments HDAWG) sequencer and the built in skewing parameter of the AWG outputs.

Due to the constantly changing ToF, the alignment in time is performed in two steps. A first time alignment is required to be performed manually where laser pulse timing is recorded at the midpoint timetagger (PicoQuant Multiharp, 80 ps resolution), after which the time difference between arrival times of the pulses from the two nodes can be calculated and adjusted. This value is recorded as calibration parameter. Secondly, the reported ToF from the time synchronization system is used to automatically adjust the skewing parameter every ~15 minutes with the difference in fiber ToF with respect to the initial calibration.

I.5.5.4. OTHER MIDPOINT STABILIZATION

POLARIZATION STABILIZATION

We continuously stabilize the polarization of the incoming stabilization light using the same beat generated on the balanced photodiode as mentioned in the phase stability section (Section I.5.5.2). Because of our in-fiber polarizer, the amplitude of the beat will depend on the overlap of the incoming light with the polarizer. Maximizing this amplitude will guarantee the same polarization between the nodes, as needed for interference. Using a phase-gain detector (Analog Devices EVAL-AD8302) we can monitor the amplitude of the beat by comparing it to an in-phase RF tone (generated by Wieserlabs FlexDDS-NG DUAL) over multiple orders of magnitude. We sample the output of this phase-gain detector with an Analog Discovery 2 (Digilent), and process the error signal in a python process running a Gradient Ascent algorithm. This in turn sends commands to the EPC that adapts the polarization state and completes the control loop. The whole process can be monitored and adjusted via a Graphical User Interface.

ULTRA-NARROW FBG STABILIZATION

We adapted the control loop for the temperature stabilization of the ultra-narrow FBGs (UNF) to allow for a considerable reduction of the optical power reflected back to the SNSPDs. We achieved this by using a heterodyne beat measurement that is sensitive to the transmission through the UNF, instead of a simple power measurement at DC. This allows for multiple orders higher sensitivity, and allows us to stabilize the filters with only ≈ 10 fW of light traveling through the filter in the backwards direction.

I.5.5.5. DEPLOYED FIBER CHARACTERIZATION AND STABILITY

We use a fiber bundle with four fibers to perform all the communication between the locations. These are provided to us by KPN, a major Dutch telecom provider, and are part of their telecom infrastructure. The reality of using deployed fibers means that it is built up of sections of continuous fiber, which are spliced or connected together at various locations along the path. Therefore the losses per kilometer of deployed fiber are notably higher than the ideal losses of ≈0.2 dB km^{-1} @ 1580 nm, and can differ from fiber to fiber.

During the period of measuring over the deployed link in 2023, several parts of the fiber were adapted and re-routed as part of restructuring of the network by KPN, changing both their length (± 100 m) and loss (± 1 dB) multiple times over the span of a few weeks. Table I.5.2 shows typical loss values measured during this period. Thanks to the modular approach of our system, we have complete freedom in changing the arrival time of the photon in the midpoint, allowing for easy re-alignment of the propagation delay, both for the fiber restructuring as well as the daily expansion and contraction.

I.5.5.6. Calibrations

Entanglement generation

We employ a method where we interleave the generation of entanglement with three calibrations that measure and re-calibrate critical parameters and settings. These calibrations are an adapted version of the entanglement generation sequence that measure specific key elements of the entanglement generation: the signal-to-noise ratio (SNR), optical phase stability (PHASE) and the entangled state phase (XsweepX). Typical results of these three calibrations are shown in Fig. I.5.6. When these calibrations have passed their threshold, we proceed to measure the correlators used to calculate the entangled state fidelity, FID for short.

The first calibration is the measurement of the single-photon signal from both nodes and the background, which includes all the losses that are present in the system. We prepare the communication qubit in the $|0\rangle$ to maximize the single photon signal. The measurement is the same experimental sequence as shown in Fig. I.5.8A, where now the state generation α pulse is removed to measure the signal, and replaced by a π-rotation to measure the noise. Furthermore, the arrival time of the photons is shifted by 100 ns to measure the brightness of both nodes individually.

Second is determining the contrast and phase of the relative optical phase between the nodes. We realize this by interfering a bright pulse (1 μs) of the excitation lasers which we reflect off the diamond surface, and follows the exact path as the NV-center emission from there. By varying the setpoint of the phase in the stabilization scheme, we can measure a full interference fringe at the SNSPDs as seen in Fig. I.5.6B and characterize the residual phase noise of the system at the specific time window where single photons interfere. Furthermore, this calibration is used to set the phase of the optical interference at any point along this fringe, which can be used to optimize the entangled state fidelity [38]. We show the capability of changing the optical phase to two different setpoints of 0° and 180°.

The third and last calibration is the measurement of the entangled state phase, which has an offset with respect to the optical phase setpoint. Using the single-click protocol we create a correlated spin-spin state that we can use to probe this phase. We do this by measuring correlations in the rotated basis X on Node Delft, while varying the readout basis in the Bloch sphere equator plane for Node The Hague. We can extract this entangled state phase by fitting the resulting oscillation with a single cosine, see Fig. I.5.2C. We feed-forward this phase in the entanglement measurements to always generate the $\Psi^{\pm} = \frac{1}{\sqrt{2}}(|01\rangle \pm |10\rangle)$ during the entanglement generation.

EXPERIMENTAL SETUP PERFORMANCE

We maintain similar performance parameters of the experimental setup by performing calibrations of many different settings at different timescales. On a daily timescale, performance parameters of the communication qubit are re-calibrated:

1. Laser power (see Fig. I.5.14)
2. Single-Shot Readout
3. Microwave qubit control (π, $\pi/2$, α)
4. Optical excitation (optical π pulse) for entanglement generation attempt
5. QFC efficiency

Roughly every 20 minutes, a set of shorter timescale calibrations are run. Some are dependent on performance parameters that are available live during or right after a measurement set. See Fig. I.5.14 for the flowchart showing the calibrations and decisions made. As discussed in the previous section, we require several types of measurements to calibrate the phase of the entangled state. If in any of those measurements we are outside of the bound of acceptance, we restart the sequence. Additionally, the FID measurement sequence is cut into smaller blocks of 10k (30k) successful CR-checks for the heralded (delayed-choice) metropolitan distance experiments. After each block, the CR-check passing rate is checked against the average CR-check rate during the SNR sequence (per node). If the passing rate is below this value, we exit the FID sequence and continue. We do this because the CR-check passing rate is a value that includes many derived underlying performance parameters of the setup as a whole, e.g. laser wavelengths, laser power, objective position and others. If any of those values changed substantially the CR-check passing rate is negatively impacted, which we use as a signal that an underlying parameter of the experiment is drifting off ideal and subsequently we break out of FID data taking. As can be seen in the flowchart, afterwards all calibrations are restarted, and we start from a calibrated setup with the SNR sequence, which is when we expect the highest CR check passing rate, and as such, use that to define our threshold for the rest of the experiment.

I.5.5.7. MODELING THE GENERATED ENTANGLED STATE

To assist in setting up the experiment and simulating the outcomes, we employ a Monte-Carlo simulation based on the model described in [38]. This is an extensive description of generating entanglement between remote nodes using the single-click protocol. It considers the spin-spin density matrix, based on the detection events where at most two photons reach the central detectors. By calculating the probability of each detection pattern and its corresponding spin-state, it arrives at the average density matrix given non photon-number resolving detectors. It takes into account many physical parameters that have an impact on the entangled state fidelity, such as photon loss, photon indistinguishably, and the photon wavepacket shape. It also includes several experimental parameters such as the effects of residual phase noise, dephasing noise and darkcount probability. We noticed that in contrast to the 13 MHz Full-Width Half Maximum (FWHM) spectral diffusion found in [38], a FWHM of 25 MHz represents the fidelity vs. window length trend better.

In the experiments presented in the main text we do not apply a post-processing correction using the Charge-Resonance check after the readout of the spin-state. This correction can be done to identify sequences where one of the nodes is in the NV^0 state, and no longer optically responsive to the excitation laser, but only in a post-processed fashion. To accurately model the effect of including events when the NV-center is ionized on the fidelity with the ideal state, we extend the model by including the probability of one of the nodes being ionized. We assume that, when an NV photon from a particular node in the midpoint is detected, this node can not be in the ionized state, but the other node can be with a probability p_{ion}. If the event in the midpoint is due to a noise photon, either of the nodes can be in the ionized state. This probability is measured by saving the CR-outcomes after the readout sequence. We include this ionized state as a third level of our qubit, that is outside the space addressed by our microwave control. When applying a readout pulse however, it will be read out as the $|1\rangle$ (=dark) state. The single shot readout (SSRO) fidelity of the solid-state NV qubits are given in Table I.5.3. State readout correction is performed according to iterative Bayesian unfolding as described in [56].

An overview of all the simulation parameters used and their measured/used value for the simulation is given in Table I.5.4. We have also simulated near-term performance of the same link based on SnV centers (keeping the collection efficiency the same), which have 16 times higher coherent photon emission probability per optical excitation, full use of the improved QFC technology and improved phase stability. For additional insight, we have simulated the infidelity contribution of the protocol error α and the SNR to the entangled state, as can be seen in Figure I.5.15.

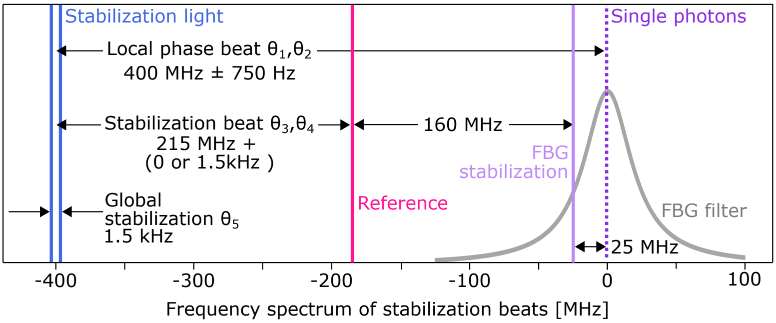

Figure I.5.5: **Overview of beat frequencies and lay-out of optical fields used.** Frequency of relevant optical fields for the phase lock in the midpoint. The grey Lorentzian shape is the ultra-narrow fiber-bragg grating filter (FBG). It is stabilized using a 160 MHz beat generated by the reference laser and a frequency-shifted tap-off that is back-propagated through the flank of the FBG (25 MHz from the transmission peak). The stabilization light is located far from the filter resonance, detuned by 400 MHz from the filter peak and excitation laser/single-photons, which is locked by the local phase lock controllers θ_1 and θ_2. This stabilization light is reflected off the FBG and interferes with the reference laser generating a ≈ 215 MHz beat, which is stabilized by the fast phase lock controller θ_3 and θ_4. The slight offset between the nodes of 1.5 kHz is measured by the SNSPDs and input to controller θ_5, to close the phase lock between Delft and The Hague.

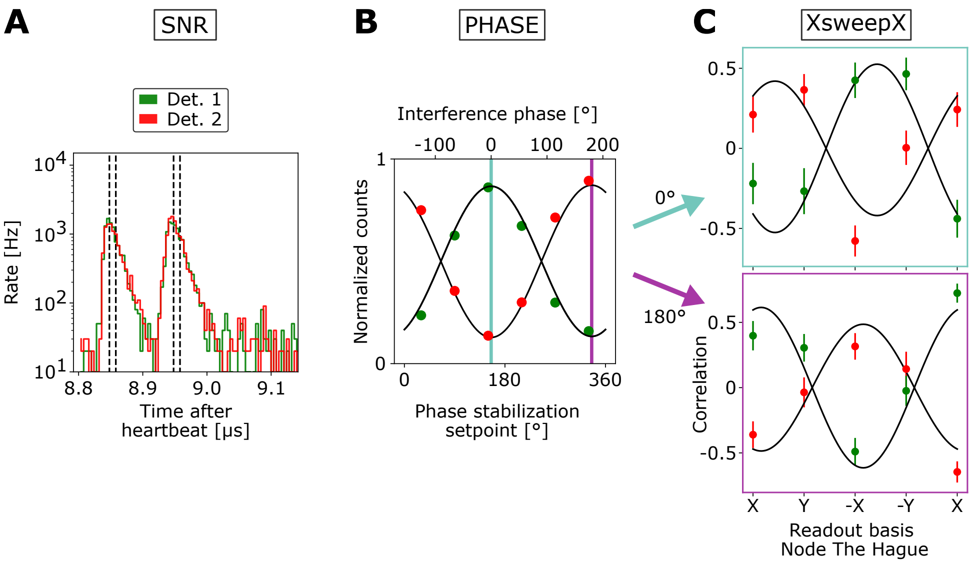

Figure I.5.6: **Outcomes of calibration sequence to perform entanglement generation.** Typical calibration outcomes of: **(A)** signal strength (SNR) where the dotted lines show the used 'signal' window for both nodes respectively. The same windows are used to measure the 'noise' when the NV qubit state is rotated to the $|1\rangle$ (=dark) state. **(B)** Optical phase stability (PHASE), with fitted contrast (black lines). The vertical lines project to the top horizontal axis to determine the interference phase for the following measurements. **(C)** The entangled state phase (XsweepX) for an interference phase of 0° and 180°, showing the capabilities of the stabilization system to set a specific phase setpoint. The fitted phases (black solid lines) are 219(6) and 14(6) for the interference phase 0° and 180°, respectively.

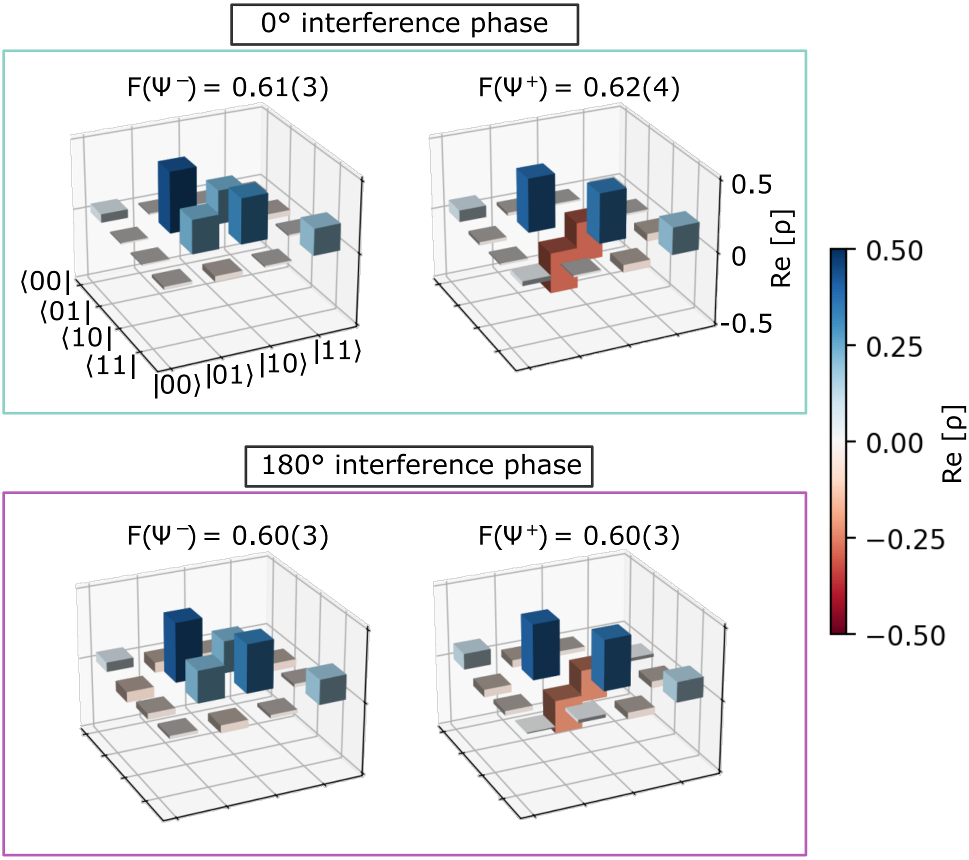

Figure I.5.7: **Bayesian estimation of density matrix for both phase setpoints, using the post-selected entanglement generation scheme, with both nodes in the same lab in Delft.** We measure all two-spin correlators $\langle M_i M_j \rangle$ with $M_{i,j} \in [X, Y, Z]$ and use Bayesian estimation for tomography [57, 58] to find the most likely density matrix. The calibration measurements in Fig. I.5.6 allow us to generate the same entangled state, at two different optical phase setpoints. The overlap with the ideal state for the most likely density matrix is given as numerical value, that is above 0.6 for both phase setpoints and detector outcomes.

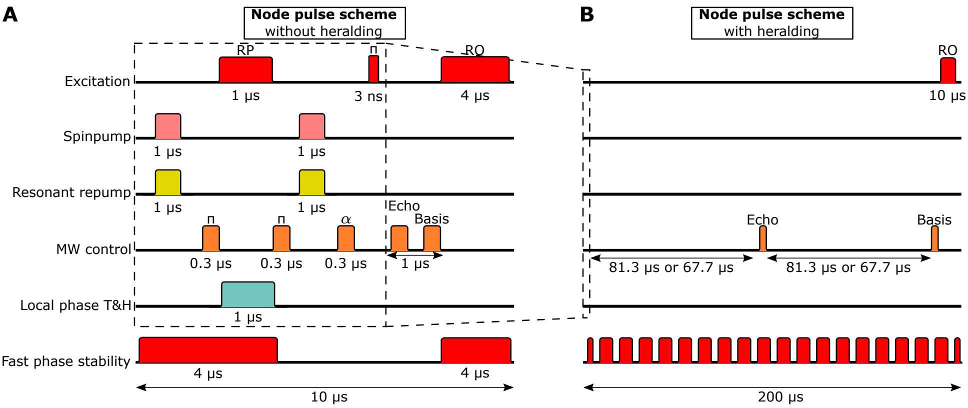

Figure I.5.8: **Relative timing of control pulses on the nodes for entanglement generation without (A) and with (B) heralding.(A)** Local node pulse scheme for the duration of one heartbeat when performing entanglement generation without heralding. Red and yellow pulses are laser, orange are microwave pulses, blue-green is electrical feedback. The NV center is (re-)initialized in the correct spin and charge state via pumping resonant with $|1\rangle$ (637 nm) and the ZPL of NV^0 (575 nm), respectively. We limit resonant optical excitation during the reflection pulse (RP) we need for local phase stability by preparing the qubit state in the opposite spin state a using microwave π-pulse. After the local phase stability, we initialize the spin into the $|0\rangle$ state, create the unequal superposition with a microwave pulse with rotation angle α, and optically excite using a short optical excitation, completing the spin-photon entangled state generation. A microwave π-pulse echos the spin state, and a $\frac{\pi}{2}$-pulse selects the readout basis for the resonant optical readout that follows. **(B)** Node pulse scheme during entanglement generation. This sequence now takes 20 heartbeat periods $(200\,\mu s)$. All pulses required to perform the local phase stability and spin-photon entanglement are repeated exactly as in (A). However, now the rephasing echo pulse is played at its calibrated value of 82 μs(68 μs) for Node Delft (The Hague), while the stabilization light still is periodically sent to the midpoint such that phase stability feedback can be applied there. The total duration of 200 μs is for one whole entanglement generation attempt where wait time padding is added node specifically (not shown) to allow for a common repetition period when dealing with the different node-midpoint communication delays.

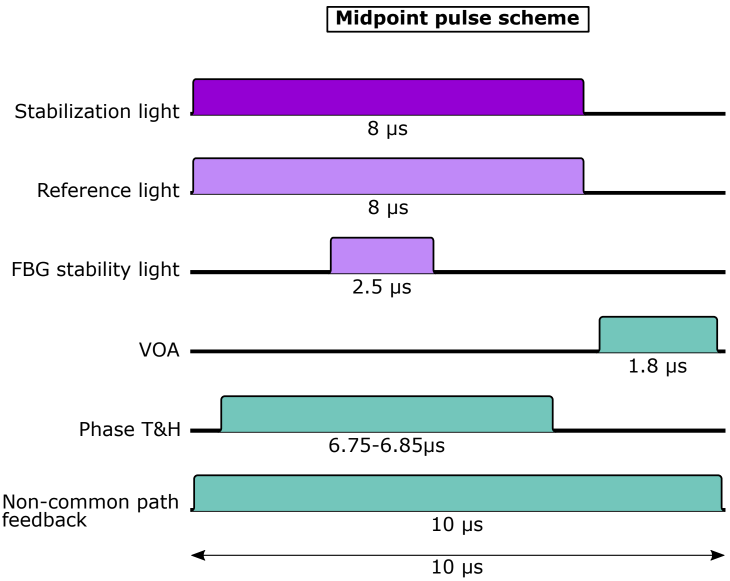

Figure I.5.9: **Relative timing of midpoint pulse scheme for the duration of one heartbeat**. This sequence is agnostic to the experiment is run. Purple colors are telecom wavelength laser light, blue-green is electrical signal. Stabilization light is converted light coming from the nodes. The reference and FBG stability light are both originated from the telecom laser at the midpoint. The error signal for the fast lock is processed by a Track and Hold (T&H) amplifier before being processed by the controllers. Variable optical attenuators are used to shield the detectors during the times where stabilization/reference light is propagating in the system, and they are only opened for 2 μs where single photons from the nodes can arrive. The global control task is not modulated, as the feedback bandwidth is much slower than the low-pass filtering of the error signal (150 Hz). For all above pulse schemes holds that absolute block sizes are not to scale, the denoted time duration is leading.

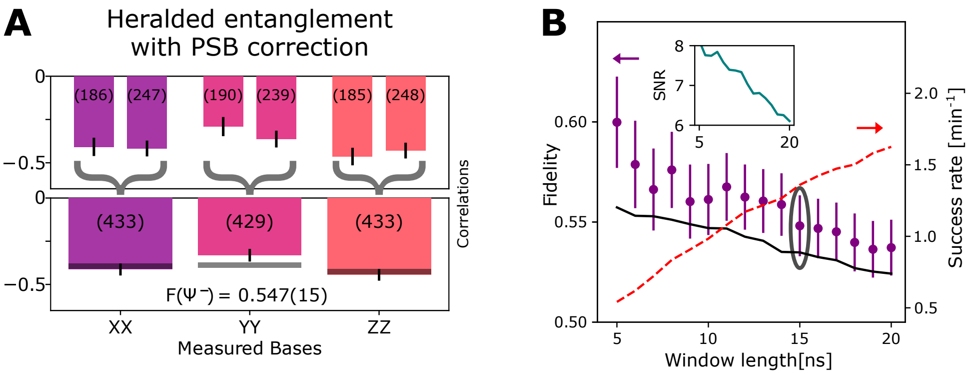

Figure I.5.10: **Correlation measurement for full heralding with correction on discarding events accompanied by a measured PSB photon.** **(A)** Upper plot shows XX, YY and ZZ correlations per detector, lower for both detectors combined. Bars indicate measured data, the number in parenthesis indicate the amount of events. Horizontal lines indicate the theoretical model. The calculated fidelity is significantly above 0.5 **(B)** State fidelity and entanglement generation rate for varying photon acceptance window length. Inset shows signal-to-noise ratio for the same window lengths. All measurement outcomes are corrected for tomography errors, errorbars are 1 standard deviation.

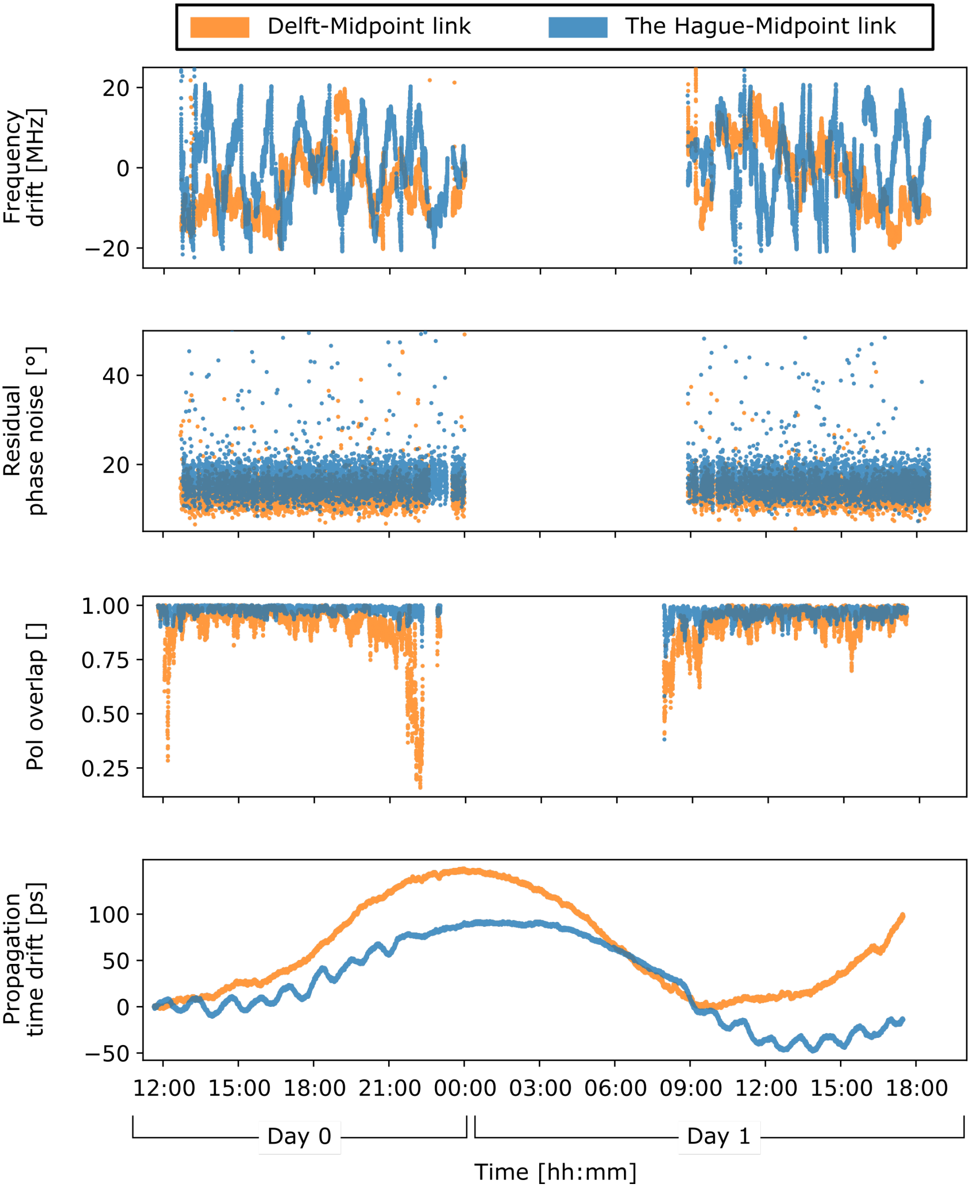

Figure I.5.11: **Continuous data of important parameters monitored over deployed fiber link**. From top to bottom: the frequency drift, phase noise, polarization and time of flight as measured by the individual systems and logged into a central database. For the frequency, phase and polarization we have conditioned the data on the respective feedback system being active. The pause in the system overnight was due to one of the feedback systems being out of lock, which got reset the next morning.

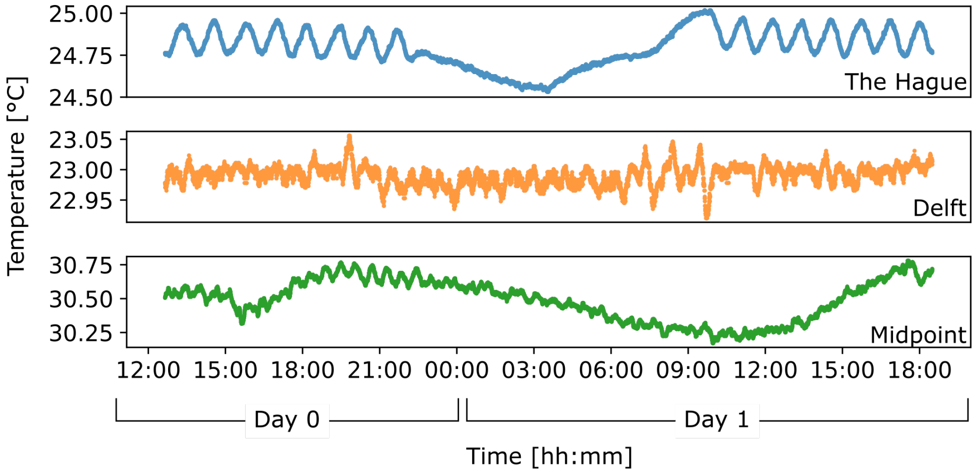

Figure I.5.12: **Temperature logging of the three locations during the same time as the continuous data logging of Fig. I.5.11.** Some of the features shown in Fig. I.5.11, such as the frequency drifts, seem to be correlated with the measured temperature variations on the node.

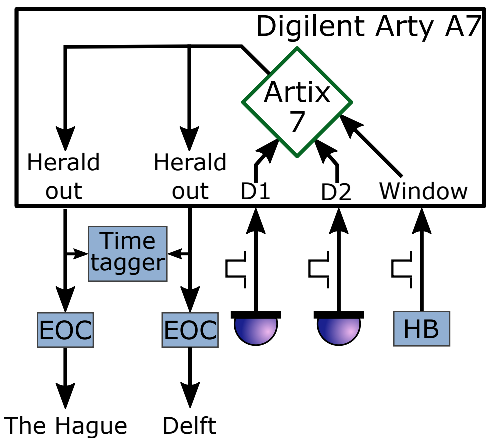

Figure I.5.13: **Hardware lay-out of the FPGA used for heralding.** Single photon detection signals are processed by custom FPGA-code on the Digilent Arty A7. If photons arrive within the externally derived acceptance window from the heartbeat (HB), a heralding signal is sent to both locations through an Electrical-to-Optical-Converter (EOC). The heralding signal is also recorded on the timetaggers on all the three locations.

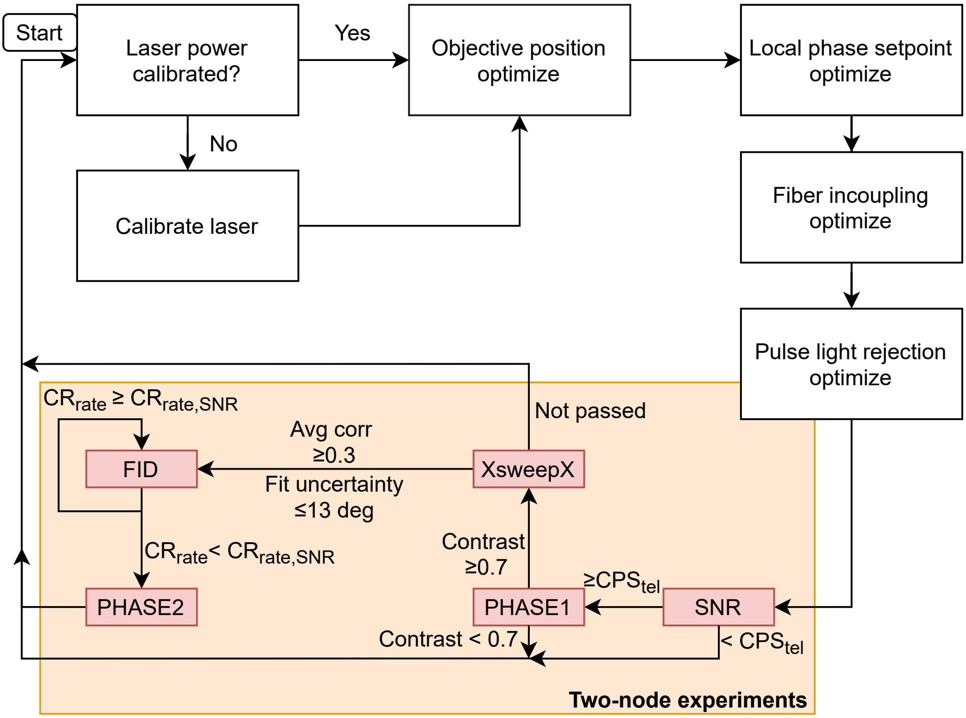

Figure I.5.14: **Flowchart for calibrations and performing the two-node experiments of measuring the fidelity of the entangled state.** Between the different steps of the measurement sequence thresholds are checked of measured parameters that decide continuation of the sequence. Calibrations are started with a signal-to-noise (SNR) measurement, where the counts-per-shot of telecom signal from the nodes (CPS_{tel}) is checked. We continue with PHASE and XsweepX and check their respective parameters. If all thresholds are satisfied, we continue with the fidelity measurements (FID) until the Charge Resonance passing rate (CR_{rate}) drops below the calibrated value it had during the SNR ($CR_{rate,SNR}$). Finally, we do another PHASE check before we restart the entire cycle.

I.5

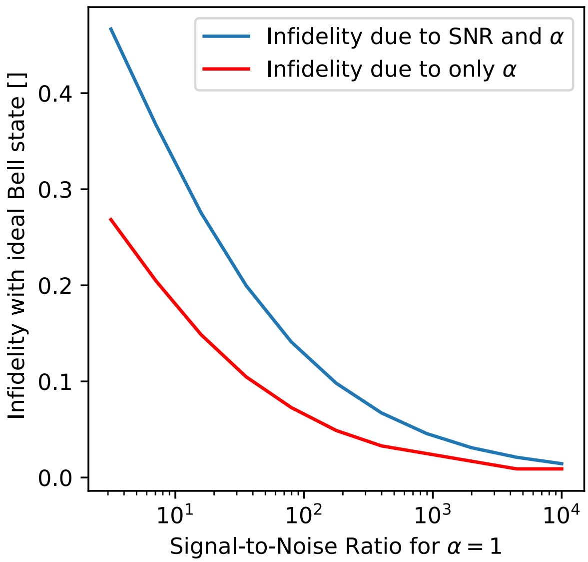

Figure I.5.15: **Impact of the protocol error α on the entangled state fidelity for different signal-to-noise ratios (SNRs).** The red (bottom) line shows the infidelity contribution with respect to the ideal Bell state with only the protocol error α as contribution to this infidelity scaling as $1-\alpha$. The blue line (top) is the infidelity contribution both due to the SNR and α, having a higher infidelity. The SNR is defined as , which is defined at $\alpha = 1$. Note that every point on both lines has an optimized α such that the infidelity contribution is the lowest, at the given SNR.

Table I.5.1: **Comparison of the QFCs used in the experiment.**

QFC	Node	Non-linear medium	Efficiency (front to end)	Noise $[s^{-1}\,GHz^{-1}]$	Eval. at filter bandwidth
QuTech [23, 35]	The Hague	ppLN waveguide	50%	2104	50 MHz
Fraunhofer ILT [36]	Delft	bulk KTA	48%	19	374 GHz

Table I.5.2: **Parameters of the losses and delays over the quantum channel.**

Link	Loss local	Loss deployed fiber	Total	Typ. Round-trip time, drift
The Hague to midpoint	3 dB QFC, 4.9 dB filters	5.2 dB, 0.51 $dB\,km^{-1}$	13.1 dB	103.16 µs ±40 $ps\,h^{-1}$
Delft to midpoint	4 dB QFC, 4.5 dB filters	5.6 dB, 0.39 $dB\,km^{-1}$	13.9 dB	145.31 µs ±80 $ps\,h^{-1}$

Table I.5.3: **Error budget of deployed link post-selected and heralded entangled states.** Parameters noted with * are averages of data measured between the fidelity measurements, other are calibrated in separate experiments. The probability to detect a photon is given for $\alpha = 1$. If only one value is mentioned it is considered equal for both nodes. The infidelity contribution is given as if it was the only error present, to make direct comparison easier. Note that due to the large contribution of noise counts, the infidelity of the final simulated state with all the contributions taken into account does not follow the sum of the individual contributions.

Simulation parameter	Delayed-choice		Fully heralded	
	Value	Error con.	Value	Error con.
Det. prob.* (Delft, DH) []	10.6e-6, 8.4e-6	28.1%	10.0e-6, 7.1e-6	26.5%
α []	0.25 and 0.25		0.25 and 0.25	
Backgr. counts* (Det1, Det2) [Hz]	40.3, 42.8		23.8, 22.0	
Double excitation probability []	0.04, 0.1	5.5%	0.04, 0.1	5.8%
Res. phase noise std* [°]	35	10.1%	41.1	12.3%
Dephasing probability []	0.01, 0.01	2.3%	0.02, 0.04	4.0%
Spectral diffusion FWHM [MHz]	25	6.5%	25	6.9%
Beam splitter imperfections []	0.95		0.95	
Detection window length [ns]	10		15	
Optical Excitation Rabi angle [°]	150, 150	-	150, 150	-
Ionization probability* []	0.035, 0.045%	5.4%	0.046	6.2%
PSB collection efficiency []	0.1, 0.1	-	0.0, 0.0	-
Simulated error (all params)	-	42.9%	-	45.8%
Simulated Fidelity	0.568, 0.576	-	0.544	-
Measured error	-	43.2%, 42.4%	-	46.6%
Avg. SSRO fidelity	95.14%, 94.49%	-	94.13%, 94.98%	

Table I.5.4: **Error budget of near-term and future improvements.** For the near-term performance, we simulated an improved ZPL fraction of the SnV, the implementation of the improved QFC on both nodes, and an improvement of the local phase-stabilization. For future improvements on the system with we have added improvements in qubit coherence via dynamical decoupling, reduction of double excitation via shorter optical excitation,reduced ionization by better control of the charge state of the emitter and improved mode overlap at the central beam splitter.

Simulation parameter	Near-term		Future	
	Value	Error con.	Value	Error con.
Det. prob. (Delft, DH)[]	16x10e-6, 16x10e-6	4.2%	16x10e-6, 16x10e-6	4.2%
α []	0.05 and 0.05		0.05 and 0.05	
Backgr. counts (Det1, Det2) [Hz]	5.0, 5.0		5.0, 5.0	
Double excitation probability []	0.04, 0.04	2.15%	0.01, 0.01	0.54%
Res. phase noise std [°]	15	1.7%	15	1.7%
Dephasing probability []	0.02, 0.04	3.0%	0.01, 0.01	1.0%
Spectral diffusion FWHM [MHz]	13	3.9%	13	1.3%
Beam splitter imperfections []	0.95		0.99	
Detection window length [ns]	15	-	15	-
Optical Excitation Rabi angle [°]	150, 150	-	150, 150	-
Ionization probability []	0.046	4.7%	0.01	1.0%
PSB collection efficiency []	0.1, 0.1	-	0.1, 0.1	-
Simulated error (all params)	-	18.9%	-	10.0%
Simulated Fidelity	0.811	-	0.90	-

REFERENCES

[1] H. J. Kimble, *The quantum internet,* Nature **453**, 1023 (2008).

[2] S. Wehner, D. Elkouss, and R. Hanson, *Quantum internet: A vision for the road ahead,* Science **362**, eaam9288 (2018).

[3] H. Buhrman, R. Cleve, J. Watrous, and R. de Wolf, *Quantum fingerprinting,* Phys. Rev. Lett. **87**, 167902 (2001).

[4] M. Ben-Or and A. Hassidim, *Fast quantum byzantine agreement,* in *Proceedings of the Thirty-Seventh Annual ACM Symposium on Theory of Computing*, STOC '05 (Association for Computing Machinery, New York, NY, USA, 2005) p. 481–485.

[5] D. Gottesman, T. Jennewein, and S. Croke, *Longer-baseline telescopes using quantum repeaters,* Phys. Rev. Lett. **109**, 070503 (2012).

[6] J. F. Clauser, M. A. Horne, A. Shimony, and R. A. Holt, *Proposed experiment to test local hidden-variable theories,* Phys. Rev. Lett. **23**, 880 (1969).

[7] D. L. Moehring, P. Maunz, S. Olmschenk, K. C. Younge, D. N. Matsukevich, L.-M. Duan, and C. Monroe, *Entanglement of single-atom quantum bits at a distance,* Nature **449**, 68–71 (2007).

[8] S. Ritter, C. Nölleke, C. Hahn, A. Reiserer, A. Neuzner, M. Uphoff, M. Mücke, E. Figueroa, J. Bochmann, and G. Rempe, *An elementary quantum network of single atoms in optical cavities,* Nature **484**, 195 (2012).

[9] J. Hofmann, M. Krug, N. Ortegel, L. Gérard, M. Weber, W. Rosenfeld, and H. Weinfurter, *Heralded Entanglement Between Widely Separated Atoms,* Science **337**, 72 (2012).

[10] H. Bernien, B. Hensen, W. Pfaff, G. Koolstra, M. S. Blok, L. Robledo, T. H. Taminiau, M. Markham, D. J. Twitchen, L. Childress, and R. Hanson, *Heralded entanglement between solid-state qubits separated by three metres,* Nature **497**, 86–90 (2013).

[11] R. Stockill, M. J. Stanley, L. Huthmacher, E. Clarke, M. Hugues, A. J. Miller, C. Matthiesen, C. Le Gall, and M. Atatüre, *Phase-Tuned Entangled State Generation between Distant Spin Qubits,* Physical Review Letters **119**, 010503 (2017).

[12] L. Stephenson, D. Nadlinger, B. Nichol, S. An, P. Drmota, T. Ballance, K. Thirumalai, J. Goodwin, D. Lucas, and C. Ballance, *High-Rate, High-Fidelity Entanglement of Qubits Across an Elementary Quantum Network,* Physical Review Letters **124**, 110501 (2020).

[13] V. Krutyanskiy, M. Galli, V. Krcmarsky, S. Baier, D. Fioretto, Y. Pu, A. Mazloom, P. Sekatski, M. Canteri, M. Teller, J. Schupp, J. Bate, M. Meraner, N. Sangouard, B. Lanyon, and T. Northup, *Entanglement of Trapped-Ion Qubits Separated by 230 Meters,* Physical Review Letters **130**, 050803 (2023).

[14] P. Drmota, D. Main, D. Nadlinger, B. Nichol, M. Weber, E. Ainley, A. Agrawal, R. Srinivas, G. Araneda, C. Ballance, and D. Lucas, *Robust Quantum Memory in a Trapped-Ion Quantum Network Node,* Physical Review Letters **130**, 090803 (2023).

[15] M. Pompili, C. Delle Donne, I. te Raa, B. van der Vecht, M. Skrzypczyk, G. Ferreira, L. de Kluijver, A. J. Stolk, S. L. N. Hermans, P. Pawełczak, W. Kozlowski, R. Hanson, and S. Wehner, *Experimental demonstration of entanglement delivery using a quantum network stack,* npj Quantum Information **8**, 1 (2022).

[16] M. Pompili, S. L. N. Hermans, S. Baier, H. K. C. Beukers, P. C. Humphreys, R. N. Schouten, R. F. L. Vermeulen, M. J. Tiggelman, L. dos Santos Martins, B. Dirkse, S. Wehner, and R. Hanson, *Realization of a multinode quantum network of remote solid-state qubits,* Science **372**, 259 (2021).

[17] S. L. N. Hermans, M. Pompili, H. K. C. Beukers, S. Baier, J. Borregaard, and R. Hanson, *Qubit teleportation between non-neighbouring nodes in a quantum network,* Nature **605**, 663 (2022).

[18] P. Drmota, D. P. Nadlinger, D. Main, B. C. Nichol, E. M. Ainley, D. Leichtle, A. Mantri, E. Kashefi, R. Srinivas, G. Araneda, C. J. Ballance, and D. M. Lucas, *Verifiable blind quantum computing with trapped ions and single photons,* Phys. Rev. Lett. **132**, 150604 (2024).

[19] M. Bock, P. Eich, S. Kucera, M. Kreis, A. Lenhard, C. Becher, and J. Eschner, *High-fidelity entanglement between a trapped ion and a telecom photon via quantum frequency conversion,* Nature Communications **9**, 1998 (2018).

[20] V. Krutyanskiy, M. Meraner, J. Schupp, V. Krcmarsky, H. Hainzer, and B. P. Lanyon, *Light-matter entanglement over 50 km of optical fibre,* npj Quantum Information **5**, 1 (2019).

[21] M. Bock, P. Eich, S. Kucera, M. Kreis, A. Lenhard, C. Becher, and J. Eschner, *High-fidelity entanglement between a trapped ion and a telecom photon via quantum frequency conversion,* Nature Communications **9**, 1998 (2018).

[22] M. Schäfer, B. Kambs, D. Herrmann, T. Bauer, and C. Becher, *Two-stage, low noise quantum frequency conversion of single photons from silicon-vacancy centers in diamond to the telecom c-band,* Advanced Quantum Technologies , 2300228 (2023), https://onlinelibrary.wiley.com/doi/pdf/10.1002/qute.202300228 .

[23] A. Tchebotareva, S. L. Hermans, P. C. Humphreys, D. Voigt, P. J. Harmsma, L. K. Cheng, A. L. Verlaan, N. Dijkhuizen, W. de Jong, A. Dréau, and R. Hanson, *Entanglement between a Diamond Spin Qubit and a Photonic Time-Bin Qubit at Telecom Wavelength,* Physical Review Letters **123**, 063601 (2019).

[24] E. Bersin, M. Sutula, Y. Q. Huan, A. Suleymanzade, D. R. Assumpcao, Y.-C. Wei, P.-J. Stas, C. M. Knaut, E. N. Knall, C. Langrock, N. Sinclair, R. Murphy, R. Riedinger, M. Yeh, C. Xin, S. Bandyopadhyay, D. D. Sukachev, B. Machielse, D. S. Levonian, M. K. Bhaskar, S. Hamilton, H. Park, M. Lončar, M. M. Fejer, P. B. Dixon, D. R. Englund, and

M. D. Lukin, *Telecom networking with a diamond quantum memory,* PRX Quantum **5** (2024), 10.1103/prxquantum.5.010303.

[25] C. Bradley, J. Randall, M. Abobeih, R. Berrevoets, M. Degen, M. Bakker, M. Markham, D. Twitchen, and T. Taminiau, *A Ten-Qubit Solid-State Spin Register with Quantum Memory up to One Minute,* Physical Review X **9**, 031045 (2019).

[26] V. Krutyanskiy, M. Canteri, M. Meraner, V. Krcmarsky, and B. Lanyon, *Multimode ion-photon entanglement over 101 kilometers,* PRX Quantum **5**, 020308 (2024).

[27] T. van Leent, M. Bock, F. Fertig, R. Garthoff, S. Eppelt, Y. Zhou, P. Malik, M. Seubert, T. Bauer, W. Rosenfeld, W. Zhang, C. Becher, and H. Weinfurter, *Entangling single atoms over 33 km telecom fibre,* Nature **607**, 69 (2022).

[28] C. M. Knaut, A. Suleymanzade, Y.-C. Wei, D. R. Assumpcao, P.-J. Stas, Y. Q. Huan, B. Machielse, E. N. Knall, M. Sutula, G. Baranes, N. Sinclair, C. De-Eknamkul, D. S. Levonian, M. K. Bhaskar, H. Park, M. Lončar, and M. D. Lukin, *Entanglement of nanophotonic quantum memory nodes in a telecom network,* Nature **629**, 573 (2024).

[29] D. Lago-Rivera, S. Grandi, J. V. Rakonjac, A. Seri, and H. de Riedmatten, *Telecom-heralded entanglement between multimode solid-state quantum memories,* Nature **594**, 37–40 (2021).

[30] X.-Y. Luo, Y. Yu, J.-L. Liu, M.-Y. Zheng, C.-Y. Wang, B. Wang, J. Li, X. Jiang, X.-P. Xie, Q. Zhang, X.-H. Bao, and J.-W. Pan, *Postselected entanglement between two atomic ensembles separated by 12.5 km,* Phys. Rev. Lett. **129**, 050503 (2022).

[31] J.-L. Liu, X.-Y. Luo, Y. Yu, C.-Y. Wang, B. Wang, Y. Hu, J. Li, M.-Y. Zheng, B. Yao, Z. Yan, D. Teng, J.-W. Jiang, X.-B. Liu, X.-P. Xie, J. Zhang, Q.-H. Mao, X. Jiang, Q. Zhang, X.-H. Bao, and J.-W. Pan, *Creation of memory–memory entanglement in a metropolitan quantum network,* Nature **629**, 579 (2024).

[32] D. Lago-Rivera, J. V. Rakonjac, S. Grandi, and H. d. Riedmatten, *Long distance multiplexed quantum teleportation from a telecom photon to a solid-state qubit,* Nature Communications **14**, 1889 (2023).

[33] C. Cabrillo, J. I. Cirac, P. García-Fernández, and P. Zoller, *Creation of entangled states of distant atoms by interference,* Physical Review A **59**, 1025–1033 (1999).

[34] S. Bose, P. L. Knight, M. B. Plenio, and V. Vedral, *Proposal for Teleportation of an Atomic State via Cavity Decay,* Physical Review Letters **83**, 5158 (1999).

[35] A. J. Stolk, K. L. van der Enden, M.-C. Roehsner, A. Teepe, S. O. J. Faes, C. E. Bradley, S. Cadot, J. van Rantwijk, I. te Raa, R. A. J. Hagen, A. Verlaan, J. Biemond, A. Khorev, R. Vollmer, M. Markham, A. Edmonds, J. Morits, T. Taminiau, E. van Zwet, and R. Hanson, *Telecom-Band Quantum Interference of Frequency-Converted Photons from Remote Detuned NV Centers,* PRX Quantum **3**, 020359 (2022).

[36] J. F. Geus, F. Elsen, S. Nyga, A. J. Stolk, K. L. van der Enden, E. J. van Zwet, C. Haefner, R. Hanson, and B. Jungbluth, *Low-noise short-wavelength pumped frequency down-conversion for quantum frequency converters,* Optica Quantum **2**, 189 (2024).

[37] A. Dréau, A. Tchebotareva, A. E. Mahdaoui, C. Bonato, and R. Hanson, *Quantum frequency conversion of single photons from a nitrogen-vacancy center in diamond to telecommunication wavelengths,* Phys. Rev. Appl. **9**, 064031 (2018).

[38] S. L. N. Hermans, M. Pompili, L. D. S. Martins, A. R.-P. Montblanch, H. K. C. Beukers, S. Baier, J. Borregaard, and R. Hanson, *Entangling remote qubits using the single-photon protocol: an in-depth theoretical and experimental study,* New Journal of Physics **25**, 013011 (2023).

[39] E. F. Dierikx, A. E. Wallin, T. Fordell, J. Myyry, P. Koponen, M. Merimaa, T. J. Pinkert, J. C. J. Koelemeij, H. Z. Peek, and R. Smets, *White rabbit precision time protocol on long-distance fiber links,* IEEE Transactions on Ultrasonics, Ferroelectrics, and Frequency Control **63**, 945 (2016).

[40] C. A. Ryan, J. S. Hodges, and D. G. Cory, *Robust Decoupling Techniques to Extend Quantum Coherence in Diamond,* Physical Review Letters **105**, 200402 (2010).

[41] M. H. Abobeih, J. Cramer, M. A. Bakker, N. Kalb, M. Markham, D. J. Twitchen, and T. H. Taminiau, *One-second coherence for a single electron spin coupled to a multi-qubit nuclear-spin environment,* Nature Communications **9**, 2552 (2018).

[42] P. Lodahl, *Quantum-dot based photonic quantum networks,* Quantum Science and Technology **3**, 013001 (2017).

[43] C. Bradac, W. Gao, J. Forneris, M. E. Trusheim, and I. Aharonovich, *Quantum nanophotonics with group iv defects in diamond,* Nature Communications **10**, 5625 (2019).

[44] N. T. Son, C. P. Anderson, A. Bourassa, K. C. Miao, C. Babin, M. Widmann, M. Niethammer, J. Ul Hassan, N. Morioka, I. G. Ivanov, F. Kaiser, J. Wrachtrup, and D. D. Awschalom, *Developing silicon carbide for quantum spintronics,* Applied Physics Letters **116**, 190501 (2020).

[45] M. Ruf, N. H. Wan, H. Choi, D. Englund, and R. Hanson, *Quantum networks based on color centers in diamond,* Journal of Applied Physics **130**, 070901 (2021).

[46] J. V. Rakonjac, S. Grandi, S. Wengerowsky, D. Lago-Rivera, F. Appas, and H. d. Riedmatten, *Transmission of light–matter entanglement over a metropolitan network,* Optica Quantum **1**, 94–102 (2023).

[47] M. Ruf, M. Weaver, S. van Dam, and R. Hanson, *Resonant excitation and purcell enhancement of coherent nitrogen-vacancy centers coupled to a fabry-perot microcavity,* Physical Review Applied **15**, 024049 (2021).

[48] D. Riedel, I. Söllner, B. J. Shields, S. Starosielec, P. Appel, E. Neu, P. Maletinsky, and R. J. Warburton, *Deterministic enhancement of coherent photon generation from a nitrogen-vacancy center in ultrapure diamond,* Phys. Rev. X **7**, 031040 (2017).

[49] A. Sipahigil, R. E. Evans, D. D. Sukachev, M. J. Burek, J. Borregaard, M. K. Bhaskar, C. T. Nguyen, J. L. Pacheco, H. A. Atikian, C. Meuwly, R. M. Camacho, F. Jelezko, E. Bielejec, H. Park, M. Lončar, and M. D. Lukin, *An integrated diamond nanophotonics platform for quantum-optical networks,* Science **354**, 847–850 (2016).

[50] M. Pasini, N. Codreanu, T. Turan, A. Riera Moral, C. F. Primavera, L. De Santis, H. K. C. Beukers, J. M. Brevoord, C. Waas, J. Borregaard, and R. Hanson, *Nonlinear quantum photonics with a tin-vacancy center coupled to a one-dimensional diamond waveguide,* Phys. Rev. Lett. **133**, 023603 (2024).

[51] P.-J. Stas, Y. Q. Huan, B. Machielse, E. N. Knall, A. Suleymanzade, B. Pingault, M. Sutula, S. W. Ding, C. M. Knaut, D. R. Assumpcao, Y.-C. Wei, M. K. Bhaskar, R. Riedinger, D. D. Sukachev, H. Park, M. Lončar, D. S. Levonian, and M. D. Lukin, *Robust multi-qubit quantum network node with integrated error detection,* Science **378**, 557 (2022), https://www.science.org/doi/pdf/10.1126/science.add9771 .

[52] V. Krutyanskiy, M. Canteri, M. Meraner, J. Bate, V. Krcmarsky, J. Schupp, N. Sangouard, and B. Lanyon, *Telecom-Wavelength Quantum Repeater Node Based on a Trapped-Ion Processor,* Physical Review Letters **130**, 213601 (2023).

[53] N. Kalb, A. A. Reiserer, P. C. Humphreys, J. J. W. Bakermans, S. J. Kamerling, N. H. Nickerson, S. C. Benjamin, D. J. Twitchen, M. Markham, and R. Hanson, *Entanglement distillation between solid-state quantum network nodes,* Science **356**, 928–932 (2017).

[54] I. T. Raa, H. K. Ervasti, P. J. Botma, L. C. Visser, R. Budhrani, J. F. van Rantwijk, S. P. Cadot, J. Vermeltfoort, M. Pompili, A. J. Stolk, M. J. Weaver, K. L. van der Enden, D. de Leeuw Duarte, M. Teng, J. van Zwieten, and F. Grooteman, *QMI - Quantum Measurement Infrastructure, a Python 3 framework for controlling laboratory equipment,* (2023).

[55] A. J. Stolk, J. J. B. Biemond, K. L. van der Enden, L. van Dooren, E. J. van Zwet, and R. Hanson, *Extendable optical phase synchronization of remote and independent quantum network nodes over deployed fibers,* (2024).

[56] M. Pompili, *Multi-Node Quantum Networks with Diamond Qubits,* Ph.D. thesis, Delft University of Technology (2021).

[57] C. Granade, J. Combes, and D. G. Cory, *Practical bayesian tomography,* New Journal of Physics **18**, 033024 (2016).

[58] C. Granade, C. Ferrie, I. Hincks, S. Casagrande, T. Alexander, J. Gross, M. Kononenko, and Y. Sanders, *Qinfer: Statistical inference software for quantum applications,* Quantum **1**, 5 (2017).

I.5

I.6

CONCLUSIONS AND OUTLOOK

But now they say, "congratulations"
Worked so hard, forgot how to vacation
They ain't never had the dedication
People hatin', say we changed and look, we made it
Yeah, we made it

Post Malone, *Congratulations*, Stony, 2016

In this Chapter I summarize the results of "Part I: Experimental" of this thesis and highlight the intermediary and final results of the successful metropolitan-scale entanglement generation experiment. Then, based on these findings and accrued knowledge of the technological challenges, I present promising avenues to continue advancing the field of quantum networks.

I.6.1. SUMMARY

Chapter I.3 showed the successful first step in proving that the quantum network hardware platform can create indistinguishable photons originating from distinguishable sources. We have interfered photons emitted by remote, independently operated and spectrally detuned NV center-based quantum network nodes using quantum frequency conversion to the telecom L-band. The conversion process is simultaneously used to frequency stabilize the interfering photons, a design that can readily be used for large distance separation between the nodes. With this result, the first iteration of the quantum network hardware platform is validated and ready to be used in entanglement generation experiments.

Chapter I.4 presented the technical background of the phase stabilization architecture. We investigated the necessary feedback bandwidth of the stabilization tasks and quantified the performance of each of them. We characterized the resulting optical phase stability of the fully deployed system over a continuous period of 10 hours, and found a short-term stability standard deviation of $\sigma \approx 35\,\mathrm{deg}$ and a long-term stability of the average optical phase to within a few degrees. With this, we have successfully proven that the phase stabilization architecture could be used for the metropolitan-scale entanglement experiment.

Chapter I.5 demonstrated the full capabilities of the quantum network hardware platform as set out at the start of this thesis. We performed heralded entanglement generation between two independently operated quantum network nodes separated by 10km that are linked with a midpoint station via 25km of deployed optical fiber. By capitalizing on the full heralding capabilities of the network link in combination with real-time feedback logic on the long-lived qubits, we demonstrated the delivery of a predefined entangled state on the nodes irrespective of the heralding detection pattern with a fidelity of 0.534(15) at a rate of $1.3\,\mathrm{min}^{-1}$. This quantum network hardware platform establishes an extensible architecture for exploring metropolitan-scale quantum networks and is compatible with different qubit systems.

In the following sections I will discuss the future of quantum networks both from an academic and commercial point of view.

I.6.2. NEAR-TERM RESEARCH PROSPECTS

For academic research prospects we limit the discussion to a Technology Readiness Level (TRL) below 6, as I believe it to be the most fitting levels for an academic environment, see Table II.1.1 of Chapter II.1 for an overview of the levels. This range spans from observing basic principles to technology validation in the relevant environment. In the next sections I will discuss the prospects of fundamental research to enable quantum network scaling that can be performed in TRL 1-5, which will focus on bottom-up improvements on qubits, quantum chip design and proof-of-concept quantum network experiments. After that, the Commercialization section will focus on further development necessary to build large-scale quantum networks that are TRL 6+.

I.6.2.1. IMPROVED PHOTON EMISSION

Research in building physical systems for scaling quantum network is largely spread over several topics: improving quantum emitters for increased entanglement generation rates and improving fidelity [1, 2], scaling of number of qubits per quantum chip [1, 3], increasing the number of connected nodes [4] and increasing the distance between the nodes (Part I of this thesis) [5–8]. Although the NV center has been incredibly useful as demonstration platform for scaling quantum networking, it is close to reaching its end-of-life of its current implementation. With the limited 3% ZPL emission and SIL-based collection that is relatively inefficient, the starting point of entanglement generation rates is handicapped by its fundamentals (PSB collection ranges $\approx 5-13\%$ [9, 10]). This translates to fidelity as well when making use of the 'fast' single-photon entanglement generation scheme, as highlighted in Chapter I.5. There, a larger α was traded off against SNR, reducing the state fidelity. With larger signal, both the SNR increases and a smaller α can be chosen, boosting the fidelity both ways. A larger signal also opens the possibility to move back to a two-photon entanglement scheme, removing the protocol error α altogether, and reducing system complexity by removing stringent phase stability requirements, see Chapter I.4.

We can boost this signal by embedding the NV center in an open microcavity [11–15], yet this does not solve the scaling per-chip issue. Conversely, we can replacing the NV center by another color center that has fundamentally better optical properties in its effective ZPL emission, such as SiV, GeV, SnV and PbV [1]. We have estimated that using an SnV in the experiment of Chapter I.5 would yield a heralded state fidelity above 0.8 at the same entanglement rate as the NV, when all QFCs used are the low-noise NORA QFCs.

I.6.2.2. SCALING PLATFORMS

The benefit of other group-IV color centers and their symmetric inversion axis is their compatibility with photonic structures [16] and embedded photonic crystal cavities [17–20], allowing for scaling the fabrication of multiple qubits per chip and routing photons on-chip [1, 21]. These methods have had little success for NV centers given their susceptibility to electric field and strain. Academically it is worthwhile to explore these diamond-based platforms, and the SnV as first candidate given its recent progress and compatibility to existing techniques of communication qubit control [22–28]. When experimental developments amount to more advanced qubit and local memory control for the SnV [29, 30], the higher ZPL fractions and on-chip scalability will allow for near-term demonstration systems that can explore increasingly more complex quantum networking applications with multiple communication qubits. Additionally, it can be a demonstration platform for more advanced network control when integrated in a quantum internet software stack. Specific next experimental goals can include performing verified blind quantum computing on a solid-state qubit platform and multiple-qubit reconfigurable routing demonstrations through link-layer control of the hardware systems [31–33]. Essentially, experiments that can be localized to *at most two nodes*, which can include multiple (communication) qubits per node, are suitable for further SnV-based experimental efforts in quantum networking applications.

I.6.2.3. Scaling limits

Managing more than two nodes is unfeasible in academic environments for the coming years. In the expectation that each node becomes continuously more advanced in functionality, long-term stability and hardware device management overhead will limit the ability for coordination beyond two prototype systems. Multiple (> 2) nodes will only be feasibly controllable by an academic team if the research goals are less focused on pushing the full system capabilities itself, and they can make use of a *standardized* node that is close to turn-key in operability. Then, the research attention can shift back to the fundamentals and we can expect multiple nodes to be operable for experimental implementation of different color-center qubits, testing of scaling on-chip structures, improving sub-systems (midpoint measurement systems, optical switching capabilities, QFCs, software control) or experimentally verifying network architectures.

Furthermore, while promising as academic platform, the usability of the group-IV color centers in diamond scaling beyond academia is not a given from a practical point of view. With challenges in strain tuning, microwave delivery and heating and controlling additional nuclear spins for memory purposes, the individual SnV performance has several years of development before it can be used as building block in future quantum networks [1, 15, 21, 34]. Even then, fabrication of diamond devices is a highly specialized skill in the full logistical chain from diamond growth, to the introduction of the color center (growth, implantation) and fabrication of the eventual structures surrounding the qubits [15, 21]. Also the scaling of diamond fabrication beyond dozens of diamond-only chips will have to be developed largely from the ground up, as the current semiconductor industry is not natively *diamond compatible*. A concentrated effort of a *diamond foundry* can help relieve the scaling bottleneck and concentrate skills and expertise, see Section I.6.3.2.

I.6

I.6.2.4. Beyond diamond as solid-state platform

The semiconductor industry can be leveraged to scale production of quantum chips for quantum networking by making use of silicon platforms in several ways. Most promising technologies include hybrid photonic structures where only the quantum emitter is kept in diamond and integrated in optimized (non-diamond) photonic structures [3, 35–37]. This reduces the reliability on diamond fabrication, yet allows for the benefits of CMOS, photonic integrated circuits (PICs) and programming [38]. Moving fully away from diamond, there in progress in ions embedded in other material nanophotonic cavities, e.g. $^{171}\mathrm{Yb}:\mathrm{YVO}^4$ [2, 39]. A promising direction from a chip-scalability perspective is to have quantum emitters with spin fully in silicon-type structures: color centers in silicon [40–43] and silicon-carbite [44] are being engineered, as well as integration of Erbium dopants in silicon [45, 46]. Here, the inherent silicon fabrication scalability argument outweighs the still limited control of all potential qubits that can be made in those platforms [47]. Still, recent progress in entanglement generation between separate silicon T-centers shows the potential for continued success [48]. If silicon-based qubit control can rival the color centers in diamond, with their native telecom-wavelength compatibility, on-chip photon routing, inherent platform scalability and the existing standardized fabrication of silicon technology, these platforms have the potential to outperform diamond-based systems.

I.6.3. COMMERCIALIZATION

Beyond TRL 5+ lays the opportunity to pursue technology development that is more towards scaling quantum networks. The system requirements that led to successful demonstration of the quantum network hardware platform are foreshadowing how to scale beyond the two-node and metropolitan-scale system. In scaling to multiple nodes at long distances, independent and long-term operation, I identify three key categories of potential next technology development directions: miniaturization, gadgets and full-stack systems. These categories are beyond the scope of academia, and are aimed at commercial development to guarantee their success. I share the ideas on commercialization because:

> It's not about the idea, but about the execution of the idea.

I.6.3.1. MINIATURIZATION

Any deployable quantum node will have to be of manageable size, and fit to standards of telecommunication and data centers. Generally, this means a standard 19“-rack format, and preferably as few of them as possible. The current quantum network layout is comprised of 2 full-size 19“-racks, an optical table, and a full sized frame around the table for additional hardware devices and cabling. Engineering efforts will have to reduce this fully to 19“-racks. Other quantum computing systems have shown similar size reductions, also those involving optics [49]. For the system described in this thesis, significant effort can be put in miniaturization of optics, electronics and laser system integration. Free-space optics can be aligned more easily in precision-milled molds in standardized 1/2/3U boxes or through optics soldering, which is area-efficient when employed in three dimensional geometries [50]. The most improvements can be made for optics to be developed on-chip as PIC [35, 36]. Close collaboration with an integrated photonics foundry can provide tailored solutions for specific implementations and challenges [51, 52].

Electronics should also be consolidated to single devices as much as possible. Especially electronics that depend on signals to and from each other (microcontroller and qubit control, timetagger, timing distribution) should be integrated into one product per node, which is currently an ongoing effort directed by the Delft scale-up Qblox within the Quantum Internet Alliance (QIA) [53], for example. Similarly, rack-based and centralized control of laser systems will greatly reduce the footprint with a server rack [54, 55]. Custom cryogenic systems can also be made compatible to racks [56, 57].

I.6.3.2. GADGETS

Individual subsystem development can be turned into its own specific product, sometimes named a *gadget*: a product that does a minimal amount of tasks, but executes them well. From the quantum network hardware platform we can distill several gadgets that, with proper implementation, have high probability to be desirable products. I omit gadgets that are in development by several companies, e.g. the aforementioned Qblox *qubit controller*.

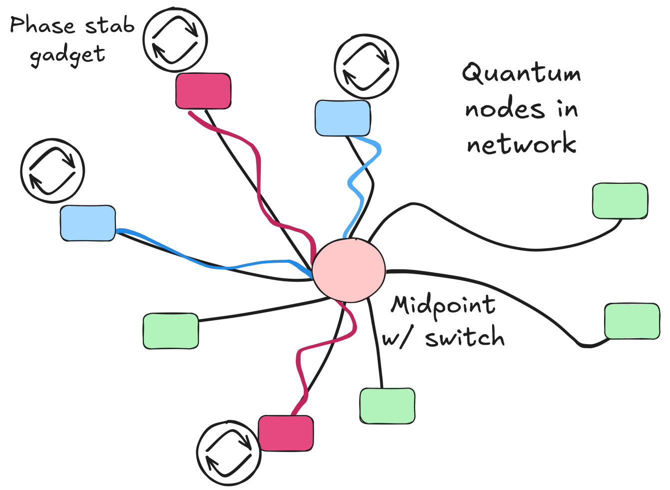

Figure I.6.1: Schematic of a future quantum network, where users and their quantum node (rectangular box) can entangle with each other (blue, pink) over the midpoint (circle). Reconfiguration at the midpoint allows for multiple nodes to be connected using shared resources. Included here is the visualization of a phase stabilizer gadget integrated in the nodes.

Quantum Frequency Converter

Many of the currently used quantum communication qubits operate at visible wavelength [58], and depend on quantum frequency conversion to become telecom compatible [5, 8, 59–61]. Since telecom-native qubits are still in development, there is a need for QFCs. Currently, construction of QFCs is mostly done by research groups and used in academic research [62–66], mostly due to their specific implementation. Differences come in through the entanglement generation schemes based on polarization or time-bin, but also in long- or short-wavelength conversion, or the specific implementation of how it can be built, as described in Section I.2.5.1, I.2.5.2 and [67]. In this thesis we have also used a QFC built by Fraunhofer ILT, which in this category, has leading performance in terms of its conversion efficiency, low noise injection and practical operational long-term stability. This is a system that comes closest to commercialization, which I expect with another iteration of practical engineering can be turned into a marketable gadget. Future development include frequency conversion on-chip, reducing area footprint and allowing for quantum chip integration [51]. The availability of a commercial QFC also opens the possibility for more research groups to benefit from this technology, as many might not have the expertise to both develop communication qubits and the QFC.

Phase stabilizer

Going forward, single-click entanglement schemes will remain relevant in achieving high-rate entanglement generation for long-distance connections. The complexity overhead of phase stabilization, as shown in Chapter I.4 and Chapter I.5), can be reason to step back to a two-photon entanglement scheme with reduced rate. Still, for quantum network applications where entanglement fidelity can be traded off against rate, a quantum network

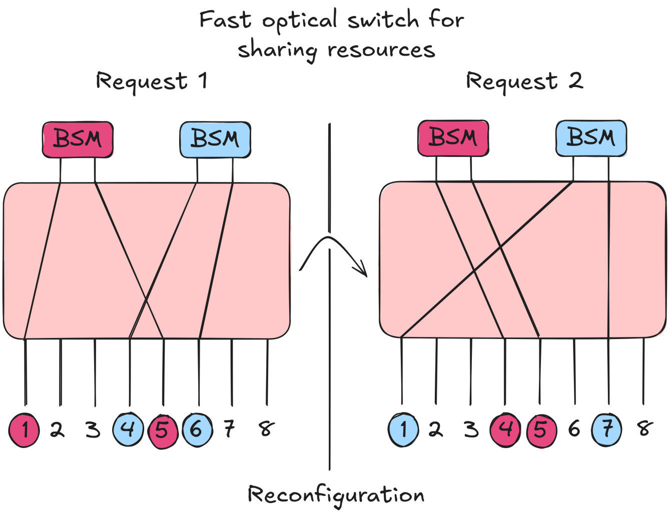

Figure I.6.2: Fast optical switching allows multiple users to be routed over the same midpoint, sharing Bell state measurement (BSM) resources, see Fig. I.6.1. Over multiple rounds, reconfiguration of the switch can connect different users in a short time frame.

should be able to use the single-photon scheme. A turn-key solution that stabilizes the phase of the photon path with low error and operational stability would enable the flexibility to switch between high fidelity, lower rate, or lower fidelity, higher rate. This product will also be useful for twin-field quantum key distribution networks, where similar phase stabilization requirements are demanded [68, 69].

DIAMOND FOUNDRY

As mentioned in Section I.6.2.4, fabrication of nanostructures and qubit integration in diamond will need to see a path to reliability and scalability if it ever wants to match up against the silicon industry. A specialized effort that tackles the challenge of diamond growth, qubit integration, nanofabrication and subsequent characterization will solve a bottleneck in the logistical chain towards scaling diamond-based quantum chips.

OPTICAL SWITCH

To generate entanglement between different users in an efficient manner a start topology will have to be employed, connecting several nodes to one measurement station. This station will connect end users based on the requests they make, necessitating fast switching of optical signals to reconfigure its connections to make optimal use of the available single-photon measurement resources in the form of a Bell state measurement (BSM), as shown in Fig. I.6.2. This optical switch will have to be able fast (sub-microsecond switching time), should allow for high suppression $O(100)$dB when using stabilization lasers (see Chapter I.4) as well have < 1 dB insertion loss in pass-through mode to not be an insignificant loss channel for long-distance single photon transmission. Where initially switch performance matters most, later the size of the physical switch and scalability of input-output connectivity will become more important, suggesting a move to on-chip switching, an active area of research [70]. Additionally, on top of the hardware of this switch, software and control can be built that manages entanglement generation requests [71].

Hardware Layer Operating System

Software and control methods to manage the different layers in the quantum network stack are concurrently being developed next to hardware. A recent demonstration showed an operating system for executing applications on quantum network nodes in a research setting [72]. Development in this field is key for future, complex quantum networks, but without hardware to run these control systems on, is not marketable except for the pursuit of developing an intellectual property portfolio. Since any complex quantum network requires stable and reliable quantum hardware systems, a quantum hardware control stack to manage solely the *hardware layer* is vital in providing scalability. In this thesis we have shown a first iteration of such a quantum hardware control stack, see Chapter I.2.7 and Fig. I.2.7. While this provided the necessary stability to execute the metropolitan-scale entanglement generation between two nodes, redesign is necessary to scale to tens of nodes and achieve industry-standard of $> 99.9\%$ headless operation time [73]. This should include security-by-design principles, and will likely move to a more state machine-like operating system. It will simultaneously keep track of performance metrics and executing dependency graph calibration routines automatically, while providing a dedicated communication line for the other network layers. Such a *hardware OS* will be useful for both research or commercial quantum network nodes. The unique selling point of this stack will be its inherent compatibility to distributed quantum nodes.

I.6.3.3. FULL-STACK SYSTEMS

The success of the commercialization prospects described in the previous Sections I.6.3.1-I.6.3.2 all depend on the actual *use* of their suggestions. Miniaturization efforts only are worth their investment if the deployment requirements are necessary, i.e. if quantum internet systems end up at datacenters and telecom stations. A similar argument holds for the gadgets. Although their first use could be in academia, exponential growth of sales depends on their integration in systems that are built for scale.

I propose that it is possible to develop such a system: a full-stack quantum internet commercialization effort in hardware and software, which can act as *integrator* for the gadgets above, and for other gadget-like products being developed in the quantum technology landscape. The benefit of such a commercial effort is that interfacing of all the layers in this stack can be managed and optimized. The risk is that developing an entire stack in both hard- and software is costly. Still, the call for full-stack system development is broadcast widely by national and European quantum ecosystems [74], although few rise up to the challenge of its execution. Most full-stack *quantum computing* system development has found its rise in the USA by startup companies[1], with few doing the same in Europe[2] and even less in the Netherlands[3]. Driven by the expectation that quantum networks will enable scaling towards useful quantum computing, an opportunity presents itself for an expert quantum internet operator to deliver on this scaling catalyst.

[1] Some of which are Rigetti, PsiQuantum, Quantinuum (through acquisition of Honeywell), IonQ, QuEra
[2] IQM, Pasqal
[3] Quix

REFERENCES

[1] M. Ruf, N. H. Wan, H. Choi, D. Englund, and R. Hanson, *Quantum networks based on color centers in diamond,* Journal of Applied Physics **130**, 070901 (2021).

[2] A. Ruskuc, C.-J. Wu, E. Green, S. L. N. Hermans, J. Choi, and A. Faraon, *Scalable Multipartite Entanglement of Remote Rare-earth Ion Qubits,* (2024).

[3] N. H. Wan, T.-J. Lu, K. C. Chen, M. P. Walsh, M. E. Trusheim, L. De Santis, E. A. Bersin, I. B. Harris, S. L. Mouradian, I. R. Christen, E. S. Bielejec, and D. Englund, *Large-scale integration of artificial atoms in hybrid photonic circuits,* Nature **583**, 226 (2020).

[4] M. Pompili, S. L. N. Hermans, S. Baier, H. K. C. Beukers, P. C. Humphreys, R. N. Schouten, R. F. L. Vermeulen, M. J. Tiggelman, L. dos Santos Martins, B. Dirkse, S. Wehner, and R. Hanson, *Realization of a multinode quantum network of remote solid-state qubits,* Science **372**, 259 (2021).

[5] T. van Leent, M. Bock, F. Fertig, R. Garthoff, S. Eppelt, Y. Zhou, P. Malik, M. Seubert, T. Bauer, W. Rosenfeld, W. Zhang, C. Becher, and H. Weinfurter, *Entangling single atoms over 33 km telecom fibre,* Nature **607**, 69 (2022).

[6] Y. Zhou, P. Malik, F. Fertig, M. Bock, T. Bauer, T. van Leent, W. Zhang, C. Becher, and H. Weinfurter, *Long-lived quantum memory enabling atom-photon entanglement over 101 km of telecom fiber,* PRX Quantum **5**, 020307 (2024).

[7] J.-L. Liu, X.-Y. Luo, Y. Yu, C.-Y. Wang, B. Wang, Y. Hu, J. Li, M.-Y. Zheng, B. Yao, Z. Yan, D. Teng, J.-W. Jiang, X.-B. Liu, X.-P. Xie, J. Zhang, Q.-H. Mao, X. Jiang, Q. Zhang, X.-H. Bao, and J.-W. Pan, *Creation of memory–memory entanglement in a metropolitan quantum network,* Nature **629**, 579 (2024).

[8] C. M. Knaut, A. Suleymanzade, Y.-C. Wei, D. R. Assumpcao, P.-J. Stas, Y. Q. Huan, B. Machielse, E. N. Knall, M. Sutula, G. Baranes, N. Sinclair, C. De-Eknamkul, D. S. Levonian, M. K. Bhaskar, H. Park, M. Lončar, and M. D. Lukin, *Entanglement of nanophotonic quantum memory nodes in a telecom network,* Nature **629**, 573 (2024).

[9] B. Hensen, H. Bernien, A. E. Dréau, A. Reiserer, N. Kalb, M. S. Blok, J. Ruitenberg, R. F. L. Vermeulen, R. N. Schouten, C. Abellán, W. Amaya, V. Pruneri, M. W. Mitchell, M. Markham, D. J. Twitchen, D. Elkouss, S. Wehner, T. H. Taminiau, and R. Hanson, *Loophole-free Bell inequality violation using electron spins separated by 1.3 kilometres,* Nature **526**, 682 (2015).

[10] O. Ubbens, *A Unified Model to Predict Excited State Cyclicity of Nitrogen Vacancy Centres in Diamond,* Master's thesis, QuTech, Delft University of Technology (2022).

[11] K. J. Vahala, *Optical microcavities,* Nature **424**, 839–846 (2003).

[12] R. Albrecht, A. Bommer, C. Deutsch, J. Reichel, and C. Becher, *Coupling of a single nitrogen-vacancy center in diamond to a fiber-based microcavity,* Phys. Rev. Lett. **110**, 243602 (2013).

[13] D. Riedel, I. Söllner, B. J. Shields, S. Starosielec, P. Appel, E. Neu, P. Maletinsky, and R. J. Warburton, *Deterministic enhancement of coherent photon generation from a nitrogen-vacancy center in ultrapure diamond,* Phys. Rev. X **7**, 031040 (2017).

[14] E. Janitz, M. K. Bhaskar, and L. Childress, *Cavity quantum electrodynamics with color centers in diamond,* Optica **7**, 1232 (2020).

[15] M. Ruf, *Cavity-enhanced quantum network nodes in diamond*, Ph.D. thesis, Delft University of Technology (2021).

[16] R. E. Evans, A. Sipahigil, D. D. Sukachev, A. S. Zibrov, and M. D. Lukin, *Narrow-linewidth homogeneous optical emitters in diamond nanostructures via silicon ion implantation,* Phys. Rev. Appl. **5**, 044010 (2016).

[17] A. Sipahigil, R. E. Evans, D. D. Sukachev, M. J. Burek, J. Borregaard, M. K. Bhaskar, C. T. Nguyen, J. L. Pacheco, H. A. Atikian, C. Meuwly, R. M. Camacho, F. Jelezko, E. Bielejec, H. Park, M. Lončar, and M. D. Lukin, *An integrated diamond nanophotonics platform for quantum-optical networks,* Science **354**, 847–850 (2016).

[18] R. E. Evans, M. K. Bhaskar, D. D. Sukachev, C. T. Nguyen, A. Sipahigil, M. J. Burek, B. Machielse, G. H. Zhang, A. S. Zibrov, E. Bielejec, H. Park, M. Lončar, and M. D. Lukin, *Photon-mediated interactions between quantum emitters in a diamond nanocavity,* Science **362**, 662 (2018).

[19] A. E. Rugar, S. Aghaeimeibodi, D. Riedel, C. Dory, H. Lu, P. J. McQuade, Z.-X. Shen, N. A. Melosh, and J. Vučković, *Quantum Photonic Interface for Tin-Vacancy Centers in Diamond*, Physical Review X **11**, 031021 (2021).

[20] K. Kuruma, B. Pingault, C. Chia, D. Renaud, P. Hoffmann, S. Iwamoto, C. Ronning, and M. Lončar, *Coupling of a single tin-vacancy center to a photonic crystal cavity in diamond,* Applied Physics Letters **118**, 230601 (2021).

[21] M. Pasini, *Nanophotonics with Diamond Color Centers: Quantum Optics and Entanglement Protocols*, Ph.D. thesis (2024).

[22] A. E. Rugar, C. Dory, S. Aghaeimeibodi, H. Lu, S. Sun, S. D. Mishra, Z.-X. Shen, N. A. Melosh, and J. Vučković, *Narrow-Linewidth Tin-Vacancy Centers in a Diamond Waveguide,* ACS Photonics **7**, 2356 (2020).

[23] L. De Santis, M. E. Trusheim, K. C. Chen, and D. R. Englund, *Investigation of the stark effect on a centrosymmetric quantum emitter in diamond,* Phys. Rev. Lett. **127**, 147402 (2021).

[24] R. Debroux, C. P. Michaels, C. M. Purser, N. Wan, M. E. Trusheim, J. Arjona Martínez, R. A. Parker, A. M. Stramma, K. C. Chen, L. de Santis, E. M. Alexeev, A. C. Ferrari, D. Englund, D. A. Gangloff, and M. Atatüre, *Quantum control of the tin-vacancy spin qubit in diamond,* Phys. Rev. X **11**, 041041 (2021).

[25] J. Arjona Martínez, R. A. Parker, K. C. Chen, C. M. Purser, L. Li, C. P. Michaels, A. M. Stramma, R. Debroux, I. B. Harris, M. Hayhurst Appel, E. C. Nichols, M. E. Trusheim, D. A. Gangloff, D. Englund, and M. Atatüre, *Photonic indistinguishability of the tin-vacancy center in nanostructured diamond,* Phys. Rev. Lett. **129**, 173603 (2022).

[26] E. I. Rosenthal, C. P. Anderson, H. C. Kleidermacher, A. J. Stein, H. Lee, J. Grzesik, G. Scuri, A. E. Rugar, D. Riedel, S. Aghaeimeibodi, G. H. Ahn, K. Van Gasse, and J. Vučković, *Microwave Spin Control of a Tin-Vacancy Qubit in Diamond,* Physical Review X **13**, 031022 (2023).

[27] G. Pieplow, M. Belhassen, and T. Schröder, *Efficient microwave spin control of negatively charged group-iv color centers in diamond,* Phys. Rev. B **109**, 115409 (2024).

[28] J. M. Brevoord, L. De Santis, T. Yamamoto, M. Pasini, N. Codreanu, T. Turan, H. K. Beukers, C. Waas, and R. Hanson, *Heralded initialization of charge state and optical-transition frequency of diamond tin-vacancy centers,* Phys. Rev. Appl. **21**, 054047 (2024).

[29] I. B. Harris, C. P. Michaels, K. C. Chen, R. A. Parker, M. Titze, J. Arjona Martínez, M. Sutula, I. R. Christen, A. M. Stramma, W. Roth, C. M. Purser, M. H. Appel, C. Li, M. E. Trusheim, N. L. Palmer, M. L. Markham, E. S. Bielejec, M. Atatüre, and D. Englund, *Hyperfine spectroscopy of isotopically engineered group-iv color centers in diamond,* PRX Quantum **4**, 040301 (2023).

I.6

[30] R. A. Parker, J. Arjona Martínez, K. C. Chen, A. M. Stramma, I. B. Harris, C. P. Michaels, M. E. Trusheim, M. Hayhurst Appel, C. M. Purser, W. G. Roth, D. Englund, and M. Atatüre, *A diamond nanophotonic interface with an optically accessible deterministic electronuclear spin register,* Nature Photonics **18**, 156 (2024).

[31] J. F. Fitzsimons and E. Kashefi, *Unconditionally verifiable blind quantum computation,* Physical Review A **96**, 012303 (2017).

[32] S. Gauthier, G. Vardoyan, and S. Wehner, *A control architecture for entanglement generation switches in quantum networks,* in *Proceedings of the 1st Workshop on Quantum Networks and Distributed Quantum Computing*, QuNet '23 (Association for Computing Machinery, New York, NY, USA, 2023) p. 38–44.

[33] S. Gauthier, T. Vasantam, and G. Vardoyan, *An on-demand resource allocation algorithm for a quantum network hub and its performance analysis,* (2024).

[34] X. Guo, A. M. Stramma, Z. Li, W. G. Roth, B. Huang, Y. Jin, R. A. Parker, J. Arjona Martínez, N. Shofer, C. P. Michaels, C. P. Purser, M. H. Appel, E. M. Alexeev, T. Liu, A. C. Ferrari, D. D. Awschalom, N. Delegan, B. Pingault, G. Galli, F. J. Heremans, M. Atatüre, and A. A. High, *Microwave-based quantum control and coherence protection of tin-vacancy spin qubits in a strain-tuned diamond-membrane heterostructure,* Phys. Rev. X **13**, 041037 (2023).

[35] A. W. Elshaari, W. Pernice, K. Srinivasan, O. Benson, and V. Zwiller, *Hybrid integrated quantum photonic circuits,* Nature Photonics **14**, 285 (2020).

[36] E. Pelucchi, G. Fagas, I. Aharonovich, D. Englund, E. Figueroa, Q. Gong, H. Hannes, J. Liu, C.-Y. Lu, N. Matsuda, J.-W. Pan, F. Schreck, F. Sciarrino, C. Silberhorn, J. Wang, and K. D. Jöns, *The potential and global outlook of integrated photonics for quantum technologies,* Nature Reviews Physics **4**, 194 (2022).

[37] L. Li, L. D. Santis, I. B. W. Harris, K. C. Chen, Y. Gao, I. Christen, H. Choi, M. Trusheim, Y. Song, C. Errando-Herranz, J. Du, Y. Hu, G. Clark, M. I. Ibrahim, G. Gilbert, R. Han, and D. Englund, *Heterogeneous integration of spin–photon interfaces with a CMOS platform,* Nature **630**, 70 (2024).

[38] W. Bogaerts, D. Pérez, J. Capmany, D. A. B. Miller, J. Poon, D. Englund, F. Morichetti, and A. Melloni, *Programmable photonic circuits,* Nature **586**, 207 (2020).

[39] J. M. Kindem, A. Ruskuc, J. G. Bartholomew, J. Rochman, Y. Q. Huan, and A. Faraon, *Control and single-shot readout of an ion embedded in a nanophotonic cavity,* Nature **580**, 201 (2020).

[40] W. Redjem, A. Durand, T. Herzig, A. Benali, S. Pezzagna, J. Meijer, A. Y. Kuznetsov, H. S. Nguyen, S. Cueff, J.-M. Gérard, I. Robert-Philip, B. Gil, D. Caliste, P. Pochet, M. Abbarchi, V. Jacques, A. Dréau, and G. Cassabois, *Single artificial atoms in silicon emitting at telecom wavelengths,* Nature Electronics **3**, 738 (2020).

[41] Y. Baron, A. Durand, P. Udvarhelyi, T. Herzig, M. Khoury, S. Pezzagna, J. Meijer, I. Robert-Philip, M. Abbarchi, J.-M. Hartmann, V. Mazzocchi, J.-M. Gérard, A. Gali, V. Jacques, G. Cassabois, and A. Dréau, *Detection of Single W-Centers in Silicon,* ACS Photonics **9**, 2337 (2022).

[42] D. B. Higginbottom, A. T. K. Kurkjian, C. Chartrand, M. Kazemi, N. A. Brunelle, E. R. MacQuarrie, J. R. Klein, N. R. Lee-Hone, J. Stacho, M. Ruether, C. Bowness, L. Bergeron, A. DeAbreu, S. R. Harrigan, J. Kanaganayagam, D. W. Marsden, T. S. Richards, L. A. Stott, S. Roorda, K. J. Morse, M. L. W. Thewalt, and S. Simmons, *Optical observation of single spins in silicon,* Nature **607**, 266 (2022).

[43] A. DeAbreu, C. Bowness, A. Alizadeh, C. Chartrand, N. A. Brunelle, E. R. MacQuarrie, N. R. Lee-Hone, M. Ruether, M. Kazemi, A. T. K. Kurkjian, S. Roorda, N. V. Abrosimov, H.-J. Pohl, M. L. W. Thewalt, D. B. Higginbottom, and S. Simmons, *Waveguide-integrated silicon T centres,* Optics Express **31**, 15045 (2023).

[44] S. Majety, P. Saha, V. A. Norman, and M. Radulaski, *Quantum information processing with integrated silicon carbide photonics,* Journal of Applied Physics **131**, 130901 (2022).

[45] L. Weiss, A. Gritsch, B. Merkel, and A. Reiserer, *Erbium dopants in nanophotonic silicon waveguides,* Optica **8**, 40 (2021).

[46] A. Gritsch, A. Ulanowski, and A. Reiserer, *Purcell enhancement of single-photon emitters in silicon,* Optica **10**, 783 (2023).

[47] S. Simmons, *Scalable fault-tolerant quantum technologies with silicon color centers,* PRX Quantum **5**, 010102 (2024).

[48] P. Inc, F. Afzal, M. Akhlaghi, S. J. Beale, O. Bedroya, K. Bell, L. Bergeron, K. Bonsma-Fisher, P. Bychkova, Z. M. E. Chaisson, C. Chartrand, C. Clear, A. Darcie, A. DeAbreu, C. DeLisle, L. A. Duncan, C. D. Smith, J. Dunn, A. Ebrahimi, N. Evetts, D. F. Pinheiro, P. Fuentes, T. Georgiou, B. Guha, R. Haenel, D. Higginbottom, D. M. Jackson, N. Jahed, A. Khorshidahmad, P. K. Shandilya, A. T. K. Kurkjian, N. Lauk, N. R. Lee-Hone, E. Lin, R. Litynskyy, D. Lock, L. Ma, I. MacGilp, E. R. MacQuarrie, A. Mar, A. M. Khah, A. Matiash, E. Meyer-Scott, C. P. Michaels, J. Motira, N. K. Noori, E. Ospadov, E. Patel, A. Patscheider, D. Paulson, A. Petruk, A. L. Ravindranath, B. Reznychenko, M. Ruether, J. Ruscica, K. Saxena, Z. Schaller, A. Seidlitz, J. Senger, Y. S. Lee, O. Sevoyan, S. Simmons, O. Soykal, L. Stott, Q. Tran, S. Tserkis, A. Ulhaq, W. Vine, R. Weeks, G. Wolfowicz, and I. Yoneda, *Distributed Quantum Computing in Silicon,* (2024).

[49] I. Pogorelov, T. Feldker, C. D. Marciniak, L. Postler, G. Jacob, O. Krieglsteiner, V. Podlesnic, M. Meth, V. Negnevitsky, M. Stadler, B. Höfer, C. Wächter, K. Lakhmanskiy, R. Blatt, P. Schindler, and T. Monz, *Compact ion-trap quantum computing demonstrator,* PRX Quantum **2**, 020343 (2021).

[50] Fraunhofer ILT, *Packaging,* Accessed through Wayback Machine 20 Aug 2024 (2019).

[51] X. Wang, X. Jiao, B. Wang, Y. Liu, X.-P. Xie, M.-Y. Zheng, Q. Zhang, and J.-W. Pan, *Quantum frequency conversion and single-photon detection with lithium niobate nanophotonic chips,* npj Quantum Information **9**, 1 (2023).

I.6

[52] K. Alexander, A. Bahgat, A. Benyamini, D. Black, D. Bonneau, S. Burgos, B. Burridge, G. Campbell, G. Catalano, A. Ceballos, C.-M. Chang, C. J. Chung, F. Danesh, T. Dauer, M. Davis, E. Dudley, P. Er-Xuan, J. Fargas, A. Farsi, C. Fenrich, J. Frazer, M. Fukami, Y. Ganesan, G. Gibson, M. Gimeno-Segovia, S. Goeldi, P. Goley, R. Haislmaier, S. Halimi, P. Hansen, S. Hardy, J. Horng, M. House, H. Hu, M. Jadidi, H. Johansson, T. Jones, V. Kamineni, N. Kelez, R. Koustuban, G. Kovall, P. Krogen, N. Kumar, Y. Liang, N. LiCausi, D. Llewellyn, K. Lokovic, M. Lovelady, V. Manfrinato, A. Melnichuk, M. Souza, G. Mendoza, B. Moores, S. Mukherjee, J. Munns, F.-X. Musalem, F. Najafi, J. L. O'Brien, J. E. Ortmann, S. Pai, B. Park, H.-T. Peng, N. Penthorn, B. Peterson, M. Poush, G. J. Pryde, T. Ramprasad, G. Ray, A. Rodriguez, B. Roxworthy, T. Rudolph, D. J. Saunders, P. Shadbolt, D. Shah, H. Shin, J. Smith, B. Sohn, Y.-I. Sohn, G. Son, C. Sparrow, M. Staffaroni, C. Stavrakas, V. Sukumaran, D. Tamborini, M. G. Thompson, K. Tran, M. Triplet, M. Tung, A. Vert, M. D. Vidrighin, I. Vorobeichik, P. Weigel, M. Wingert, J. Wooding, and X. Zhou, *A manufacturable platform for photonic quantum computing,* (2024).

[53] Quantum Internet Alliance, *Products and platforms,* Accessed through Wayback Machine 27 May 2024 (2024).

[54] NKT Photonics, *Koheras ACOUSTIK – modular line card fiber laser,* Accessed through Wayback Machine 9 Aug 2024 (2024).

[55] TOPTICA, *Laser Rack Systems,* Accessed through Wayback Machine 15 Aug 2024 (2024).

[56] Single Quantum, *Cryogenics: A "cool" environment for our SNSPDs,* Accessed through Wayback Machine 2 Aug 2024 (2024).

[57] attocube, *Compact Mobile Cryogenics,* Accessed through Wayback Machine 22 July 2024 (2024).

[58] L. Stephenson, D. Nadlinger, B. Nichol, S. An, P. Drmota, T. Ballance, K. Thirumalai, J. Goodwin, D. Lucas, and C. Ballance, *High-Rate, High-Fidelity Entanglement of Qubits Across an Elementary Quantum Network,* Physical Review Letters **124**, 110501 (2020).

[59] V. Krutyanskiy, M. Meraner, J. Schupp, V. Krcmarsky, H. Hainzer, and B. P. Lanyon, *Light-matter entanglement over 50 km of optical fibre,* npj Quantum Information **5**, 1 (2019).

[60] V. Krutyanskiy, M. Canteri, M. Meraner, J. Bate, V. Krcmarsky, J. Schupp, N. Sangouard, and B. Lanyon, *Telecom-Wavelength Quantum Repeater Node Based on a Trapped-Ion Processor,* Physical Review Letters **130**, 213601 (2023).

[61] E. Bersin, M. Sutula, Y. Q. Huan, A. Suleymanzade, D. R. Assumpcao, Y.-C. Wei, P.-J. Stas, C. M. Knaut, E. N. Knall, C. Langrock, N. Sinclair, R. Murphy, R. Riedinger, M. Yeh, C. Xin, S. Bandyopadhyay, D. D. Sukachev, B. Machielse, D. S. Levonian, M. K. Bhaskar, S. Hamilton, H. Park, M. Lončar, M. M. Fejer, P. B. Dixon, D. R. Englund, and M. D. Lukin, *Telecom networking with a diamond quantum memory,* PRX Quantum **5** (2024), 10.1103/prxquantum.5.010303.

[62] N. Curtz, R. Thew, C. Simon, N. Gisin, and H. Zbinden, *Coherent frequency-down-conversion interface for quantum repeaters,* Optics Express **18**, 22099 (2010).

[63] H. Takesue, *Single-photon frequency down-conversion experiment,* Physical Review A **82**, 013833 (2010).

[64] S. Zaske, A. Lenhard, C. A. Keßler, J. Kettler, C. Hepp, C. Arend, R. Albrecht, W.-M. Schulz, M. Jetter, P. Michler, and C. Becher, *Visible-to-Telecom Quantum Frequency Conversion of Light from a Single Quantum Emitter,* Physical Review Letters **109**, 147404 (2012).

[65] M. Bock, P. Eich, S. Kucera, M. Kreis, A. Lenhard, C. Becher, and J. Eschner, *High-fidelity entanglement between a trapped ion and a telecom photon via quantum frequency conversion,* Nature Communications **9**, 1998 (2018).

[66] F. Mann, H. M. Chrzanowski, F. Gewers, M. Placke, and S. Ramelow, *Low-noise quantum frequency conversion in a monolithic cavity with bulk periodically poled potassium titanyl phosphate,* Phys. Rev. Appl. **20**, 054010 (2023).

[67] A. J. Stolk, *Going the distance: Metropolitan scale entanglement of NV-centers over deployed telecom fiber*, Ph.D. thesis, QuTech, Delft University of Technology (2024).

[68] M. Lucamarini, Z. L. Yuan, J. F. Dynes, and A. J. Shields, *Overcoming the rate–distance limit of quantum key distribution without quantum repeaters,* Nature **557**, 400 (2018).

I.6

[69] M. Pittaluga, M. Minder, M. Lucamarini, M. Sanzaro, R. I. Woodward, M.-J. Li, Z. Yuan, and A. J. Shields, *600-km repeater-like quantum communications with dual-band stabilization,* Nature Photonics **15**, 530 (2021).

[70] X. Chen, J. Lin, and K. Wang, *A review of silicon-based integrated optical switches,* Laser & Photonics Reviews **17**, 2200571 (2023).

[71] S. Gauthier, G. Vardoyan, and S. Wehner, *An Architecture for Control of Entanglement Generation Switches in Quantum Networks,* IEEE Transactions on Quantum Engineering **4**, 1 (2023).

[72] C. D. Donne, M. Iuliano, B. van der Vecht, G. M. Ferreira, H. Jirovská, T. van der Steenhoven, A. Dahlberg, M. Skrzypczyk, D. Fioretto, M. Teller, P. Filippov, A. R.-P. Montblanch, J. Fischer, B. van Ommen, N. Demetriou, D. Leichtle, L. Music, H. Ollivier, I. t. Raa, W. Kozlowski, T. Taminiau, P. Pawełczak, T. Northup, R. Hanson, and S. Wehner, *Design and demonstration of an operating system for executing applications on quantum network nodes,* (2024).

[73] Gaurab Bose, *Google Cloud: Standard Tier Data Transfer now offers a 99.9% availability SLA,* Accessed through Wayback Machine 9 Feb 2024 (2023).

[74] J. F. van Wijnen, *Financieel Dagblad: 'Straks eindigt Nederland zonder eigen kwantumcomputer',* Accessed through archive.today 4 July 2024 (2024).

II

Business & Society

II.1

INTRODUCTION

Parts of this Introduction also appear in the Introduction of Part I of this thesis

The development of the computer has propelled humanity into the Information Age by providing exponential increase in computational powers for many years in a row, later known as Moore's law [1]. To fulfill that need, technological ecosystems built for and around the computer have transformed the economy worldwide [2], with over $500 billion in sales in the semiconductor industry alone in 2023 [3, 4]. The industry spans the hardware manufacturers (e.g. TSMC, Samsung, Apple), to the hardware that makes the hardware (e.g. ASML), to all kinds of software development that has led to increased productivity and new ways of data processing. A second revolution started when all these computers became interconnected: The internet was born. Now every computing device could be used to share information, use the enormous power of high performance computing (HPC) centers for complex calculations or processing vast amounts of data (e.g. banking, E-commerce). With all data now zipping around the globe, the field of cybersecurity filled the gap to ensure secure transfer of information [5].

We realized soon that there are limits to what a classical computer can do. Certain computational algorithms simply do not scale well enough with the growing complexity of the problem they tackle. A paradigm shift was necessary to not build bigger computers, but a different kind of computer. The quantum computer. By using the laws of quantum physics, we can process data in a fundamentally different way. In this world we do not encode information in bits, but encode quantum information in qubits (quantum bits) [6]. Throughout the years, many quantum algorithms that used these qubits were introduced that could be run on a (to be built) general-purpose quantum computer. They provide significant speed-ups for complex computational problems with respect to their classical counterparts: chemistry and physics simulations for drug and material discovery [7, 8], financial modeling [9, 10], logistical optimization [11], machine learning [12] and more. There are many academic and commercial endeavors that use different types of qubits, of which the most used are: ion, neutral atoms, superconducting, color vacancy, carbon nanotubes and photonic[1]. They aim to build a fault-tolerant quantum computer that provably is better at the previously mentioned computations than a classical computer is.

In fact, we need more than *one* quantum computer, we need *many*. And when we have many, they are to be connected to enable a new revolution in quantum computing. We need to build a **quantum network**.

Quantum networks are the *only* way through which quantum computers can share quantum information.

It is impossible to send quantum information between quantum computers through the classical internet, we have to remain quantum.

[1] Companies such as Google, IBM, Amazon, Microsoft, Rigetti, PsiQuantum, Photonic Inc. QuEra and Quantum Brilliance, as examples

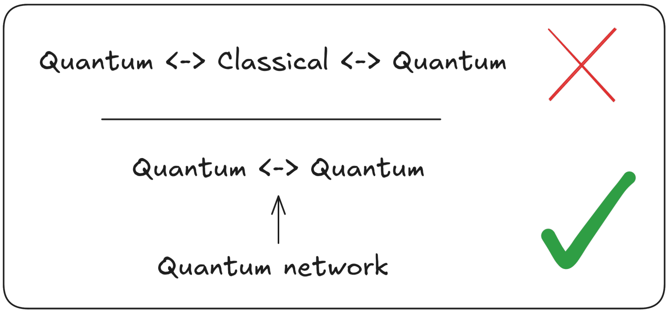

Quantum networks are the catalyst to scaling quantum computers with chip-to-chip communication, connecting future high-performance quantum computing centers (HPQCs) and bridging the interface between different kinds of quantum computing platforms [13], to build a full fledged quantum internet [14, 15]. There are applications we know of that are only able to work in quantum networks, some of which are: distributed quantum computing [16], secure delegated quantum computing in the cloud [17, 18], quantum equivalents of message authentication [19], digital signatures [20] and anonymous transmission [21–23]. Leaning on the historical leap the internet has enabled for the computer, we expect many more applications to follow once quantum computers are enabled in connectivity. Still, the argument alone of speeding up the development of useful quantum computers warrants a worldwide push to build scalable quantum networks. The experimental Part I of this thesis discusses at length the technological development of a quantum network hardware platform.

Quantum networks will revolutionize quantum computing, transform existing industries and have widespread societal impact.

Here, in Part II, I focus on the impact that quantum networks as *deep tech* will have on industry, business and society. Especially given the tornado of change that the internet brought to computing, we have to expect that quantum networks, or as overarching term, the *quantum internet*, will have similar disruptive capabilities to the quantum computing landscape. Subsequently, this will have consequences for businesses, the quantum computing and telecommunications industry especially, and society as a whole.

I am uniquely positioned to give an informed view on the industrial and societal impact of the quantum internet. Never-before seen ideas or inventions usually find validation of their intended purpose in academic environments. The technology readiness level (TRL) of these ideas extend generally until experimental proof of concepts (TRL 3), the validation of this technology in the lab (TRL 4) or in a relevant environment (TRL 5), see Table II.1.1. Beyond these levels, academia is rarely the appropriate platform to grow technology usability, as TRL 5+ involves deploying technology (outside the lab) usually at (paying) customers. There are exceptions to this general statement, as the system

II.1

TRL	Description	
TRL 1	Basic principles	Academic
TRL 2	Technology concept	
TRL 3	Proof of concept	
TRL 4	Lab verification	
TRL 5	Relevant environment verification	
TRL 6	Demonstration in a relevant environment	Commercial
TRL 7	System prototype in operational environment	
TRL 8	System completed and qualified through test and demonstration	
TRL 9	System proven through successful operation	

Table II.1.1: Technology readiness levels (TRLs)

presented in Part I of this thesis is a prime example - we have shown quantum networking technology to be validated in a relevant environment (TRL 5), bordering on a technology demonstration (TRL 6). This has allowed me to form a vision on the rollout of an extensive quantum internet from a technological point of view, on the interfaces this technology might have to existing industries and what ethical, legal, societal and policy implications (ELSPI) this carries. We delve deeper into these subjects in the following Chapters.

Thesis "business & society" goal
Develop use cases of the quantum internet within an existing industry and assess the ethical, legal, societal and policy implications of the development of a future quantum internet.

II.1.1. THESIS “PART II” OVERVIEW

Chapter II.2 describes the tools necessary for generating deep tech awareness and how to develop useful insights in a deep tech subject like the quantum internet. I discuss how science communication can help to generate awareness and why industry use case development of quantum networks is essential. Lastly, I highlight the importance of responsible technology innovation to address the ELSPI of the quantum internet and present a relevant framework of assessment through the *ten principles for responsible quantum innovation* developed by Mauritz Kop *et al.* [24].

Chapter II.3 is a C-level executive guide to the risks and opportunities that the quantum internet offers. Written in 2022, this Chapter presents a short and high-level introduction into the different kinds of technology that quantum communication as a field offers, from quantum key distribution (QKD) to interconnected quantum computers, and describes its risks and opportunities per topic. It provides an overview of the status quo of technological development (at the time this was published) and governmental investments that specifically mention to target the development of the quantum internet.

Chapter II.4 presents a quantum internet use case analysis for the automotive industry. We utilize a method where megatrends - trends that have an effect on the entirety of their respective industry - of both fields are identified and qualitatively compared for both short (< 10 years) and long (≥ 10 years) time scales. For the long-term (≥ 10 years) we develop a comprehensive list of use cases for the quantum internet within the automotive sector. These results allow for further development of targeted research directions for both domains.

Chapter II.5 evaluates the status of the development of a responsible future quantum internet. Through horizon scanning, domain expert trend analysis and guided workshops led by the Centre for Quantum & Society, we present a desired future conceptualized by stakeholders within the scope of the quantum internet. Simultaneously, we examine the alignment of the situation today and the desired future of the quantum internet ELSPI to the ideals of the ten principles for responsible quantum innovation. Based on the outcomes we recommend further action to ensure continued development of a responsible quantum internet.

Chapter II.6 summarizes the outcomes of Part II of this thesis and presents the future of commercializing this technology.

II.1

REFERENCES

[1] G. Moore, *Cramming more components onto integrated circuits,* (1965).

[2] P. E. Ceruzzi, *A History of Modern Computing* (MIT Press, 2003).

[3] Semiconductor Industry Association, *Global Semiconductor Sales Decrease 8.2% in 2023; Market Rebounds Late in Year,* Accessed through Wayback Machine 23 May 2024 (2024).

[4] Deloitte, *2024 Semiconductor Industry Outlook,* Accessed through Wayback Machine 27 July 2024 (2024).

[5] D. Comer, *Computer Networks and Internets* (Prentice Hall, 2009).

[6] B. Schumacher, *Quantum coding,* Physical Review A **51**, 2738–2747 (1995).

[7] A. Aspuru-Guzik, A. D. Dutoi, P. J. Love, and M. Head-Gordon, *Simulated quantum computation of molecular energies,* Science **309**, 1704 (2005).

[8] M. B. Hastings, D. Wecker, B. Bauer, and M. Troyer, *Improving quantum algorithms for quantum chemistry,* Quantum Info. Comput. **15**, 1–21 (2015).

[9] D. J. Egger, C. Gambella, J. Marecek, S. McFaddin, M. Mevissen, R. Raymond, A. Simonetto, S. Woerner, and E. Yndurain, *Quantum computing for finance: State-of-the-art and future prospects,* IEEE Transactions on Quantum Engineering **1**, 1 (2020).

[10] L. Leclerc, L. Ortiz-Gutiérrez, S. Grijalva, B. Albrecht, J. R. K. Cline, V. E. Elfving, A. Signoles, L. Henriet, G. Del Bimbo, U. A. Sheikh, M. Shah, L. Andrea, F. Ishtiaq, A. Duarte, S. Mugel, I. Cáceres, M. Kurek, R. Orús, A. Seddik, O. Hammami, H. Isselnane, and D. M'tamon, *Financial risk management on a neutral atom quantum processor,* Phys. Rev. Res. **5**, 043117 (2023).

[11] S. Harwood, C. Gambella, D. Trenev, A. Simonetto, D. Bernal, and D. Greenberg, *Formulating and solving routing problems on quantum computers,* IEEE Transactions on Quantum Engineering **2**, 1 (2021).

[12] J. Biamonte, P. Wittek, N. Pancotti, P. Rebentrost, N. Wiebe, and S. Lloyd, *Quantum machine learning,* Nature **549**, 195–202 (2017).

[13] M. J. Weaver, P. Duivestein, A. C. Bernasconi, S. Scharmer, M. Lemang, T. C. v. Thiel, F. Hijazi, B. Hensen, S. Gröblacher, and R. Stockill, *An integrated microwave-to-optics interface for scalable quantum computing,* Nature Nanotechnology **19**, 166 (2024).

[14] H. J. Kimble, *The quantum internet,* Nature **453**, 1023 (2008).

[15] S. Wehner, D. Elkouss, and R. Hanson, *Quantum internet: A vision for the road ahead,* Science **362**, eaam9288 (2018).

[16] M. Caleffi, M. Amoretti, D. Ferrari, J. Illiano, A. Manzalini, and A. S. Cacciapuoti, *Distributed quantum computing: A survey,* Computer Networks , 110672 (2024).

[17] A. Broadbent, J. Fitzsimons, and E. Kashefi, *Universal Blind Quantum Computation,* in *2009 50th Annual IEEE Symposium on Foundations of Computer Science* (2009) pp. 517–526.

[18] J. F. Fitzsimons and E. Kashefi, *Unconditionally verifiable blind quantum computation,* Physical Review A **96**, 012303 (2017).

[19] H. Barnum, C. Crépeau, D. Gottesman, A. Smith, and A. Tapp, *Authentication of quantum messages,* in *The 43rd Annual IEEE Symposium on Foundations of Computer Science, 2002. Proceedings.* (IEEE, 2002) pp. 449–458.

[20] D. Gottesman and I. Chuang, *Quantum Digital Signatures,* arXiv:quant-ph/0105032 (2001).

[21] M. Christandl and S. Wehner, *Quantum Anonymous Transmissions,* in *Advances in Cryptology - ASIACRYPT 2005*, edited by B. Roy (Springer, Berlin, Heidelberg, 2005) pp. 217–235.

[22] J. Bouda and J. Sprojcar, *Anonymous Transmission of Quantum Information,* in *2007 First International Conference on Quantum, Nano, and Micro Technologies (ICQNM'07)* (2007) pp. 12–12.

[23] A. Unnikrishnan, I. J. MacFarlane, R. Yi, E. Diamanti, D. Markham, and I. Kerenidis, *Anonymity for practical quantum networks,* Phys. Rev. Lett. **122**, 240501 (2019).

[24] M. Kop, M. Aboy, E. D. Jong, U. Gasser, T. Minssen, I. G. Cohen, M. Brongersma, T. Quintel, L. Floridi, and R. Laflamme, *Ten principles for responsible quantum innovation,* Quantum Science and Technology **9**, 035013 (2024).

II.2

METHODS

This Chapter discusses the ways with which the deep tech development of quantum networks can be supported from a business and societal perspective.

II.2.1. Tools for Deep Tech Awareness and Insights

To continue developing deep tech like quantum networking, we require insights into and improvement of the technology's usability, marketability and societal acceptance. In this thesis, we tackle these topics through several means: science communication, industry use case analysis and evaluation of the status of responsible innovation. This covers a large part of the ecosystem surrounding quantum technologies from general public awareness, to business development and ethical, legal and societal aspects (ELSA) and policy implications (ELSPI). We discuss each topic below.

II.2.1.1. Science Communication

Gaining broad public acceptance for a technology's purpose helps facilitate support for its development [1–5]. Acceptance of technology starts with understanding what it can potentially do and how that will affect people's daily or professional life. This is an important step, because understanding often translates to public funding (initially), in hopes that eventually the deep tech graduates to a useful product and contributes positively to the economy. Along this entire process it is helpful that as many people as possible are informed about the technology straight from domain experts to prevent the spread of misinformation and so-called *magic-thinking*: mislabeling of what particular technology does due to lack of understanding [6].

An accessible way to inform the general audience is science communication. Scientists and domain-experts can spread the word of their work and explain the often difficult topics of science and technology in understandable language. This can be done through talks, workshops, social/traditional media, open-forum discussions or even casually within family or friends. The positive effect of this communication goes both ways: the public becomes more informed on science and the scientist gains experience in public speaking and transforming complex information to an understandable format. In itself, science communication is a way to create general awareness of deep tech and allows for developing insights into its acceptance and integration into businesses and society. To help achieve that awareness, a substantial portion of this thesis includes communicating its scientific results and technological context to a general and professional public, as shown in Chapter 1. Furthermore, Chapter II.3 is a guide for C-level executives on the risks and opportunities of the quantum internet for their business.

II.2.1.2. Industry Use Case Analysis

The future viability of quantum networks as technology relies on its applications and on the industry integration that follow from these applications. In order to widen the dialogue and understanding of the viability of use cases from quantum network applications, it is helpful to perform use case analyses of integration of quantum networks in industries. Several efforts already have attempted similar analyses for quantum computing [7–9], however quantum network analyses mostly give overviews on use cases and applications [10, 11]. In Chapter II.4, a quantum internet use case analysis for the automotive industry is presented. We utilize a method where megatrends - trends that have an effect on the entirety of their respective industry - of both fields are identified and qualitatively compared for both short (< 10 years) and long (≥ 10 years) time scales. Further details of the method and how it is applied can be found in Chapter II.4.

II.2.1.3. Responsible Innovation

The development of deep tech has the potential to be of substantial consequence for society: for better or worse, or both. Due to the wide scope of the consequences that deep tech development can have, we denote these aspects and implications by the ELSA or ELSPI, as introduced before. In the pursuit of life-changing technology, guardrails will have to be created in order for the technology to end up well-integrated in society, i.e. how can this new technology most benefit society, minimize risk of negative (side-)effects and remain ethical. These guardrails can find their effect into technology development in many ways, for example in research mindset, general awareness, policy and lawmaking. We can generalize this statement and call for *responsible innovation*, a systematic approach to anticipate and manage societal risks and opportunities that may arise when a new technology is developed [12]. For quantum technologies, a first proposal has been made to develop ten guiding principles for responsible quantum innovation [13]. These principles, the topics they represent, their aim and responsible research and innovation (RRI) value [14, 15] are shown in Table II.2.1. In Chapter II.5 we use the principles to assess the present situation of responsible innovation of the quantum internet, as well as evaluate a *desired future* of the quantum internet integrated in society, developed through a collaborative foresight exercise organized by the Centre for Quantum & Society.

II.2

Category	Topic	Aim	RRI-value	Principle
Safeguarding				
	Information security	Addressing security threats	Anticipation & Reflection	1. Make information security an integral part of QT
	Dual use	Addressing risks of dual use	Anticipation & Reflection	2. Proactively anticipate the malicious use of quantum applications
	Quantum race	Addressing a winner-takes-all dynamic	Anticipation & Reflection	3. Seek international collaboration based on shared values
Engaging				
	Quantum gap	Engaging states	Openness & Transparency	4. Consider our planet as the sociotechnical environment in which QT should function
	IP	Engaging institutions	Openness & Transparency	5. Incentivise innovation while being as open as possible and as closed as necessary
	Inclusion	Engaging people	Diversity & Inclusion	6. Pursue diverse R&D communities in terms of disciplines and people
Advancing				
	Societal relevance	Advancing society	Responsiveness & Adaptation to change	7. Link quantum R&D explicitly to desirable societal goals
	Complementary innovation	Advancing technology	Responsiveness & Adaptation to change	8. Actively stimulate sustainable, cross-disciplinary innovation
	Responsibility	Advancing our understanding of responsible QT	Responsiveness & Adaptation to change	9. Create an ecosystem to learn about the possible uses and consequences of QT applications
	Education and Dialogue	Advancing our collective thinking and education about QT and its impact	Responsiveness & Adaptation to change	10. Facilitate dialogues with stakeholders to better envision the future of QT

Table II.2.1: Ten principles for responsible quantum innovation as described in [13].

REFERENCES

[1] M. Kurath and P. Gisler, *Informing, involving or engaging? science communication, in the ages of atom-, bio- and nanotechnology,* Public Understanding of Science **18**, 559 (2009).

[2] C. Mooney, *Do scientists understand the public?* Bulletin of the American Academy of Arts and Sciences **63**, 5 (2010).

[3] P. E. Vermaas, *The societal impact of the emerging quantum technologies: a renewed urgency to make quantum theory understandable,* Ethics and Information Technology **19**, 241 (2017).

[4] F. Van Dam, L. De Bakker, A. M. Dijkstra, and E. A. Jensen, *Science communication: An introduction*, Vol. 1 (World Scientific, 2020).

[5] T. M. Roberson, *On the Social Shaping of Quantum Technologies: An Analysis of Emerging Expectations Through Grant Proposals from 2002–2020,* Minerva **59**, 379 (2021).

[6] A. Gell, *Technology and Magic,* Anthropology Today **4**, 6 (1988).

[7] A. Bayerstadler, G. Becquin, J. Binder, T. Botter, H. Ehm, T. Ehmer, M. Erdmann, N. Gaus, P. Harbach, M. Hess, J. Klepsch, M. Leib, S. Luber, A. Luckow, M. Mansky, W. Mauerer, F. Neukart, C. Niedermeier, L. Palackal, R. Pfeiffer, C. Polenz, J. Sepulveda, T. Sievers, B. Standen, M. Streif, T. Strohm, C. Utschig-Utschig, D. Volz, H. Weiss, and F. Winter, *Industry quantum computing applications,* EPJ Quantum Technology **8**, 25 (2021).

[8] Bova, Francesco, Goldfarb, Avi, and Melko, Roger G., *Commercial applications of quantum computing,* EPJ Quantum Technol. **8**, 2 (2021).

[9] P. A. Ganeshamurthy, K. Ghosh, C. O'Meara, G. Cortiana, and J. Schiefelbein-Lach, *Bridging the Gap to Next Generation Power System Planning and Operation with Quantum Computation,* (2024).

[10] L. de Forges de Parny, O. Alibart, J. Debaud, S. Gressani, A. Lagarrigue, A. Martin, A. Metrat, M. Schiavon, T. Troisi, E. Diamanti, P. Gélard, E. Kerstel, S. Tanzilli, and M. Van Den Bossche, *Satellite-based quantum information networks: use cases, architecture, and roadmap,* Communications Physics **6**, 1 (2023).

[11] Veriqloud, *Quantum Protocol Zoo,* (2024).

[12] U. Gasser, E. De Jong, and M. Kop, *A call for responsible quantum technology,* Nature Physics , 1 (2024).

[13] M. Kop, M. Aboy, E. D. Jong, U. Gasser, T. Minssen, I. G. Cohen, M. Brongersma, T. Quintel, L. Floridi, and R. Laflamme, *Ten principles for responsible quantum innovation,* Quantum Science and Technology **9**, 035013 (2024).

II.2

[14] R. von Schomberg, *A Vision of Responsible Research and Innovation,* in *Responsible Innovation* (John Wiley & Sons, Ltd, 2013) Chap. 3, pp. 51–74.

[15] G. Declich, M. Berliri, and A. Alfonsi, *Responsible Research and Innovation (RRI) and Research Ethics,* in *Ethics, Integrity and Policymaking: The Value of the Case Study*, edited by D. O'Mathúna and R. Iphofen (Springer, Cham (CH), 2022).

II.3

The Quantum Internet: A New Frontier in Communication

K.L. van der Enden, W. Kozlowski

In the global race towards the development of useful Quantum Computers (QCs), there is a need to interconnect these computers so that they can exchange quantum information. The Quantum Internet (QI) provides this by harnessing the power of entanglement, allowing QCs to unlock new applications of Quantum Computing in computational speed, privacy and security. With current encryption standards at risk of being broken by QCs, the first step towards a QI is the implementation of quantum safe encryption and communication through Quantum Key Distribution (QKD). With QKD products commercially available, QKD networks are built as we speak, also with governmental support. More advanced functionality of the QI is enabled by connecting QCs through entanglement, allowing them to exchange quantum information. This has been shown in academic environments and commercialization of the QI is at its infancy, but has the potential to become a game-changing enabling technology for Quantum Computing.

This chapter is translated into English from the original Chapter "Das Quanteninternet: neue Möglichkeiten der Kommunikation" that appeared in the book "Chancen und Risiken von Quantentechnologien: Praxis der zweiten Quantenrevolution für Entscheider in Wirtschaft und Politik". Usage by courtesy of Nature Springer.

Our technology landscape has for the past decades been filled with marvelous developments that all have an important property in common: interconnectivity. At the advent of the Information Age, the computer brought an exponential increase in computational power that has transformed our lives in a way very few dared to dream of. This transformation was extended with the ability to interconnect these computational devices to bring together people and technology in a web that spans the world, now known as *the Internet*. We are currently in the midst of the same development with Quantum Computing and the Quantum Internet, where we benefit from having gone through these motions in the collective remembrance of engineers around the globe to preemptively predict, develop and build an infrastructure to support the sending and receiving of quantum information between Quantum Computers (QCs). Similar to the Internet, the Quantum Internet will unlock new applications of Quantum Computing in computational speed, privacy and security. For example, Quantum Key Distribution (QKD), perhaps the best-known application of the Quantum Internet so far, provides us with much stronger cybersecurity guarantees compared to what is possible classically, by utilizing the fundamental quantum physical properties of light to detect eavesdroppers. Because this application is very relevant for cybersecurity standards now and for the coming years, we will first discuss why exactly we need QKD and what problem it solves and how, and show the opportunities for organizations to use this technology. We will do the same for the Quantum Internet and explain how we can extend the usefulness of quantum networks to QCs and their applications.

II.3.1. Quantum Key Distribution

II.3.1.1. Encryption at risk

Almost all cryptographic methods used in cybersecurity rely on the computational complexity to *crack the code* with which we encrypt sensitive data. Both symmetric (e.g. AES) and asymmetric (RSA) encryption algorithms use keys and complex calculations to encrypt and decrypt data. Calculations so complex that, provided the keys are long enough, any supercomputer on earth would not be able to crack. This changed with the introduction of Quantum Computing, where certain quantum algorithms turned out to be able to crack these keys with much more ease than any classical computation can. Shor's algorithm can find the key-pair used in RSA [1], and even Grover's search algorithm can bring a speed up to cracking AES, putting AES-128 at risk [2]. With commercial QCs expected to be introduced towards 2030 [3], all data encrypted using current standardized encryption methods is at risk to be decrypted. And not only for data generated and sent when a QC exists, but also for data generated right now: the confidentiality risk is retroactive[1].

II.3.1.2. Post-Quantum Cryptography and Quantum Keys

There are two main approaches to protecting one's data against the aforementioned risk. First, to make use of encryption methods for which there is not yet currently a known

[1] Imagine a hacker stealing encrypted data today, to be able to uncover sensitive data such as national security data, healthcare data and banking transactions in a future where they have access to a powerful Quantum Computer

quantum-advantage counterpart, known as Post-Quantum-Cryptography (PQC). Several national security agencies have already issued a directive to drop RSA, use at least AES-256 and consider PQC methods to ensure forward secrecy for QC attacks [4–6]. The National Institute of Standards and Technology (NIST) is finalizing a list of audited PQC algorithms in 2022 that can be used for forward standardization of encryption [7]. However, since there will always be a risk that a classical security algorithm can be hacked using quantum methods yet to be developed, the best solution will have to be sought in the quantum world with the second approach: Quantum Key Distribution.

Quantum Key Distribution (QKD) uses single particles of light, photons, that are sent between parties that wish to securely communicate. Specialized equipment derives quantum mechanically generated encryption keys from that light with the guarantee that no-one has been able to intercept these keys. With these keys the user can encrypt and send data exactly like we do now over the Internet, Several QKD algorithms exist, well known are BB84 [8] and E91 [9]. Under the right conditions these key-exchange algorithms are resilient against an attacker with unlimited classical and quantum computational power.

QKD can make use of the existing fiber network of the Internet and uses fibers reserved to only send its own signals over, however the communication distance of QKD presently is limited to tens of kilometers. In order to extend the network, physically secure repeaters need to be deployed that result in a loss of end-to-end security: one cannot guarantee the absolute security of these repeaters. These networks are called trusted repeater networks. For point-to-point connections this is not yet a reason for concern and they have shown to be useful for inter/intra-datacenter connections or direct connections between known and trusted government institutions such as election results in Switzerland [10]. As QKD technology improves, higher levels of security are unlocked. For example with Measurement-Device-Independent QKD, or MDI-QKD, a protocol that is still secure even when a repeater is untrusted. However, the hardware and infrastructural requirements to implement this protocol are more complex and are still in development. The most secure key-sharing can be done using Device-Independent QKD, which requires QCs to produce keys over the Quantum Internet. A table of maturity levels per key-sharing protocol is shown in Table II.3.1.

II.3.1.3. COMMERCIAL QKD NETWORKS

QKD is a reality today, with many commercial vendors selling readily available *QKD boxes* that are rack-mountable devices that perform key distribution with its counterpart, delivering keys to a classical computer/server on demand with rates of only kilobits per second. More notable vendors are Toshiba, Quintessence Labs and ID Quantique, among a myriad of startup companies providing similar services. Several QKD enabled networks exist around the world that we know of[2], some even spanning thousands of kilometers using trusted repeater nodes, e.g. in China [11–13]. These networks almost all use fiber-based communications, however they have already matured to the point where academical demonstrations showed successful QKD using satellites free-space communication [14]. This success is aimed to continue with several initiatives called forth towards the development of intercontinental satellite-QKD networks [15, 16].

[2]And likely many we *do not* know the location of due to national/business security reasons

Table II.3.1: Overview of the maturity level of QKD protocols

Key-sharing protocol	**Maturity level**
Trusted Repeater QKD	Global commercially available
MDI-QKD	Successful demonstration use-case in 2021 [17]
DI-QKD	Limited experimental results shown in academic research institutes [18–20]

II.3.1.4. Challenges

The main challenge of QKD is scalability in number of users, distance between nodes and bandwidth. It is hard for businesses to implement a change in their security policy, especially one that is new and relatively costly[3]. However, with national security agencies strongly advising adoption of PQC and QKD on the long term, many companies and institutions will have to follow suit in upgrading their security standards in the coming years, especially those organizations that are or want to be certified for an information security management system such as DIN EN ISO/IEC 27001. Additionally, as QKD technology improves, so will adoption among first movers that can afford to. However, to cross country borders and allow users over hundreds of kilometers to share keys, an investment will have to be made to provide a trusted repeater network, adopt better QKD systems such as MDI-QKD, or wait for competitive QKD techniques that allow for further-distance communication [21–23]. Lastly, we will require standardization of key-exchange protocols and QKD-traffic management. Standard multiplexing technologies that allow for high bandwidths over fiber for the Internet are not directly applicable to a QKD network. With a growing number of end-users this additional quantum network will need to be managed and controlled much like current Internet Service Providers (ISPs) manage the Internet backbone.

II.3.1.5. Opportunities

Already by reading this Chapter, you have taken the first step to be at the forefront to reshape the future of your organization in the direction of quantum security. It is of utmost importance for organizations to properly assess the risk profile of data gathered, processed and distributed. Critical data(streams) will have to be timely upgraded with enhanced cryptographic methods such as PQC and QKD. Globally overhauling complete IT systems to be *quantum safe* could have a greater impact than the Y2K preparation [24]. Therefore, mapping out flows of information and identifying encryption protocols and standards used in your organization can prepare you for the changes you will need to make, today. Furthermore, this is the ideal time for new players to enter the QKD market and for hardware companies to join the development in creating QKD technology. Proven QKD technology is already on the market, and this is expected to increase significantly with a growing amount of consumers [25]. The value-chain of QKD technology extends to the enabling technologies as well – telecom infrastructure in fiber and space, software and chip manufacturing [26]. Additionally, governments around the globe directly support

[3] The key-sharing *QKD boxes* are still specialized and relatively costly equipment, but additional costs also incur for access to a fiber network over which this key sharing can occur. With increased adoption rolling out, it is of course expected for overhead costs of the QKD network and the cost of key-sharing hardware to go down.

QKD initiatives to create large-scale networks especially for society vital organizations [16, 27].

II.3.2. QUANTUM INTERNET

With an increasing amount of QCs being built around the world, we need a supporting infrastructure not just to exchange information, but to exchange quantum information, the information that quantum devices use for their calculations. The only way in which QCs can share quantum information is by making use of the special properties of entanglement. There is no classical alternative that can do the same. The platform that will provide this service is the Quantum Internet.

> The Quantum Internet is an interconnected system of QCs that generate and distribute entanglement with which they can exchange quantum information.

Leading Quantum Internet research professors have identified six stages of the development of the Quantum Internet based on the functionality available to the end-users [28]. From the QKD section we know that the trusted repeater networks already exist, this is the first stage. As we reach new stages, new functionality becomes possible, such as end-to-end secure QKD, private quantum computing in the cloud and many others.

II.3.2.1. ENTANGLEMENT AS RESOURCE FOR QUANTUM COMMUNICATION

The underlying principle that makes the Quantum Internet work is Entanglement, a special state of two or more quantum bits (qubits) in which the individual qubits can no longer be described independently of each other, their properties become correlated at the physical level. For two qubits one can imagine as if they are special coins where after a coin flip of one, the other will always show the same flip-outcome as the first[4]. Entanglement can, in principle, exist no matter how far apart these qubits are, making it an interesting resource for networking, see Figure 1.

This unusual phenomenon was highly controversial for many years, with Einstein not believing that entanglement could be such a fundamental part of nature calling it "spooky action at a distance". He claimed that there must be another explanation and that quantum physics must be incomplete [29]. However, in 2015 a famous experiment in Delft essentially proved Einstein to be wrong [30]. Quantum Information between QCs is exchanged by moving information encoded in qubits from one QC to another, which is called the teleportation of a qubit state: The laws of physics prevent the copying of qubits, and this information thus disappears from the sender, to appear at the receiver[5]. This quantum teleportation is only possible between qubits that are entangled, and their entanglement is consumed upon the act of teleportation. Entanglement is therefore a

[4]For normal coin flips it is statistically impossible to show perfect correlation of outcomes, the best one can do there is 50%. Qubits on the other hand can theoretically go up to a correlation of 100% all the time, showing the mind-blowing property of entanglement.

[5]An important note: teleportation does *not* happen instantaneously, there is still *classical* feedback required to verify the qubit that is teleported, which makes the communication speed still bounded by the speed of light.

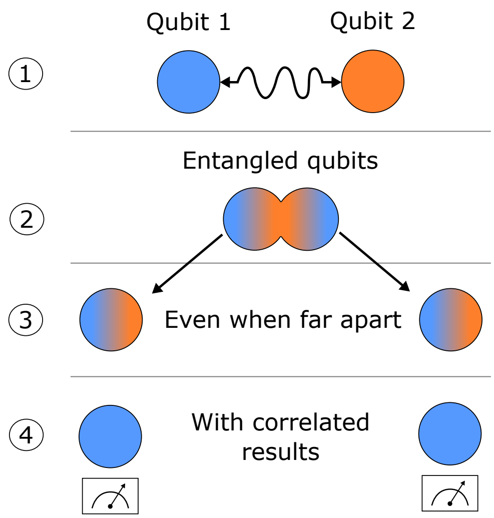

Figure II.3.1: Entanglement generation and correlated results

resource to exchange quantum information through qubits, a resource that will have to be continuously generated and stored to then be consumed to sustain continuous transferring of quantum information: The Quantum Internet provides and manages Entanglement-as-a-Service (EaaS).

II.3.2.2. Applications: Enhanced privacy and security

Much like the user-cloud infrastructure many organizations use now, eventually it will be possible for you as user to maintain your own QC and go on the Quantum Internet to a Quantum Cloud provider, an additional powerful tool that is added to your existing IT infrastructure. When we are able to connect QCs through the Quantum Internet, many interesting applications arise for computing, security and privacy, powered by the properties of entanglement. A few examples:

It will be possible to perform blind quantum computations: running quantum algorithms on an untrusted quantum server in the cloud, without the quantum server having any knowledge of the information that is being processed [31]. Even if the provider would attempt to learn any secrets, it simply cannot. This application is pivotal for retaining privacy and ownership of data in the cloud, removing the potential of maleficent governments or companies to backdoor their way into our data. Beyond that, we will be able to leverage the power of many QCs through distributed quantum computation, like distributed systems are used nowadays. The Quantum Internet is therefore an enabling technology to harness the power of combined quantum computation capabilities. The Quantum Internet also allows us to anonymously send information between parties, such that the knowledge of who the sender/receiver is only remains between them. An essential technology enabling an unprecedented level of anonymity applauded by privacy enthusiasts, and undoubtedly critically observed by governmental security agencies around the world.

II.3.2.3. State of the art and challenges ahead

The Quantum Internet is at its infancy as of writing, with many academic researcher institutes having access to and actively developing small quantum networks, with the world-record at three QCs connected over 30 meters distance [32] and two over 1.3 kilometers [33]. The QCs used are specifically optimized for quantum communication. The speed of these networks is limited – only few qubits can be entangled per second and considerable effort is being made to improve the quantum hardware to increase this performance metric. Future applications will require bandwidths that are order of magnitude higher than is available today. Furthermore, there have also been standards proposed to manage the Quantum Internet [34], with demonstrations showing a full quantum network stack operating and managing computation and communication between two QCs [35]. There are many institutes, *hubs* and governments around the globe dedicated to the advancement of the Quantum Internet: University of Chicago is at the heart of the US's Department of Energy €550 million program for QI [36], Quantum Delta in the Netherlands can distribute €615 million [37] and Germany pledged €2 billion [38] for quantum technologies, with both programs citing specific Quantum Internet targets. Some hubs already have start-up spin-offs that attempt to commercialize their specific Quantum Internet technologies or develop components for that value-chain. Important technologies are high-quality optics, cryogenics and electronic control systems, as well as software and quantum network algorithm development. Cross-disciplinary collaborations are also being made, most recently by Fraunhofer ILT and the Dutch research center QuTech to intensify efforts towards building a Quantum Internet [39].

With the Quantum Internet at a research stage of development, there are numerous challenges that can and will be tackled in the coming years. In the next years there will be more proof-of-concept demonstrations that solidify the expectations set out for this technology. A Quantum Internet over metropolitan distance and complex remote quantum computations in a near-production environment must be shown to work still.

II.3.2.4. Opportunities

Although many of the above challenges involve the work of quantum scientists, there is an equal amount of *classical* hardware and engineering solutions required to satisfy the aforementioned goals. It is therefore important for businesses and institutes to actively engage in conversation with the Quantum Internet development hubs and institutes to collaboratively figure out where an overlap in expertise can be made for both hardware and software. The coming years will be aimed at proving that the Quantum Internet is possible, with different technologies competing for the best performance parameters for a Quantum Internet that is a decade away. This gives an enormous first-mover advantage opportunity. Not only in hardware, but especially in software, as this can be created largely agnostically from the quantum hardware available. Software development could already be started now and continue largely independently of changes to the underlying quantum hardware. Through standardization of quantum communication protocols and development of specific software and hardware for the quantum network stack, early adopters can grow with government aid towards an expected global multi-billion dollar market [40, 41].

II.3.2.5. FORWARD VISION

Where the Internet brought forth a surge in applications that transformed our lives, we expect the same to happen with the Quantum Internet. There must be many more interesting applications that can benefit from interconnected QCs, history has taught us that much. The best course of action for any business leader today is to be vigilant and visioning [42]. Vigilance to be aware of the milestones made towards a real-world Quantum Internet and keep themselves and direct stakeholders visioning about how the Quantum Internet can determine the future of their business. For the short term, businesses can appoint someone responsible who can develop the knowledge of how and to what extent quantum communication can fit their organization.

II.3.3. CONCLUSION

The threat of the Quantum Computer towards breaking current encryption is a risk for the exchange of data on the Internet. However, with alternative encryption methods like Post-Quantum Cryptography and quantum-safe exchange of keys with Quantum Key Distribution we can protect ourselves from this risk when timely implemented. The first stage of quantum enhanced security through the usage of QKD hardware is commercially available and QKD networks are built as we speak with governmental support. This is only the first step towards a Quantum Internet that will harness the power of entangled Quantum Computers to unlock new applications of Quantum Computing in computational speed, privacy and security. Although still in a research phase, significant investments towards this new technology is being made by institutes around the world, as the Quantum Internet is a technology that will enable a second revolution for applications of the Quantum Computer. Leaders of organizations are highly encouraged to be proactive in recognizing milestone developments and when and how their business can make use of the Quantum Internet.

REFERENCES

[1] P. W. Shor, *Polynomial-time algorithms for prime factorization and discrete logarithms on a quantum computer,* SIAM Review **41**, 303 (1999).

[2] M. e. a. Grassl, *Applying grover's algorithm to aes: quantum resource estimates,* in *Post-Quantum Cryptography* (Springer, 2016) pp. 29–43.

[3] E. Lucero, *Unveiling our new Quantum AI campus,* Google (2021).

[4] AIVD, *Bereid je voor op de dreiging van quantumcomputers,* AIVD (2021).

[5] ANSSI, *Should quantum key distribution be used for secure communications?* ANSII (2020).

[6] BSI, *Bsi veröffentlicht leitfaden zum aktuellen stand der quantensicheren kryptografie,* BSI (2021).

[7] G. Alagic, J. Alperin-Sheriff, D. Apon, D. Cooper, Q. Dang, J. Kelsey, Y.-K. Liu, C. Miller, D. Moody, R. Peralta, *et al., Status report on the second round of the nist post-quantum cryptography standardization process,* US Department of Commerce, NIST (2020), 10.6028/NIST.IR.8309.

[8] C. H. Bennett and G. Brassard, *Quantum cryptography: Public key distribution and coin tossing,* Theoretical Computer Science **560**, 7 (2014).

[9] A. K. Ekert, *Quantum cryptography based on bell's theorem,* Physical review letters **67**, 661 (1991).

[10] IDQuantique, *Securing data transfer for elections: Ethernet encryption with quantum key distribution,* IDQ Use Case (2017).

[11] BT, *Bt and toshiba install uk's first quantum-secure industrial network between key uk smart production facilities,* BT Newsroom (2020).

[12] C. Elliott and H. Yeh, *DARPA quantum network testbed*, Tech. Rep. (BBN TECHNOLOGIES CAMBRIDGE MA, 2007).

[13] Y.-A. Chen, Q. Zhang, T.-Y. Chen, W.-Q. Cai, S.-K. Liao, J. Zhang, K. Chen, J. Yin, J.-G. Ren, Z. Chen, S.-L. Han, Q. Yu, K. Liang, F. Zhou, X. Yuan, M.-S. Zhao, T.-Y. Wang, X. Jiang, L. Zhang, W.-Y. Liu, Y. Li, Q. Shen, Y. Cao, C.-Y. Lu, R. Shu, J.-Y. Wang, L. Li, N.-L. Liu, F. Xu, X.-B. Wang, C.-Z. Peng, and J.-W. Pan, *An integrated space-to-ground quantum communication network over 4,600 kilometres - Nature,* Nature **589**, 214 (2021).

[14] S.-K. Liao, W.-Q. Cai, W.-Y. Liu, L. Zhang, Y. Li, J.-G. Ren, J. Yin, Q. Shen, Y. Cao, Z.-P. Li, F.-Z. Li, X.-W. Chen, L.-H. Sun, J.-J. Jia, J.-C. Wu, X.-J. Jiang, J.-F. Wang, Y.-M. Huang, Q. Wang, Y.-L. Zhou, L. Deng, T. Xi, L. Ma, T. Hu, Q. Zhang, Y.-A. Chen, N.-L. Liu, X.-B. Wang, Z.-C. Zhu, C.-Y. Lu, R. Shu, C.-Z. Peng, J.-Y. Wang, and J.-W. Pan, *Satellite-to-ground quantum key distribution - Nature,* Nature **549**, 43 (2017).

II.3

[15] H. Podmore, I. D'Souza, J. Cain, T. Jennewein, B. L. Higgins, Y. S. Lee, A. Koujelev, D. Hudson, and A. McColgan, *QKD terminal for Canada's Quantum Encryption and Science Satellite (QEYSSat)*, in *International Conference on Space Optics — ICSO 2020*, Vol. 11852, edited by B. Cugny, Z. Sodnik, and N. Karafolas, International Society for Optics and Photonics (SPIE, 2021) pp. 203 – 212.

[16] E. Commission, *European quantum communication infrastructure (euroqci)*, Shaping Europe's digital future (2021).

[17] J. Slater, *Untappable quantum cryptography becomes practical with mdi-qkd*, QuTech (2021).

[18] W.-Z. Liu, Y.-Z. Zhang, Y.-Z. Zhen, M.-H. Li, Y. Liu, J. Fan, F. Xu, Q. Zhang, and J.-W. Pan, *Toward a photonic demonstration of device-independent quantum key distribution*, Phys. Rev. Lett. **129**, 050502 (2022).

[19] D. P. Nadlinger, P. Drmota, B. C. Nichol, G. Araneda, D. Main, R. Srinivas, D. M. Lucas, C. J. Ballance, K. Ivanov, E. Y.-Z. Tan, P. Sekatski, R. L. Urbanke, R. Renner, N. Sangouard, and J.-D. Bancal, *Experimental quantum key distribution certified by bell's theorem,* (2022).

[20] W. Zhang, T. van Leent, K. Redeker, R. Garthoff, R. Schwonnek, F. Fertig, S. Eppelt, W. Rosenfeld, V. Scarani, C. C.-W. Lim, and H. Weinfurter, *A device-independent quantum key distribution system for distant users,* (2022).

[21] A. Boaron, G. Boso, D. Rusca, C. Vulliez, C. Autebert, M. Caloz, M. Perrenoud, G. Gras, F. Bussières, M.-J. Li, D. Nolan, A. Martin, and H. Zbinden, *Secure quantum key distribution over 421 km of optical fiber*, Phys. Rev. Lett. **121**, 190502 (2018).

[22] J.-P. Chen, C. Zhang, Y. Liu, C. Jiang, W. Zhang, X.-L. Hu, J.-Y. Guan, Z.-W. Yu, H. Xu, J. Lin, M.-J. Li, H. Chen, H. Li, L. You, Z. Wang, X.-B. Wang, Q. Zhang, and J.-W. Pan, *Sending-or-not-sending with independent lasers: Secure twin-field quantum key distribution over 509 km*, Phys. Rev. Lett. **124**, 070501 (2020).

[23] N. S. Kirsanov, N. R. Kenbaev, A. B. Sagingalieva, D. A. Kronberg, V. M. Vinokur, and G. B. Lesovik, *Long-distance quantum key distribution based on the physical loss control,* (2021).

[24] M. Harris, *The quantum y2k moment*, Physics World **32**, 40 (2019).

[25] IQT, *Quantum Key Distribution: The Next Generation – A Ten-year Forecast and Revenue Assessment: 2020 to 2029*, Tech. Rep. (2020).

[26] T. K. Paraïso, T. Roger, D. G. Marangon, I. De Marco, M. Sanzaro, R. I. Woodward, J. F. Dynes, Z. Yuan, and A. J. Shields, *A photonic integrated quantum secure communication system*, Nature Photonics **15**, 850 (2021).

[27] CORDIS, *Open european quantum key distribution testbed*, European Commission (2019).

[28] S. Wehner, D. Elkouss, and R. Hanson, *Quantum internet: A vision for the road ahead,* Science **362**, eaam9288 (2018).

[29] A. Einstein, B. Podolsky, and N. Rosen, *Can quantum-mechanical description of physical reality be considered complete?* Phys. Rev. **47**, 777 (1935).

[30] J. Markoff, *Sorry, Einstein. Quantum Study Suggests 'Spooky Action' Is Real.* New York Times (2015).

[31] A. Broadbent, J. Fitzsimons, and E. Kashefi, *Universal blind quantum computation,* in *2009 50th Annual IEEE Symposium on Foundations of Computer Science* (IEEE, 2009) pp. 517–526.

[32] M. Pompili, S. L. N. Hermans, S. Baier, H. K. C. Beukers, P. C. Humphreys, R. N. Schouten, R. F. L. Vermeulen, M. J. Tiggelman, L. dos Santos Martins, B. Dirkse, S. Wehner, and R. Hanson, *Realization of a multinode quantum network of remote solid-state qubits,* Science **372**, 259 (2021).

[33] B. Hensen, H. Bernien, A. E. Dréau, A. Reiserer, N. Kalb, M. S. Blok, J. Ruitenberg, R. F. L. Vermeulen, R. N. Schouten, C. Abellán, W. Amaya, V. Pruneri, M. W. Mitchell, M. Markham, D. J. Twitchen, D. Elkouss, S. Wehner, T. H. Taminiau, and R. Hanson, *Loophole-free bell inequality violation using electron spins separated by 1.3 kilometres,* Nature **526**, 682 (2015).

[34] A. Dahlberg, M. Skrzypczyk, T. Coopmans, L. Wubben, F. Rozpundefineddek, M. Pompili, A. Stolk, P. Pawełczak, R. Knegjens, J. de Oliveira Filho, R. Hanson, and S. Wehner, *A link layer protocol for quantum networks,* in *Proceedings of the ACM Special Interest Group on Data Communication*, SIGCOMM '19 (Association for Computing Machinery, New York, NY, USA, 2019) p. 159–173.

[35] M. Pompili, C. Delle Donne, I. te Raa, B. van der Vecht, M. Skrzypczyk, G. Ferreira, L. de Kluijver, A. J. Stolk, S. L. N. Hermans, P. Pawełczak, W. Kozlowski, R. Hanson, and S. Wehner, *Experimental demonstration of entanglement delivery using a quantum network stack,* npj Quantum Information **8**, 1 (2022).

[36] DOE, *From long-distance entanglement tobuilding a nationwide quantum internet,* Report of the DOE: Quantum Internet Blueprint Workshop (2020).

[37] Quantum Delta NL, *Quantum delta nl awarded 615 million euro from netherlands' national growth fund to accelerate quantum technology,* Quantum Delta NL (2021).

[38] *Eckpunkte des konjunkturprogramms: Corona-folgen bekämpfen, wohlstand sichern, zukunftsfähigkeit stärken,* Bundesministerium der Finanzen (2020).

[39] Fraunhofer-Gesellschaft, *Fraunhofer and qutech unite to champion quantum internet,* Fraunhofer-Gesellschaft (2021).

[40] E. Gibney, *Quantum gold rush: the private funding pouring into quantum start-ups,* Nature **574**, 22 (2019).

II.3

[41] J. Dargan, *15 countries with national quantum initiatives,* Quantum Insider (2021).

[42] W. D. O. Jonathan Ruane, Andrew McAfee, *Quantum Computing for Business Leaders: Will the reality live up to the hype?* Accessed through Wayback Machine 3 Jan 2022 (2022).

II.4

Quantum Internet Use Case Analysis for the Automotive Industry

K. L. van der Enden,[*] R. Kirschner,[*,1,2] M. Krumtünger[1], A. Wilms[3,4,†]

[1] *Formerly at Porsche Digital GmbH, Stralauer Allee 12, 10245 Berlin, Germany*
[2] *Currently at Audi AG, Auto-Union-Str. 1, 85057 Ingolstadt, Germany*
[3] *Porsche Digital GmbH, Stralauer Allee 12, 10245 Berlin, Germany*
[4] *Dahlem Center for Complex Quantum Systems, Freie Universität Berlin, 14195 Berlin, Germany*

A future quantum internet brings promising applications related to security, privacy and enabling distributed quantum computing. Integration of these concepts into the future trends of the automotive sector is of considerable interest, as it enables both the development of practical quantum internet use cases and the adoption of innovative technologies in the automotive sector. In this work we analyze cross-platform megatrends in both the quantum internet and the automotive industry, identifying mutually beneficial regions of interest. In the short-term (< 10 years) hardware miniaturization and automation of quantum internet technology provides a synergy interface between the two domains. For the long-term (≥ 10 years) we develop a comprehensive list of use cases for the quantum internet within the automotive sector. We find considerable relevancy of augmenting autonomous driving, vehicle ad hoc networks and sensor fusion with blind quantum computing, anonymous transmission and quantum cryptographic tools. These results can be used to target future research, engineering and venture developments for both domains. Furthermore, our approach can be applied to other industries, enabling a structured methodology for identifying and developing feasible use cases for the quantum internet in diverse domains.

[*] These authors contributed equally to this work.
[†] Porsche Digital correspondence to: alissa.wilms@porsche.digital

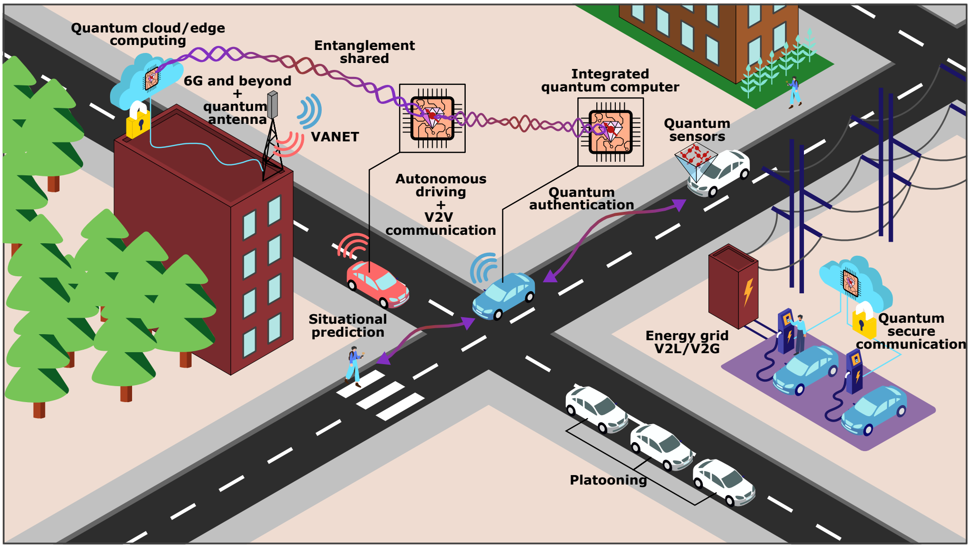

Figure II.4.1: **Future quantum enabled automotive**. A sketch of an envisioned future of the automotive integrated with quantum technologies. Cars have integrated quantum computers on board, entangled with other cars and quantum (edge) servers. Entanglement is either generated live while driving via quantum antennas that operate in parallel with 6G networks and beyond, or pre-loaded in quantum memories while charging. Charging infrastructure has intelligent load balancing for vehicle-to-load/grid (V2L/V2G), where cars quantum securely communicate, use quantum digital signatures in their handshake, allowing payment to be processed. Vehicles drive autonomously individually or together in platooning order. They set up vehicle-to-vehicle ad-hoc networks (V2V, VANET) to make driving decisions, aid in situational prediction and verify identities via quantum authentication. Cars can be equipped with quantum sensors to aid positional tracking for self-driving capabilities.

II.4.1. Introduction

The automotive sector has been progressing towards integrating computational, communication and sensor technology in vehicles to enhance the user experience and strengthen safety measures, among many other improvements [1, 2]. Current trends in the automotive sector require the integration of cutting-edge technology, such as AI, 5/6G networks and batteries to enable automated driving, over-the-air (OTA) software updates and electrification [3]. The introduction of these and further new technologies may make vehicles a higher risk to be vulnerable to cyber attack vectors, which is an active area of concern [4–9]. In parallel, the last decades have shown considerable advancement in the quantum technology research fields of quantum computing, quantum internet and quantum sensing. These technologies promise to solve particular complex computational problems [10–13], provide quantum-secure communication and ability for networked quantum computing [14, 15], and enhanced sensing [16–18], respectively. Quantum technologies have the potential to provide the innovation required to satisfy the increased needs in technological capabilities and security requirements for the envisioned future trends in the automotive sector. In addition, due to their novelty, applications of quantum technologies could bring forth use cases within the automotive sector that previously had not been considered.

Current quantum and automotive technological development and use cases mostly manifested in the field of quantum computing, focused on algorithms for traffic routing and factory process optimization, supporting machine learning approaches for autonomous driving and improved batteries for electric vehicles [19–22]. Conversely, little attention has been given to exposing the automotive domain to the possible applications that the quantum internet provides. However, with a future quantum internet having promising applications in secure and privacy enhancing communication and enabling distributed quantum computing, the benefit of employing these concepts in the automotive sector can be substantial. Furthermore, the automotive domain works on development cycles that make for a natural match with quantum research topics, of which many are on a decade timeline towards being a commercial product. Reciprocally, the quantum internet domain can benefit from an additional source of practical applications for the technologies they develop.

Given the current state of the art, it remains uncertain which, if any, of these potential applications could be realized in practice. This analysis explores their potential of implementation under the assumption of an optimal scenario. We utilize a method where megatrends - trends that have an effect on the entirety of their respective industry - of both fields are identified and qualitatively compared for both short (< 10 years) and long (≥ 10 years) time scales. First, we will cover the need-to-know of the quantum internet and its relevant applications in Section II.4.1.1. We then introduce the automotive field in Section II.4.1.2 and show why these two sectors are well matched for developing mutual use cases. Next, we will describe the megatrends of both respective sectors in Section II.4.2. We investigate the long and short term trends of the quantum internet in Section II.4.2.1 and II.4.2.1, respectively. We repeat this for the automotive for the long and short term trends in Section II.4.2.2 and II.4.2.2, respectively. Then, we perform a qualitative comparison of these trends and underlying sub-trends in terms of their mutual interfacing and developmental relevance in Section II.4.3.1. On this analysis we perform a synergy evaluation in Section II.4.3.2, allowing us to extract the trends that have the largest potential to build business cases around. Finally, we show newly developed potential use cases for the future of the automotive sector and make a qualitative assessment of the potential relevance of quantum internet applications within these use cases in Section II.4.3.3.

II.4.1.1. QUANTUM INTERNET

Analogous to how the current (classical) internet enabled a revolution for the classical computer, interconnecting quantum computers promises a similar revolution to quantum computing. Such a network of interconnected quantum computers is a quantum internet. Unlike a solely classical network where information is transmitted using classical bits, a quantum internet will transmit quantum bits (qubits) between quantum computers. Due to their quantum nature, these qubits cannot be sent over the classical internet, thus a different method of transmission of quantum information is required. A key property that enables sharing of quantum information is quantum entanglement. Entanglement between qubits can be generated with various methods and for telecommunication compatibility, generally involve using so-called flying qubits, single particles of light (photons). Once entanglement is generated, it can be consumed to teleport quantum information [23, 24, 24], the quantum equivalent of sending classical information. In contrast to the classical, quantum information cannot be copied (no-cloning theorem [25]), it disappears at the sender and appears at the receiver. In part, the property of the no-cloning theorem allows detection of when outside intervention on quantum communication is attempted, making it an opportune technology for verification of security of communication channels [26]. The downside of this property is that amplification of signals is impossible, and repetition of quantum information is not straightforward - one must employ the use of specialized quantum repeaters that use similar underlying quantum properties to mediate long-distance (> 100 km) communication [27].

A particular application of entanglement is to securely generate classical encryption keys between different parties using entangled photons. This is known as Quantum Key Distribution (QKD) [26, 28, 29], a technology that is available commercially and implemented worldwide [30–34]. The usage of QKD is to generate these classical encryption keys that are secure against classical and quantum attacks, in contrast to current quantum unsafe cryptographic protocols (RSA, AES) [10, 11]. While currently accepted post-quantum cryptographic (PQC) algorithms are classical and quantum secure [35], they are not proven to be so indefinitely. QKD offers the alternative to be both currently and in the future provably classical and quantum secure. Still, the functionality of QKD ends with key generation, whereas the previously defined quantum internet has the ability to go beyond that - it has the ability to let quantum computers communicate in a network. The rest of the paper will mostly focus on the latter capabilities.

Complex and widely rolled out quantum networks have yet to be built, however there is widespread confidence that such networks will come to exist in the future, which is strengthened by considerable public funding in pursuit of that goal [36]. Currently, the cutting-edge of quantum networks allows for two and multi-node networks within research lab environments [37, 38], and successful advances are made in building different kinds of quantum networks at metropolitan scales using commercially available fiber networks [39–41]. The quantum internet has use cases defined at different levels of functionality in the developmental process towards these complex networks [15]. We continue discussing the relevant functionality levels and quantum internet applications for this paper in Section II.4.2.1.

II.4.1.2. Automotive

The global vehicle manufacturing industry is over a century old and reached $2.6 trillion in revenue in 2023 [42]. It employs in the EU almost 13 million people indirectly, of which 2.4 million directly [43], making it a cornerstone of the economy covering around 7% of all jobs in the EU. Technological developments are constantly integrated into new automobiles to introduce new or improved features for customers, or to adhere to changed regulations. As such, the spending of the automotive industry on R&D is the highest of all industrial sectors in the European Union with €59 billion in 2021 [44], and a significant contributor to technology patenting with 587k patents filed between 2010 and 2019 by the top 20 world patent holders in the automotive industry [45].

The automobile integration of technology accelerated in the information age driven by regulations, user demands and the pursuit of technological advancements, resulting in cars have increasingly become more of a computer on wheels [46–51]. User interfaces are on (touch)screens, control of automotive functionality is relinquished to digital processing and car access can be keyless, to name a few. This trend continued with the introduction of sensory-awareness and driving assistance for enhanced safety and driver comfort, aiming towards full autonomous driving in any situation [52]. There are many challenges to be solved in achieving that goal, not only involving the self-contained challenge of an autonomous driving vehicle interacting in traffic, but also in the security of data-transmission of sensitive information. In addition, these systems will need to be robust against rogue actors trying to gain access to driving systems individually or to vehicle fleets [5, 53].

Furthermore, new vehicles are now connected to the internet. This enabled improved customer functionality for navigation and entertainment and enabled the possibility for vehicle-to-everything (V2X) communication, which includes over-the-air (OTA) diagnostics and updating of soft- and firmware, and smart-grid integration [3, 54, 55]. However, cybersecurity is becoming a key focus point for vehicle system development that permeates through the entire software stack of vehicle and V2X management software [6, 53].

To uphold extensive and thorough safety standards, vehicles must be compliant with regulations such as International Organization for Standardization (ISO) 26262[1]. Furthermore, technology in cars aims to be robust and reliable, requiring only intermittent maintenance for eroding or moving parts. These design requirements have impact on integrating new technologies in the Product Development Process (PDP) of automobiles, allowing only the introduction of new features after rigorous tests and verification of long-term operability. The phase before starting the PDP is the pre-Production Development Process (pre-PDP). In this initial stage, essential requirements are outlined to determine whether a new technology can be successfully integrated into the vehicle [57]. These pre-PEP requirements are shared between the vehicle manufacturer and their suppliers to form a mutual framework for product integration.

To formulate pre-PDP requirements for this paper, we extract the requirements set in the selection matrix for sensor component requirements from [58], generalizing it as a method for technology transfer of a new technology to the vehicle ecosystem, which makes it applicable to quantum technologies. We present a non-exhaustive list of several of the most important requirements that are relevant to this analysis and discuss them further in Section II.4.2.2.

In general, PDP cycles from concept to start of production can take up to 5 years [59]. The automotive sector thus has to predict and steer future technological trends for their purpose beyond this 5 year timeline to evaluate their benefits, limitations and determine necessary steps for automotive-specific integration. It is this timeline that makes for a natural match with quantum research topics, of which many are on a decade timeline towards being a commercial product. This makes it an interesting candidate for matching pre-PDP requirements to current (< 10 years) quantum internet development tracks. In addition, the timeline of predicting long term (≥ 10 years) use cases in the automotive sector aligns with the long term vision of quantum internet applications gaining usefulness as technological functionality increases. This allows for analyzing the intersection of future use cases in the automotive with applications of the quantum internet, which is

[1] Road vehicles - Functional safety [56]

discussed in Section II.4.3.3.

II.4.2. Megatrends

To conduct a thorough use case analysis, we need to identify key trends in both the quantum internet and automotive industries for the long and short term. Trends that have an effect on the entirety of their respective industry are called megatrends. We discuss long and short term trends of the quantum internet in Section II.4.2.1 and II.4.2.1, respectively. We repeat this for the automotive for the long and short term trends in Section II.4.2.2 and II.4.2.2, respectively. We present the results of the interfacing analysis of the megatrends in Section II.4.3.

II.4.2.1. Megatrends Quantum Internet

The quantum internet is at an early developmental stage, enabling us to identify two megatrend directions: Trends for future applications (≥ 10 years) [15] and known protocols [60] on one hand, and trends in current research tracks (< 10 years) on the other. The latter are trending research tracks that are pursued to reach the future applications.

Quantum Internet Future Trends

We can infer future application megatrends through recent research publications and guidance brought by institutional and industrial consortia [36, 61]. From this, we distinguish three categories that we discuss below:

a. *Interconnected quantum computing*
b. *Quantum cryptography*
c. *Quantum sensors*

The trends identified are highlighted in bold in the text.

Interconnected quantum computing

Interconnecting quantum computers is the leading trend in the field. With the knowledge that interfacing classical computers brought a second revolution to the information age, the quantum internet has the possibility to provide a similar revolution to quantum computing. Hence, **distributed quantum computing** is a sought after application that could accelerate reaching useful quantum computing. Furthermore, networked quantum computing capabilities also allow for **blind quantum computing** (BQC) [62, 63], where clients can run calculations on a server that will remain blind to what the client executes. This is expected to become an important cornerstone for future privacy and geographical-safe computing. Lastly, **anonymous transmission** of quantum information can provide built-in privacy for quantum networks [64–66].

Quantum cryptography

A separate category of quantum communication focuses specifically on quantum-enabled cryptography, where protocols are developed that use properties of the quantum internet.

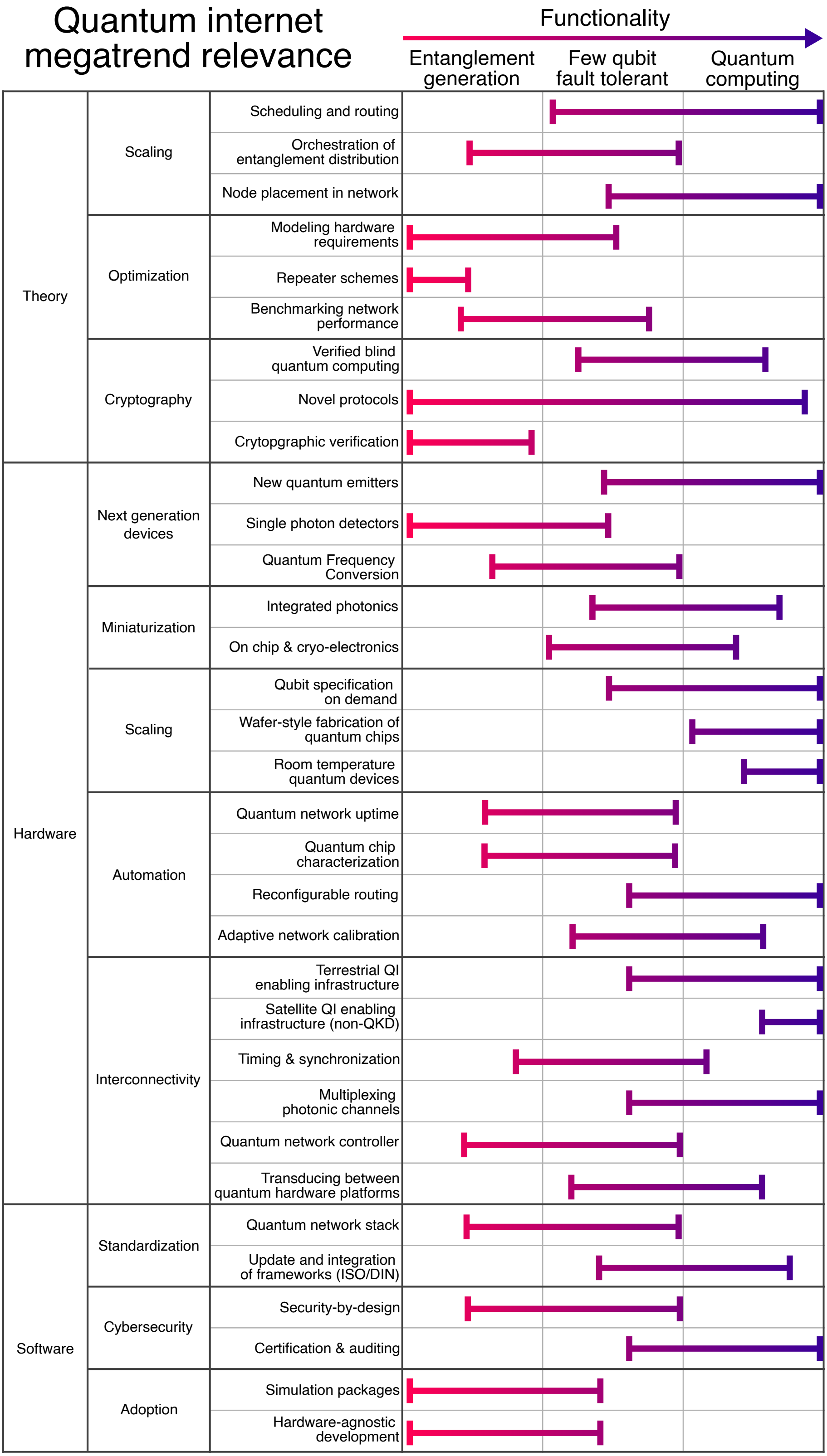

Quantum internet megatrend relevance
Functionality
Entanglement generation
Few qubit fault tolerant
Quantum computing
Theory
Scaling
Scheduling and routing
Orchestration of entanglement distribution
Node placement in network
Optimization
Modeling hardware requirements
Repeater schemes
Benchmarking network performance
Cryptography
Verified blind quantum computing
Novel protocols
Crytopgraphic verification
Hardware
Next generation devices
New quantum emitters
Single photon detectors
Quantum Frequency Conversion
Miniaturization
Integrated photonics
On chip & cryo-electronics
Scaling
Qubit specification on demand
Wafer-style fabrication of quantum chips
Room temperature quantum devices
Automation
Quantum network uptime
Quantum chip characterization
Reconfigurable routing
Adaptive network calibration
Interconnectivity
Terrestrial QI enabling infrastructure
Satellite QI enabling infrastructure (non-QKD)
Timing & synchronization
Multiplexing photonic channels
Quantum network controller
Transducing between quantum hardware platforms
Software
Standardization
Quantum network stack
Update and integration of frameworks (ISO/DIN)
Cybersecurity
Security-by-design
Certification & auditing
Adoption
Simulation packages
Hardware-agnostic development

Figure II.4.2: **Quantum internet megatrends.** List of quantum internet trends divided by category. We evaluate when this trend will be relevant at what functionality level of the quantum internet.

A way to prevent quantum attacks on current quantum unsafe cryptographic protocols (RSA, AES) [10, 11] is to replace message authentication and sender non-repudiation by their quantum equivalents. These protocols are **quantum authentication** [67] and **quantum digital signatures** [68–70]. Additionally, in geographies where data retention is regulated or where particular data of customers is confidential (e.g. General Data Protection Regulation (GDPR) in the European Union), **quantum encryption with certified data deletion** at scale could simplify compliance and prevent mistakes [71].

Furthermore, as discussed in the Section II.4.1.1, at early stages of the quantum internet, classical **encryption with QKD** is an accessible technology that will continue to be relevant going forward [26, 28]. Lastly, consideration for distributed algorithms is dealing with faulty participants in networked decisions and how to get to an agreement among them. This is known as the Byzantine agreement problem. With V2X interconnectivity, faulty or malicious data exchange can lead to safety issues [8, 53], requiring to use Byzantine fault tolerant protocols [72, 73]. We therefore include that quantum communication can offer a faster version known as **fast Byzantine agreement** [74].

QUANTUM SENSORS

When a quantum internet is rolled out, we see the possibility of being able to use a distributed network of quantum sensors. This can be in the form of **quantum internet-of-things (QIoT)**. Another known application is to enhance the precision of distributed **clock synchronization** using quantum resources [75]. However, in this application we include the usage of classical technology that helps distribute sub-nanosecond level timing distribution [76]. Separately, quantum sensors can precisely measure acceleration offering 50 to 100-fold improvements in sensor stability over their classical counterparts [77, 78]. This is a crucial technology for autonomous driving that complements global navigational satellite systems (GNSS) in GNSS-denied environments (tunnels, cities) to enable inertia navigation. Thus, enhanced **position tracking** is a relevant application of a distributed network of quantum sensors [79].

QUANTUM INTERNET RESEARCH TRENDS

In this section we will define research trends, and perform a mapping of those trends to their technological maturity in the quantum internet domain. We will use this maturity mapping to determine whether there is a relevant interface between the quantum internet trends and design considerations in the automotive pre-PDP requirements and discuss the results in Section II.4.3.1.

In defining the research trends, we aim to cover the entire quantum internet domain in three categories:

a. *Theory*
b. *Hardware*
c. *Software*

The boundary between all three categories is fluid. In the category *theory*, we recognize protocol development, analytical/numerical modeling of algorithms and projected hardware performance. This is distinguished from *software*, which we categorize as development of software and architecture design that can directly be applied to code bases, libraries or specifically to (drivers of) software-controlled hardware. Lastly, with *hardware* we cover the qubit platforms and classical control systems that control and interface with the quantum hardware.

The trends that we recognize in these three categories are shown in Figure II.4.2 based on expert knowledge and global quantum internet research. While this list is carefully selected, it is non-exhaustive and exact trend recognition can vary by expertise. We recommend revisiting this list periodically to ensure its relevancy.

We have mapped projected relevancy of each quantum internet megatrend to the functionality scale as defined in [15], shown in Figure II.4.2 on the horizontal axis. We start at the level of entanglement generation, a necessary basic task in quantum networking. If we extend such a network with few fault tolerant qubits we enhance the network's capabilities with small quantum computations and quantum memory. The last stage is to have full-fledged quantum computing mediated by a quantum internet, allowing arbitrary distributed quantum computing over multiple hardware systems. This range defines the area where quantum internet applications beyond (trusted node) QKD lie. Although all trends described are current topics of research and considerations, every trend has a different relevancy along the functionality levels of the quantum internet. To take one example, even though wafer-style fabrication is an important consideration at the early stages of building quantum internet technologies, these considerations only become significantly relevant when the qubit-platform has matured to be at least few-qubit fault tolerant.

We perform this mapping specifically to functionality level to be platform agnostic. Some quantum hardware platforms are further developed in their functionality level than others, however the underlying trends and the functionality relevance remain the same. In the following sections we discuss the trends per quantum internet research domain.

THEORY

Towards the **scaling** of larger networks, more protocol and architecture development is required both for orchestration of entanglement distribution and scheduling and routing of entanglement generation requests [80, 81]. In contrast to the classical internet, most of these concepts in the quantum internet space are unexplored. Furthermore, quantum systems give rise to the challenge of optimal node placement in networks [82]. Theoretical models can provide tools to model hardware requirements, aiding their development and provide **optimizations**. The same holds for building frameworks to **benchmark quantum network performance** [83, 84]. Separately we consider **cryptography** as active area of research. Continued research is relevant to discover various ways of verified blind quantum computing. The application of cryptographic protocols and developing novel protocols can help enable quantum internet use cases, as has been shown for verified blind quantum computing [63, 85].

Hardware

The quantum internet domain is in search for improved quantum devices, carrying the name of **next generation devices** - those that go beyond the current state of the art in qubit performance [86–88]. Since we are focusing on quantum communication, we recognize the required enhancement in photon emission and detection, i.e. finding new quantum emitters and improved single photon detection [89]. For improved connectivity and looking forward to integrated devices, quantum frequency conversion hardware is being developed and pushed to efficiency limits both in conversion and in its applications of entanglement generation (time-bin, polarization encoding) [90–94].

Looking forward, with increased functionality of quantum devices comes the necessity of **miniaturization** of photon manipulation towards integrated photonics [95–98], and moving to on-chip classical control electronics similar to quantum computing [99, 100]. This is combined with the drive to scale up quantum devices - more qubits per surface area as well as streamlined production processes with standardized outcomes and tolerance definition. Quantum device operation is potentially simplified if they could operate closer to room temperature, however this is a trend we only see relevant in the scaling of quantum computing systems.

Current state-of-the-art quantum network systems report uptimes of 78% without human operator over the course of 17 days [101]. Compared to classical internet industry standards of 99.9% [102], continued work on **automation** of various layers in quantum networks is a necessity. This includes automated characterization of quantum chips, automatic routing reconfiguration [103] and adaptive recalibration of connection parameters (entanglement fidelity, rate, etc.) in mature networks.

Lastly, the quality and availability of **interconnectivity** of different quantum devices is trending. Both in developing terrestrial and orbital quantum internet infrastructure [104, 105], but also more directly in the challenges of distributing timing and synchronization of quantum devices on a network. Interconnectivity bandwidth can be improved from singular photonic channels to multiplexing on photonic channels to achieve the quantum analogy to wavelength-division multiplexing [106]. Additionally, the concept of a quantum network controller is only in its infancy due to state-of-the-art quantum networks having at most several nodes, simplifying the control architecture. However, for many-node networks such a controller is paramount in delivering interconnectivity on demand. Finally, the physical transduction of quantum information encoded in different formats (photons, phonons, microwaves) is a building block in connecting different quantum hardware platforms [107].

Software

Standardization of control and software frameworks is essential for ensuring hardware interoperability, reducing costs, and simplifying maintenance. This includes agreement on a quantum network stack, of which initial attempts have been made already [108, 109]. We recognize that the development of a quantum network stack is broad in itself, however it suffices for this analysis to group these developments under one trend. In standardization, there will be a requirement to continue updating standards as ISO or

German Institute for Standardization (DIN), which is only relevant at higher maturity of quantum systems.

Especially standards aimed at **cybersecurity** and information management systems will keep up with the advancement of quantum technology. This makes certifying and auditing of quantum soft- and hardware a relevant trend in the long term, and the development of standards in the near term according to security-by-design principles.

Finally, **adoption** of quantum communication tools is driven by the accessibility of simulation packages, both for software integration and application analysis [110–112].

II.4.2.2. MEGATRENDS AUTOMOTIVE

Megatrends across the entire automotive sector are defined by umbrella automotive organizations. Without loss of generality we focus on the German umbrella association (VDA) and their defined megatrends up to a timeline of 2030 [113, 114]. We extend that timeline towards ≥ 10 years from publishing of this paper, given its continuous relevancy.

First, we will discuss these future trends and then introduce the previously mentioned pre-PDP requirements. Then, in Section II.4.3.3, we present the outcomes of the interfacing analysis between the automotive megatrends and quantum internet future applications.

AUTOMOTIVE FUTURE TRENDS

The VDA defines the following megatrend categories:

a. *Autonomous driving and connectivity*
b. *Infrastructure*
c. *Mobility and logistics*
d. *Production*
e. Materials
f. Drivetrain and vehicle
g. Energy carrier and storage

We highlight in italic the megatrends we will discuss in this paper. The selected megatrends are those that actively use the classical internet, making them relevant to the quantum internet future applications and research tracks. The other megatrends related to material science and mechanical movement do not have a predicted significant relevance to quantum interconnectivity. From a quantum technology point of view, they would be more relevant to quantum computing (quantum chemistry, optimization) [115–117].

In the following paragraphs we give details about the above selected megatrend categories and their underlying trends. Additionally, for each trend we developed several use cases without assessment of their business viability. This allows the possibility for future cross-interaction of use cases between the automotive and quantum internet domains, even though their business viability might be uncertain today. The complete list of megatrend categories, trends and use cases is shown along the vertical axis of Figure II.4.5.

Autonomous driving and connectivity

The main megatrend for the future of automotive is **autonomous driving**. As defined by the Society of Autonomous Engineers (SAE), there are 6 levels of automation in driving. They range from L-0 being solely the human as driver to L-5 where the vehicle is able to drive autonomously in any environment without failure [52]. Many different components and yet to be developed technology need to be integrated in vehicles and surrounding infrastructure for L-5 to be achievable, of which we recognize several trends.

First, the act of **cooperative driving** together with **secure V2X communication** is an emerging field within autonomous driving, giving rise to the need for vehicle ad-hoc networks (VANETs) - vehicles only need interconnectivity with each other if actual interaction is expected , e.g. at an intersection [55]. These ad hoc networks require self-organization, real-time communication and secure (anonymous) transmission, to mention a few features.. For more organized and higher abstraction level connectivity, **network management** is necessary for e.g. latency control. Vehicles will also need to be able to perform **situational prediction** of previously unknown situations and ensure the data they receive is correct. They are mission driven: a vehicle must successfully assess situations and be able to autonomously make decisions and execute actions on the road, while remaining functionally safe for the driver and other traffic participants. Data collection of the environment is performed through **sensors and fusion of sensor data** which needs to be processed in real-time [118]. Lastly, selective data collected necessary in order to perform autonomous movements will have to be private and treated securely, making **data privacy & ownership** a trend in this category.

Infrastructure

Together with the electrification transition of vehicles and the requirement to be more interconnected, existing infrastructure needs changes to support these transitions. A trend in infrastructure development is combining the car as battery with the **energy grid**, which involves organization of load-balancing systems for charging, vehicle-to-load (V2L) and vehicle-to-grid (V2G) systems that all have to comply with cybersecurity standards. Additionally, infrastructure needs to support cars communicating with each other and the (quantum) internet via digital or quantum channels which we denote by **physical communication**.

Mobility

Collaboration of vehicles in traffic is the separate trend of mobility. Developments in this trend mostly focus on **swarming, fleeting and platooning** of vehicles within intermodal traffic management.

Production

Separately from how a vehicle operates once produced, we see relevant trends in the production facilities and the management of factory processes. Manufacturers are strongly interested in constantly reducing their resources and costs by increasing the efficiency of the production. Value chains and assembly lines are aimed to be optimized by making use of the Internet of Things through the digital connection of machines, buildings, and plant locations, but also through the subsequent use of artificial intelligence and machine learning. Extensive connectivity in factory plants enable using swarm effects for production facilities. Machines could organize themselves in a swarm to share information and learn from each other [119]. With more automated production, coordination of intelligent machines and timing needs to be synchronized. Furthermore, sources of data that are being shared within the factory need to be verified, i.e. data ownership requires guarantees. Furthermore, we see a continued need for secure data tracking during the entire production chain and secure interfacing with the factory network as trend.

PRE-PDP REQUIREMENTS

In this section we discuss the pre-PDP requirements that are suited for assessing interfacing relevancy with the current research tracks of the quantum internet.

VEHICLE & INFRASTRUCTURE

We define this category of requirements as system requirements for products that are aimed to be included in a vehicle and the (out-of-vehicle) infrastructure necessary to support it. In order to assess interfaces with other products, a **characterized performance** of each integrated product needs to be known and verified. These parameters are well defined in many kinds of product requirement documents (PRDs). Furthermore, the smaller the product can be, the better. A car has limited volume, and this makes **miniaturization** of products essential. Then, to increase the possibility of interfacing, replacing or upgrade parts, the **modularity** of the product must be taken into account. Lastly, the ease with which products are set up is its **deployability**.

REGULATIONS

With the automotive being a highly regulated sector with different rules per country, all products need to pass externally imposed regulations and laws. Additionally, they need to adhere to internal regulations that are generally manufacturer specific. We focus on the regulations that matter for this analysis, being **cybersecurity** in the form of UNECE R155[2]/R156[3], ISO 27001[4], ISO/SAE 21434[5] and the recently introduced EU Digital Operational Resilience Act, to name a few relevant regulations out of many that apply to this sector. In addition, we recognize the importance of compliance with **energy consumption** regulations both for fossil-fueled and electric vehicles. One of the key requirements that distinguishes the automotive from most other consumer product fields is the need for technology to be **resilient against extreme environments**. Semiconductor technology in a vehicle can only be used if it is operable in almost any environment on earth

[2] UN Regulation No. 155: Cyber security and cyber security management system [120]
[3] UN Regulation No. 156: Software update and software update management system [121]
[4] *Information security, cybersecurity and privacy protection* [122]
[5] *Road vehicles - Cybersecurity engineering* [123]

and with road conditions that cause vibrations and even corrosion (ISO 16750[6]). Some components require extreme temperature range resistance from −55 °C to 125 °C due to a combination of low and high temperatures generated by both the outside environment and heat generation of the vehicle itself [124, 125]. Furthermore, products require a well assessed safety risk during crash conditions. These types of requirements are rarely considered in the development of quantum technologies as a whole, making it a highly relevant topic for interfacing analysis.

Quality

Product quality must be consistent and thus **reproducible** within specified **tolerances** and should also retain its quality during production and after. Those requirements are product and original equipment manufacturer (OEM) specific, and will also be described in the product requirement documents.

Long-term availability

In the product requirement documents the long-term availability of the product must be stated, as vehicle product lines can run for years and thus **manufacturing continuity** has to be preserved. Additionally, the raw materials or parts used require **supply-chain availability**, which for quantum devices becomes relevant when rare-earth or other highly specific materials are used [126, 127].

Change management

During the (pre-)PDP the possibility of making changes to the products will have to be possible to mediate interfacing. After production, the **product service life** must correspond to the service life of a vehicle. Additionally, firm- and software updates in the form of **OTA updates** to products will have to be possible for the whole life cycle of ≥ 10 years.

II.4.3. Interfacing Analysis

We now turn to the interfacing analysis, divided into three parts. First, we interface the pre-PDP requirements to the quantum internet trends in Figure II.4.3 and discuss the results in Section II.4.3.1. Then we compare these outcomes with the maturity mapping of Figure II.4.2 to obtain a synergy evaluation of the automotive and quantum internet trends in Figure II.4.4 and Section II.4.3.2. Lastly, we interface the future trends of the quantum internet to currently foreseen use cases of the automotive future trends in Figure II.4.5 and discuss the use cases in Section II.4.3.3.

The structure of the following interfacing figures is a framework to elucidate mutual influences at different trend timelines: pre-PDP versus quantum internet megatrends in Figure II.4.3 and automotive use cases versus quantum internet applications in Fig-

[6] *Road vehicles - Environmental conditions and testing for electrical and electronic equipment* [124]

ure II.4.5. Because of the mutual influence of the domains on each other, these figures are to be read bidirectionally.

II.4.3.1. QUANTUM INTERNET RESEARCH TRENDS & PRE-PDP REQUIREMENTS

In this section we will describe the outcomes of the interfacing analysis of the quantum internet research trends and the pre-PDP requirements, shown in Figure II.4.3. We list the research trends of the quantum internet that were previously discussed in Section II.4.2.1 and shown in Figure II.4.2 on the vertical axis. On the horizontal axis we list the pre-PDP requirements from Section II.4.2.2 and together evaluate the bidirectional relevancy of these trends to each other. We define relevancy to be low when we evaluate the trends to have no interface with each other, they exist completely parallel to each other. The relevancy is high when the trends have a high degree of interfacing: they can mutually benefit from expert knowledge or requirements from the other domain. In the following sections we will discuss the interfacing of the pre-PDP requirements per quantum internet megatrend category.

THEORY

Trends in quantum internet theory developments are largely disconnected from production requirements. We can state that the megatrends of optimization and cryptography are a layer before being considered as pre-PDP requirement. Quantum cryptography is solely related to cybersecurity aspects of pre-PDP requirements, as they will have to comply to regulatory standards. This interface is one-directional, only the pre-PDP requirements can provide input for quantum cryptography developments, but the outcome of this research likely has little influence on the demands from the automotive side. Lastly, the availability of characterized performance is requested through the product requirement documents and thus modeling of hardware requirements and network performance will be essential.

HARDWARE

The highest relevancy in interfacing can be found in the hardware megatrends, which is a natural overlap given that the pre-PDP requirements are largely hardware focused.

NEXT-GEN & MINIATURIZATION

Hardware megatrends directly relate to product integration into a vehicle. It is a necessity to have characterized performance of quantum internet hardware, as the automotive will demand clear performance requirements. This is valuable knowledge for hardware development strategies: the automotive can co-determine, with their use-cases, the minimum viable performance for the quantum connection, e.g. in required entanglement generation rate, fidelity, memory coherence and uptime. Additionally, the development of next generation quantum devices needs to take manufacturing continuity and supply-chain availability into account, which is highly relevant as several promising qubit systems are derived from rare-earth metals or diamond [86].

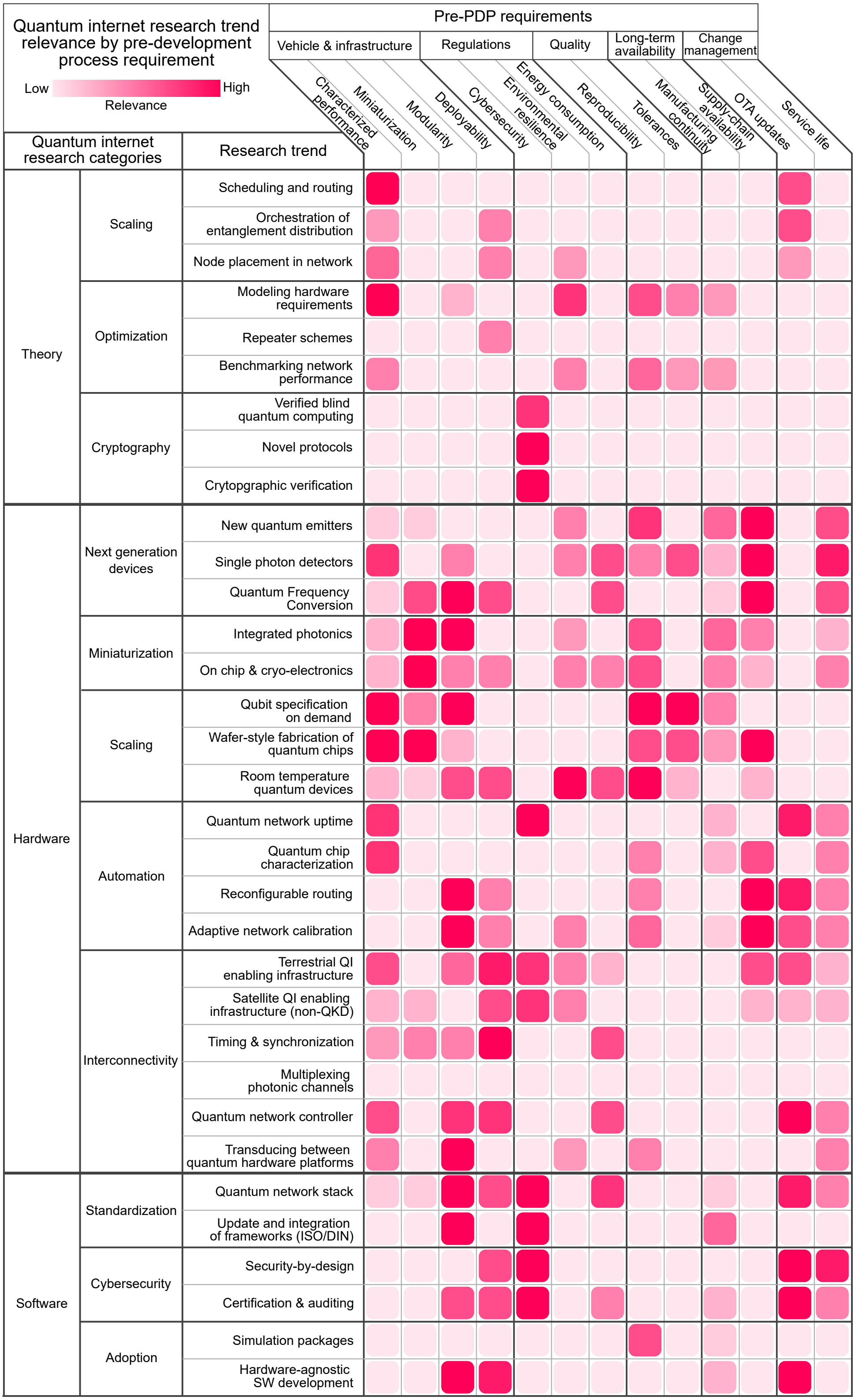
Quantum internet research trend relevance by pre-development process requirement
Low
High
Relevance
Pre-PDP requirements
Vehicle & infrastructure
Regulations
Quality
Long-term availability
Change management
Characterized performance
Miniaturization
Modularity
Deployability
Cybersecurity
Environmental resilience
Energy consumption
Reproducibility
Tolerances
Manufacturing continuity
Supply-chain availability
OTA updates
Service life
Quantum internet research categories
Research trend
Theory
Scaling
Scheduling and routing
Orchestration of entanglement distribution
Node placement in network
Optimization
Modeling hardware requirements
Repeater schemes
Benchmarking network performance
Cryptography
Verified blind quantum computing
Novel protocols
Crytopgraphic verification
Hardware
Next generation devices
New quantum emitters
Single photon detectors
Quantum Frequency Conversion
Miniaturization
Integrated photonics
On chip & cryo-electronics
Scaling
Qubit specification on demand
Wafer-style fabrication of quantum chips
Room temperature quantum devices
Automation
Quantum network uptime
Quantum chip characterization
Reconfigurable routing
Adaptive network calibration
Interconnectivity
Terrestrial QI enabling infrastructure
Satellite QI enabling infrastructure (non-QKD)
Timing & synchronization
Multiplexing photonic channels
Quantum network controller
Transducing between quantum hardware platforms
Software
Standardization
Quantum network stack
Update and integration of frameworks (ISO/DIN)
Cybersecurity
Security-by-design
Certification & auditing
Adoption
Simulation packages
Hardware-agnostic SW development

Figure II.4.3: **Quantum internet and pre-PDP requirements analysis.** We evaluate the relevancy of quantum internet research trends and the categorized pre-PDP requirements. Relevancy of the trend intersection can be read bidirectionally. Note that there are more pre-PDP requirements than evaluated here, only the most relevant requirements for this analysis have been selected.

Miniaturization is a trend present in both the pre-PDP and quantum internet research, thus interfaces well. The automotive can provide significant guidance on the miniaturization requirements. Besides 'the smaller the better'always taking preference, together both domains can determine the threshold of trading off functionality of new quantum internet hardware with respect to its integration complexity. The efforts towards miniaturization on the quantum internet hardware are already largely in line with the automotive demands: especially integrated photonics and on-chip electronics provide order of magnitudes reduction in packing volume of both quantum hardware and classical control technology compared to their current free-space or in-fiber counterparts. Furthermore, miniaturization could reduce overall energy consumption, especially relevant for electric vehicles.

SCALING & AUTOMATION

The scaling of quantum hardware systems will help satisfy pre-PDP requirements. Standardized qubit specifications and mass-producing quantum chips will ensure reproducibility and be within set tolerance requirements in quantum performance. This will also aid in determining compatibility with car control hardware. With improved specificity of device capabilities, (quantum) control hardware can be miniaturized further and integration can be better defined. The same arguments hold for more standardized fabrication methods. Together they can also guarantee manufacturing continuity and reproducibility of the product, especially when considering the production of 93 million vehicles yearly worldwide [128].

In quantum internet automation we recognize interfaces in pre-PDP modularity and reconfigurability. Automated calibrations and rerouting can help to guarantee network uptime, even if parts of the quantum network are (temporarily) offline or unavailable. The hard- and software that organized this reconfiguration will have to be OTA update compatible and also should receive (security) software updates/support, hence the interfacing with the pre-PDP service life requirement.

INTERCONNECTIVITY

With the introduction of the internet and connecting vehicles to a telecommunications infrastructure, collaborative efforts were made to integrate vehicles computer systems with those infrastructures for navigation, in-vehicle-entertainment and OTA updates. We see a possibility in extending these efforts even further towards integrated quantum internet systems not only for the vehicles itself, but also for designing and setting requirements for the terrestrial and orbital quantum internet infrastructure and its future network controllers. In that context, the interconnectivity trends interface with most pre-PDP requirements pertaining to vehicle & infrastructure and regulatory compliance.

Software

The standardization of both hardware and software related to quantum internet technology results in this field producing its own standards corresponding to their newly developed products [129]. The output of this megatrend thus becomes an input for the regulatory pre-PDP requirements, where required standards can now include quantum related standardization as well.

This is opposite for cybersecurity, as this has become a cornerstone and topic weaved in almost every digital aspect of the automotive. Here the quantum internet domain has to adapt: clear guidelines and standards describe the security practices, auditing and complying to already existing standards. For any software to be deployable in a car, security-by-design and certification will have to be implemented. The progression from academic and research software to a software product can thus learn from the requirements set by the automotive, which is in part based on governmental (e.g. GDPR and Network and Information Security Directive (NIS2) in the European Union) or industry standards defined by e.g. ISO or DIN.

Although adoption of quantum internet related software is an important megatrend, we see little relevance to the pre-PDP requirements. We do recognize that long life maintainability of software products can be achieved with more certainty if software is continuously developed and maintained by many users and developers. A broad adoption of (open-source) code-bases can aid in achieving that goal, while allowing transparency around security protocols being implemented.

II.4.3.2. Synergy evaluation

To further assess the viability of collaboration on the short term (< 10 years) between the automotive sector and the quantum internet, we perform a synergy evaluation as shown in Figure II.4.4. There we evaluate two parameters:

1. Where in functionality level is each quantum internet megatrend relevant? (vertical axis)
2. How relevant is that megatrend for the pre-PDP requirements? (horizontal axis)

This combination allows us to map which quantum internet research trends have the ideal combination of being both near-term relevant in their development and highly relevant as pre-PDP requirements. It is those trends that allow for two-way exchange of expertise and requirements. We highlight the synergy region, the region in which we expect to find the largest potential for synergy between the automotive and quantum internet domains. We can interpret the bottom of the synergy region to be the near term use case opportunity and the top mostly long term, however all to be within the < 10 year timeline given by the pre-PDP requirements.

We are only able to perform the synergy evaluation to the pre-PDP requirements, as they are evaluated against the quantum internet megatrends, of which we both have detailed assessments. Such an assessment is not yet possible to be made for the automotive megatrends as the quantum internet applications are on the ≥ 10 year timeline. We discuss the topics that are part of the synergy region in the following sections.

SYNERGY REGIONS

VEHICLE & INFRASTRUCTURE

Miniaturization has significant potential for synergy with the pre-PDP vehicle and infrastructure requirements. As mentioned in Section II.4.3.1, we identify short-term interfaces in miniaturization:

- Form factor
- Integration complexity
- Environmental resilience
- Modularity
- Power consumption

LONG-TERM AVAILABILITY

From a hardware perspective, it is vital that the next generation devices of the quantum internet support long-term availability of its used raw materials and production processes. This is especially relevant for the short-term, as many new quantum devices are actively being developed to be used in quantum networking as communication qubit.

REGULATIONS

A natural synergy is found in the development of standardization in general and cybersecurity, specifically. The automotive can provide input on these topics in advance of any quantum internet related product entering the market. Clear stated requirements from regulations can provide a smooth transition of new quantum technology from experimental to a commercial vehicle-deployable one. To ensure this transition, it is beneficial that quantum product certification will align with e.g. ISO 27001, 21434 or 16750 standards. Conversely, the automotive is highly dependent on the development of the quantum network stack and will need to adapt their systems based on the requirements that this stack demands of their hard- and software. For instance, to operate the quanutum network stack, the availability of particular antennas for communication functionalities could necessary. Additionally, specific requirements on the vehicle's real-time computing power and data transfer bandwidths are also to be expected.

II.4

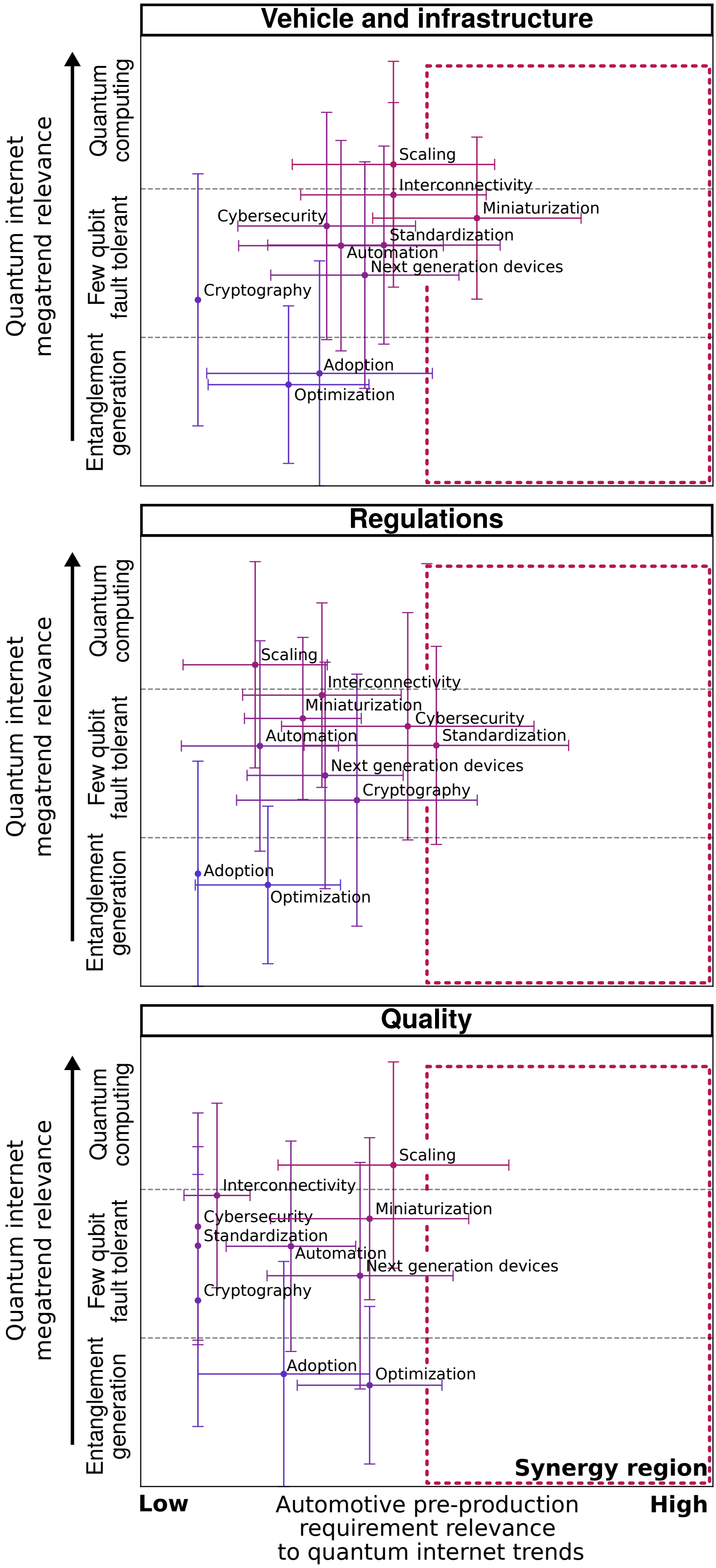
Vehicle and infrastructure
Quantum internet megatrend relevance
Quantum computing
Few qubit fault tolerant
Entanglement generation
Scaling
Interconnectivity
Miniaturization
Cybersecurity
Standardization
Automation
Next generation devices
Cryptography
Adoption
Optimization
Regulations
Quantum internet megatrend relevance
Quantum computing
Few qubit fault tolerant
Entanglement generation
Scaling
Interconnectivity
Miniaturization
Cybersecurity
Automation
Standardization
Next generation devices
Cryptography
Adoption
Optimization
Quality
Quantum internet megatrend relevance
Quantum computing
Few qubit fault tolerant
Entanglement generation
Scaling
Interconnectivity
Miniaturization
Cybersecurity
Standardization
Automation
Next generation devices
Cryptography
Adoption
Optimization
Synergy region
Low
Automotive pre-production requirement relevance to quantum internet trends
High

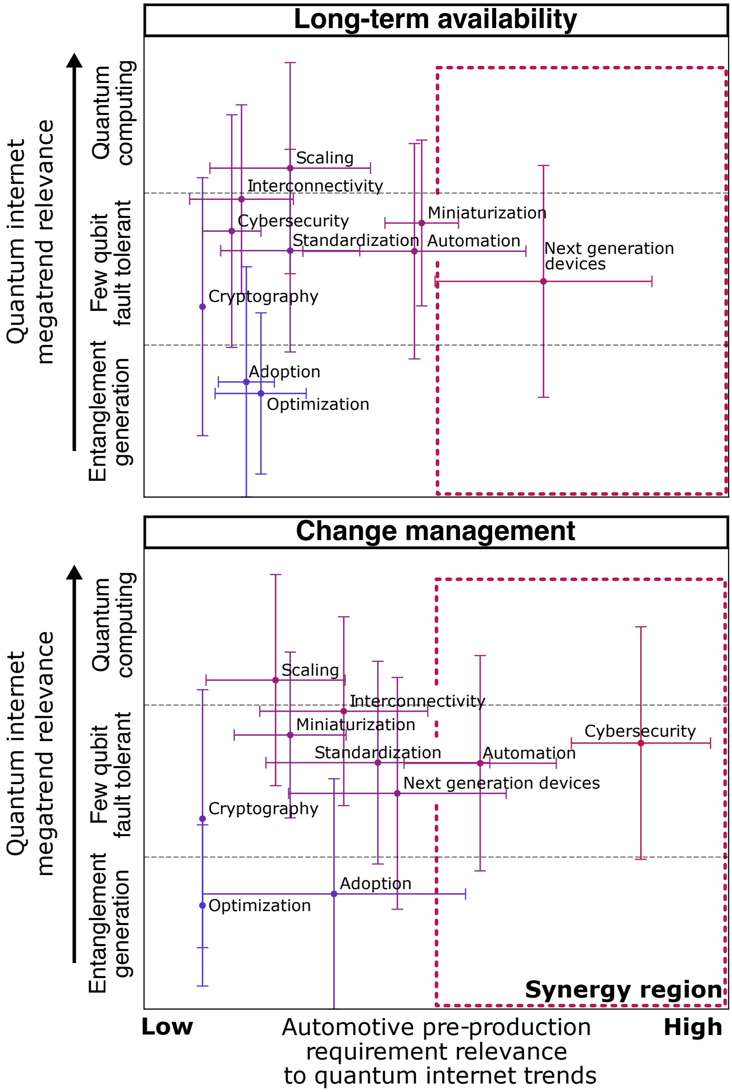

Figure II.4.4: **Synergy evaluation**: We evaluate the quantum internet megatrends of Figure II.4.2 and the relevancy of the quantum internet megatrends with the automotive pre-PDP requirements of Figure II.4.3 to obtain a synergy mapping. For the quantum internet megatrends we group the research topics per subcategory and show when it will become relevant on the quantum internet functionality scale of the vertical axis. We perform the same mapping for the pre-PDP interfacing analysis on the horizontal axis based on the data collected in Figure II.4.3 and evaluate every pre-PDP category separately as denoted at the top of each graph. The dots show the averages of the relevancy per subcategory grouping of Figure II.4.2 (vertical axis) and Figure II.4.3 (horizontal axis). The bars signify the average range (vertical axis) and one standard deviation of the relevancy (horizontal axis) per subcategory grouping. The dotted lines frame the synergy region, the region of interest where the potential for synergy between the automotive pre-PDP requirements and the quantum internet trends is the highest. This region covers all functionality levels of the quantum internet which allows this mapping to remaining hardware agnostic and cover near term and long term synergies within the < 10 year evaluation timeline.

Change management

We find strong synergy for the quantum internet domain to incorporate cybersecurity in their products, matching with the same requirement for vehicles. as well as enabling software-powered automation of hardware systems. It is much easier to integrate security-by-design in fresh code bases for new products. Certification demands and operational automation are additionally better to be integrated at the start of a product development process than after. These product development considerations are a hard requirement for the eventual breakthrough of a quantum internet product in any mature industry.

Quality

There is a small opportunity for quantum internet hardware scaling to be relevant in quality requirements at pre-PDP. Especially in reproducibility and tolerances the automotive can provide their input on qubit parameters. Other trends of this category are not sufficiently in the synergy region.

II.4.3.3. Automotive Future Trends & Quantum Internet Applications

The final interfacing analysis we make is of the future trends of the automotive, defined in Section II.4.2.2, with the quantum internet future trends of Section II.4.2.1. We developed a list of potential automotive use cases out of the future trends through a structured brainstorming approach of challenge-solution fits [130, 131]. The challenges are developed from the automotive megatrends and solutions are proposed by the future applications of the quantum internet.

The automotive use cases are shown on the vertical axis of Figure II.4.5, and we assessed the potential of applying quantum internet applications (horizontal axis) to these use cases.

Autonomous driving and connectivity

The autonomous driving and connectivity megatrend has relationships across the entire range of quantum internet applications. Use-cases pertaining to optimization of routes and traffic are both related to distributed quantum computing as well as enhanced sensing: having more quantum computing power available in a distributed fashion can allow for improved calculations on efficient traffic flows. Especially the creation of VANETs can benefit from blind quantum computing and anonymous transmission in communication and complex decision processing (see Sec. II.4.2.1). The quantum communication protocols we already know to provide enhanced privacy, security or anonymity are potentially relevant for all automotive use cases related to communication or security.

Furthermore, local autonomous decisions can be aided with enhanced sensory input from quantum sensors. As previously discussed, quantum accelerometers can aid GNSS-denied areas by enabling inertia-navigation (see Sec. II.4.2.1), offering a substantial enhancement of accelerometer stability 50-100 fold over their classical equivalent.

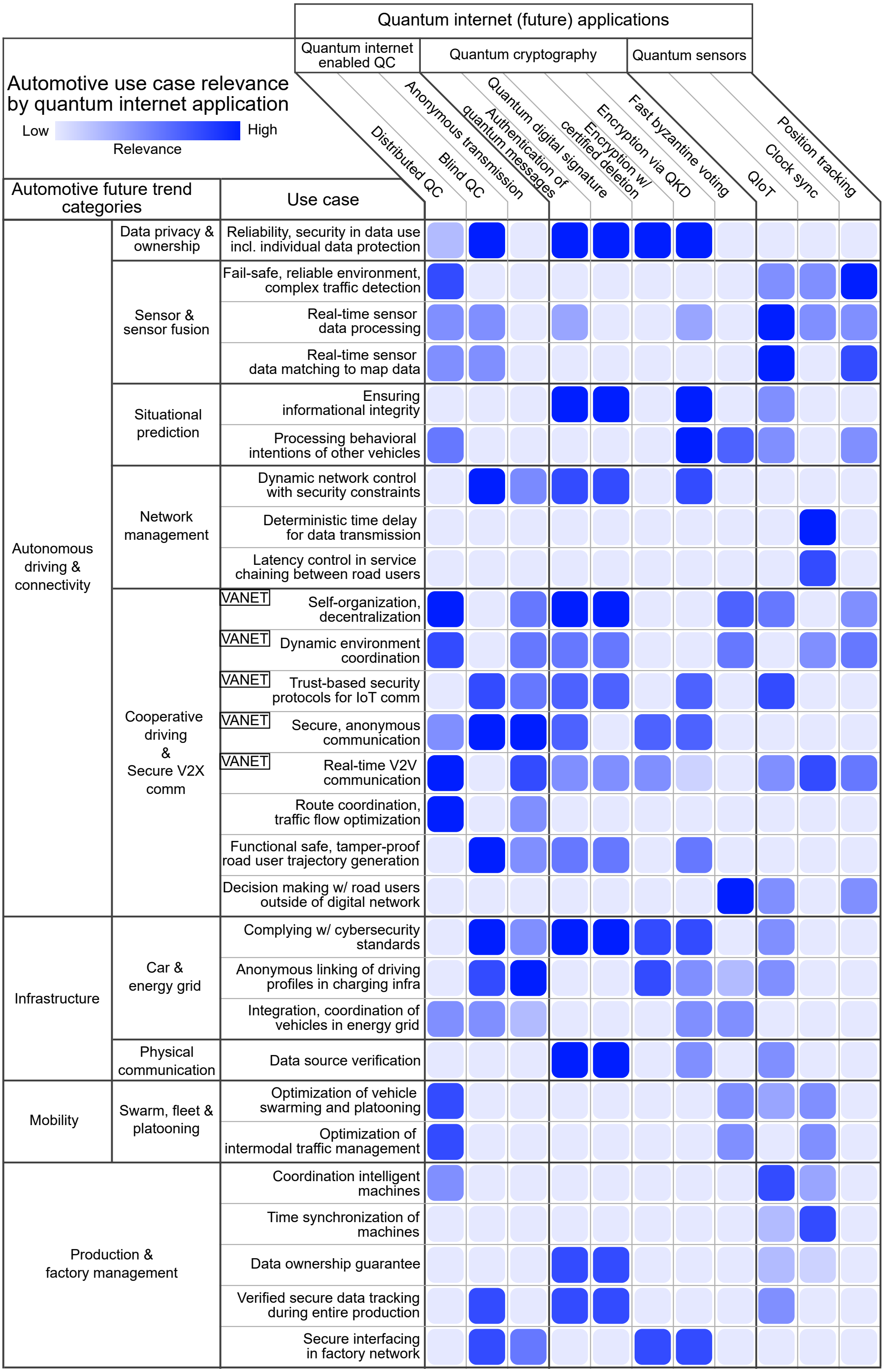
Quantum internet (future) applications
Quantum internet enabled QC
Quantum cryptography
Quantum sensors
Automotive use case relevance by quantum internet application
Low
High
Relevance
Distributed QC
Blind QC
Anonymous transmission
Authentication of quantum messages
Quantum digital signature
Encryption w/ certified deletion
Encryption via QKD
Fast byzantine voting
QIoT
Clock sync
Position tracking
Automotive future trend categories
Use case
Autonomous driving & connectivity
Data privacy & ownership
Reliability, security in data use incl. individual data protection
Sensor & sensor fusion
Fail-safe, reliable environment, complex traffic detection
Real-time sensor data processing
Real-time sensor data matching to map data
Situational prediction
Ensuring informational integrity
Processing behavioral intentions of other vehicles
Network management
Dynamic network control with security constraints
Deterministic time delay for data transmission
Latency control in service chaining between road users
Cooperative driving & Secure V2X comm
VANET Self-organization, decentralization
VANET Dynamic environment coordination
VANET Trust-based security protocols for IoT comm
VANET Secure, anonymous communication
VANET Real-time V2V communication
Route coordination, traffic flow optimization
Functional safe, tamper-proof road user trajectory generation
Decision making w/ road users outside of digital network
Infrastructure
Car & energy grid
Complying w/ cybersecurity standards
Anonymous linking of driving profiles in charging infra
Integration, coordination of vehicles in energy grid
Physical communication
Data source verification
Mobility
Swarm, fleet & platooning
Optimization of vehicle swarming and platooning
Optimization of intermodal traffic management
Production & factory management
Coordination intelligent machines
Time synchronization of machines
Data ownership guarantee
Verified secure data tracking during entire production
Secure interfacing in factory network

Figure II.4.5: **Automotive megatrends, use cases and the quantum internet future applications.** We list the automotive future trends (vertical axis) as discussed in Section II.4.2.2, defined by the German umbrella association for automotive [113]. We developed several use cases per trend and evaluate the relevancy of those use cases to quantum internet future applications (horizontal axis). The relevancy can be read bidirectionally for each trend.

Other quantum sensors can provide enhanced light detection and ranging (LiDAR), offering a factor 4 theoretical improvement in signal-to-noise ratio compared to optimal classical radar and a theoretical factor $\sqrt{2}$ improvement in precision for target distance measurement [132]. This topic can be combined for sensors to enable high precision multi-parameter optimization.

Additionally we recognize the potential of fast Byzantine voting (see Sec. II.4.2.1) to aid local decision making between ensembles of vehicles interacting in traffic situations. This can allow for fewer-round decision making as well as preventing bad actors from disturbing traffic flow or reducing the safety of traffic participants [53, 133]. Important to note is that, although the concepts of Byzantine voting are well developed within classical and quantum information theory, applications within the context of automotive as described specifically using quantum connectivity require the collaboration and input from both domains to find solutions that can be applied to real-life challenges. Such a collaboration benefits specifically from finding solutions that provide an improvement that can proven theoretically (from quantum network theory perspective) and has potential to be implemented practically (from the automotive perspective).

Infrastructure

There are interfaces between the megatrend of infrastructure around electric charging/V2L/V2G (see Sec. II.4.2.2) and cybersecurity with blind quantum computing, anonymous transmission, and all quantum cryptography protocols pertaining to authentication and verification (see Sec. II.4.2.1). We recognize that the quantum internet can provide tools to ensure anonymity. Quantum authentication and signatures can help provide data source verification resistant to quantum attacks. Fast Byzantine voting can aid in finding consents in a V2G connected network, as it is a network with many actors with fast and live changes on power demands, while ensuring privacy among cars and without requiring privileged members or leader election. This could be used for the coordination of vehicles at charging stations, even if one car shares misinformation.

Not mentioned in Figure II.4.5 are the reverse use cases where automotive technology can provide use cases for the quantum internet. Their implementation is too uncertain to consider in the relevancy analysis. For example, the concept of quantum edge computing becomes feasible with the appropriate infrastructure support from telecommunications and the automotive. Quantum processing tasks can be delegated in a blind or non-blind way to a more powerful quantum computer close by, while having a smaller quantum computer available locally in the vehicle that has the ability to teleport information to/from this edge quantum computer.

Complementary, we notice the possibility of vehicle-supporting infrastructure to provide quantum states either (1) statically through charging ports, where a car is loaded with quantum states to an integrated quantum memory or even (2) dynamically even while driving through free-space connections we shall denote as quantum antennas. Proposed research directions can include:

- Optimization of geographical positioning of quantum antennas within urban areas
- Protocol development and standardization of free-space communication architectures to distribute flying qubits
- Development of antenna hardware for multiple-party sending and receiving of single photons for entanglement generation

Beneficial to this cause is the development of the 6G standard, which conceptually attempts to incorporate the requirement that quantum networks could put on the classical internet, i.e. low-latency and incorporation of quantum-generated classical encryption keys. This trend will continue for communication standards beyond 6G, allowing for continued integration of quantum networks within communication standards.

Mobility & logistic concepts

The mobility & logistic concepts megatrend focuses on new types of logistical concepts that can be applicable for management of vehicles and transport systems. As such, it is a topic that has considerably less overlap with quantum internet future trends. Only a few interfaces stand out: first, the organization and planning of swarming and platooning using distributed quantum computing resources. This can be performed with minimal (dynamical) input from the vehicles themselves. Second, vehicle-group alignment in decision making through fast Byzantine voting and clock distribution. This latter trend can benefit from focused collaborative research of quantum computer scientists and the automotive, as mentioned above in Section II.4.3.3, to identify whether or not there is an (theoretical) advantage in leveraging these quantum internet applications for swarms or platoons.

Not mentioned in Figure II.4.5 are potentially new mobility concepts that include ridesharing and flexible car renting. These could potentially benefit from integration with cross-platform financing using a quantum money scheme[7] to verify payments [134, 135], to securely verify identities using quantum digital signatures. Recently this has been shown to be applicable to e-commerce platforms [136], which is conceptually similar to the transactions surrounding flexible car renting. However, while valuable ideas for future applications, these use cases are too uncertain in relevancy for the automotive and thus omitted from the interfacing analysis.

Production

We specifically see a role for privacy preserving analytics in the digital and data trend of production, to guarantee the security and uniqueness of data processed and generated in production factories using quantum authentication and signatures.

[7] A quantum money scheme is a cryptographic protocol that uses the concepts of superposition and no-cloning to ensure its uniqueness and prevent counterfeiting.

II.4.4. Conclusion

We have presented a multi-layered use case analysis of the quantum internet's current research tracks and long-term applications applied to all facets of the automotive industry. We employed a method where cross-platform megatrend relevancy is qualitatively assessed. This method was successful in finding potential synergies between trends in the quantum internet and the automotive. Given the generality of the method it can further be applied to any arbitrary industry, allowing for a structured approach to cross-platform use case development of the quantum internet.

We compiled megatrends of the quantum internet based on current research tracks for a <10 year horizon and mapped their relevancy by level of quantum internet functionality. This comprehensive mapping is a first attempt at a hardware-agnostic trend analysis in the quantum internet domain. This will serve as foundation for further use case research for other industries than the automotive. With this mapping we have qualitatively evaluated which of these quantum internet megatrends have mutual relevance with pre-production engineering process requirements for the automotive sector.

Together these two mappings combined to a synergy evaluation where strong synergy potential has been found in quantum internet hardware miniaturization and automation for vehicle & infrastructure development, as well as for quantum internet software development on the quantum network stack to provide input on regulations for the automotive. Additionally, we find that supply-chain availability is a strong driver for allowing next generation quantum hardware to be included in the vehicle development cycle.

We evaluated megatrends on the ≥ 10 year horizon and produced a list of future use cases for the automotive. We assessed which quantum internet future applications are of potential interest to add value or functionality to the automotive use case. We have found that connected quantum sensors have the potential to serve in high precision multi-parameter optimization. Additionally, there is considerable potential for incorporating blind quantum computing, anonymous transmission and quantum authentication and signatures to augment the security and privacy aspects of V2G and autonomous driving, in particular in VANETs.

II.4.5. Recommendation for Action

We have identified potential interfaces for quantum internet applications to be integrated into automotive products and processes. However, this analysis assumes optimal implementation conditions that may be difficult to achieve in practice. The deployment of these applications requires deep knowledge of quantum technologies as well as expertise on manufacturing, engineering production processes and more. Accumulating this knowledge requires a substantial investment both from the quantum internet and the automotive domain in research and development. Venturing into this shared domain poses significant strategic risks due to the many challenges and unclear feasibility of quantum technologies. Pursuing such an initiative is therefore only recommended for companies with a first mover strategy, or those willing to take high-risk, long-term endeavors.

A possible route for the automotive industry to develop in this area is to build up know-how in the field of the quantum internet through academic collaborations. By leveraging those collaborations, the automotive industry can gain exposure to the quantum internet domain at an early stage without substantial investments. They can take a passive approach by observing the activities in the quantum internet domain, or choose a more active approach by participating in co-creating novel applications and communicate pre-development requirements. The earlier such a collaboration is started, the higher the probability that assimilation of quantum internet applications is eased in the automotive ecosystem. The close collaboration between the automotive industry and academic groups therefore occupies a crucial role in driving a shared development. In the academic context, the automotive pre-PDP requirements and knowledge about mass production could benefit the quantum internet field at this early stage. Venturing, cooperatively funded projects and commercial testbeds of relatively mature applications (miniaturization, environmental resilience, sensor integration) could further strengthen the intersection of these domains.

Lastly, the extensive analysis of this paper helped identify several fundamental research topics that are unexplored that provide interesting possibilities for an academic or start-up venture collaboration between the quantum internet and automotive: theoretical and algorithm development for quantum communication powered VANETs focused on fast Byzantine voting, adversarial-proof decision making and collaborative QIoT for multi-parameter optimization can be first steps towards predicting quantum advantage of quantum enabled interconnected vehicles.

DISCLAIMER

The results, opinions and conclusions expressed in this publication are not necessarily those of Porsche Digital GmbH or Audi AG.

ACKNOWLEDGEMENTS

We would like to thank Prof. Dr. ir. Ronald Hanson, Dr. Mahdi Manesh, Claudia Schwarz, Stefan Zerweck and Mattias Ulbrich for their support and the opportunity to perform this analysis. Dr. Clemens Wickboldt, Amirtharaj Amirthalingam and Dr. Sjoerd Loenen for the critical discussions and feedback on the manuscript. Laura Ohff, Dr. Marie-Christine Slater for useful discussions at the start of this project.

Funding: We acknowledge funding the Dutch Research Council (NWO) through the project “QuTech Part II Applied-oriented research” (project number 601.QT.001). We further acknowledge funding through the BMBF (HYBRID) and Porsche Digital GmbH.
Competing interests: The authors declare no competing interests.
Data and materials availability: The data supporting this manuscript is available at 4TU.ResearchData [137].

II.4

REFERENCES

[1] NHTSA, *Automated Vehicles for Safety - NHTSA,* .

[2] L. Lakshmanan, *The story of evolution of the in-car infotainment system (with special throwback to the 1990s),* (2024).

[3] G. Abdelkader, K. Elgazzar, and A. Khamis, *Connected Vehicles: Technology Review, State of the Art, Challenges and Opportunities,* Sensors **21**, 7712 (2021).

[4] S. Checkoway, D. McCoy, B. Kantor, D. Anderson, H. Shacham, S. Savage, K. Koscher, A. Czeskis, F. Roesner, and T. Kohno, *Comprehensive experimental analyses of automotive attack surfaces,* in *20th USENIX Security Symposium (USENIX Security 11)* (USENIX Association, San Francisco, CA, 2011).

[5] H. Olufowobi and G. Bloom, *Connected Cars: Automotive Cybersecurity and Privacy for Smart Cities,* in *Smart Cities Cybersecurity and Privacy*, edited by D. B. Rawat and K. Z. Ghafoor (Elsevier, 2019) Chap. 16, pp. 227–240.

[6] S. K. Khan, N. Shiwakoti, P. Stasinopoulos, and Y. Chen, *Cyber-attacks in the next-generation cars, mitigation techniques, anticipated readiness and future directions,* Accident Analysis & Prevention **148**, 105837 (2020).

[7] J. Takahashi, M. Iwamura, and M. Tanaka, *Security Threat Analysis of Automotive Infotainment Systems,* in *2020 IEEE 92nd Vehicular Technology Conference (VTC2020-Fall)* (2020) pp. 1–7.

[8] I. Pekaric, C. Sauerwein, S. Haselwanter, and M. Felderer, *A taxonomy of attack mechanisms in the automotive domain,* Computer Standards & Interfaces **78**, 103539 (2021).

[9] V. Renganathan, E. Yurtsever, Q. Ahmed, and A. Yener, *Valet attack on privacy: a cybersecurity threat in automotive Bluetooth infotainment systems,* Cybersecurity **5**, 30 (2022).

[10] P. Shor, *Algorithms for quantum computation: discrete logarithms and factoring,* in *Proceedings 35th Annual Symposium on Foundations of Computer Science* (1994) pp. 124–134.

[11] L. K. Grover, *A fast quantum mechanical algorithm for database search,* in *Proceedings of the twenty-eighth annual ACM symposium on Theory of Computing*, STOC '96 (Association for Computing Machinery, New York, NY, USA, 1996) pp. 212–219.

[12] S. Lloyd, *Universal Quantum Simulators,* Science **273**, 1073 (1996).

[13] J. Preskill, *Quantum Computing in the NISQ era and beyond,* Quantum **2**, 79 (2018).

[14] H. J. Kimble, *The quantum internet,* Nature **453**, 1023 (2008).

[15] S. Wehner, D. Elkouss, and R. Hanson, *Quantum internet: A vision for the road ahead,* Science **362**, eaam9288 (2018).

[16] W. C. Campbell and P. Hamilton, *Rotation sensing with trapped ions,* Journal of Physics B: Atomic, Molecular and Optical Physics **50**, 064002 (2017).

[17] C. Degen, F. Reinhard, and P. Cappellaro, *Quantum sensing,* Reviews of Modern Physics **89**, 035002 (2017).

[18] S. Pirandola, B. R. Bardhan, T. Gehring, C. Weedbrook, and S. Lloyd, *Advances in photonic quantum sensing,* Nature Photonics **12**, 724 (2018).

[19] S. Yarkoni, F. Neukart, E. M. G. Tagle, N. Magiera, B. Mehta, K. Hire, S. Narkhede, and M. Hofmann, *Quantum Shuttle: traffic navigation with Quantum computing,* in *Proceedings of the 1st ACM SIGSOFT International Workshop on Architectures and Paradigms for Engineering Quantum Software*, APEQS 2020 (Association for Computing Machinery, New York, NY, USA, 2020) pp. 22–30.

[20] O. Burkacky, L. Pautasso, and N. Mohr, *Will quantum computing drive the automotive future,* (2020).

[21] A. Bayerstadler, G. Becquin, J. Binder, T. Botter, H. Ehm, T. Ehmer, M. Erdmann, N. Gaus, P. Harbach, M. Hess, J. Klepsch, M. Leib, S. Luber, A. Luckow, M. Mansky, W. Mauerer, F. Neukart, C. Niedermeier, L. Palackal, R. Pfeiffer, C. Polenz, J. Sepulveda, T. Sievers, B. Standen, M. Streif, T. Strohm, C. Utschig-Utschig, D. Volz, H. Weiss, and F. Winter, *Industry quantum computing applications,* EPJ Quantum Technology **8**, 25 (2021).

[22] S. Yarkoni, A. Alekseyenko, M. Streif, D. Von Dollen, F. Neukart, and T. Bäck, *Multi-car paint shop optimization with quantum annealing,* in *2021 IEEE International Conference on Quantum Computing and Engineering (QCE)* (IEEE, 2021) pp. 35–41.

[23] D. Bouwmeester, J.-W. Pan, K. Mattle, M. Eibl, H. Weinfurter, and A. Zeilinger, *Experimental quantum teleportation,* Nature **390**, 575 (1997).

[24] R. Van Meter, *Teleportation,* in *Quantum Networking* (John Wiley & Sons, Ltd, 2014) Chap. 4, pp. 79–89.

[25] W. K. Wootters and W. H. Zurek, *A single quantum cannot be cloned,* Nature **299**, 802 (1982).

[26] C. H. Bennett and G. Brassard, *Quantum cryptography: Public key distribution and coin tossing,* Theoretical Computer Science Theoretical Aspects of Quantum Cryptography – celebrating 30 years of BB84, **560**, 7 (2014).

[27] R. Van Meter, *Purification and entanglement swapping-based repeaters,* in *Quantum Networking* (John Wiley & Sons, Ltd, 2014) Chap. 10, pp. 195–217.

[28] A. K. Ekert, *Quantum cryptography based on Bell's theorem,* Physical Review Letters **67**, 661 (1991).

[29] R. Van Meter, *Quantum key distribution,* in *Quantum Networking* (John Wiley & Sons, Ltd, 2014) Chap. 5, pp. 91–111.

[30] M. Stanley, Y. Gui, D. Unnikrishnan, S. Hall, and I. Fatadin, *Recent progress in quantum key distribution network deployments and standards,* in *Journal of Physics: Conference Series*, Vol. 2416 (IOP Publishing, 2022) p. 012001.

[31] ID Quantique, *Quantum-Safe Security Products,* (2024).

[32] Toshiba, *Quantum Key Distribution - What Is QKD? How Does It Work?* (2024).

[33] MagiQ Technologies, *MagiQ QPN™| Network Security | Somerville, MA,* (2024).

[34] Quintessence Labs, *QOptica™ Quantum Key Distribution Product Sheet,* .

[35] NIST, *Post-quantum cryptography standardization,* (2024).

[36] Horizon Europe, *Quantum Internet Alliance - Phase1,* .

[37] P. C. Humphreys, N. Kalb, J. P. J. Morits, R. N. Schouten, R. F. L. Vermeulen, D. J. Twitchen, M. Markham, and R. Hanson, *Deterministic delivery of remote entanglement on a quantum network,* Nature **558**, 268 (2018).

[38] M. Pompili, S. L. N. Hermans, S. Baier, H. K. C. Beukers, P. C. Humphreys, R. N. Schouten, R. F. L. Vermeulen, M. J. Tiggelman, L. dos Santos Martins, B. Dirkse, S. Wehner, and R. Hanson, *Realization of a multinode quantum network of remote solid-state qubits,* Science **372**, 259 (2021).

[39] J.-L. Liu, X.-Y. Luo, Y. Yu, C.-Y. Wang, B. Wang, Y. Hu, J. Li, M.-Y. Zheng, B. Yao, Z. Yan, D. Teng, J.-W. Jiang, X.-B. Liu, X.-P. Xie, J. Zhang, Q.-H. Mao, X. Jiang, Q. Zhang, X.-H. Bao, and J.-W. Pan, *A multinode quantum network over a metropolitan area,* (2023).

[40] J. V. Rakonjac, S. Grandi, S. Wengerowsky, D. Lago-Rivera, F. Appas, and H. d. Riedmatten, *Transmission of light–matter entanglement over a metropolitan network,* Optica Quantum **1**, 94 (2023).

[41] A. J. Stolk, K. L. van der Enden, M.-C. Slater, I. te Raa-Derckx, P. Botma, J. van Rantwijk, J. J. B. Biemond, R. A. J. Hagen, R. W. Herfst, W. D. Koek, A. J. H. Meskers, R. Vollmer, E. J. van Zwet, M. Markham, A. M. Edmonds, J. F. Geus, F. Elsen, B. Jungbluth, C. Haefner, C. Tresp, J. Stuhler, S. Ritter, and R. Hanson, *Metropolitan-scale heralded entanglement of solid-state qubits,* Science Advances **10**, eadp6442 (2024).

[42] IBISWorld, *IBISWorld - Industry Market Research, Reports, and Statistics,* (2024).

[43] The European Automobile Manufacturers' Association, *The automobile industry: Pocket guide 2023/2024,* (2023).

[44] The European Automobile Manufacturers' Association, *R&D investment by top 10 industrial sectors in the EU,* (2023).

[45] A. Hafner and D. Modic, *European automotive technological innovation systems in the age of disruption: The suppliers' view,* Research in Social Change **12**, 53 (2020).

[46] M. Broy, *Challenges in automotive software engineering,* in *Proceedings of the 28th international conference on Software engineering*, ICSE '06 (Association for Computing Machinery, New York, NY, USA, 2006) pp. 33–42.

[47] H.-T. Lim, L. Völker, and D. Herrscher, *Challenges in a future ip/ethernet-based in-car network for real-time applications,* in *2011 48th ACM/EDAC/IEEE Design Automation Conference (DAC)* (2011) pp. 7–12.

[48] S. Greengard, *Automotive systems get smarter,* Commun. ACM **58**, 18–20 (2015).

[49] G. Macher, A. Höller, E. Armengaud, and C. Kreiner, *Automotive embedded software: Migration challenges to multi-core computing platforms,* in *2015 IEEE 13th International Conference on Industrial Informatics (INDIN)* (2015) pp. 1386–1393.

[50] N. Navet and F. Simonot-Lion, *Automotive embedded systems handbook* (CRC press, 2017).

[51] O. Burkacky, J. Deichmann, and J. P. Stein, *Automotive software and electronics 2030,* (2019).

[52] SAE International, *J3016_202104: Taxonomy and Definitions for Terms Related to Driving Automation Systems for On-Road Motor Vehicles,* .

[53] S. Malik and W. Sun, *Analysis and Simulation of Cyber Attacks Against Connected and Autonomous Vehicles,* in *2020 International Conference on Connected and Autonomous Driving (MetroCAD)* (2020) pp. 62–70.

[54] N. Lu, N. Cheng, N. Zhang, X. Shen, and J. W. Mark, *Connected Vehicles: Solutions and Challenges,* IEEE Internet of Things Journal **1**, 289 (2014).

[55] E. Farsimadan, F. Palmieri, L. Moradi, D. Conte, and B. Paternoster, *Vehicle-to-Everything (V2X) Communication Scenarios for Vehicular Ad-hoc Networking (VANET): An Overview,* in *Computational Science and Its Applications – ICCSA 2021*, edited by O. Gervasi, B. Murgante, S. Misra, C. Garau, I. Blečić, D. Taniar, B. O. Apduhan, A. M. A. C. Rocha, E. Tarantino, and C. M. Torre (Springer International Publishing, Cham, 2021) pp. 15–30.

[56] ISO, *ISO 16750-1:2023 Road vehicles - Environmental conditions and testing for electrical and electronic equipment,* (2023).

[57] S. Rudert and J. Trumpfheller, *Well considered - the product development process,* (2015).

[58] H. Winner, S. Hakuli, and G. Wolf, *Sensorik fuŕ fahrerassistenzsysteme,* in *Handbuch Fahrerassistenzsysteme: Grundlagen, Komponenten und Systeme für aktive Sicherheit und Komfort* (Springer-Verlag, 2011) Chap. 15, pp. 221–228.

[59] E. Filipovic and A.-M. Großmann, *Npd knowledge transfer via standards and patents? a case study,* in *ISPIM Conference Proceedings* (The International Society for Professional Innovation Management (ISPIM), filipovic2014npd) p. 1.

II.4

[60] S. Singh, M. Doosti, N. Mathur, M. Delavar, A. Mantri, H. Ollivier, and E. Kashefi, *Towards a unified quantum protocol framework: Classification, implementation, and use cases,* (2023), arXiv:2310.12780 [quant-ph] .

[61] D. Awschalom, K. K. Berggren, H. Bernien, S. Bhave, L. D. Carr, P. Davids, S. E. Economou, D. Englund, A. Faraon, M. Fejer, S. Guha, M. V. Gustafsson, E. Hu, L. Jiang, J. Kim, B. Korzh, P. Kumar, P. G. Kwiat, M. Lončar, M. D. Lukin, D. A. Miller, C. Monroe, S. W. Nam, P. Narang, J. S. Orcutt, M. G. Raymer, A. H. Safavi-Naeini, M. Spiropulu, K. Srinivasan, S. Sun, J. Vučković, E. Waks, R. Walsworth, A. M. Weiner, and Z. Zhang, *Development of Quantum Interconnects (QuICs) for Next-Generation Information Technologies,* PRX Quantum **2**, 017002 (2021).

[62] A. Broadbent, J. Fitzsimons, and E. Kashefi, *Universal Blind Quantum Computation,* in *2009 50th Annual IEEE Symposium on Foundations of Computer Science* (2009) pp. 517–526.

[63] J. F. Fitzsimons and E. Kashefi, *Unconditionally verifiable blind quantum computation,* Physical Review A **96**, 012303 (2017).

[64] M. Christandl and S. Wehner, *Quantum Anonymous Transmissions,* in *Advances in Cryptology - ASIACRYPT 2005*, edited by B. Roy (Springer, Berlin, Heidelberg, 2005) pp. 217–235.

[65] J. Bouda and J. Sprojcar, *Anonymous Transmission of Quantum Information,* in *2007 First International Conference on Quantum, Nano, and Micro Technologies (ICQNM'07)* (2007) pp. 12–12.

[66] A. Unnikrishnan, I. J. MacFarlane, R. Yi, E. Diamanti, D. Markham, and I. Kerenidis, *Anonymity for practical quantum networks,* Phys. Rev. Lett. **122**, 240501 (2019).

[67] H. Barnum, C. Crépeau, D. Gottesman, A. Smith, and A. Tapp, *Authentication of quantum messages,* in *The 43rd Annual IEEE Symposium on Foundations of Computer Science, 2002. Proceedings.* (IEEE, 2002) pp. 449–458.

[68] D. Gottesman and I. Chuang, *Quantum digital signatures,* (2001), arXiv:quant-ph/0105032 [quant-ph] .

[69] I. V. Puthoor, R. Amiri, P. Wallden, M. Curty, and E. Andersson, *Measurement-device-independent quantum digital signatures,* Physical Review A **94**, 022328 (2016).

[70] F.-L. Chen, W.-F. Liu, S.-G. Chen, and Z.-H. Wang, *Public-key quantum digital signature scheme with one-time pad private-key,* Quantum Information Processing **17**, 10 (2017).

[71] A. Broadbent and R. Islam, *Quantum encryption with certified deletion,* in *Theory of Cryptography: 18th International Conference, TCC 2020, Durham, NC, USA, November 16–19, 2020, Proceedings, Part III 18* (Springer, 2020) pp. 92–122.

[72] J.-H. Chen, M.-R. Chen, G.-Q. Zeng, and J.-S. Weng, *Bdfl: A byzantine-fault-tolerance decentralized federated learning method for autonomous vehicle,* IEEE Transactions on Vehicular Technology **70**, 8639 (2021).

[73] C.-F. Cheng, G. Srivastava, J. C.-W. Lin, and Y.-C. Lin, *Fault-tolerance mechanisms for software-defined internet of vehicles,* IEEE Transactions on Intelligent Transportation Systems **22**, 3859 (2021).

[74] M. Ben-Or and A. Hassidim, *Fast quantum byzantine agreement,* in *Proceedings of the Thirty-Seventh Annual ACM Symposium on Theory of Computing*, STOC '05 (Association for Computing Machinery, New York, NY, USA, 2005) p. 481–485.

[75] V. Giovannetti, S. Lloyd, and L. Maccone, *Quantum-enhanced positioning and clock synchronization,* Nature **412**, 417 (2001).

[76] M. Lipiński, T. Włostowski, J. Serrano, and P. Alvarez, *White rabbit: A ptp application for robust sub-nanosecond synchronization,* in *2011 IEEE International Symposium on Precision Clock Synchronization for Measurement, Control and Communication* (IEEE, 2011) pp. 25–30.

[77] S. Templier, P. Cheiney, Q. d'Armagnac de Castanet, B. Gouraud, H. Porte, F. Napolitano, P. Bouyer, B. Battelier, and B. Barrett, *Tracking the vector acceleration with a hybrid quantum accelerometer triad,* Science Advances **8**, eadd3854 (2022).

[78] C. Salducci, Y. Bidel, M. Cadoret, S. Darmon, N. Zahzam, A. Bonnin, S. Schwartz, C. Blanchard, and A. Bresson, *Quantum sensing of acceleration and rotation by interfering magnetically launched atoms,* Science Advances **10**, eadq4498 (2024).

[79] B. Battelier, B. Barrett, L. Fouché, L. Chichet, L. Antoni-Micollier, H. Porte, F. Napolitano, J. Lautier, A. Landragin, and P. Bouyer, *Development of compact cold-atom sensors for inertial navigation,* in *Quantum Optics*, Vol. 9900 (SPIE, 2016) pp. 21–37.

[80] S. Gauthier, G. Vardoyan, and S. Wehner, *A control architecture for entanglement generation switches in quantum networks,* in *Proceedings of the 1st Workshop on Quantum Networks and Distributed Quantum Computing*, QuNet '23 (Association for Computing Machinery, New York, NY, USA, 2023) p. 38–44.

[81] S. Gauthier, T. Vasantam, and G. Vardoyan, *An on-demand resource allocation algorithm for a quantum network hub and its performance analysis,* (2024), arXiv:2405.18066 [quant-ph] .

[82] J. Rabbie, K. Chakraborty, G. Avis, and S. Wehner, *Designing quantum networks using preexisting infrastructure,* npj Quantum Information **8**, 1 (2022).

[83] G. Vardoyan, M. Skrzypczyk, and S. Wehner, *On the quantum performance evaluation of two distributed quantum architectures,* ACM SIGMETRICS Performance Evaluation Review **49**, 30 (2022).

II.4

[84] Á. G. Iñesta and S. Wehner, *Performance metrics for the continuous distribution of entanglement in multiuser quantum networks,* Physical Review A **108**, 052615 (2023).

[85] P. Drmota, D. P. Nadlinger, D. Main, B. C. Nichol, E. M. Ainley, D. Leichtle, A. Mantri, E. Kashefi, R. Srinivas, G. Araneda, C. J. Ballance, and D. M. Lucas, *Verifiable blind quantum computing with trapped ions and single photons,* (2024).

[86] C. Bradac, W. Gao, J. Forneris, M. E. Trusheim, and I. Aharonovich, *Quantum nanophotonics with group iv defects in diamond,* Nature Communications **10**, 5625 (2019).

[87] N. T. Son, C. P. Anderson, A. Bourassa, K. C. Miao, C. Babin, M. Widmann, M. Niethammer, J. Ul Hassan, N. Morioka, I. G. Ivanov, F. Kaiser, J. Wrachtrup, and D. D. Awschalom, *Developing silicon carbide for quantum spintronics,* Applied Physics Letters **116**, 190501 (2020).

[88] S. Simmons, *Scalable Fault-Tolerant Quantum Technologies with Silicon Color Centers,* PRX Quantum **5**, 010102 (2024).

[89] I. Esmaeil Zadeh, J. W. N. Los, R. B. M. Gourgues, V. Steinmetz, G. Bulgarini, S. M. Dobrovolskiy, V. Zwiller, and S. N. Dorenbos, *Single-photon detectors combining high efficiency, high detection rates, and ultra-high timing resolution,* APL Photonics **2**, 111301 (2017).

[90] M. Bock, P. Eich, S. Kucera, M. Kreis, A. Lenhard, C. Becher, and J. Eschner, *High-fidelity entanglement between a trapped ion and a telecom photon via quantum frequency conversion,* Nature Communications **9**, 1998 (2018).

[91] A. Dréau, A. Tchebotareva, A. E. Mahdaoui, C. Bonato, and R. Hanson, *Quantum frequency conversion of single photons from a nitrogen-vacancy center in diamond to telecommunication wavelengths,* Phys. Rev. Appl. **9**, 064031 (2018).

[92] T. van Leent, M. Bock, R. Garthoff, K. Redeker, W. Zhang, T. Bauer, W. Rosenfeld, C. Becher, and H. Weinfurter, *Long-Distance Distribution of Atom-Photon Entanglement at Telecom Wavelength,* Physical Review Letters **124**, 010510 (2020).

[93] M. Schäfer, B. Kambs, D. Herrmann, T. Bauer, and C. Becher, *Two-stage, low noise quantum frequency conversion of single photons from silicon-vacancy centers in diamond to the telecom c-band,* Advanced Quantum Technologies , 2300228 (2023).

[94] J. Geus, F. Elsen, S. Nyga, A. Stolk, K. van der Enden, E. van Zwet, C. Haefner, R. Hanson, and B. Jungbluth, *Low-noise short-wavelength pumped frequency down-conversion for quantum frequency converters,* (2023).

[95] A. Sipahigil, R. E. Evans, D. D. Sukachev, M. J. Burek, J. Borregaard, M. K. Bhaskar, C. T. Nguyen, J. L. Pacheco, H. A. Atikian, C. Meuwly, R. M. Camacho, F. Jelezko, E. Bielejec, H. Park, M. Lončar, and M. D. Lukin, *An integrated diamond nanophotonics platform for quantum-optical networks,* Science **354**, 847–850 (2016).

[96] P.-J. Stas, Y. Q. Huan, B. Machielse, E. N. Knall, A. Suleymanzade, B. Pingault, M. Sutula, S. W. Ding, C. M. Knaut, D. R. Assumpcao, Y.-C. Wei, M. K. Bhaskar, R. Riedinger, D. D. Sukachev, H. Park, M. Lončar, D. S. Levonian, and M. D. Lukin, *Robust multi-qubit quantum network node with integrated error detection,* Science **378**, 557 (2022).

[97] M. Pasini, N. Codreanu, T. Turan, A. R. Moral, C. F. Primavera, L. D. Santis, H. K. C. Beukers, J. M. Brevoord, C. Waas, J. Borregaard, and R. Hanson, *Nonlinear quantum photonics with a tin-vacancy center coupled to a one-dimensional diamond waveguide,* (2023), arXiv:2311.12927 [quant-ph] .

[98] R. A. Parker, J. Arjona Martínez, K. C. Chen, A. M. Stramma, I. B. Harris, C. P. Michaels, M. E. Trusheim, M. Hayhurst Appel, C. M. Purser, W. G. Roth, D. Englund, and M. Atatüre, *A diamond nanophotonic interface with an optically accessible deterministic electronuclear spin register,* Nature Photonics **18**, 156 (2024).

[99] J.-S. Park, S. Subramanian, L. Lampert, T. Mladenov, I. Klotchkov, D. J. Kurian, E. Juarez-Hernandez, B. Perez-Esparza, S. R. Kale, K. T. Asma Beevi, S. Premaratne, T. Watson, S. Suzuki, M. Rahman, J. B. Timbadiya, S. Soni, and S. Pellerano, *A Fully Integrated Cryo-CMOS SoC for Qubit Control in Quantum Computers Capable of State Manipulation, Readout and High-Speed Gate Pulsing of Spin Qubits in Intel 22nm FFL FinFET Technology,* in *2021 IEEE International Solid-State Circuits Conference (ISSCC)*, Vol. 64 (2021) pp. 208–210.

[100] A. Ruffino, T.-Y. Yang, J. Michniewicz, Y. Peng, E. Charbon, and M. F. Gonzalez-Zalba, *A cryo-CMOS chip that integrates silicon quantum dots and multiplexed dispersive readout electronics,* Nature Electronics **5**, 53 (2022).

[101] A. J. Stolk, K. L. van der Enden, M.-C. Roehsner, A. Teepe, S. O. J. Faes, C. E. Bradley, S. Cadot, J. van Rantwijk, I. te Raa, R. A. J. Hagen, A. Verlaan, J. Biemond, A. Khorev, R. Vollmer, M. Markham, A. Edmonds, J. Morits, T. Taminiau, E. van Zwet, and R. Hanson, *Telecom-Band Quantum Interference of Frequency-Converted Photons from Remote Detuned NV Centers,* PRX Quantum **3**, 020359 (2022).

[102] Gaurab Bose, *Google Cloud: Standard Tier Data Transfer now offers a 99.9% availability SLA,* Accessed through Wayback Machine 9 Feb 2024 (2023).

[103] K. Chakraborty, F. Rozpedek, A. Dahlberg, and S. Wehner, *Distributed routing in a quantum internet,* (2019), arXiv:1907.11630 [quant-ph] .

[104] C. Simon, *Towards a global quantum network,* Nature Photonics **11**, 678 (2017).

[105] L. de Forges de Parny, O. Alibart, J. Debaud, S. Gressani, A. Lagarrigue, A. Martin, A. Metrat, M. Schiavon, T. Troisi, E. Diamanti, P. Gélard, E. Kerstel, S. Tanzilli, and M. Van Den Bossche, *Satellite-based quantum information networks: use cases, architecture, and roadmap,* Communications Physics **6**, 1 (2023).

[106] C. Reimer, M. Kues, P. Roztocki, B. Wetzel, F. Grazioso, B. E. Little, S. T. Chu, T. Johnston, Y. Bromberg, L. Caspani, D. J. Moss, and R. Morandotti, *Generation of multi-photon entangled quantum states by means of integrated frequency combs,* Science **351**, 1176 (2016).

[107] M. J. Weaver, P. Duivestein, A. C. Bernasconi, S. Scharmer, M. Lemang, T. C. v. Thiel, F. Hijazi, B. Hensen, S. Gröblacher, and R. Stockill, *An integrated microwave-to-optics interface for scalable quantum computing,* Nature Nanotechnology **19**, 166 (2024).

[108] A. Dahlberg, M. Skrzypczyk, T. Coopmans, L. Wubben, F. Rozpundefineddek, M. Pompili, A. Stolk, P. Pawełczak, R. Knegjens, J. de Oliveira Filho, R. Hanson, and S. Wehner, *A link layer protocol for quantum networks,* in *Proceedings of the ACM Special Interest Group on Data Communication*, SIGCOMM '19 (Association for Computing Machinery, New York, NY, USA, 2019) p. 159–173.

[109] A. Dahlberg, B. v. d. Vecht, C. D. Donne, M. Skrzypczyk, I. t. Raa, W. Kozlowski, and S. Wehner, *NetQASM—a low-level instruction set architecture for hybrid quantum–classical programs in a quantum internet,* Quantum Science and Technology **7**, 035023 (2022).

[110] T. Coopmans, R. Knegjens, A. Dahlberg, D. Maier, L. Nijsten, J. de Oliveira Filho, M. Papendrecht, J. Rabbie, F. Rozpędek, M. Skrzypczyk, L. Wubben, W. de Jong, D. Podareanu, A. Torres-Knoop, D. Elkouss, and S. Wehner, *NetSquid, a NETwork Simulator for QUantum Information using Discrete events,* Communications Physics **4**, 1 (2021).

[111] X. Wu, A. Kolar, J. Chung, D. Jin, T. Zhong, R. Kettimuthu, and M. Suchara, *SeQUeNCe: a customizable discrete-event simulator of quantum networks,* Quantum Science and Technology **6**, 045027 (2021).

[112] QuTech, *Quantum Network Explorer ADK,* (2024).

[113] Forschungsvereinigung Automobiltechnik, Verband der Automobilindustrie, *Die Automobilitaẗ der Zukunft,* (2021).

[114] Forschungsvereinigung Automobiltechnik, Verband der Automobilindustrie, *Roadmap fur̈ die Automobilitaẗ der Zukunft,* (2021).

[115] A. Aspuru-Guzik, A. D. Dutoi, P. J. Love, and M. Head-Gordon, *Simulated quantum computation of molecular energies,* Science **309**, 1704 (2005).

[116] M. B. Hastings, D. Wecker, B. Bauer, and M. Troyer, *Improving quantum algorithms for quantum chemistry,* Quantum Info. Comput. **15**, 1–21 (2015).

[117] B. G. Q. Team, J. Klepsch, J. R. Finžgar, F. Kiwit, L. Hölscher, M. Erdmann, L. Müller, C. Kumar, and A. Luckow, *Quantum computing for automotive applications: From algorithms to applications,* (2024), arXiv:2409.14183 [quant-ph] .

II.4

[118] S. Campbell, N. O'Mahony, L. Krpalcova, D. Riordan, J. Walsh, A. Murphy, and C. Ryan, *Sensor Technology in Autonomous Vehicles : A review,* in *2018 29th Irish Signals and Systems Conference (ISSC)* (2018) pp. 1–4.

[119] plus10, *Allow machines to learn from each other across manufacturers,* (2022).

[120] UNECE, *UN Regulation No. 155 - Cyber security and cyber security management system,* (2021).

[121] UNECE, *UN Regulation No. 156 - Software update and software update management system,* (2021).

[122] ISO, *ISO/IEC 27001:2022 Information security, cybersecurity and privacy protection - Information security management systems - Requirements,* (2022).

[123] ISO/SAE, *ISO/SAE 21434:2021 Road vehicles - Cybersecurity engineering,* (2021).

[124] ISO, *ISO 26262-1:2018 Road Vehicles - Functional Safety,* (2018).

[125] A. Seeck, J. C. Gail, B. Lorenz, M. Zöller, U. Seiffert, E. Fritzsche, H. Mankau, C. Repmann, A. Eilemann, M. Jung, E. Pantow, A. Wiebelt, and J. Honeder, *Anforderungen, zielkonflikte, grundlagen,* in *Vieweg Handbuch Kraftfahrzeugtechnik* (Springer Fachmedien Wiesbaden, 2021) p. 15–123.

[126] U. Mans, J. Robbers, J. Rabbie, and T. van der Veen, *Mapping quantum supply chains: Towards european technology sovereignty in an emerging industry,* (2023).

[127] U. Mans, J. Robbers, J. Rabbie, and T. van der Veen, *Mapping the supply chains for quantum communication: Towards european technology sovereignty in an emerging industry,* (2023).

[128] OICA, *2023 production statistics,* (2023).

[129] IETF, *Quantum internet research group (qirg),* (2024).

[130] C. Meinel, L. Leifer, and H. Plattner, *Design thinking: Understand-improve-apply* (Springer, 2011).

[131] A. Wilms, R. Kirschner, and M. Manesh, *Der Prozess des agilen Forschungs- und Techniktransfers – ein Erfahrungsbericht aus der Industrie am Beispiel der Porsche Digital GmbH,* in *Chancen und Risiken von Quantentechnologien*, edited by A. Wilms and F. Neukart (Springer Fachmedien, Wiesbaden, 2022) pp. 89–100.

[132] G. Slepyan, S. Vlasenko, D. Mogilevtsev, and A. Boag, *Quantum Radars and Lidars: Concepts, realizations, and perspectives,* IEEE Antennas and Propagation Magazine **64**, 16 (2022).

[133] H. Liu, C.-W. Lin, E. Kang, S. Shiraishi, and D. M. Blough, *A Byzantine-Tolerant Distributed Consensus Algorithm for Connected Vehicles Using Proof-of-Eligibility,* in *Proceedings of the 22nd International ACM Conference on Modeling, Analysis and Simulation of Wireless and Mobile Systems*, MSWIM '19 (Association for Computing Machinery, New York, NY, USA, 2019) pp. 225–234.

II.4

[134] S. Wiesner, *Conjugate coding,* SIGACT News **15**, 78–88 (1983).

[135] D. Gavinsky, *Quantum Money with Classical Verification,* in *2012 IEEE 27th Conference on Computational Complexity* (2012) pp. 42–52.

[136] X.-Y. Cao, B.-H. Li, Y. Wang, Y. Fu, H.-L. Yin, and Z.-B. Chen, *Experimental quantum e-commerce,* Science Advances **10**, eadk3258 (2024).

[137] K. L. van der Enden, R. Kirschner, M. Krumtünger, and A. Wilms, *Data supporting manuscript,* (2024).

II.5

ADVANCING A RESPONSIBLE FUTURE QUANTUM INTERNET

K. L. van der Enden, G. Profitiliotis, D. Croese

We evaluate the status of the development of a responsible future quantum internet (QI). Through horizon scanning, domain expert trend analysis and guided workshops, we present a desired future (DF) conceptualized by stakeholders within the scope of the ethical, legal, societal aspects (ELSA) and policy implications (ELSPI) of the QI. We examine the alignment of the present situation and the DF of the QI ELSPI to the ideals of the ten principles for responsible quantum innovation [1]. Most principles in the DF are well aligned to the ideal, except for the misalignment in intellectual property (IP) and dual use, revealing the precarious balance of well intended policy suggestions and effective outcomes. Additionally, there is an overemphasis placed on the principal of societal relevance in the DF, risking overseeing other principles in the future steering of the ELSPI. The present situation is in moderate alignment with the principles, however trending to misalignment on IP and international collaboration due to QI commercialization and the push for geopolitical sovereignty. For continued success of a responsible quantum internet, we recommend further investigation on the prevention of dual use quantum internet applications, closer involvement of commercial entities in ELSPI ideation, continued recognition of base-layer technology research and stakeholder education on QI applications.

The results of this chapter have been published in *2024 IEEE International Conference on Quantum Computing and Engineering (QCE)*.

II.5.1. Introduction

The development of quantum technologies has seen great advancements in the last decade driven by the potential to revolutionize computation, communication and sensing [2–5]. In parallel to quantum computing, the development of technology that allows quantum computers to share quantum information is now more relevant than ever. This *quantum internet* (QI) is making its way to become a powerhouse in accelerating the pace to useful quantum computing by enabling distributed quantum computing, inherently secure communication and anonymous transmission [6].

Although profoundly unique and useful from a security and computational perspective, the development of the QI equally poses risks for bad actors to operate with impunity, can cause international informational network isolation and inequality in (quantum) resource access. With the several levels of functionality of the QI rapidly increasing in Technology Readiness Level (TRL) [6], it is of importance to evaluate the ethical, legal, societal and policy implications (ELSPI) of a future QI [7]. Previous work has introduced guardrails to steer innovation without hindering its progress with the *ten principles for responsible quantum innovation* [1].

In order to facilitate an ELSPI analysis of a future QI, it is necessary to actively consider such a future. Without consideration of the future, humans are bounded by the simulation heuristic, i.e. a difficult to imagine future tends to be seen as unlikely. Simultaneously, different stakeholders do not necessarily share the same mental model of the future, which is a breeding ground for unrecognized assumptions and biases. A way to counteract both challenges is to follow a process of collaborative foresight conceptualization [8].

To facilitate foresight ideation and co-create a so-called *desired future* (DF) for the QI, the Dutch ‘Centre for Quantum and Society’ sponsored the transdisciplinary strategic foresight project ’Scenarios for Quantum Networks’[1]. For this project, the Centre organized a series of workshops where a diverse group of representatives of academic, industrial, governmental and civil society stakeholders were invited to participate in a collaborative scenario development process of the QI in 2050[2]. In total more than 50 people participated, including a 10 person core team of experts from a diverse background within the quantum ecosystem to be present along the entire process of the DF creation.

In this paper we evaluate the status of the development of a responsible future QI. We utilize the *ten principles for responsible quantum innovation* and evaluate the status quo and DF of the QI along the principles’ ideals. First we will discuss the process towards the creation of this DF in Section II.5.2 and present its outcomes in Section II.5.3. We build on these results and qualitatively assess the progression towards the principles’ ideals of the collectively determined DF and repeat this assessment for the status quo and inclination of trends. This combined evaluation in Section II.5.5 allows us to make a normalized comparison between now and the desired long-term future, opening up the discussion on the direction of the ELSPI in achieving a responsible future QI.

[1]Project conducted by Dr. G. Profitiliotis in 2023-2024.
[2]The timeline of 2050 is set to symbolically represent a long-term future.

II.5.2. DESIRED FUTURE CONCEPTUALIZATION

Pioneered by Pierre Wack at Royal Dutch Shell, the art of *Scenario Planning* brings a structured approach to develop possible futures and strategies based on them [9]. This approach recognized that for successful scenario planning different points of view are crucial to prevent group thinking. Stakeholders also have mental models of the future, which have to be actively challenged, leading to re-interpretation of reality. We extend the scenario planning exercise with an explicit expression of the stakeholders' favorable future [10]. The complete steps of the methodology are:

Process to create a desired future

1. Setting the focal topic
2. Exploration of topic's influential factors (horizon scanning)
3. Ranking these factors by impact and uncertainty
4. Generate extreme scenarios representing two key uncertainties
5. Build these scenarios focusing on the implications they have on the topic
6. Explicit articulation of a DF extracted from (4-5)

For this paper the focal topic has been set to the *ELSPI of the QI*, and in the next sections we go more into detail of steps 2-5.

II.5.2.1. HORIZON SCANNING

In order to fulfill step 2 of the methodology a systematic identification, monitoring and examination of relevant elements surrounding the topic has been performed, known as horizon scanning [11]. This scanning starts with identifying signals of new developments within the scope of the topic that potentially could influence the future in a broad sense. Signals are perceived indicators of small or local phenomena that have the potential to grow in scale and reach [12]. Horizon scanning therefore covers as many domains as possible, from politics, law, policy, natural environment and economy to technology and its impact on society. In total close to 200 signals have been found across all domains that surround the topic of the QI, which have been grouped into 14 *seeds of the future* based on theme and collective fundamentals, finalizing step 3.

II.5.2.2. SCENARIO BUILDING

To spark discussion and expand the perspectives of the stakeholders, two future uncertainties were carefully selected to form a *scenario logics matrix* (step 4), shown in Fig. II.5.1. The two axes of this matrix must be uncorrelated and opposite ends of both axes are extreme opposite outcomes of the uncertainties.

The act of world building in these polarized scenarios has the power to extract underlying assumptions, break group thinking and form the *likes* and *dislikes* about each of the scenarios. The four outcomes align to Dator's archetypes of generalized futures [13] as shown in Fig. II.5.1. They describe either the continued growth of the current situ-

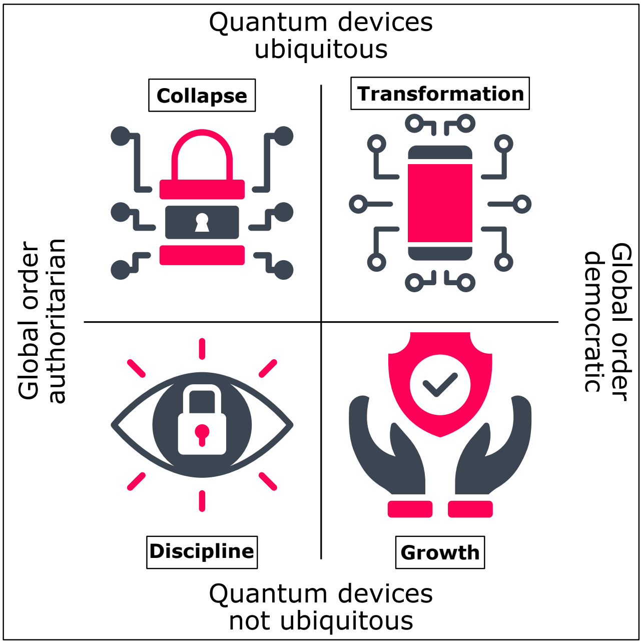

Figure II.5.1: The chosen scenario logics matrix of extreme opposites of uncertain outcomes of the future. The scenarios are used in a world building exercise from which we can extract a DF. The four scenarios follow Dator's archetypes of generalized futures.

ation (Growth) or for the situation to completely inverse (Collapse). Additionally, we can describe a world where radical changes occur in all directions (Transformation) or scarcity prevails and rules and (environmental) regulations are prioritized to enable human survival (Discipline).

We continue with step 5, where stakeholders developed each of these scenarios from the point of view of The Netherlands in a European context. In all scenarios the implications of future applications of the QI were explored [6]. Although this world building process aims to be as unbiased as possible, we need to recognize that all participants are currently living in a democratic society. This leads to an inherent sense that an authoritarian regime is not desirable and a democratic order is desired. Additionally, all participants are part of the quantum ecosystem, which makes it likely to inherently favor the success of the QI. Even though during this process it was stressed that participants should be as objective as possible in their world building, it is impossible to claim that this has occurred completely without bias.

After this session, almost 40 participants in eight parallel groups of diverse composition explored in further detail the ELSPI of the QI in the Netherlands situated in the four scenarios. Each group was assigned to assess the implications of the QI either in the energy or healthcare sector, as example domains that play a critical part in society that combines technology with people's well-being. Then, groups exercised the ELSPI of the QI in their worlds, its (un)intentional benefits in their assigned scenario, also taking the opposing stance on the negative effects that QI applications can pose within these domains[3]. Lastly, they were encouraged to make recommendations for preemptive actions in the quantum network sector to be taken in 2024 to steer their scenario into a direction that was acceptable to them. This concludes step 5 of the process to create a DF.

II.5.3. DESIRED FUTURE

From the guided discussions and topics presented by the participants, we process a list of 18 outcomes of what collectively is framed to be the DF of the ELSPI of the QI, shown in Fig. II.5.2. These outcomes are mapped in *alignment* to each of the ten principles in Fig. II.5.2. We take each principle's definition and detailed description and map whether or not the DF outcome is aligned to the ideal that the principle describes. This assessment is the authors' expert opinion. Each DF outcome can have alignment with some and misalignment for other principles, simultaneously. As example we take the DF outcome 'worldwide quantum internet enables digital inclusion that is secure and robust': With the push for information security inherent in this statement it is aligned to P1, and with expressing desire to give quantum internet access to everyone, it is aligned to P4. However, with unconstrained and global access to quantum internet facilities, malicious activity could secretly take place over secure communication channels, which is in misalignment to the prevention of dual uses of P2. We find the other principles not relevant to this DF outcome, and this finalizes the mapping for this outcome.

The normalized alignment of Fig. II.5.2 is shown on the radial axis in Fig. II.5.3, where the width of the spokes is the normalized number of interfaces of the principle in the DF. We can interpret Fig. II.5.3 as a measure of two parameters. First, the *balance* of the importance placed on each principle in the DF, where an ideal future gives all ten principles equal attention (equal and widest spoke width). Even though it cannot be expected that all topics that are covered in the workshop sessions would have equal representations, they are aimed to be equal enough that any topics that participants would over- or under-represent, will stand out. Second, the alignment of the principle in the DF to the ideal that the principle represents (radial axis). In the DF crafted by the stakeholder participants, we recognize that all principles are well aligned to the ideal except for *dual use* (P2) and *intellectual property* (P5).

[3]Criminal activity being undetectable, dependence on governing entities to provide secure transmissions, quantum secure connections used to obfuscate means to control the population, etc.

Ten principles for responsible quantum innovation →	1 Information security	2 Dual use	3 Quantum race	4 Quantum gap	5 Intellectual Property	6 Inclusion	7 Societal relevance	8 Complementary innovation	9 Responsibility	10 Education and dialogue
Desired future outcomes										
Restrict harmful use of the quantum internet by preventing monopolies, aiming to overcome geopolitical rivalry		✓	✓		✗					
Nation-state pursuit of self-sufficiency in strategic domains, co-shaping R&D to build technology beneficial for people			✗	✗		✓	✓			
Consistent strategies, policy and guardrails for public/private actors to guarantee funding technology for societal benefit				✓			✓	✓		
Actively bridge dialogue between quadruple helix and facilitate constructive interaction							✓			✓
Worldwide quantum internet enables digital inclusion that is secure and robust	✓	✗		✓						
Privacy as human right further prevents state misuse of quantum networks in surveillance and conformism	✓	✗		✓						
Emphasis on 'quantum for good' erodes financial inequalities between citizens			✓	✓		✓	✓			✓
Open public discourse promotes evidence-based understanding of the benefits of quantum networks		✗							✓	
ELSPI are continually studied to steer responsible quantum innovation		✓					✓		✓	
International trade in quantum technology is unrestricted and free of protectionist policies			✓		✓ / ✗					
Vibrant business ecosystem without Big Tech and targeted government investment towards societal needs							✓	✓		
Responsible innovation and self-reflection prevent exploitative capitalism of quantum network technology						✓				
Education is inclusive and freely accessible, cultivating quantum talent across all disciplines						✓				✓
International cooperative scientific research is open and drives standardization of norms and protocols			✓		✓ / ✗					
Broad stakeholder involvement to prevent corruption that would erode the use of quantum technologies for good										✓
Quantum networking drives more direct democratic processes	✓						✓ / ✗			
Environmental impact of quantum technology development is anticipated and managed responsibly							✓			
Quantum networks help address environmental degradation through sensing and monitoring		✗					✓			
Number of interfaces	3	6	5	5	4	4	9	2	2	4
Normalized alignment	5	1.7	4	4	1.7	5	4.7	5	5	5

Figure II.5.2: Mapping of the desired future conceptualization outcomes if they are *aligned* (✓), *misaligned* (✗) or unrelated (empty) to each of the ten principles for responsible quantum innovation. The amount of interfaces is (#✓ +#✗). The alignment per principle is the sum (#✓ - #✗) normalized to the amount of interfaces of that principle and rescaled to be between [0,5]. This allows us to compare the alignment per principle, independent of the amount of interfaces of that principle in the DF. This normalized alignment is the input for the DF radial spokes of Fig. II.5.3. The split (#✓ / #✗) signifies an alignment or misalignment dependent on their interpretation, which counts as *neutral* for the alignment and as a single interface. It is included to acknowledge the existence of an interface but one that is ambiguous or double-edged.

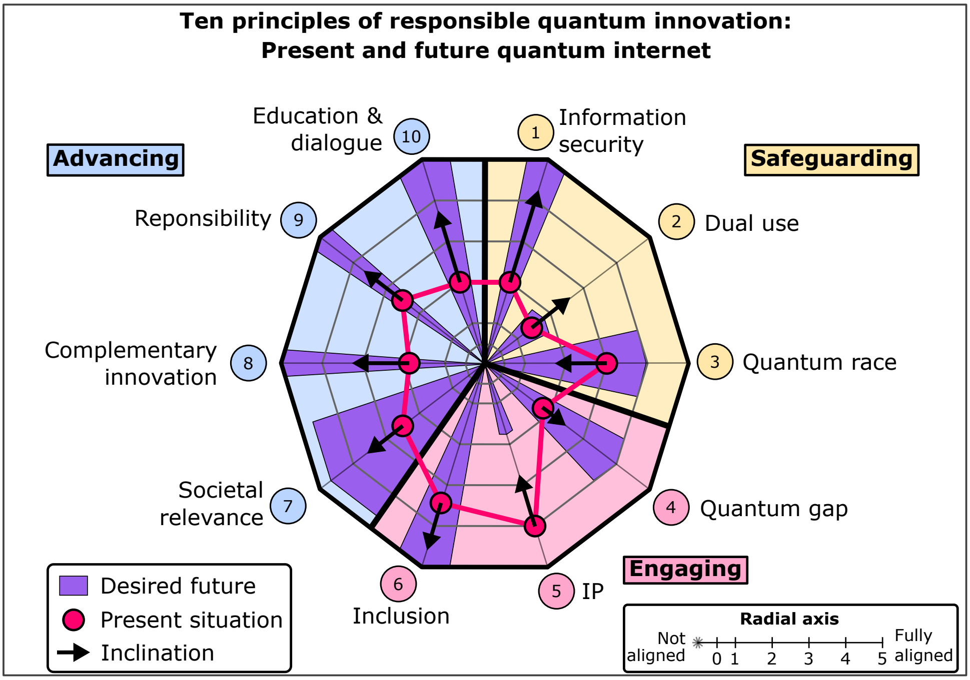

Figure II.5.3: Mapping of the status of the development of a responsible QI for the present situation (pink dots, line), where we expect the trend to incline towards (black arrow) and for the DF outcomes (purple spokes) from Fig. II.5.2. The radial axis denotes alignment to the principle, with full alignment on the outer rim and *not aligned* on the inner most rim. The normalized interface occurrence of each principle in the DF is represented by the width of the spoke. The present situation alignment is determined through the authors' expert opinion, see Section II.5.7.1.

II.5.4. PRESENT SITUATION AND INCLINATION

Alongside the DF ideation, we show an assessment of the *present situation* of the alignment with the ten principles in Fig. II.5.3, including an inclination of the alignment in the near-term future given the trends relevant at the time of writing of this paper. The placement on the alignment scale is determined by the authors' expert opinion and argumented by recent research papers and ELSPI developments. Since QI technology is still in development and fluid in directionality, we recognize that generally all ten principles are not fully developed yet, however the current assessment is a best-effort approach to provide a snapshot of the status quo. This present situation assessment as well as the following analyses are directly the authors' work and not developed in workshops. The reasoning behind the assessment per principle is listed in Chapter II.5.7.1.

II.5.5. A RESPONSIBLE FUTURE QUANTUM INTERNET

The overview of Fig. II.5.3 presents the complete status of the present situation, future inclination and DF of the ten principles of responsible quantum innovation. We observe that the conceived DF and present situation have under-representation of interface occurrence or misalignment with several principles, which we discuss below.

II.5.5.1. Analysis

A possible explanation of misalignment of the *dual use* principle (P3) both in the DF and present situation is the perceived fear that *negative* connotation to QI technologies is not advised to be publicly discussed, as to not harm the *positive* reputation the QI has in delivering enhanced security. We observe that this results in DF outcomes that are misaligned with P3. The same argument holds for the present situation: it is not a *positive* narrative to discuss misuse of quantum technologies other than to protect against adversarial use of those same technologies. With history showing to prepare for misuse of any new technology that has potential for destructive power, the QI domain requires this as well.

A different type of explanation can be found for the misalignment of the *IP* principle (P5) in the DF, where outcomes were formulated in favor of unrestricted and free of protectionist trade policies. This endangers the implementation of methods to protect a market if new risks are feared to destabilize a healthy economy. With one of the desired outcomes being to 'restrict harmful use of the QI by preventing monopolies' (see Fig. II.5.2) we risk closing the possibility for large technology players to rise up from the average. Although clearly with its flaws [14, 15], the existence of *Big Tech* does open up the possibility for enormous private R&D spending (€140 billion in 2023 combined of the top 5 R&D spenders [16]) and the development of market-driven standardization that is much harder to achieve in an otherwise fragmented sector [17]. Preemptively decimating the possibility of large-cap QI companies risks missing out on developing a world-leading quantum industrial sector. As such, a balance of these topics needs to be found to remain aligned with P5.

In the present situation however the public discourse on P5 is more balanced. This is a consequence of the lower TRL of the QI domain, where most knowledge development occurs at research institutes, allowing for more transparency, collaboration and open research. With the TRL of the domain increasing over time, commercialization efforts can result in more secrecy and proprietary information [18]. Together with a current worldwide political push for sovereignty [19–21], relating to *quantum race* (P3), the future inclination of both principles tilts towards misalignment (inward facing arrows in Fig. II.5.3).

The *societal relevance* principle (P7) is overemphasized in occurrence in the DF conceptualization relative to the other principles (widest spoke in Fig. II.5.3). This is explained by the assumption that the QI domain should find (societal) useful applications as driver for technological development. This trend is in line with technological solutionism to solve global environmental challenges [22], in which quantum technologies can potentially play a significant role [23, 24]. While this emphasis has good intentions, it has the potential side-effect of limiting technology research only for those purposes. The definition of P7 allows for advancing *base-layer* technologies [7], however this is a nuance that stakeholders potentially oversee in the quest for solving humanity's global challenges. Additionally, a relative overemphasis of a principle risks removing attention from others, exemplified by the relative unbalanced representation of occurrences in the DF, should thus be avoided.

II.5.5.2. POINTS OF FUTURE INTEREST

To improve on the balance of representation and alignment of several principles in the DF and present situation, we make several recommendations for future discussions on the ELSPI of the QI:

(1) Create a critical review of currently known applications of the malicious use of QI technologies. This allows stakeholders to have an improved understanding of the risks involved and allows for ideation on prevention or enhanced safeguarding of dual use applications (P2).

(2) Closer involvement of (quantum) industry in QI ELSPI discussions. This opens the possibility to include a balancing voice on how industry views proposed policy and market regulation (P3, 5).

(3) Actively emphasize the necessity of funding base-layer research that is not considered to be of direct societal relevance to prevent over-regulation of (commercial) research (P7).

(4) Educate stakeholders on the QI and expand to include more expert future stakeholders. The more stakeholders are aware of the field they will participate in, the better their steering towards the principles can be (P1, 8, 9, 10).

II.5.5.3. LIMITATIONS OF ASSESSMENT

The DF conceptualization through workshops is bounded by its process as described in Section II.5.2 and the participants itself, which has its limitations. We suggest several process improvements. For more consistency and to allow for full understanding of the QI context, we suggest to have the same participants in every workshop round and to allot more time or sessions to fully cover all discussions. This allows for intermediate assessment and steering of principle representation. Furthermore, we suggest to expand the scope of the DF to include influences from other important technological trends (AI, biotech, sustainability) which are expected to have mutual interactions with quantum technologies, covering a more complete conceptualization within responsible innovation.

Lastly, although the DF is crafted through stakeholders, the principle alignment assessment of the DF and present situation is performed solely by the authors. This assessment can benefit from a broader perspective or involvement of principle-domain experts.

II.5.6. CONCLUSION

We have presented an evaluation of the development towards a responsible future QI, assessing both the status quo and a collectively conceptualized DF along the ideal of the ten principles of quantum innovation. Most principles in the DF are well aligned to the ideal, however we found there to be significant misalignment in the DF of principles related to *IP* and *dual use*, revealing the precarious balance of well intended policy suggestions and effective outcomes. This misalignment is possibly driven by the unpopularity of discussing *negative* effects of quantum technologies, as well as an under-representation of commercial entity stakeholders in the DF ideation process. Additionally, there is an overemphasis on the principal of societal relevance in the DF, risking overseeing other principles in the future steering of the ELSPI. The present situation has on average moderate alignment with the principles, with most trends showing inclination in the direction of the ideal, except for the principles *IP* and *quantum race*, driven by the trends of quantum technology commercialization and the intention of geopolitical sovereignty.

For continued success of a responsible QI, we recommend further rounds of workshops with stakeholders with improved consistency and expanded technological scope. For the quantum ecosystem we recommend further investigation on the prevention of dual use QI applications, closer involvement of commercial entities in ELSPI ideation, continued recognition of base-layer technology research and stakeholder education on QI applications and developments.

II.5.7. SUPPLEMENTARY MATERIALS

Table II.5.1: Seeds of the future selected as *trends* of the quantum internet across as many domains as possible.

Trends	Reasoning
Magical thinking influencing the dialogue between quantum scientists and public groups	Beliefs in "magical" capabilities of quantum technologies, fueled by over-hyping, movies and other media, conspiracy theories, misinformation, or pseudoscience, might lead to misinterpretations and might influence the productive interaction of quantum scientists and citizens.
Citizens taking action to preserve their privacy with regards to personal data	Citizens might make use of relevant regulations, paid services, and adaptations of their personal habits to protect their privacy in the face of growing digital surveillance capabilities.
Digital technologies becoming unobtrusive, serving the desire for genuine human experiences	The prioritization of genuine digital experiences that resonate with the values, interests, and traditions might lead to a human preference for unobtrusive technology that is not overwhelming but rather enhances daily life without compromising authenticity or overshadowing the essence of human experiences.
Global crises increasing the adoption of more pragmatic and proactive attitudes in individuals	Frequent exposure to global challenges might give rise to an even more increased sense of agency, responsibility, and practical action towards the future, with people deciding to behave more proactively and take more direct control over their lives.
Corporate users of quantum computing using it as a cloud service	The convergence of cloud services with advanced computing and storage techniques, as well as with other key technologies, and the integration of the classical and quantum clouds might lead most corporate clients to adopt quantum computing via global cloud services.
Fear of decryption and hacking driving adoption of quantum networks	The escalating threats of decryption, hacking, and cyberattacks by state and non-state actors might make private and public organizations, as well as citizens, prioritize quantum networks for enhanced security.
Space-based assets enabling a fully connected world on Earth and into space	Satellites and other space systems might enable a transformative expansion of connectivity by facilitating the worldwide integration of Internet of Things networks, and by providing internet access to all regions on Earth, including remote ones, and in outer space.
Advances in next generation network technologies and spatial computing enabling humans and Artificially Intelligent agents to blend virtual and real worlds	The fusion of immersive technologies, such as high-fidelity cloud rendering, wearable devices, and 5G & 6G networks, might enable humans and AI agents to seamlessly interact and make decisions in both virtual and real worlds.
Artificial Intelligence and quantum technologies enhancing each other's progress, catalyzing their integration	The synergy and mutual reinforcement of the progress of Artificial Intelligence and quantum technologies might deepen their relationship and lead to their integration in a way that makes them indistinguishable for end users
Access to raw material sources affecting the availability of materials essential for making and using quantum devices	The geopolitical and environmental challenges regarding the extraction and availability of critical raw materials alongside the exploration of new sources might significantly influence the production and availability of materials essential for the fabrication and functioning of quantum devices.
Few corporate players dominating the global communication infrastructure	The increasing involvement of Big Tech companies and investing firms in communication infrastructure, especially at the physical layer, might lead to a limited number of players controlling the global communication infrastructure.

II.5

Shortage of quantum talent in EU and the US limiting economic potential	An aging and declining population and a growing skills gap might result in a quantum workforce shortage in Europe and the US, hindering the growth of a quantum business ecosystem and its economic potential.
Governments controlling quantum network technologies for geopolitical reasons	The strategic importance of quantum technologies in defense and national security and geopolitical power dynamics might prompt governments to exert control over the development, deployment, and governance of quantum networks.
EU implementing regulation to meet the demand for digital infrastructures as a public good	Discrepancy between who pays for and who benefits from digital infrastructures, advocacy from civil society and industry, combined with grassroots efforts to transform foundational digital infrastructures into public goods might prompt the EU to explore regulations that ensure fair distribution of both the costs and benefits.

II.5.7.1. Present situation alignment

Below we list the reasoning behind the alignment of the present situation with the *ten principles of responsible quantum innovation* as shown in Fig. II.5.3.

P1: Information security

Even though quantum networks are poised to bring (quantum) enhanced data connections that are both quantum and classically secure, the integration of such technology within already secure layers of soft- and hardware is at its infancy. Software development of systems that aid in controlling research-level hardware is not built with security-by-design principles. With only limited hardware products in this domain available, also the usage of these systems is highly specialized and placed at customer's controlled environments, dampening the need for extensive *hacker-proof* bolstering of the products. However, it is clear to the QI domain that for this technology to succeed, security principles need to be adopted and implemented, and significant trends are recognized in doing so. Further adoption of purchasable soft- and hardware will drive security-by-design development through cybersecurity certification and scrutiny.

P2: Dual use

The potential malicious use of the QI is barely recognized as a risk that needs to be addressed[4]. This is expected by the prevalent narrative that the technology domain looks for *useful* applications as a way to generate momentum, raise (government) funds and positive public awareness around the topics of quantum technologies. Unfortunately the consequence is that very little attention is given to the prevention or of the guardrailing of malicious use of the QI. However, the awareness that the development of new technology comes with the responsibility of it being a double edged sword indicates that with technology maturing, more attention will be given to *dual use* both from the public and private sector [26]. An example within the quantum computing domain is the initial

[4] Without explicitly mentioning QI, it is a widely recognized threat that a powerful quantum computer will be able to break classical cryptosystems of RSA and AES [25], putting most current classical information sharing at risk of being *hacked*. Given that a QI will contribute to enabling such a powerful quantum computer, it is arguable that the development of a QI contributes to this and other dual uses of quantum computing. In this paper we refer to other malicious uses that abuse the power only a QI has, with minimal consideration of quantum computing threats.

attempts at understanding if a *quantum virus scanner* is possible [27], and initial attempts at developing the concept of a *quantum honeypot* [28]. Still, the lack of attention of dual use applications the desired future conceptualization is a counter indicator that more active attention needs to be given to the (prevention of) potential misuse of quantum networking technologies, which needs to be translated into additional funding in this space.

P3: Quantum race

In the present day, fundamental research from academic institutions is published openly (pre-print) alongside journal publications. Collaboration between universities and businesses is common and encouraged, both within and between supra-national states as the EU and the USA [29–31]. However, there have been and continue to be, trends towards limiting international collaboration: Export laws specifically targeted at quantum technologies [19], more direct scrutiny of foreign investments [20] and the push for inter-state exclusivity on product supply through e.g. Strategic Technologies for Europe Platform (STEP) [21] driven by critical supply-chain availability [32]. These trends contribute to a diminished push for international collaboration, even risking a geopolitical race dynamic. This is strong indication that trends are moving away both from the alignment of the principle as well as from the intended desired future.

P4: Quantum gap

This principle deals with the consideration of our planet as the sociotechnical environment in which quantum technologies should function. It aims to promote equitable and fair access to quantum technologies. As how most fundamental research topics start, only wealthy countries and institutes have the funds to attempt ground breaking research that does not have a proven use for society yet. The higher the TRL of such a technology develops, the more affordable and accessible this is expected to be for consumers and less developed countries: where the internet was only accessible and extremely complex to operate 70 years ago, it is now in the palm of the hands of most people globally [33]. Simultaneously efforts are being made to educate a larger part of society through outreach, school education and the development of accessible programming kits both for quantum computing and QI [34–38]. This means that right now the quantum gap is significant, albeit understandable, but with future cost reduction and expansion of use cases the QI can make its way to become an accessible technology globally.

P5: Intellectual Property

Innovation in quantum technologies is globally incentivized by sizable government programs (globally \$50B committed public funding over 10 years) and private investments (globally \$1.2B in 2023) [39]. Therefore the current landscape ranks decent on public IP development, which is also reflected by the exponential increase in patents granted in quantum technologies over the last years [40]. Transparency in academic science has been made easier through the internet and pre-print archives allowing direct sharing of latest (non-peer reviewed) results. Lately however, with more privately owned companies taking on quantum technology R&D, not all results are publicly shared or sharing is delayed. This trend can still be regarded as part of the principle ‘as open as possible and closed as necessary', where only information is shared when beneficial also to the entity sharing it, and not doing so when it hurts a competitive advantage. However, the trend of more closed research seems highly likely to progress, given the international quantum race trend of P3, which turns into a negative feedback loop. The more secrecy is held by one actor, the more inclined others are to follow to not only *give out* their information if nothing comes in return.

P6: Inclusion

Availability of talent in the quantum technology domain is severely under pressure. Currently this is already tackled from many angles, including migration of high educated workers and covering (re-)education of a workforce that is not schooled in the specific field of quantum. Academic institutes, start-ups and especially scale-ups recognize that a wide range of technical and soft skill backgrounds is necessary for fast growth and for gathering the knowledge and skills to achieve the goals they have set out. This combined allows for a significant alignment with P6, including a recognized increase trend in diversifying the workforce, given the necessity of the exponential growth the QI domain will find itself in. This is in line with the desired future conceptualization, where broad education and cross-sector R&D has been highlighted as an important outcome to work towards.

P7: Societal relevance

Quantum R&D within the QI domain is at a stage where development towards societal relevant goals are long-term, not current driving forces. With the expectation that the QI will accelerate useful quantum computing, its focal point is in providing the means to enact the goals set from the quantum computing domain and extend them into enhanced security and privacy. As such, the alignment with the societal relevancy goal of P7 is moderate: The long-term societal goals exist, but are not yet reflected in the technology that is being built. We expect that the alignment with societal relevance increases as more quantum networks are built, deployed and used by quantum computing customers.

P8: Complementary innovation

Most of the QI technology developments have been limited to academic research institutes. While internally enabling some cross-discipline innovation, this is not yet extended into economical or societal spillover. With increased TRL and need for scalability, the semiconductor and telecommunications industry can help in accelerating the deployment of a distributed QI both terrestrially (fiber) and through the air (6G). Furthermore, with additional use case development also other industries, e.g. the automotive (see Chapter II.4), can actively help stimulate innovation between domains.

P9: Responsibility

The attention that responsible innovation within quantum technologies receives is steadily increasing, while mostly being pushed by a handful of institutions, centers and professors[5]. Their background is mostly outside-in assessment of the technology fields from law,

[5] Examples are University of Oxford with the *Reponsible Technology institute* [41, 42], University of Amsterdam with *Quantum Impact on Societal Security Consortium* [43], Stanford Law School with *Stanford Center for*

policy or science communication. Lately more work on responsible innovation has been published in technology oriented journals [48], allowing for more traction of this field within the technology R&D community. With continued funding of collaborative centers, the involvement of quantum technology experts and other disciplines, the inclination is that responsible innovation will become more interweaved in QI development.

P10: Education & dialogue

This paper is an example of the results of an active dialogue between different stakeholders which included a basic explanatory session to familiarize all participants with quantum technologies broadly, and the QI specifically. Globally, efforts of accessibility to quantum education is facilitated by Massive Open Online Courses (MOOCs), but they are mostly oriented at STEM educated participants worldwide. Funding towards education in quantum technologies is made available to the skilled individual starting in the quantum industry, but a more publicly funded approach is necessary to inform a wider audience. This makes the present situation of quantum education and dialogue at a reasonably acceptable start, but with much room to grow to become part of our collective thinking.

Responsible Quantum Technology [44], Leiden University with *Quantum and Society* research group [45], Delft University of Technology with *TPM Quantum Lab* [46], and related to this Chapter Quantum Delta NL with the *Centre for Quantum and Society* [47]

II.5

REFERENCES

[1] M. Kop, M. Aboy, E. D. Jong, U. Gasser, T. Minssen, I. G. Cohen, M. Brongersma, T. Quintel, L. Floridi, and R. Laflamme, *Ten principles for responsible quantum innovation*, Quantum Science and Technology **9**, 035013 (2024).

[2] H. J. Kimble, *The quantum internet*, Nature **453**, 1023 (2008).

[3] C. Degen, F. Reinhard, and P. Cappellaro, *Quantum sensing*, Reviews of Modern Physics **89**, 035002 (2017).

[4] Bova, Francesco, Goldfarb, Avi, and Melko, Roger G., *Commercial applications of quantum computing*, EPJ Quantum Technol. **8**, 2 (2021).

[5] A. Bayerstadler, G. Becquin, J. Binder, T. Botter, H. Ehm, T. Ehmer, M. Erdmann, N. Gaus, P. Harbach, M. Hess, J. Klepsch, M. Leib, S. Luber, A. Luckow, M. Mansky, W. Mauerer, F. Neukart, C. Niedermeier, L. Palackal, R. Pfeiffer, C. Polenz, J. Sepulveda, T. Sievers, B. Standen, M. Streif, T. Strohm, C. Utschig-Utschig, D. Volz, H. Weiss, and F. Winter, *Industry quantum computing applications*, EPJ Quantum Technology **8**, 25 (2021).

[6] S. Wehner, D. Elkouss, and R. Hanson, *Quantum internet: A vision for the road ahead*, Science **362**, eaam9288 (2018).

[7] M. Kop, *Quantum-ELSPI: a novel field of research*, Digital Society **2**, 20 (2023).

[8] T. Fuller and K. Loogma, *Constructing futures: A social constructionist perspective on foresight methodology*, Futures Futures Methodologies, **41**, 71 (2009).

[9] P. Wack, *Scenarios: uncharted waters ahead*, Harvard business review **63**, 72 (1985).

[10] W. L. Schultz, *Futures fluency: explorations in leadership, vision, and creativity* (University of Hawai'i at Manoa, 1995).

[11] H. T. Greely, *Governing emerging technologies—looking forward with horizon scanning and looking back with technology audits*, Global Public Policy and Governance **2**, 266 (2022).

[12] G. Profitiliotis, *HLCP Futures Masterclasses Pilot 2022-2023: Horizon Scanning*, (2022).

[13] J. Dator, *Alternative futures at the manoa school*, Jim Dator: A Noticer in Time: Selected work, 1967-2018 , 37 (2019).

[14] F. Foer, *World without mind: The existential threat of big tech* (Penguin, 2018).

[15] R. Hendrikse, I. Adriaans, T. J. Klinge, and R. Fernandez, *The Big Techification of Everything*, Science as Culture **31**, 59 (2022).

[16] E. Nindl, H. Confraria, F. Rentocchini, L. Napolitano, A. Georgakaki, E. Ince, P. Fako, A. Tübke, J. Gavigan, H. Hernández Guevara, P. Pinero Mira, J. Rueda Cantuche, S. Banacloche Sanchez, G. De Prato, and E. Calza, *The 2023 EU industrial R&D investment scoreboard* (Publications Office of the European Union, 2023).

[17] N. Petit, *Big Tech and the Digital Economy: The Moligopoly Scenario* (Oxford University Press, 2020).

[18] M. Kop, M. Aboy, and T. Minssen, *Intellectual property in quantum computing and market power: a theoretical discussion and empirical analysis,* Journal of Intellectual Property Law & Practice **17**, 613 (2022).

[19] H. Omaar, *The U.S. Approach to Quantum Policy,* ITIF Center for Data Innovation (2023).

[20] *Regulation (EU) 2019/452 of the European Parliament and of the Council of 19 March 2019 establishing a framework for the screening of foreign direct investments into the Union,* (2019).

[21] European Commission, *Proposal for a REGULATION OF THE EUROPEAN PARLIAMENT AND OF THE COUNCIL establishing the Strategic Technologies for Europe Platform ('STEP') and amending Directive 2003/87/EC, Regulations (EU) 2021/1058, (EU) 2021/1056, (EU) 2021/1057, (EU) No 1303/2013, (EU) No 223/2014, (EU) 2021/1060, (EU) 2021/523, (EU) 2021/695, (EU) 2021/697 and (EU) 2021/241,* COM/2023/335 final (2023).

[22] H. S. Sætra, *Technology and sustainable development: The promise and pitfalls of techno-solutionism* (Taylor & Francis, 2023).

[23] J. M. Dieterich and E. A. Carter, *Opinion: Quantum solutions for a sustainable energy future,* Nature Reviews Chemistry **1**, 1 (2017).

[24] J. O'Brien, *How quantum computing could be one of the most innovative climate change solutions?* (2019).

[25] C. Rugers *et al.*, *Risk management and the quantum threat,* mathesis, Leiden University (2018).

[26] M. Troyer, E. V. Benjamin, and A. Gevorkian, *Quantum for Good and the Societal Impact of Quantum Computing,* (2024).

[27] S. Deshpande, C. Xu, T. Trochatos, Y. Ding, and J. Szefer, *Towards an Antivirus for Quantum Computers,* in *2022 IEEE International Symposium on Hardware Oriented Security and Trust (HOST)* (2022) pp. 37–40.

[28] N. Nagy, M. Nagy, G. Alazman, Z. Hawaidi, S. M. Alsulaibikh, L. Alabbad, S. Alfaleh, and A. Aljuaid, *Quantum Honeypots,* Entropy **25**, 1461 (2023).

[29] M. Everett, *EU-US Collaboration on Quantum Technologies,* (2021).

[30] *JOINT COMMUNICATION TO THE EUROPEAN PARLIAMENT, THE EUROPEAN COUNCIL AND THE COUNCIL ON "EUROPEAN ECONOMIC SECURITY STRATEGY"*, JOIN/2023/20 final (2023).

[31] United States of America: House of Representatives, *National Quantum Initiative Act,* Public Law No: 115-368 (2018).

[32] U. Mans, J. Robbers, J. Rabbie, and T. van der Veen, *Mapping the supply chains for quantum communication: Towards european technology sovereignty in an emerging industry,* (2023).

[33] H. Ritchie, E. Mathieu, M. Roser, and E. Ortiz-Ospina, *Internet,* Our World in Data (2023).

[34] Horizon 2020, *Coordination and support action for quantum technology education,* (2020).

[35] QuTech, *Quantum Network Explorer ADK,* (2024).

[36] IBM, *IBM Quantum Learning,* (2024).

[37] Google AI, *Quantum AI Educational Resources,* (2024).

[38] Microsoft, *Azure quantum learning resources,* (2024).

[39] IQM Quantum Computers, OpenOcean, Lakestar, and The Quantum Insider (TQI), *State of quantum 2024 report,* (2024).

[40] M. Aboy, T. Minssen, and M. Kop, *Mapping the Patent Landscape of Quantum Technologies: Patenting Trends, Innovation and Policy Implications,* IIC - International Review of Intellectual Property and Competition Law **53**, 853 (2022).

[41] University of Oxford, *Responsible Technology Institute,* (2024).

[42] C. Ten Holter, M. Jirotka, and P. Inglesant, *Creating a responsible quantum future: the case for a dedicated national resource for responsible quantum computing,* (2021).

[43] University of Amsterdam, *Quantum Impact on Societal Security consortium,* (2024).

[44] Stanford Law School, *Stanford Center for Responsible Quantum Technology,* (2024).

[45] Leiden University, *Julia Cramer Group - Quantum and Society,* (2024).

[46] Delft University of Technology, *TPM Quantum Lab,* (2024).

[47] Quantum Delta Nederland, *Centre for Quantum and Society,* .

[48] U. Gasser, E. De Jong, and M. Kop, *A call for responsible quantum technology,* Nature Physics **20**, 525 (2024).

II.5

II.6

CONCLUSION

"Cause too many people think they made me.
Well, if they really made me, then replace me"

The Weeknd, *Sidewalks*, 2016

In this Chapter I summarize the results of "Part II: Business & Society" of this thesis and I present my proposals to continue advancing the field of quantum networks from an industry collaboration and socially responsible innovation point of view.

II.6.1. Summary

Chapter II.3 gave a C-level executive overview on the quantum communication domain, from post-quantum cryptography (PQC) and quantum key distribution (QKD) to interconnecting quantum computers in a quantum internet. Challenges and opportunities for these sub-sectors have been discussed, which show that PQC and QKD are both cryptographic methods that are suggested to be implemented in the next years to remain safe against powerful quantum attacks. Opportunities in the quantum internet domain are further ahead, but hard- and software providers should remain on the lookout to become early stage partners as equipment manufacturer, potentially growing in a multi-billion dollar market.

Chapter II.4 showed a quantum internet use case analysis of the automotive sector. We utilized a method where cross-platform megatrends in both the quantum internet and the automotive industry are analyzed, identifying mutually beneficial regions of interest. In the short-term (< 10 years) hardware miniaturization and automation of quantum internet technology provides a synergy interface between the two domains. For the long-term (≥ 10 years) we developed a comprehensive list of use cases for the quantum internet within the automotive sector. These results allow for further development of targeted research directions for both domains.

Chapter II.5 presents a first of its kind evaluation of the status of the development of a responsible future quantum internet. By using the ten principles for responsible quantum innovation [1], we assessed the present situation of responsible quantum internet development. We repeated this assessment for a collectively conceptualized desired future where the quantum internet is prominently integrated in society. We find moderate alignment to the principles in the present situation, but recognize overemphasis of principles in the desired future. We finalized this analysis with comments on the limitations of the assessment and desired future conceptualization process, and suggestions on how to proceed with responsible innovation analyses in the future.

The research presented in this 'Part II' of this thesis is one of the first efforts in developing use cases and assess responsible innovation for quantum networks integrated with industry and society. We discuss the future of continued integration of quantum networks in both topics separately below.

II.6.2. Quantum networks for industries

With the successful development use case analysis of Chapter II.4, there is a foundation for further use case research for other industries than the automotive. After the most viable industries are identified and similar analyses with them are performed, I propose that a meta-analysis of all use cases and interfaces can be performed to find cross-disciplinary overlap, allowing to unite expertise from different industries to tackle the same challenges. An example consortium as such has been created at small scale for quantum computing [2]. Industry leaders can benefit to be receptive to collaborative use case development projects with quantum experts, and possibly find quantum internet use cases that benefit both the industrial and quantum domains.

II.6.3. RESPONSIBLE QUANTUM NETWORKS FOR SOCIETY

Responsible innovation in the second quantum revolution is an emerging field of research and was first discussed in ethics around 2017 [3]. In the years before, several policy manifestos were released by governmental bodies of the EU, Great Britain and Germany [4–6], prompting the assessment of responsible research and innovation (RRI) for quantum technologies. Since then, the field of responsible quantum innovation has grown, with several organizations performing research on responsible quantum innovation from ELSPI oriented views. As emerging research field it aims to have the understanding of its findings be broadcast to all relevant parties, from lawmaker to quantum researcher.

Still, there is a divide between the work that RRI researchers perform and the transfer of that knowledge to quantum researchers/engineers working on the technology itself. This divide risks a lack of input the other way around as well, where policy is made with limited input from the quantum researcher. Although this distinction is understandable given the inherent domain differences between technology development and those researching ELSPI, it becomes less understandable knowing that eventually it can be policy makers that can bound technological development. AI regulation in the EU [7] is a recent example of policy restrictions that could clash with innovation [8]. There has to remain a constant feedback between the *boots on the ground* quantum researcher and those implementing legal and policy frameworks. The visibility of ELSPI research is a factor that can increase interaction between these two domains, which is enhanced by cross-disciplinary journal paper publications e.g. recently an ELSPI call-for-action was published in Nature Physics [9]. This trend should continue in reasonable numbers such that continuous exposure of ELSPI to the quantum community is ensured. This in turn can encourage researchers to actively participate in workshops, steering committees or other forms of expert groups, allowing policy makers to make informed decisions on quantum regulation.

II.6.3.1. CENTRE FOR QUANTUM & SOCIETY

More directly, the research that is performed by the Centre for Quantum & Society in the Netherlands remains vital in spreading awareness, gathering quantum ecosystem participants to perform foresight studies and develop tools that can help organizations navigate quantum innovation and their impact. As suggested in Chapter II.5, continued foresight studies based on the approach and work performed in that Chapter will be of interest going forward. Especially the desired future conceptualization should be continued on a regular basis, where guided workshops take the same quantum ecosystem participants, that are well informed on quantum networking, through the desired future creation process. Intermediary checks or post-workshop follow-ups can be included that assess the alignment to the *ten principles of quantum innovation*, as performed in Chapter II.5, with principle domain experts weighing in on the alignment of the desired future. This can prevent biases in the judging of desired future - principle alignment, and bring more statistical validity when more experts weigh in on the topic.

II.6.4. Commercializing quantum networks

This thesis has contributed towards commercializing quantum networks. From pushing the boundaries on technological capabilities in Part I, to assessing use cases for the automotive domain in Chapter II.4. **For direct commercialization paths of quantum networks, a breakdown of technology driven commercial next steps for quantum networks is described in detail in Chapter I.6.3**.

REFERENCES

[1] M. Kop, M. Aboy, E. D. Jong, U. Gasser, T. Minssen, I. G. Cohen, M. Brongersma, T. Quintel, L. Floridi, and R. Laflamme, *Ten principles for responsible quantum innovation,* Quantum Science and Technology **9**, 035013 (2024).

[2] A. Bayerstadler, G. Becquin, J. Binder, T. Botter, H. Ehm, T. Ehmer, M. Erdmann, N. Gaus, P. Harbach, M. Hess, J. Klepsch, M. Leib, S. Luber, A. Luckow, M. Mansky, W. Mauerer, F. Neukart, C. Niedermeier, L. Palackal, R. Pfeiffer, C. Polenz, J. Sepulveda, T. Sievers, B. Standen, M. Streif, T. Strohm, C. Utschig-Utschig, D. Volz, H. Weiss, and F. Winter, *Industry quantum computing applications,* EPJ Quantum Technology **8**, 25 (2021).

[3] C. Coenen and A. Grunwald, *Responsible research and innovation (RRI) in quantum technology,* Ethics and Information Technology **19**, 277 (2017).

[4] Innovate UK, *National strategy for quantum technologies,* Accessed through Wayback Machine 31 May 2023 (2015).

[5] W. P. Schleich, K. S. Ranade, C. Anton, M. Arndt, M. Aspelmeyer, M. Bayer, G. Berg, T. Calarco, H. Fuchs, E. Giacobino, M. Grassl, P. Hänggi, W. M. Heckl, I.-V. Hertel, S. Huelga, F. Jelezko, B. Keimer, J. P. Kotthaus, G. Leuchs, N. Lütkenhaus, U. Maurer, T. Pfau, M. B. Plenio, E. M. Rasel, O. Renn, C. Silberhorn, J. Schiedmayer, D. Schmitt-Landsiedel, K. Schönhammer, A. Ustinov, P. Walther, H. Weinfurter, E. Welzl, R. Wiesendanger, S. Wolf, A. Zeilinger, and P. Zoller, *Quantum technology: from research to application,* Applied Physics B **122**, 130 (2016).

[6] A. De Touzalin, C. Marcus, F. Heijman, I. Cirac, R. Murray, and T. Calarco, *Quantum manifesto: A new era of technology,* Accessed through Wayback Machine 9 Dec 2023 (2016).

[7] *Regulation (EU) 2024/1689 of the European Parliament and of the Council of 13 June 2024 laying down harmonised rules on artificial intelligence and amending Regulations (EC) No 300/2008, (EU) No 167/2013, (EU) No 168/2013, (EU) 2018/858, (EU) 2018/1139 and (EU) 2019/2144 and Directives 2014/90/EU, (EU) 2016/797 and (EU) 2020/1828 (Artificial Intelligence Act),* (2024).

[8] L. Laurent, *Europe has us tech in its sights. it might miss.* (2024).

[9] U. Gasser, E. De Jong, and M. Kop, *A call for responsible quantum technology,* Nature Physics , 1 (2024).

II.6

ACKNOWLEDGMENTS

It is a great privilege to add a real personal flair to this collection of scientific work. As is clear from the work itself, many people have contributed to its content directly, but many more have contributed in one way or another (in)directly to its success. It is my pleasure to thank all of you[1] below.

After a search around the US and Europe to find a fitting PhD position, I circled back to QuTech when I could not find an inspiring position in all those other places. Where before I focused on superconducting qubits, I had decided to put all options back on the table. Then, I (re)discovered the amazing promises of solid-state emitters and that the world's best research on them was being performed right under my nose. Soon I found myself in your office, **Ronald**, where you pitched me to work on the Qlink project and sold me on the idea of entanglement between Delft - The Hague in 2020! Wow! As you know, I am all for ambitious goals! We soon found a match on my excitement for the magnitude of the project, its potential impact and my entrepreneurial vision of a future beyond this PhD, where commercialization of the quantum internet can be pursued. Although the reality of the complexity of the project became more clear with every passing month, I admired your steadfastness that the monumental goals of the Qlink project would be achieved. Thank you for providing me the environment in which I could make this PhD a great success, both from a scientific and people perspective, and for giving me the opportunity to develop myself in my own ways during this entire journey. You have taught me that you can never ask too many questions, but the real trick is in actually asking them. I will make sure to do that for the rest of my career.

I believe it to be very fitting that you are my co-promotor, **Stephanie**, as it was also your initiative that started the Qlink project. Thank you for that push, without it perhaps my PhD had never existed. Although I believe the project itself took longer than you (and with you, many!) had hoped, I hope you are as proud of the final results as I am. Your group is quite unique in the work it does and with the mix of disciplines of people it requires - I am very glad that this expertise is available for collaboration and deepening of many people's work at QuTech.

With my thesis covering a broader spectrum than only experimental work, where topics as commercialization and ethics are extensively discussed, I am very glad to have a great compilation of defense committee members that represent those disciplines. It is an honor to defend my work again to **Leo Kouwenhoven**, coming back full circle after having written my MSc thesis in your group and after my work at Microsoft. It was a huge surprise to find a post-it written by you on my desk in Redmond, I even briefly considered if someone was pulling a joke on me. I look forward to defending to **Sander Otte**, I still remember your excellent solid-state lectures from my Bachelor's. Also to

[1] With so many years (also before my PhD!) in and around QuTech, if you are reading this and you are not directly mentioned in the text, hereby I acknowledge you.

Andreas Reiserer, although our professional paths never crossed, I admire your work and look forward to your sharply defined questions. I highly appreciate that **Mathias van den Bossche** agreed to be part of the committee, I look forward to your questions from an industry perspective. Lastly, thank you **Julia Cramer** for inviting yourself successfully to the committee (kidding!), I am really glad you can provide your quantum expertise from a societal impact perspective and I am excited to discuss these topics!

Arian, what can I say that has not already been said, felt or written. We were friends before this PhD and project, and much better friends after. I briefly thought it as a risk that we would work together, professionally, while being friends, but that fear was taken away completely very soon into our work. I firmly believe our teamwork led to a 1+1=3 success, where an intuitive understanding of each others way of working has significantly helped achieve our 'Herculean-task' experiments. Thank you for taking on that task with me, it was an honor and a pleasure to be working with someone as capable as you. I am very thankful for your open communication during the harder times of the project and our collaboration, I feel it deepened our personal and work relationship. I look back on our many (many, many!) hours in the lab very fondly, even though it probably gave me a Vitamin D deficiency. Somehow we managed to be extremely productive, have a smile on our faces and listen to techno in our ~~bunker~~ lab all at the same time. And if work time was not enough, our roadtrips, occasional bagels (& beans) and post-workout dinners (look at aalwwh those chkns!) were great excuses to continue talking about finance, economics, government and everything else. Also I do not think I have ever had as much fun playing with bouncy balls as with you in the empty gigantic halls of the conference center at MM2022. You are one of the most intelligent people I know, and anyone will be lucky to be working alongside or for you. Great things lie ahead for you, of that I am sure, both in your professional life and in your continued future with Vincy. I look forward to the day we can work together again!

Mariagrazia, you truly are the Taylor Swift of the entire field of quantum technologies. I have always really enjoyed having a fellow fashion-enthusiast at QuTech, and you kept me on my toes to attempt to rival the quality of your outfits. No matter what you would be tackling that day, you had more courage than me to always put the outfit *first.* I got punished for trying, ripping one of my favorite pants (at the knee) crouching underneath an optical table. As soon as you got up to speed at the Networks it was clear to me you were already ready to be running your own team, which I am quite sure you will do immediately after your PhD. I have found it quite fitting that we worked together at the start of your PhD where I pulled you into this machine learning course I was TA'ing, and that we got to work together on LT5 in the last weeks of mine (I *really* needed that FPGA board). I would have really liked to work together with you more, we got stuff DONE while having fun and singing along to your favorite Taylor songs while being interrupted by the TSITP ads. Our roadtrips are both two of my most favorite memories of my PhD, from no-mo-Joe to vibe-checking every restaurant we went to. Thank you for all the wonderful time we spent together and always having my back no matter what was going on. You are going to continue crushing those last experiments (let the lab-ghosts stay away!) and I am already excited to see what is next in store for you.

Marie-Christine, it was an absolute blessing to have you join on the Qlink project. Your insights were absolutely essential in helping debug experimental setup issues (where are the ZPL counts), in simulations and calculations (single-emitter TPQI photon counting is hard!) and, perhaps most important of all, to maintain a balance between everyone in the Qlink team. Not just to hear from someone that ‘perhaps you should go home and rest?’, but also with the retrospectives that were really quite essential in keeping our voices heard during hard times. Your segues online will forever be unrivaled! Speaking of forever (my turn for the segue!), I really felt honored to have seen you move from a Röhsner to a Slater. Your wedding made me feel like I was attending a *royal* wedding in Vienna, thank you so much again for opening up your life to Team Diamond! All the best to you and your brand new growing family, I look forward to visiting you in Vienna once again.

Thanks to the old guard of the group, **Sophie, Matteo Pompili, Simon**, you achieved something exceptional with the three-node experiment and your investigations into issues were always interesting to hear about, and surprisingly came in handy at the end of my PhD. **Sophie**, good luck with your new role back at QuTech! **Matteo**, best of luck with the tech you’re building at Lightsynq, I think you’re exactly where you’re supposed to be! I wish you and Grace a great time in the US! **Simon**, you were always kind and supportive, I wish we could have worked together more. Best of luck in Austria! **Lorenzo**, the silent-but-deadly type! Coming out with those zingers out of nowhere! Best of luck in France! **Alejandro**, I’m glad you adapted to the Team Diamond way of working. Conversations with you are always slightly unhinged and I love it. HSBC is exactly what you were looking for, best of luck pursuing the finance lifestyle, I respect it! **Matthew**, we only had brief overlap in our work-life, but I’ve very much enjoyed the hangouts we have had in the years after. Best of luck at Qphox, they’re lucky to have you!

Matteo Pasini, thank you for the fun times on the roadtrip and your confidence on the Grand Canyon hike. You *definitely* pass the vibe check, good luck in Spain! Good morning **Julia!**, it’s me Joe! Thank you for the excitement you bring to the group, during the roadtrip and always being down for a good time. I’m relieved we’ve ironed out a few wrinkles that happened along the way. Good luck with the QFC and wrapping up your PhD, never let it get you down! **Nina**, the fab-queen! I’m glad I could provide you with the coffee creamers, and in return we obtained amazing diamond fab. Good luck with your next steps, whatever they will be! Herr Fischer, **Julius**! Thank you for helping with my house in times of need! You’ve been a consistent presence in the hallways/labs and that I always appreciated that. Thanks for the laughs and fun on the roadtrip, I’ll never forget it! **Yanik**, your lab is so neat it’s almost frustrating. I’m glad the cavity project had you and **Julius** to bring to a next (resonance) level. Your always know exactly what to say or ask to make anything hilarious, and I still don’t know if this is on purpose or not. I’m glad we survived the Red Roof, and bringing the walkie-talkies was such a great idea. Good luck with your next projects! **Christopher**, I’m happy we have gotten to know each other better during the last years. Nothing really seems to get you down, no matter how hard the science of a new emitter can be. Best of luck with the last stretch, and all the best to you and your future, both professional and personal! **Hans**, thank you for being so kind on a personal level, but also always asking sharp science questions. That combo is what will make you a great professor. I wish you amazing success for all your next steps! **Christian**, it’s nice to see you’re owning the new platform! I promise my sunglasses are NOT laser goggles! **Tim**, as spiritual successor of the emitter-QFC projects I know the struggle, but I’m sure you’ll get some great results very soon. Thanks for bringing some

Berlin-vibes into the group! **Dani, Niv, Leo(nardo di Caprio)**, please keep permeating the Team Diamond spirit for the next generation of PhDs, I'm counting on you!

The office that rarely saw the holy Quadrinity! **Sjoerd**, samen uit samen thuis! From day one we had a healthy competition going (cake!), that continued with the Diamond Cup (you kept your head up, no matter how often we beat you!) all the way to the end of our PhDs. It felt like both of us were in the same trenches, and I'm glad we were able to help each other out, whether it was science, speaking or personally. You are never ashamed to ask the pressing questions, and that will continue bringing you to a successful future. Brrrbrr!! **Nicolas**! We could always say whatever is on our minds, and it fun to chat about work, life and what a PhD is like. Good luck with the last steps of yours, go write that thing! **Guido**, good luck in Stanford!

The other half of Team Diamond cannot be forgotten. **Mohamed**, I still warn people about the 'hospital food truck', you have taught me well. It was always nice to see a familiar face on the weekends and evenings in the office. **Laurens**, thank you for always being there for a nice chat or picture taking where necessary. **Christina, Margriet, Benjamin**, good luck with your PhDs and for continuing the Team Diamond spirit! **Jiwon**, you are an excellent scientist and I always enjoy that you smile and are up for a short chat at any time. Good luck with your work! On the theory side there also a few people I want to mention! **Tim Coopmans**, it's been really great to see your journey towards PI-land. You're going to continue to grow and I'm looking forward to seeing the success and papers of you and your group! **Guus**, it's funny how we would connect better outside our PhDs. I hope our paths cross again in the future, it was fun to talk in Montreal! **Francisco**, I'm glad you could find a place in quantum still, even though before you didn't seem so interested in staying ;) Best of luck with your future, both professional and personal with Janice! **Thomas**, it's very refreshing to see someone dive deeply into a very important (but hard!) topic for the future quantum internet. You're very capable and productive, I look forward to implementing your work in a real network soon. Best of luck with your PhD, and don't forget to take a break once in a while too! **Hana, Janice**, both of you grew from the slightly-shy students to professional engineer/scientist, and that's been really nice to see. Best of luck with both your futures and don't lose the weirdness! On the other spin-side, **Florian** it's been nice to keep in touch over these years after that intense time in DiCarlo's lab. Immortalized in an Intel press-kit I'm glad you found your ways all these years later to Australia! Best of luck there!

Thuisje team! Sebastian, David, Hridya, Marcel, thank you for organizing perhaps the weirdest 'Uitje' ever. I never packed so many boxes, but we all made it a huge success. **Sebastian**, it's funny that we got closer the moment you left QuTech, but I guess that is how things go sometimes. I always enjoy talking to you, and I think you should definitely pursue those ideas you have! De mannen van de techniek, in het bijzonder **Siebe, Vinod**, bedankt voor alle ondersteuning die jullie altijd konden bieden in het lab. Met een airco, opzetten van de alu balken en een altijd vriendelijke groet in de gang. Jullie werk is wat QuTech zo'n unieke plek maakt. **Régis**, thank you for taking on the hard task of finding some order in the chaos that was left from the move, being so involved with QuTech and bringing those sweets from France even though we barely met at that time. Good luck with your continued work!

Of course this list is not complete without the entire TNO-branch of the Qlink. Thank

you to **Jaco** for being so strict and closely involved in the first years, we had some discussions with sparks flying, but I know you always had the best of the project in mind! **Erwin**, it's absolutely unbelievable how you always managed to ask the *right* question that nobody wants to answer, and because of that, is the *exact* question that should be asked. Thank you for always being in a good mood and for the understanding that planning and the lab-work don't always match well. Keep asking those questions, and I hope to see pictures of your next hikes! Thank you to **Arjan, Benjamin** for all the work on the phase stabilization, you guys know how to tackle a beast of a problem! Thank you **Boudewijn, Rodolf, Leon** for all your engineering support and **Christine, Wouter, Jared** for your work on the Qlink, and to take this knowledge skillfully into QNE! Thank goodness it's always *before* Christmas! **Klaas-Jan**, thank you for standing up for the scientific team so often when this was not always what was desired of you. Your efforts are very recognized and I appreciated very much the freedom you gave to the team to let them do what they do best. **Theo**, the man of the money! I've never heard a word about funding issues, which means you did a great job to keep the train running in those final years. The Qlink-thank-you-glass-brick is prominently displayed in my house, thanks for recognizing that we needed to celebrate our achievements!

Pieter, Ingmar, Ludo, thank you for all the software support throughout these years. Your work lifted QMI and my work to the next level and ensured a (continued) future for quantum network hardware control software. **Pieter**, best of luck continuing with the QNE project, it sounds like you're exactly riding that perfect line of soft- and hardware you enjoy. **Ravi**, the same holds for you, it's been great to work together with someone that turns into a friend. I think you have the largest collection of photos of me out of anyone, including myself, but I've always been very happy to be your fashion model.

Jigsaw! **Sidney**, thank you for introducing me to working with FPGA's! It is pretty unbelievable that the board you gave me in my first month into my PhD was essential in making the heralded entanglement work in the last weeks of the experiments. No matter what you have a smile on your face, I have always appreciated that positive attitude! **Joris**, you are extremely kindhearted and a unique combination of being both a very humble, yet unbelievably capable person. The little 'tools' you developed were absolutely essential to the success of the metropolitan experiments and nothing you say to that will change my mind. Thanks to you both for developing QMI from scratch, always asking the right questions and never stopping to be amazed by the world of quantum physics.

I'm glad to thank also my German counterparts at Fraunhofer ILT! **Bernd, Florian**, you have been a consistent organizational force to keep the NORA project on track and to intensify ILT's relationships between QuTech, TNO and QIA, which will prove to be a huge enabler for success in the entire quantum networking ecosystem. Thank you for the fun hangouts, whether they were in Aachen or Delft, you are always a joy to speak to. **Fabian**, my brother from another country, I cannot thank you enough for the last minute rushes to our lab to help squeeze out those last percent of performance of your beast of a machine. We both had to make substantial sacrifices in the last months to work on it together, but the results speak for themselves and it intensified our friendship, so I'm glad it happened that way. I am really excited to see the big plans you have come to fruition, you know you always have my support on that! And I hope that leads to us working together once again in the future. Thank you for everything!

James Kroll, thanks for being a great supervisor-turned-friend. Although you did your best to scare me away from doing a PhD, that's the only thing you failed to help me with. I've always used your experimental tricks and honed them to perfection, and I'm glad we slowly were able to peel away the facade and uncover our true identities to each other. Meow! Aaaaah **Willemijn**!! *Jump, crouch, point!*, thank you for being just you! You've always been so supportive and compassionate with my work and personal life, thank you for that, you are a great friend. I'm glad you found your way after your PhD and I hope you continue doing smart things in the quantum space, because we need you! **Fokko**, it really is a small world huh. From my first-year's weekend during my Bachelor's, to working in Leo's group during my Master's and then, of course, we also overlap again during my PhD in some other way. Everyone I speak to really enjoys working with you, and I feel the same way. QBlox is lucky to have you to get those machines into the quantum internet space!

Stein, it was fun working alongside you at the start of my PhD! Best of luck with your career! **Annick**, I've never met anyone as organized as you - it was unbelievable you could join a Diamond-beach-day just a few days before your Master's defense, you have my respect for that! I'm glad you found your place in the mountains, this country was way too flat for your ambitions! **Otmar**, we realized soon that we are very alike in way of working, and that caused some late night sprints in the lab. Your work was excellent, but I'm sorry that the laser power drift fix came only a few weeks too late. Perhaps karma for breaking the AC-unit ;) Best wishes for your future at TNO, they're lucky to have you! **Adriá, Nayan**, both of you approached me for career advice at the very start of the beginning of yours. It's been an honor to provide that for you and to watch both of you grow into very fitting roles in engineering and entrepreneurship.

My future as keynote speaker would not have been possible without the support from the QuTech communications team. **Leonie**, thank you for always knowing where to find me when you needed some help, input or a collaborator for an art project (that was really fun!). The DREAM-hall is lucky to have you, they don't know what will hit them! **Aldo**, you're a character but one I enjoy greatly. QuTech profited greatly from your press-magic, although it might not always have recognized its impact enough. Thanks for all the collaborations, story-telling and help with our public releases! You're the man! Good luck in Amsterdam! **Maarten H.**, thank you for our fun conversations and the support of my entrepreneurial ideas. I'll make sure to come back to you when they solidify! **Erik**, thank you for always picking up and broadcasting the PR things I forwarded to you, you're a consistent force driving the communications team forward. **Agustina, Lua**, thank you for allowing our work to be so prominently displayed in Stroom. It was a wild ride from start to finish, but I feel we became friends along the way and I won't ever forget how art and quantum can be combined. **Heera**, you were the first at QuTech to recognize a public speaker in me. Thank you for always hyping me up and discussing future plans in the early QuTech days many years ago.

Mehdi, Mael, brothers from across the pond! I love running into you guys anywhere and everywhere, it's always fun and great to catch up on the latest goss. Qunnect will surely continue growing, keep the good vibes rolling! **Josh, Ingrid, Remon**, thank you for being the frontrunners on using fibers for quantum purposes, your first go-around on the KPN fibers made our lives a bit easier, so thanks for the all the efforts there! Best of luck with Q*BIRD! **Adriaan**, OQS is a huge success and your driving force is engraved in

its roots. Thanks for being a fun and very knowledgeable scientist to work with, you'll continue being amazing as entrepreneur. **Marjolein Bouwers**, thank you for inviting me to speak at the Royal Institution and keeping touch with me throughout the years. The Netherlands and the UK is very lucky to have you to foster innovation between the two countries, I hope our paths can cross again in the future. **Renske**, although my entrepreneurial plans are put on ice, you have always provided the fuel to that fire inside me. After our meetings I would have a million more ideas and a blazing urge to pursue my (very big) dreams. Thank you so much for that, and my story will have a definite continuation - you will be one of the first to hear about them. **Deborah, Diederick**, thank you for inviting me to the 'Scenarios for Quantum Networks'. It helped me broaden my horizons, and provided the right starting point to work on the more ELSA/ELSPI related side of the quantum internet. Best of luck with all the work you continue doing in that space! **Jesse**, you do invaluable work to keep quantum internet related topics relevant in the Netherlands and in Europe. Thank you for giving me the opportunity to shine on all those public speaking opportunities - they would have been even more enjoyable without the sanitizing gel in my eye ;).

Faiez, the realest OG, altijd goed gekleed, altijd de charme en suave, met een hart van goud. Voor mij was de omslag naar het Haganum en meteen in een vriendengroep omarmd worden echt life-changing, en heeft me een prachtige start gegeven om een nieuw leven op te bouwen. Super bedankt voor al je steun, rap-muziek-passie en je vriendschap. Je hebt een geweldig gezin, en ik ben heel blij voor je dat je een prachtige familie hebt en daar tijd mee kan besteden. **Duco, Laura**, bedankt voor het samenbrengen van zoveel interessante mensen in "Le Petit Club des Grandes Idées", dat heeft me enorm veel diepgang en enthousiasme gebracht om voor een breed publiek te blijven spreken over quantum. **Duco**, ik zal onze tijd in Duitsland nooit vergeten met een kleine heimwee naar hoe onze vriendschap toen was. Enorm veel succes met je leven in Amsterdam, ik denk aan je! **James Murdza**, thanks for the support at a distance and being so interested in quantum technology! You're a special force of nature and anyone is lucky to come across you and your work. **Merel**, I still think back to those days in the BSc student room (that doesn't exist anymore!) and it's great we were able to keep in touch throughout these years. Thank you for having me in Verbier adventures, rooftop-bars and all the lovely long talks we could have. I hope you continue finding your passion, wherever that may lead you! **Elly**, you've always been bluntly honest about my way of working. Although that style of work got me to where I am, you can rest assured that the balance has restored slightly more to what you would want for me. **Robin**, thanks for having me on your podcast! It always felt like we are kindred spirits, but just happen to not cross paths naturally enough. Continue changing the world from your kind and realistic perspective! **Esther Marquenie**, PhD, Rotterdam, COVID.. I am unsure why we haven't spoken in such a long time. You were always so supportive of my big plans, and you have been a great support during my university study career. Thank you for having been a great friend, and let's reconnect soon! **Esther Kramer, Kelbij, Jordi**, thank you for the craziness that was the 'kookclub'. Those evenings (turned nights) were both very enjoyable and therapeutic. I wish you all the best for your futures! **Frank Scholtes**, although we have been terrible at keeping touch, I want you to know I have always regarded you as my first true friend. Thank you for keeping my spirits lifted when all other kids would try to bring them down, we had the best times laughing about nothing and everything, and I seriously can't believe I ever drank Gazeuze with joy. Your kind heart is a gift to this world, but don't let it take advantage of that. **Maarten Prins**, ever since we met it was clear you had a very driven and entrepreneurial mind. I really value that we remained such good friends long after both our basketball careers ended. It's always been a breath of fresh air the way we can talk about money or success - you have a very realistic view of life and I respect you for that. And for your sake I sincerely hope you kept that Apple stock you were raving about those 15 years ago! **W.S**, I've always been in awe of your knowledge of Linux, OpSec and the digital world that comes with it. Thank you for all the hours of digital and personal support during many hardships throughout all the years, but most of all for the laughs (with tears) about the odd details we both recognize. One of these years I will join ADE again, I promise, but until then *YMFC never dies.* **Eleanor**, thank you for enduring the late nights in the command center during some very poorly planned visits. Your humor and energy is contagious, and I want to thank you for all the laughs and the time we spent together. I wish you a wonderful future! Also, Viscount Slim will indeed forever remain the best rapper name in existence.

Ron, Danielle, Sky, thank you for opening up your lives to this Dutch guy! It's been really nice to get to know you, and to bring our families together with Christmas time. I look forward to more get-togethers like that, and to see everyone again you soon!

Mam, Pap, met overtuiging kan ik zeggen dat deze dissertatie hier niet zo had kunnen staan zonder jullie. Jullie zijn een onuitputtelijke bron van liefde en ondersteuning geweest in al mijn jaren van school, studie en ook nu weer bij mijn PhD. Van personal juriste en styliste met enorm doordachte blik (mam) tot de 'professionele adviseur' die een rijsttafel aflevert op de TU (pap). Of nog laat thuis een 'gaat het goed?' in de jaren dat ik nog bij jullie woonde. Het zijn maar kleine voorbeelden van een heel boek dat ik kan vullen met de hulp die jullie hebben geboden in mijn (PhD) leven. Ik kan me geen betere ouders wensen en daarom draag ik hierbij deze promotie ook aan jullie op, zodat jullie voor altijd vereeuwigd zijn met het succes dat ik heb en wij hebben volbracht. Het feit dat we nog steeds zo close zijn koester ik elke dag. Ongeacht wat de toekomst ons brengt, een fysieke afstand zal nooit leiden tot een afstand uit hoofd en hart, wij blijven altijd entangled. Bedankt voor alles, ik hou van jullie. Live long and prosper.

Scarlett, thank you for asking to have lunch with me. Like circling planets we managed to slowly let gravity pull us closer together, until the forces brought us to a collision of minds, personalities and life. I think we are different in the exact ways we need to in order for both of us to grow, and similar in the exact ways that allow us to enjoy life together to its fullest extent. I'm so glad I bought that espresso machine *just* in time for you to be impressed with my 'coffee affinity', even though I had no idea what I was doing at the time. You have the kindest heart and the most beautiful mind, thank you for all the hours of talking, horror movie watching, cooking and coffee drinking together, but also for tolerating my ramblings or random sentences I blurt out (repetitively) when I walk around the house. I'm excited for the future we can build together, no matter what I'm convinced it will be bright, beautiful, with ubiquitous espressi, \$300M and a ranch in Montana. I love you so much, and we will always be hugbug.

Kian
Delft, March 2025

List of Publications

Papers

9. **K. L. van der Enden**[†], R. Kirschner[†], M. Krumtünger, A. Wilms. *Quantum Internet Use Case Analysis for the Automotive Industry.* arXiv.2501.19070, (2025).

8. **K. L. van der Enden**, G. Profitiliotis, D. Croese. *Advancing a Responsible Future Quantum Internet.* 2024 IEEE International Conference on Quantum Computing and Engineering (QCE), pp. 65-70.

7. A. J. Stolk, J. J. B. Biemond, **K. L. van der Enden**, L. van Dooren, E. J.van Zwet and R. Hanson. *Extendable optical phase synchronization of remote and independent quantum network nodes over deployed fibers.* Physical Review Applied **23** (1), 014077 (2025).

6. A. J. Stolk[†], **K. L. van der Enden**[†], M. C. Slater, I. te Raa-Derckx, P. Botma, J. van Rantwijk, J.B. Biemond, R. A. J. Hagen, R. W. Herfst, W. D. Koek, A. J. H. Meskers, R. Vollmer, E. J.van Zwet, M. Markham, A. M. Edmonds, J. F. Geus, F. Elsen, B. Jungbluth, C. Haefner, C. Tresp, J. Stuhler, S. Ritter and R. Hanson. *Metropolitan-scale heralded entanglement of solid-state qubits.* Sci. Adv.10, eadp6442, (2024)

5. W. D. Koek, L. van Dooren, R. A. J. Hagen, H. van Burg, M. Vaselli, J. P. J. Morits, A. J. Stolk, **K. L. van der Enden**, J. J. Benjamin Biemond, E. J. van Zwet and J. Croese. *Interferometer for phase-stabilization of quantum nodes using SIL-based color centers.* Proceedings SPIE 12911, Quantum Computing, Communication, and Simulation IV, 129111F, (2022)

4. A. J. Stolk[†], **K. L. van der Enden**[†], M. -C. Roehsner, A. Teepe, S. O. J. Faes, C. E. Bradley, S. Cadot, J. van Rantwijk, I. te Raa, R. A. J. Hagen, A. L. Verlaan, J. J. B. Biemond, A. Khorev, R. Vollmer, M. Markham, A. M. Edmonds, J. P. J. Morits, T. H. Taminiau, E. J. van Zwet and R. Hanson. *Telecom-Band Quantum Interference of Frequency-Converted Photons from Remote Detuned NV Centers.* PRX Quantum **3**, 020359, (2022)

3. J. G. Kroll, F. Borsoi, **K. L. van der Enden**, W. Uilhoorn, D. de Jong, M. Quintero-Pérez, D. J. van Woerkom, A. Bruno, S. R. Plissard, D. Car, E. P. A. M. Bakkers, M. C. Cassidy and L. P. Kouwenhoven. *Magnetic-Field-Resilient Superconducting Coplanar-Waveguide Resonators for Hybrid Circuit Quantum Electrodynamics Experiments.* Physical Review Applied **11**, 064053, (2019)

2. J. G. Kroll, W. Uilhoorn, **K. L. van der Enden**, D. de Jong, K. Watanabe, T. Taniguchi, S. Goswami, M. C. Cassidy and L. P. Kouwenhoven. *Magnetic field compatible circuit quantum electrodynamics with graphene Josephson junctions.* Nature Communications **9**, 4615, (2018)

1. A. Bruno, G. de Lange, S. Asaad, **K. L. van der Enden**, N. K. Langford and L. DiCarlo. *Reducing intrinsic loss in superconducting resonators by surface treatment and deep etching of silicon substrates.* Applied Physics Letters 106, 182601, (2015)

[†]Equally contributing authors.

BOOK CONTRIBUTIONS

1. **K.L. van der Enden** and W. Kozlowski. *Das Quanteninternet: neue Möglichkeiten der Kommunikation* appears in A. Wilms, F. Neukart, *Chancen und Risiken von Quantentechnologien.* Springer Gabler, Wiesbaden, (2023)

PATENTS

2. J. J. B. Biemond, A. J. Stolk, **K. L. van der Enden**, E. J. van Zwet, A. J. H. Meskers. *Controlled synchronisation at bandwidths beyond the limit of direct synchronisation error measurement*, (2023)

1. J. J. B. Biemond, A. J. H. Meskers, W. D. Koek, A. J. Stolk, **K. L. van der Enden**, E. J. van Zwet. *Estimation method of phase difference between two optical channels induced by optical latency variations*, (2023)

PUBLIC APPEARANCES

CONFERENCE TALKS

- *Quantum interference of telecom photons from independent quantum network nodes: Part I-Enabling technologies.*
  APS March Meeting, Chicago, USA, 2022.
- *Plotting the roadmap to the "Quantum Advantage"*.
  The Quantum Computing Summit, London, United Kingdom, 2022.
- *Quantum Internet - Opportunities and Challenges.*
  EuroScience Open Forum, Leiden, Netherlands, 2022.
- *The next generation quantum networks.*
  Q2B, Paris, France, 2023.
- *A metropolitan-scale quantum network demonstration platform using solid-state emitters in diamond.*
  NWO Physics, Veldhoven, Netherlands, 2023.
- *Towards Large-Scale Entanglement-Based Quantum Networks.*
  European Conference on Optical Communication (ECOC), Glasgow, United Kingdom, 2023.
- *Advancing a responsible quantum internet*.
  IEEE QCE, Montreal, Canada, 2024.

GENERAL AUDIENCE TALKS

- *Quantum Revolution in Computing and Internet*.
  Nyenrode lecture, Delft, Netherlands, 2021.
- *Veiliger communiceren via het Quantum Internet?*.
  Kadaster, Apeldoorn, Netherlands, 2022.
- *Quantum Delta NL: Building a European Ecosystem.*
  Minacned, Delft, Netherlands, 2022.
- *The Quantum Internet: Building the unhackable internet of the future.*
  EMERCE EDAY, Amsterdam, Netherlands, 2022.
- *Quantum Futures.*
  fanfare fanfare, Amsterdam, Netherlands, 2023.
- *The Quantum Internet: An unhackable internet of the future.*
  Royal Institution, London, United Kingdom, 2023.

CONFERENCE POSTERS

- *Towards metropolitan-scale entanglement generation for an NV based quantum network*. **NWO Physics** (online), 2021.

MEDIA APPEARANCES

- *Introductievideo Faces of Science.* **Dutch Royal Institute of Sciences**, 2022.
- *Quantenphysik: Der Schlüssel für das Internet der Zukunft?.* **Galileo**, Pro Sieben, 2022.
- Co-Host of Nationale Wetenschapscommunicatiedag. **NWO**, Den Haag, 2022.

PODCASTS

- *Quantum Internet en Quantum Computing.* **De Wereld Van Morgen Podcast**, 2020.
- *Kian van der Enden on Quantum Tech.* **Erasmus Tech Community Podcast**, 2020.
- *Kian van der Enden / Quantum Internet Researcher QuTech.* **Sociale Innovatie Podcast**, 2021.

AWARDS

- 3rd place, pitch competition. *Breaking the wall of scalable quantum networks*. **Falling Walls Baden-Württemberg**, Germany, 2024.

ART

- Scientific advisor for *Agustina Woodgate: More heat than light*. **Stroom**, The Hague, 2022.

CURRICULUM VITÆ

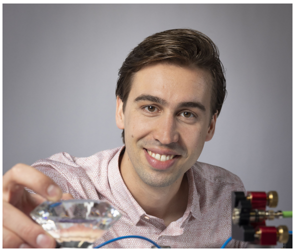

Kian Louran VAN DER ENDEN
May 19th, Delft, The Netherlands

2009-2014 **Bachelor of Science**, Applied Physics
Delft University of Technology, Delft, The Netherlands
Thesis: *"Characterization of internal quality factors in surface-treated and deep-etched superconducting CPW resonators"*
Supervisors: Dr. Alessandro Bruno and Prof. dr. Leo DiCarlo

Q1-4 2012 **Engineer & Public Relations**
Helios 3D, Delft, The Netherlands
Design and construction of modular 3D LED display with $20k budget.
Winner of Global Student SSL Contest in Guanghzou, China.

2014-2019 **Master of Science**, Applied Physics
Delft University of Technology, Delft, The Netherlands
Thesis: *"A magnetic field insensitive graphene transmon"*
Supervisors: Dr. James Kroll and Prof. dr. ir. Leo Kouwenhoven

2015-2017 **Co-founder & Chief Powertrain**
Delft Hyperloop, Delft, The Netherlands
Championship winner of the SpaceX Hyperloop Pod Competition

Q4 2018 **Research Intern Quantum Architecture**
Microsoft, Redmond, WA, USA
Supervisors: Doug Carmean and Prof. dr. ir. Leo Kouwenhoven

(Continued on next page)

2019-2025 **Ph.D, Experimental Physics**
QuTech, Delft University of Technology, Delft, The Netherlands
Thesis: *"Metropolitan-scale quantum networks with diamond qubits: Applied quantum networks for business & society"*
Promotors: Prof. dr. ir. Ronald Hanson, Prof. dr. Stephanie Wehner

2022-now **Face of Science**
The Royal Netherlands Academy of Arts and Sciences (KNAW), The Netherlands

2024-now **Quantum Technology Expert, Keynote Speaker**
Interseqt, Den Haag, The Netherlands
Specialized consulting in quantum technologies: technical expertise, sales, EU proposal development and industry keynotes.